Stiffness and Stability of Deployable Pantographic Columns

by

Igor Raskin

A thesis
presented to the University of Waterloo
in fulfilment of the
thesis requirement for the degree of
Doctor of Philosophy
in
Civil Engineering

Waterloo, Ontario, Canada, 1998

© Igor Raskin 1998

National Library of Canada
Acquisitions and Bibliographic Services
395 Wellington Street
Ottawa ON K1A 0N4
Canada

Bibliothèque nationale du Canada
Acquisitions et services bibliographiques
395, rue Wellington
Ottawa ON K1A 0N4
Canada

Your file Votre référence

Our file Notre référence

The author has granted a non-exclusive licence allowing the National Library of Canada to reproduce, loan, distribute or sell copies of this thesis in microform, paper or electronic formats.

L'auteur a accordé une licence non exclusive permettant à la Bibliothèque nationale du Canada de reproduire, prêter, distribuer ou vendre des copies de cette thèse sous la forme de microfiche/film, de reproduction sur papier ou sur format électronique.

The author retains ownership of the copyright in this thesis. Neither the thesis nor substantial extracts from it may be printed or otherwise reproduced without the author's permission.

L'auteur conserve la propriété du droit d'auteur qui protège cette thèse. Ni la thèse ni des extraits substantiels de celle-ci ne doivent être imprimés ou autrement reproduits sans son autorisation.

0-612-32853-8

Canada

The University of Waterloo requires the signatures of all persons using or photocopying this thesis. Please sign below, and give address and date.

Abstract

Straight or curved planar pantographic columns are an integral part of the three-dimensional deployable structures made of scissor-like elements. It is shown that, under the assumption of linear behaviour, the stiffness characteristics of such straight columns can be derived analytically. Equivalent bending and axial stiffnesses for uniform pantographic columns are obtained by equating their displacements to those of uniform solid columns. The behaviour of pantographic structures in bending is found to be very similar to that of conventional structures. Under axial load, the geometric non-linearity caused by the finite rotations of bars in the scissor-like elements must be taken into account. The system of non-linear equations describing the structural response in this case is solved numerically. The buckling analyses for local snap-through and global column-like types of instability are performed. The analytical procedures developed for the structures made of identical scissor-like elements are modified for non-uniform columns.

The behaviour of three-dimensional triangular and square columns in bending is considered. The analytical procedure includes the force method of analysis for a single prismatic pantographic unit and the displacement method of analysis for the whole structure. The derived expressions indicate that deflections of a spatial column consist of primary and local parts. The primary part can be obtained by superposition of the equivalent bending stiffnesses of the planar columns forming the sides of the spatial structure. The contribution of each side depends on its orientation with respect to the plane of bending. The local part of the solution originates from the support conditions at the bottom of the column. The similarities and differences in the behaviours of pantographic and solid columns are discussed.

Acknowledgements

I wish to express great thanks and appreciation to my supervisor, Professor J. Roorda, for his continued interest in my work, his constant support, guidance and encouragement. I also thank Professor S.T. Ariaratnam and other members of the Solid Mechanics Division for the valuable discussions on the problems that I encountered in the course of research. My fellow graduate students will be fondly remembered for the warm and welcoming atmosphere they created in the Division.

The financial support of the Natural Sciences and Engineering Research Council of Canada and the Ministry of Education of Ontario is acknowledged.

Contents

List of Figures

Chapter 1

Introduction

1.1 Foreword

Deployable structures have attracted growing attention from engineers, architects and researchers in recent years. This is clearly demonstrated by the two International Conferences on Mobile and Rapidly Assembled Structures - MARAS 91, held in Southampton, UK, and MARAS 96, held in Seville, Spain, as well as by the increasing number of publications on this subject found in the literature. The term "deployable" may often be substituted with the words "expandable", "foldable", "retractable" and so on. The main property of the objects described by these terms is that such systems can assume configurations in space with envelopes of essentially different volumes. Sometimes, if one thinks of an ideal structure, it is even possible to say that the dimensions of these configurations are different. We frequently use the advantages of deployable structures in everyday life without giving, in most cases, too much thought to the ideas built into them. Some examples showing the range of applications of these structures are the following. Folding road maps, umbrellas, pull-out radio aerials, clothes drying racks and foldable lawn furniture are familiar to everybody. More structural applications are: pneumatic domes, expandable arches, domes and aircraft hangars, field hospitals, storage buildings, temporary

housing, protective coverings for curing concrete on construction sites, and many others. Examples in the aerospace industry are: communication booms, space cranes and platforms, large reflectors, mesh antennas and supporting structures for them.

The choice of deployable structures in most of these cases is determined by such properties as extreme compactness during transportation and storage (the space needed is practically equal to the volume of material used), relative ease of erection and the possibility of repetitive use.

A retrospective view of deployable devices and structures throughout the human history, from the hunter chair to large span domes, has been given by Escrig (1996). The concept of foldable structures has been considered by engineers for some period of time already. Zuk and Clark (1970) listed and described a number of projects dealing with "self-erecting" structures. The authors discussed them mostly from the architectural point of view, without going into the detailed procedure of their analysis and design. As the current literature shows both the geometric and the mechanical analysis of such systems, as well as their design, are usually quite non-trivial tasks.

1.2 Deployable Structures in the Literature

1.2.1 Categories of Deployable Structures

The term "fabric architecture" encompasses rapidly assembled structures of two types: pneumatic structures and tents. The former include single-layer systems, in which the entire enclosed space is pressurized (Renner, 1996), and double-layer systems, which are assembled of inflatable flat or curved modules (Guidetti, 1996). Tents are often used to cover large areas for shows and exhibitions (Mollaert, 1996; Westbury, 1996). The two

important aspects in the design of such structures are fabric patterning and final surface stabilization.

Continuous deployable structures are usually the assemblies of triangular or quadrilateral plates connected at the corners or along the edges. These plates can form flat or curved surfaces, often used as solar cell arrays or antennas. Fig. 1.1 shows the folding sequence of the planar deployable structure suggested by Miura (1993). According to his concept, a plane subdivided into parallelograms can be folded simultaneously in two orthogonal directions through "the developable double corrugation surface". This folding principle is used for deploying membrane solar cell arrays of spacecraft in orbit. Guest and Pellegrino (1994) investigated triangulated cylinders foldable to a compact stack of plates (Fig. 1.2). Vertices of the triangles are located on the cylindrical surface and connected by straight lines, which are the sides of the triangles, and form linear hinges between them. The problem was formulated from the geometrical point of view and the phases of the folding process were studied.

Deployable tubular booms of circular cross-section are made of one or two strips of thin metal, having the shape of a circular arch in the deployed configuration. In the stored state these strips are flattened and coiled on a drum (Pellegrino, 1995). Telescopic booms also have a tubular, but much stiffer cross-section (Becchi and Dell'Amico, 1989). In addition to aerospace applications, their more down to earth uses include spyglass, pull-out pointers and radio aerials.

A very broad category of deployable trusses and frames includes a number of different systems. They can be divided into groups according to the type of elements, number of degrees of freedom during deployment, stressed or stress-free folded or deployed configurations etc. Two examples of structures that are stress-free in the deployed configuration, but have deformed members when stored, are shown in Fig. 1.3.

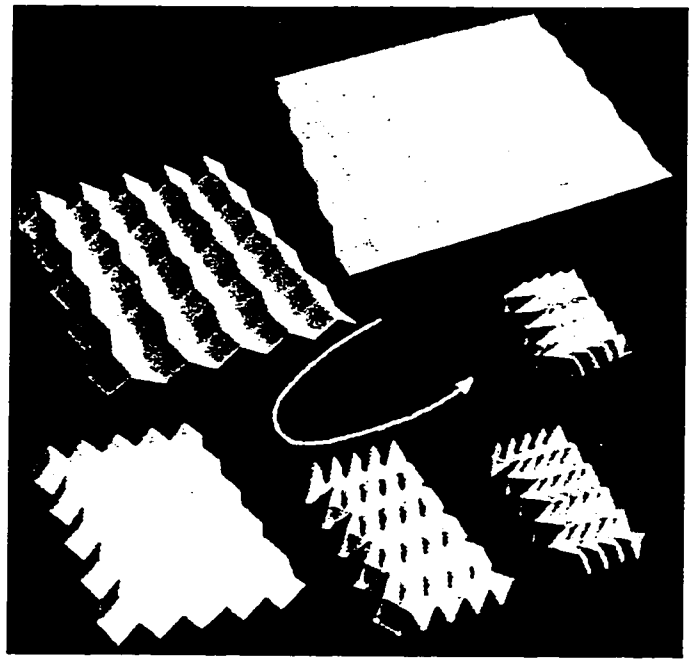

Figure 1.1: Folding a plate to "the developable double corrugation surface" (Miura, 1993).

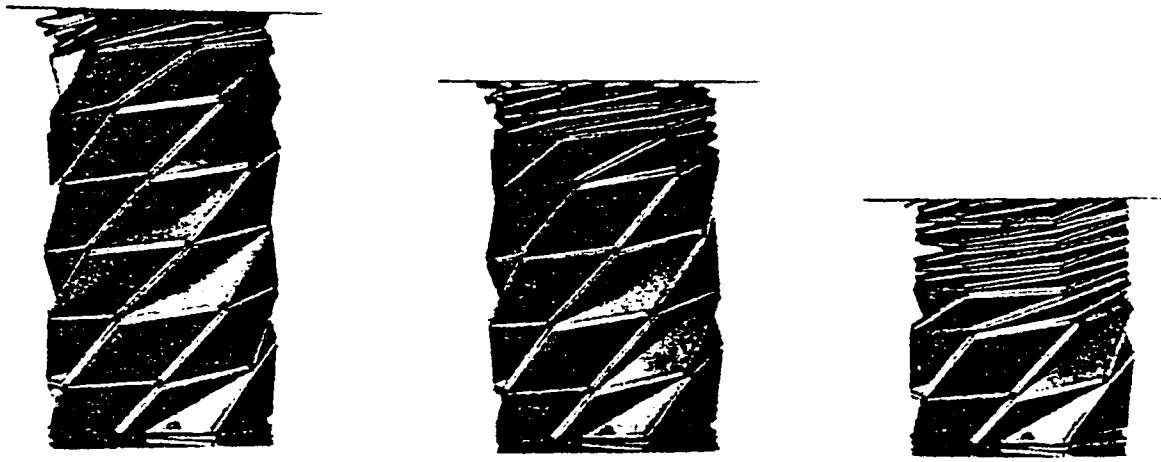

Figure 1.2: Folding sequence of a triangulated cylinder (Guest and Pellegrino, 1994a).

The first is a coilable mast by Miura (1993). The three coilable continuous longerons can be deformed to helical form and stowed into a coil when the structure is compressed in the direction of its axis. The second column, although not exactly a truss, by Hegedus (1993), consists of rigid plane elements and elastic bars (dashed lines in the figure). Under increasing axial load the bars elongate until, after the snap-through buckling of all units, the structure becomes practically flat. Both columns accumulate strain energy during the process of folding and release it during the unfolding. Another example of a system with the elements stressed in the folded state, presented by Fanning and Hollaway (1993), is shown in Fig. 1.4. This is a deployable antenna with "energy loaded joints". In the stowed configuration the compressed spring exerts a force on the sliding collar which, in turn, generates a moment about the link pin causing the joint to deploy.

Deployable trusses with multiple degrees of freedom during deployment are widely represented in the literature. Such trusses have a significant number of variable-length bars and are said to be massively actuated. Usually they are deployed one module at a time. In many cases these trusses are statically determinate, which ensures that no stress is created due to arbitrary changes in elemental lengths. If a truss is statically indeterminate, then it remains stress free if the vector of elemental length increments, also called static control, is a linear combination of the columns of the structural compatibility matrix, as was stated and proved by Ramesh et al. (1991). Hence, changing the configuration of the system under the condition of zero internal forces becomes a more complicated problem.

Mikulas et al. (1992) presented a two-dimensional truss consisting of N bays as shown in Fig. 1.5. The authors considered three approaches for achieving variable geometry of the truss by replacing different members with actuators. The number of actuators per bay, the amount of actuating required to deploy the truss and the flexibility of producing different types of deformations were used as factors to choose the design.

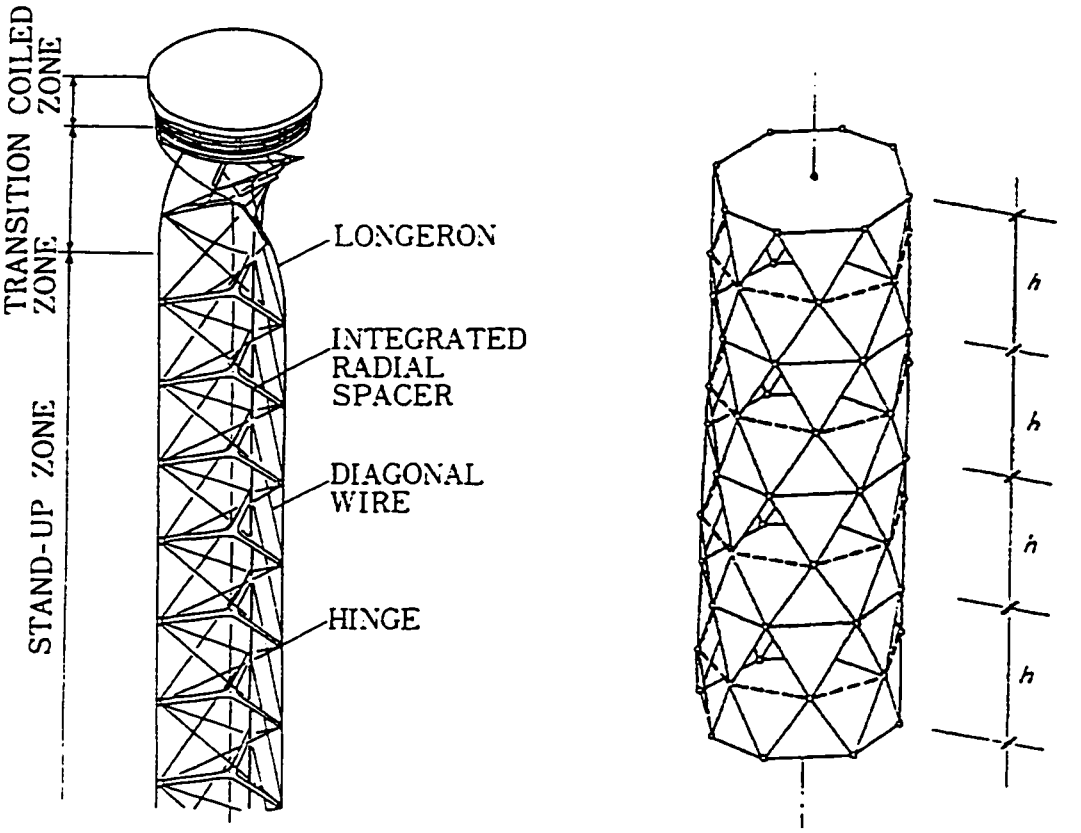

Figure 1.3: Coilable mast by Miura (1993) and deployable column by Hegedus (1993).

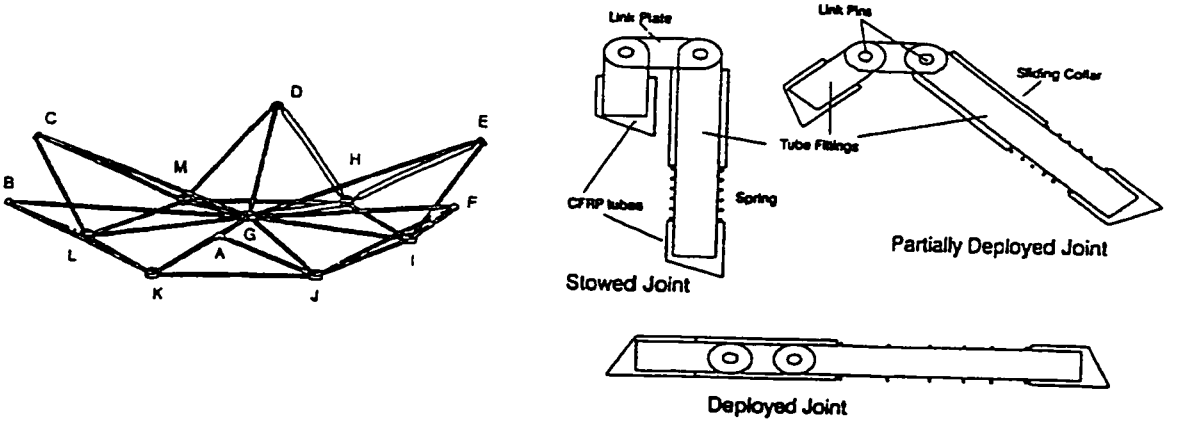

Fugure 1.4: 5.0 m deployable antenna and energy loaded joint (Fanning and Hollaway, 1993).

Three-dimensional modules of deployable trusses can be of cubic, tetrahedral, octahedral and other polyhedral configurations. Generation of the basic three-dimensional units was studied by Natori et al. (1986), and Chew and Kumar (1993). Graph theory was employed for this purpose by Warnaar and Chew (1990), and Warnaar (1992). Fig. 1.6 shows two alternatives for placing actuators in a deployable truss made of octahedral units. A variety of possibilities for changing the shape of the structure by using some or all actuators raises the issues of control and adaptability. These problems were addressed by Ramesh et al. (1989 and 1991), Miura and Furuya (1988), Miura (1989), Furuya and Isomichi (1992), Wada et al. (1989), Wada (1990) and other researchers.

Sliding joints are sometimes used to activate the process of deployment (folding) instead of variable-length members. Examples of cubic and hexagonal modules with such joints are shown in Fig. 1.7. The first module (Fig. 1.7a) has rigid bars for all members. However, if some members are known to be subjected only to axial tension or if the system can be prestressed to ensure only tensile axial forces in such members, these elements can be cables (Fig. 1.7b). The deployed hexagonal unit in Fig. 1.7c includes articulated members with intermediate hinges for the elements which are cables in the partially folded hexagonal unit in the same figure.

The number of degrees of freedom during deployment of the above structures is equal to the number of devices that vary certain geometric parameters of the system. There exists another class of deployable structures which, although highly articulated, are essentially one degree of freedom mechanisms during deployment. These so-called "pantographic structures" are described in the next Section.

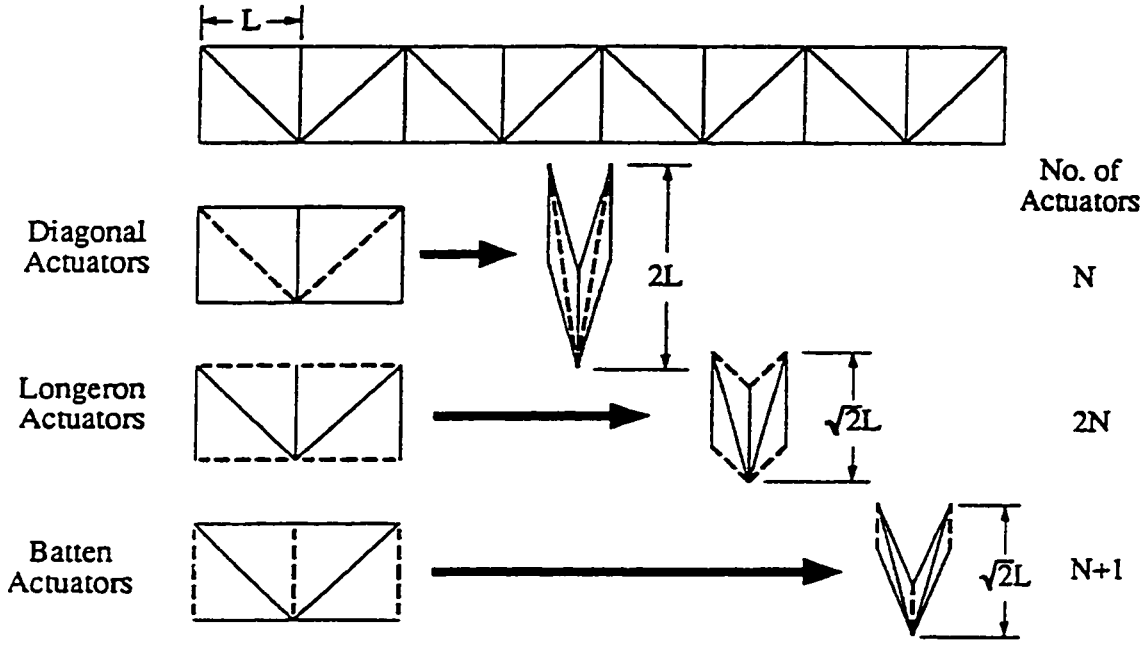

Figure 1.5: Three alternatives for placing actuators into a plane deployable truss (Mikulas et al., 1992).

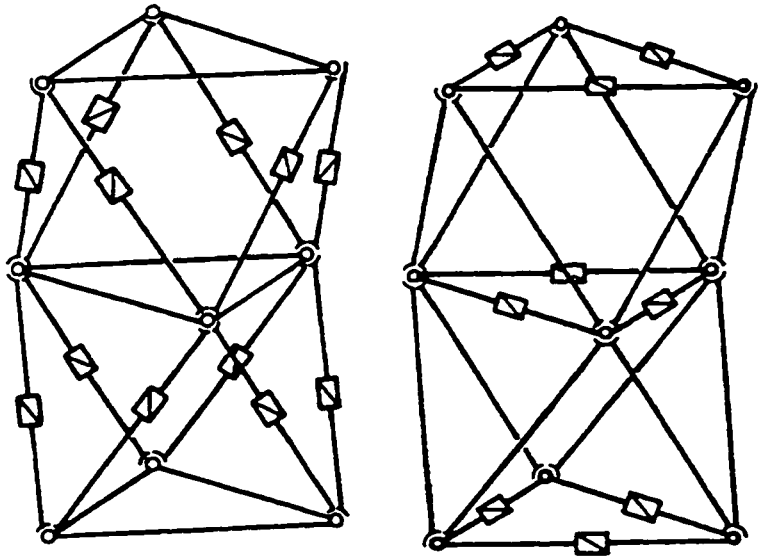

Figure 1.6: Two layouts of variable-length members in a deployable truss made of octahedral units (Miura and Furuya, 1988).

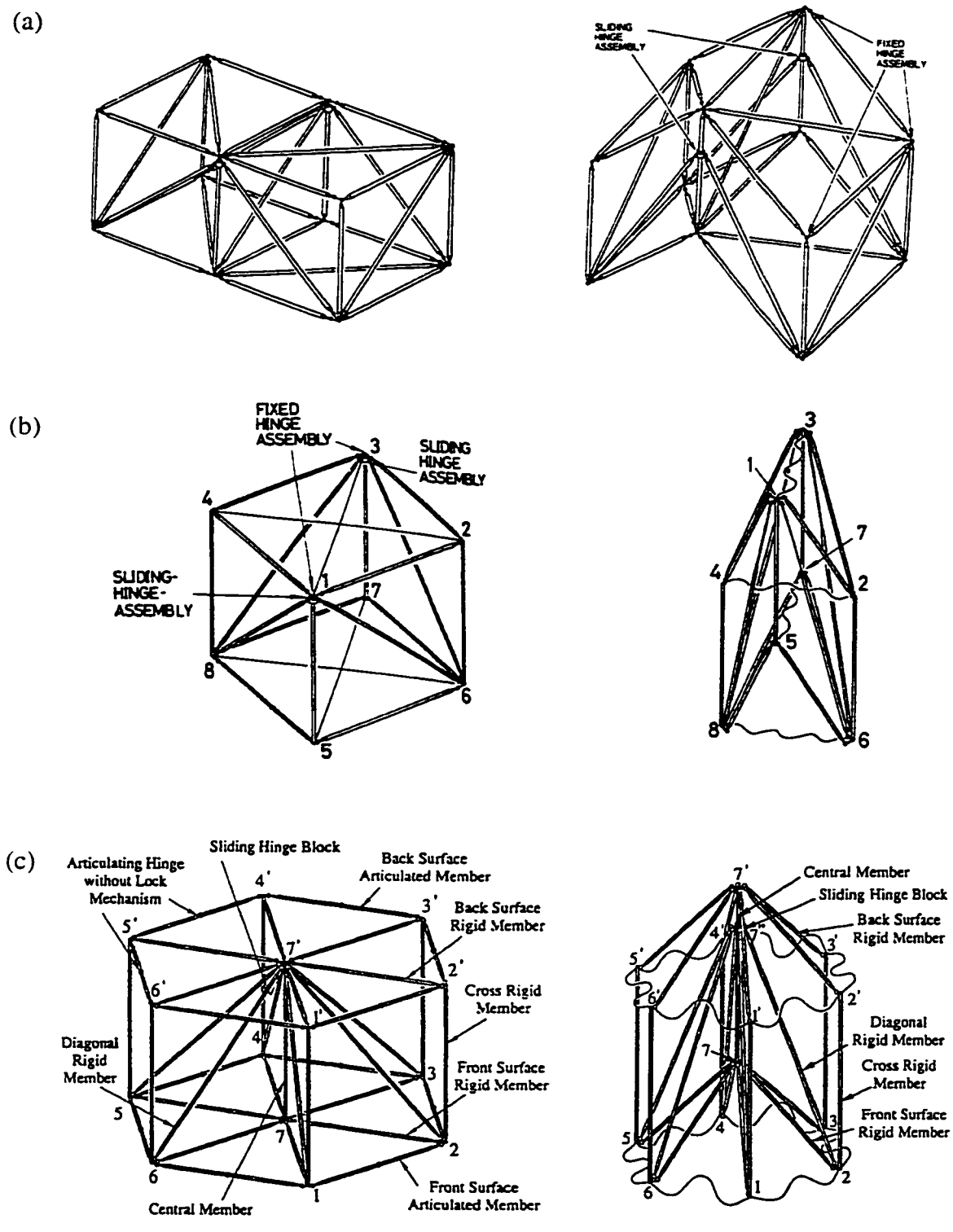

Figure 1.7: Three-dimensional deployable modules with sliding nodes: (a) by Takamatsu and Onoda (1991), (b) by Onoda (1988), (c) by Onoda et al. (1996).

1.2.2 Pantographic Structures

The dictionary defines the word "pantograph" [from Greek "panto" - all and "graph" - draw] as "an instrument for copying images on a predetermined scale consisting of four light rigid bars jointed in parallelogram form" (Webster's ..., 1981). Another commonly known use of pantographs is to carry electric current to a train from overhead wires. Inventors have extensively utilized the concept of pantograph in creating more complicated copying devices, extendible booms (McCollum, 1975; Hardin, 1978; Zanardo, 1985; Clevett et al., 1986), exhibition displays (Nodskov and Thelander, 1986; Sorenson and Gerberding, 1994; Wichman, 1992) etc. The sketches of some of these inventions are shown in Figs 1.8 to 1.12. Mechanical engineers use pantographs to create robotic manipulators (Fig. 1.13) and joints of walking machines (Yang and Lin, 1985; Ichikawa et al., 1990; Funabashi et al., 1991; Shahinpoor, 1993; Oral, 1996). Aerospace applications of the pantographs are illustrated in Figs 1.14 and 1.15.

The basic element of pantographic deployable structures is a two-dimensional pantographic unit, also called scissor-like element (SLE). The unit consists of two beam elements, with hinges at the ends, which are connected to each other at their intermediate points by a pivot allowing their relative rotation. The first introduction of such elements into structural applications is attributed to a spanish architect Emilio Perez Pinero (Makowski, 1966; Belda, 1996; Escrig, 1996). While still a student, he presented his model of a "Spatial Reticular Structure" at the UIA Congress in London in 1961 (Pinero, 1961 and 1962). Several stages of the unfolding process of this model are shown in Fig. 1.16. The structure was composed of rigid bars and flexible wire cables. Some of the cables were permanently fixed at both ends and served to terminate the deployment process. Others were fixed at one end only and had to be hooked to the structure in order to stabilize it after deployment. The members of the structure were stress-free in folded and deployed configurations, as well as during deployment (except for the stresses due to self-weight and possible prestress).

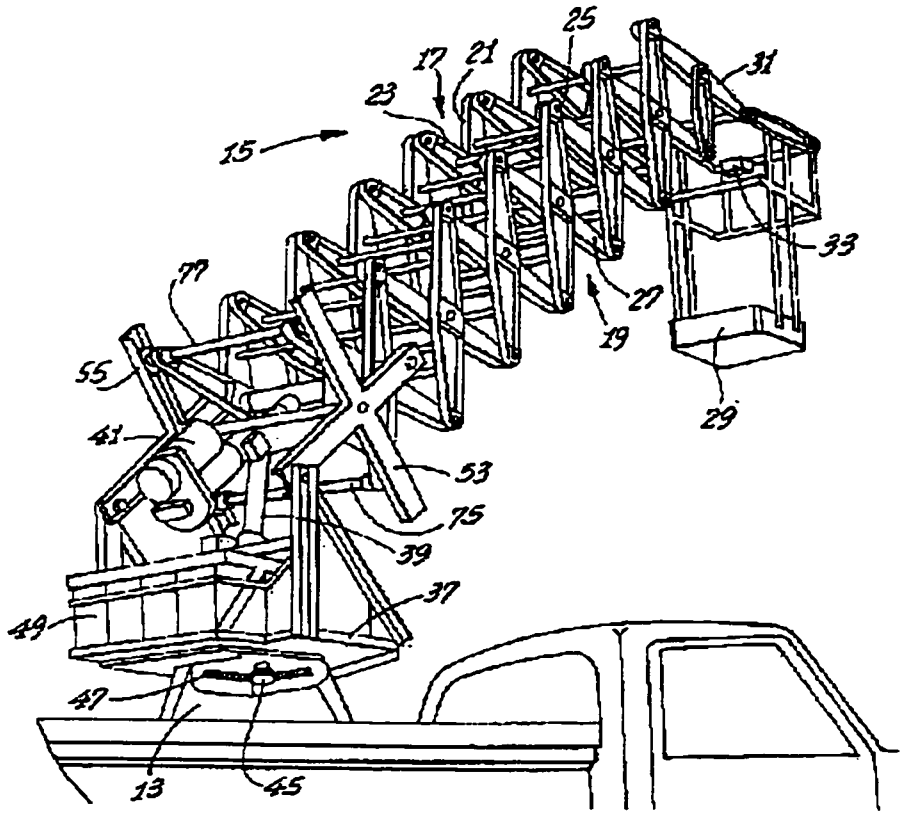

Figure 1.8: Extendible pantographic boom structure (McCollum, 1975).

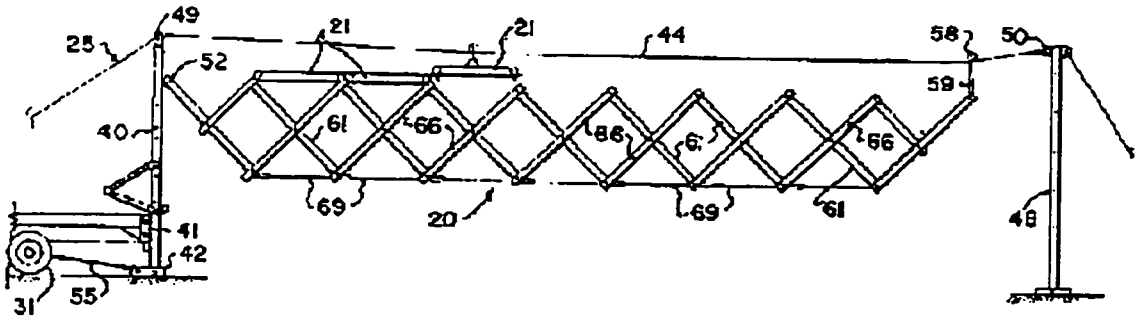

Figure 1.9: Expandable portable bridge (Clevett et al., 1986).

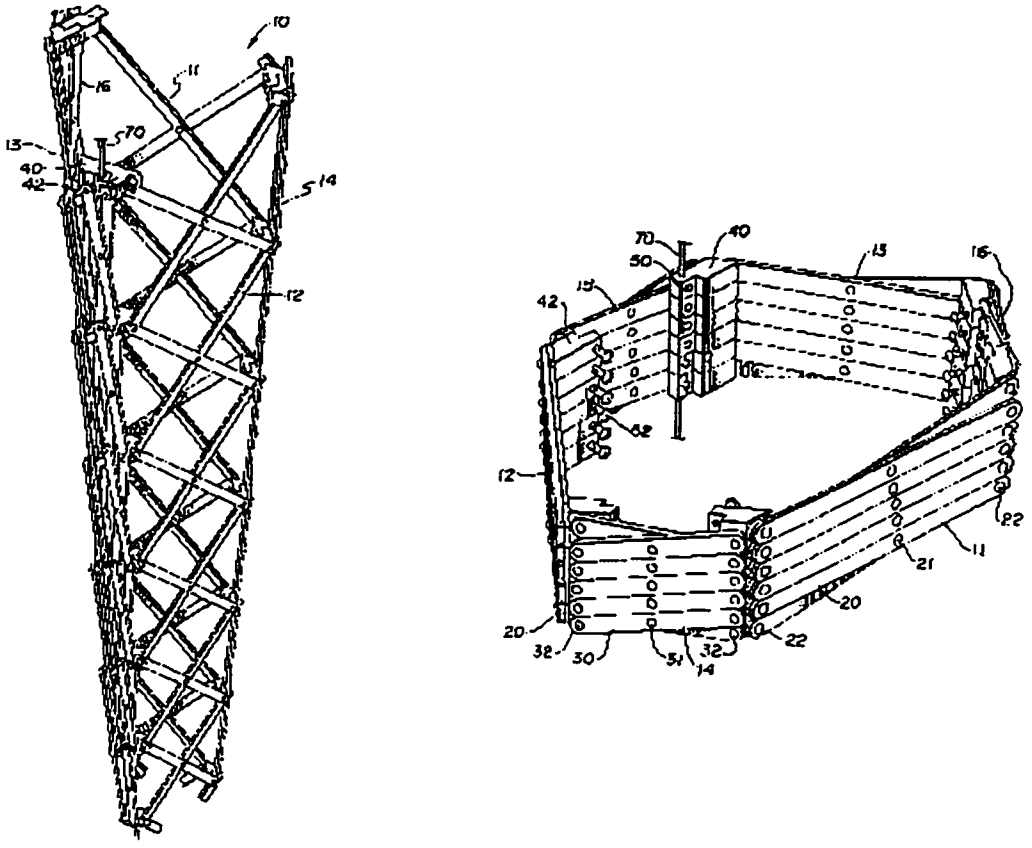

Figure 1.10: Expandable beam structure by Hardin (1978).

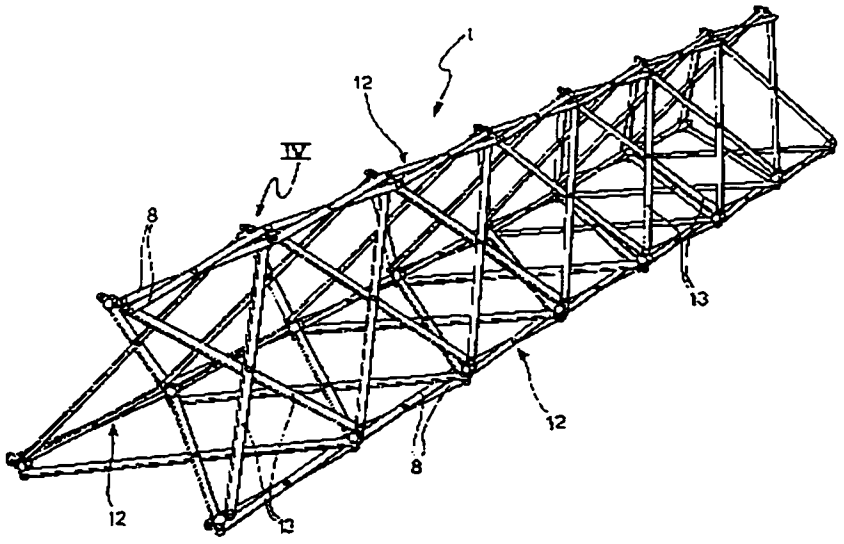

Figure 1.11: Extensible arm by Zanardo (1985).

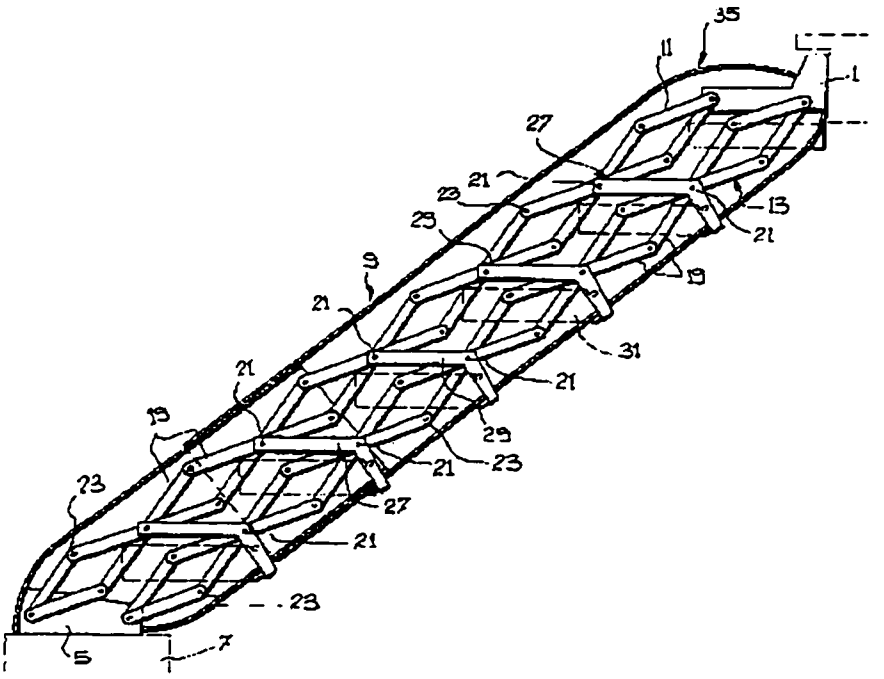

Figure 1.12: Adjustable pantographic staircase (LeBlond, 1986).

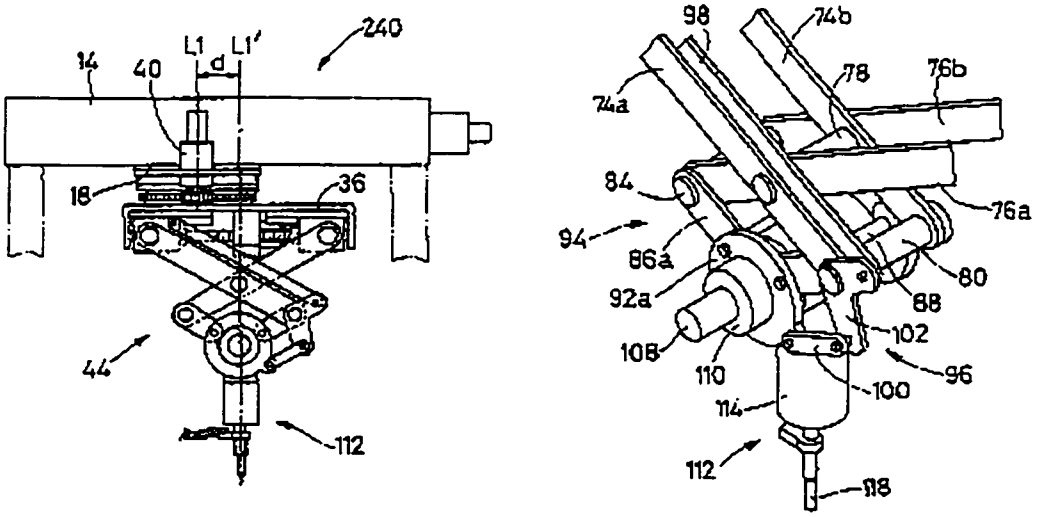

Figure 1.13: Pantograph type robot arm (Ichikawa et al., 1990).

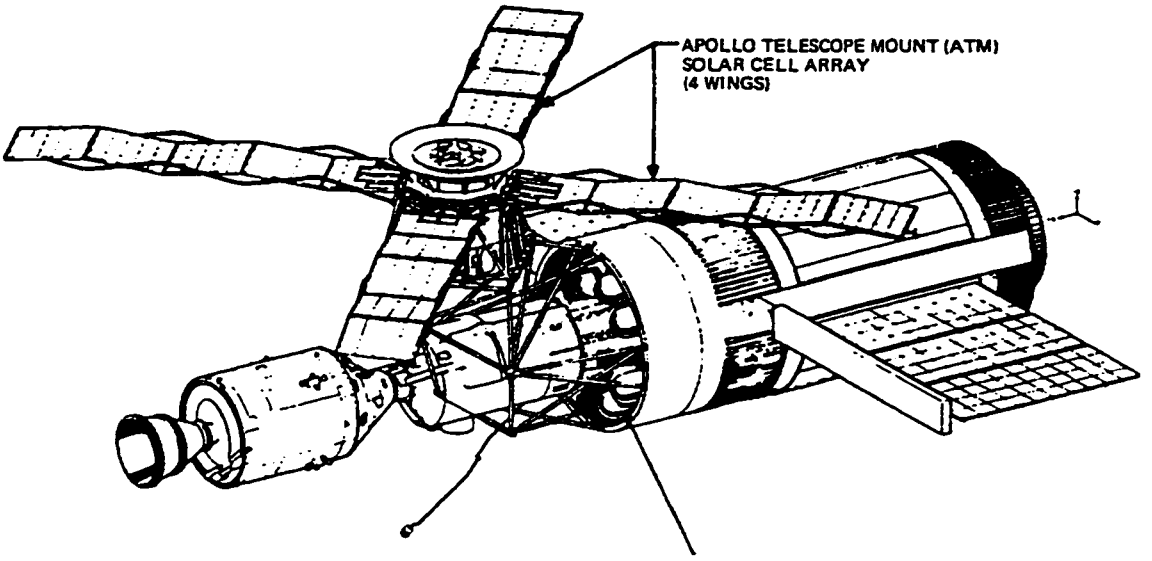

Figure 1.14: Skylab spacecraft with Apollo Telescope Mount solar cell array – four pantographic wings (Rauschenbach, 1980).

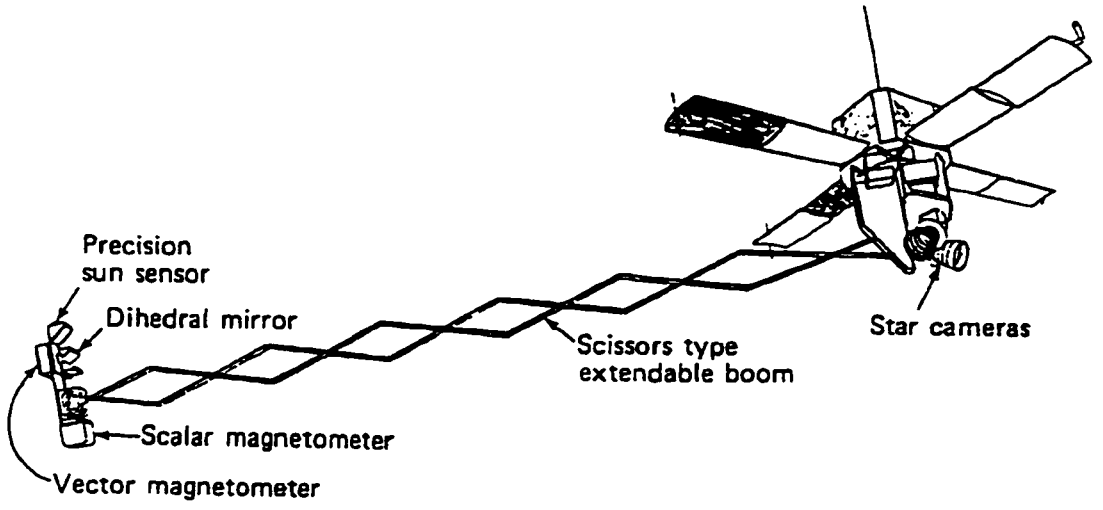

Figure 1.15: Magnetic field satellite with pantographic magnetometer boom (Smola et al., 1980).

Pinero's designs of flat and curved deployable coverings inspired other architects and engineers to follow his track. In 1976, T. Zeigler patented a "Collapsible Self-Supporting Structure" (Fig. 1.17). This structure consisted of SLEs arranged into a part of a spherical dome. The self-supporting feature of the deployed configuration of this system originated from the geometry of the elements, which was chosen in such way that during deployment most bars became bent and some of them buckled. To avoid excessive stresses in the members some pivotal connections and SLEs had to be omitted in the otherwise triangulated dome. Later Zeigler tried to overcome this problem by introducing clips and sliding connections instead of pivots in some scissor-like elements (Zeigler, 1977 and 1984).

Clarke (1984) further developed Zeigler's idea and presented a deployable, 5 metre diameter, triangulated, hemispherical dome (Fig. 1.18) with triangular cells consisting of three SLEs called "Trissors". He showed that the dome had only two states of geometric fit - compact and deployed. The geometric non-fit in all partially unfolded positions was compensated by bending of the relatively flexible struts, resulting in a snap-through action after which the structure adopted its final deployed shape. Frames of this kind are folded by applying a sufficiently strong pull at certain points resulting in a reverse snap-through. Then the structure can be easily folded back to a compact bundle.

The next step in the same direction was made by Krishnapillai (1992) who generalized the concept of self-stabilization for three-dimensional pantographic units and found a number of configurations satisfying the requirement of zero stress in folded and deployed forms (Fig. 1.19). Krishnapillai's pantographic units are regular polygons having radial, in addition to circumferential, SLEs. In circumferential SLEs the bars have the same length, whereas the difference in the lengths of the bars in the radial SLEs produces the desired snap-through effect during deployment and folding. Units of different polygonal shapes can be used to form flat slabs, as well as single- and double-curved structures.

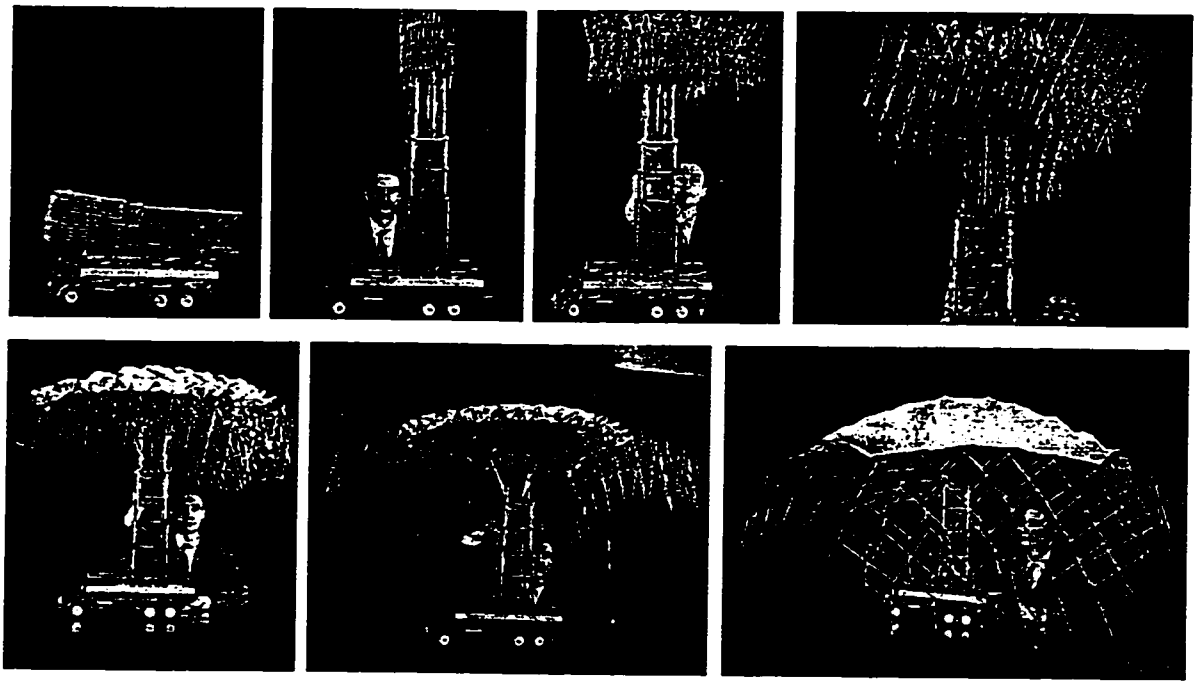

Figure 1.16: Pinero's "Spatial Reticular Structure" presented at UIA Congress (1961).

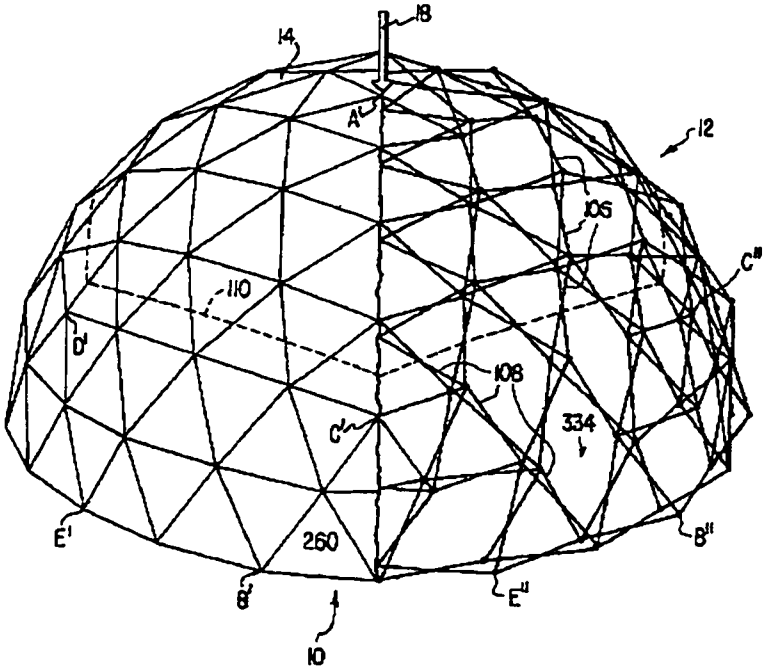

Figure 1.17: Zeigler's "Collapsible Self-Supporting Structure" (1976).

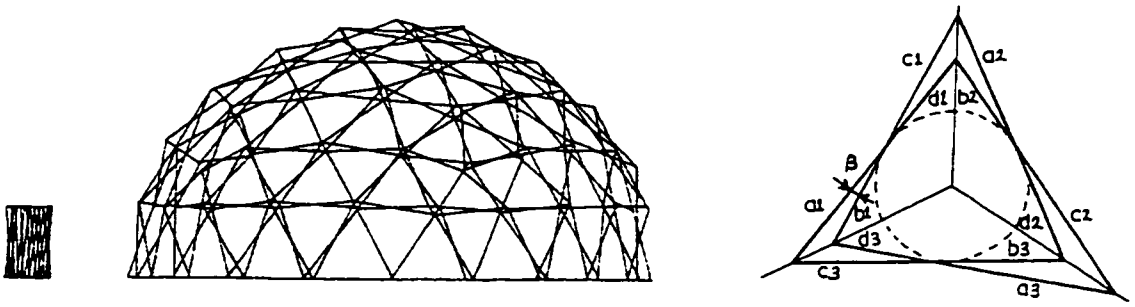

Figure 1.18: Compact and deployed configurations of a hemispherical dome and top view of a "Trissor" (Clarke, 1984).

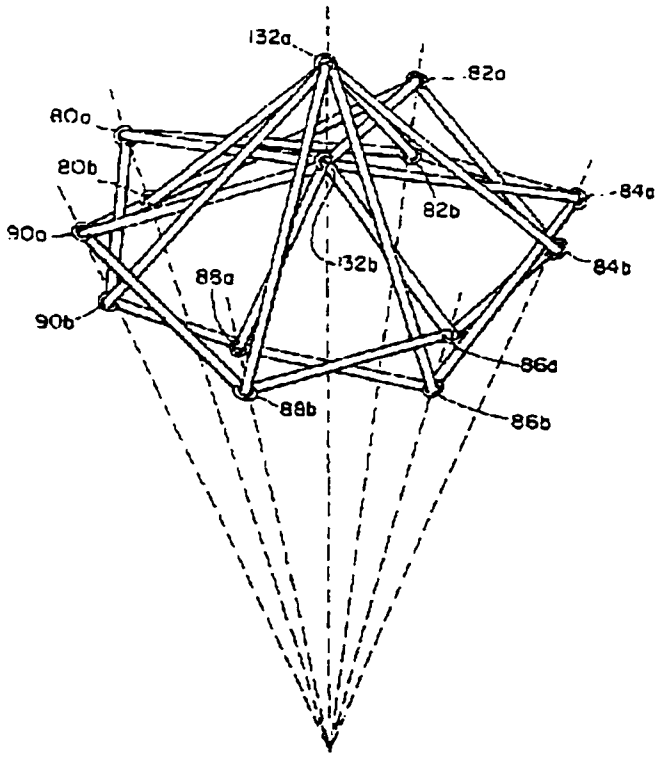

Figure 1.19: Hexagonal self-locking pantographic unit by Krishnapillai (1992).

At present, three major research centres, conducting extensive studies in the field of pantographic deployable structures, can be named. These are the School of Architecture at the University of Seville, Spain, the Departments of Architecture and Civil Engineering at MIT, USA, and the Department of Engineering at Cambridge University, UK. Dr F. Escrig, who heads the research on deployable structures in the first of these places, outlined a number of possible ways to generate three-dimensional straight and curved columns (Fig. 1.20), slabs and domes from the two-dimensional strings of SLEs (Escrig, 1984 and 1985). In addition to three-dimensional pantographic modules with the sides formed by two-dimensional SLEs, he also employed the arrangements where all bars are the diagonals of triangular or square prisms (Fig. 1.21). The latter unit type was used by Valcarcel et al. (1991) to develop spatial structures with incorporated fabric covers. The questions of generating the geometry of pantographic structures and performing their analysis are also addressed by the group in Seville (Escrig and Valcarcel, 1986 and 1991; Valcarcel et al., 1992; Morales et al., 1996; Sanchez et al., 1996). The systems they study are stress-free during deployment and therefore require additional members or locking devices to be stable in the final configuration. The perspective view of a swimming pool cover, designed at the School of Architecture and built in Seville, is shown in Fig. 1.22.

C. Gantes, in his PhD thesis at MIT, developed quantitative design principles for the structures made of Krishnapillai's units. He derived the geometric constraints that must be satisfied in order to achieve stable and stress-free states of such systems composed of prismatic and trapezoidal modules in both the deployed and collapsed configurations. A number of small- and medium-scale physical models were constructed and tested. Gantes also performed the numerical analyses of his structures by the finite element method, incorporating the discrete joint size and friction at the pivotal connections. He found that the behaviour of the deployed structures is characterized by small displacements and therefore can be considered linear. The analysis of the structural behaviour during deployment required large displacement formulation and incremental

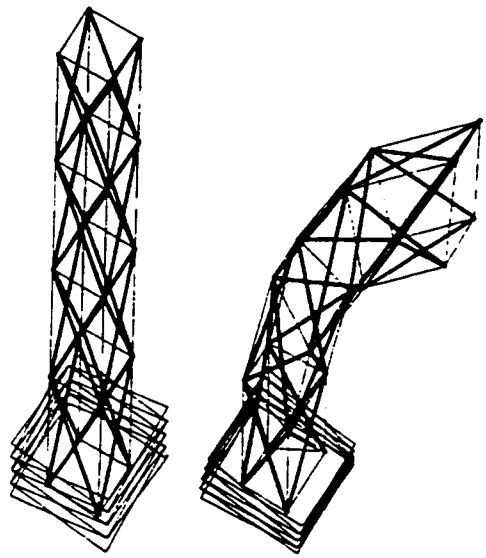

Figure 1.20: Straight and curved pantographic columns with square cross-sections (Escrig, 1984).

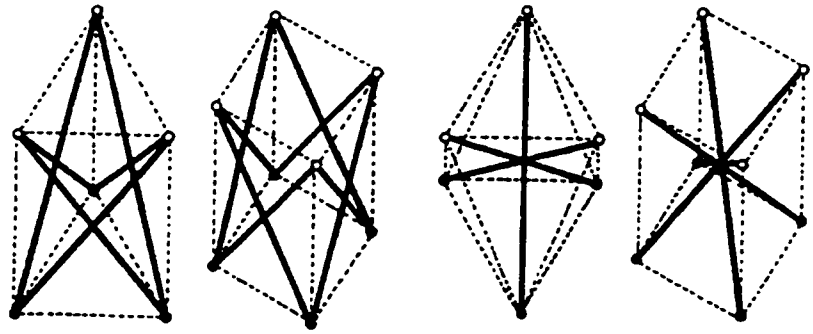

Figure 1.21: Three-dimensional pantographic modules (Escrig and Valcarcel, 1986).

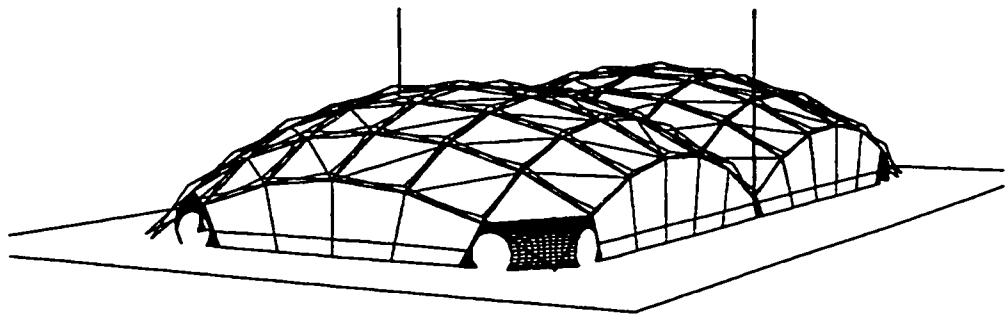

Figure 1.22: Deployable swimming pool cover in Seville, Spain (Sanchez et al., 1996).

loading to trace the load-displacement dependence beyond the limit point state corresponding to the snap-through of a structure to and from its deployed configuration. Such time and resource consuming analyses for multi-unit systems can be avoided since it was shown that their critical deployment quantities could be obtained from the respective quantities of a single unit. The results of Dr Gantes' work are described in a number of publications (Gantes, 1993 and 1996; Gantes et al., 1989, 1991, 1993 and 1994).

The Laboratory of Deployable Structures at Cambridge University, UK, is led by Dr S. Pellegrino. The research on deployable structures there is conducted in relation to their use in the aerospace industry. The deployment and prestressing of the pantographic structures by means of active and passive cables is one of the directions of study there. The three types of pantographic columns, which have been investigated analytically and through tests by Kwan and Pellegrino (1991 and 1994), Kwan et al. (1993) and You and Pellegrino (1996b), are shown in Fig. 1.23 where the cables can also be seen. The first structure is composed of two planar pantographic columns connected by another set of horizontal SLEs. This column folds into a compact bundle of bars. The second triangular column consists of prismatic triangular modules. In the folded configuration it has the form of a short triangular prism. The third column is made of octahedral units with diagonals. A set of passive cables joining pairs of points on the pantographic backbone is used to terminate the process of deployment which is driven by one or more active cables. After the columns are deployed, a state of prestress is created by further shortening the active cables. The two goals achieved by prestressing are the increase of the stiffness of the structures and the removal of the joint backlash. Besides these columns, the cable-stiffened pantographic ring structure for deployable mesh reflector was studied by You and Pellegrino (1997a). The range of applications of pantographic structures is widely broadened by the introduction of the SLE with angulated rods proposed by Hoberman (1990). Systems made of such elements (Fig. 1.24) constitute another research subject at the Laboratory (You and Pellegrino, 1996 and 1997b).

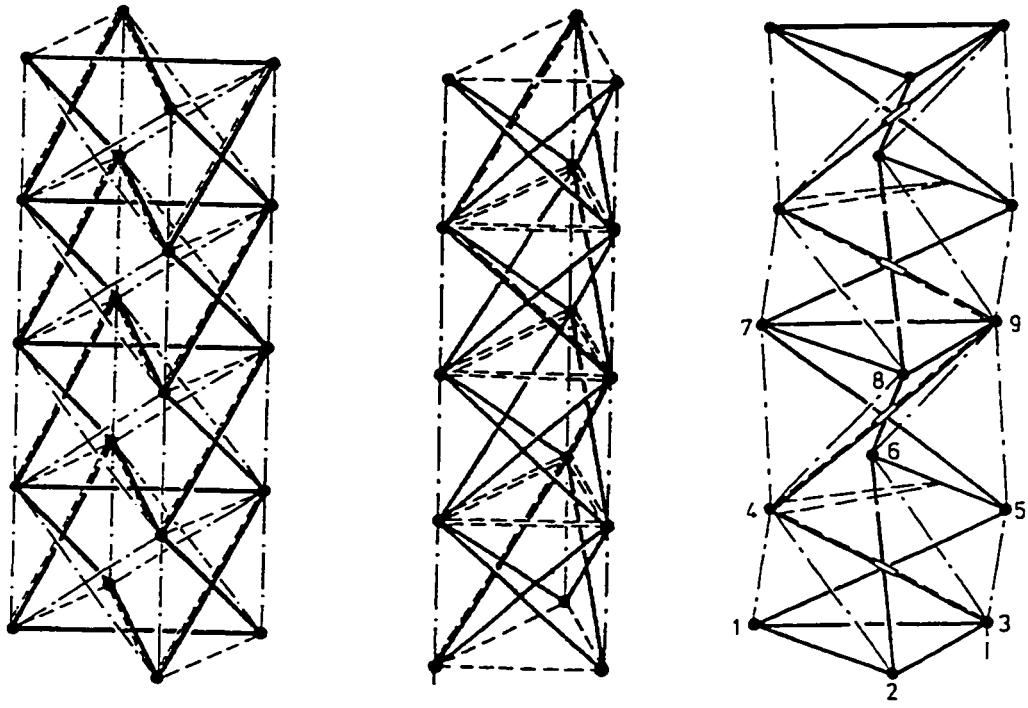

Figure 1.23: Schematic views of three types of deployable columns by Kwan et al. (1993); dashed lines are active cables, dashed-dotted lines are passive cables.

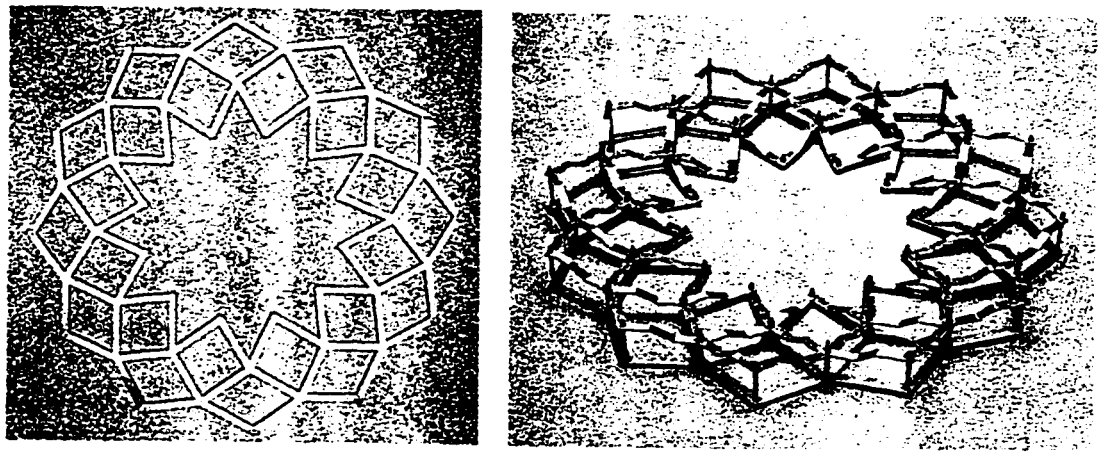

Figure 1.24: Single- and double-layer circular foldable bar structures with SLEs with angulated rods (You and Pellegrino, 1997b).

1.3 Research Motivation

Despite the completed and extensive ongoing research on pantographic assemblages outlined in the previous Section, there are still many questions about the structural behaviour of this relatively new class of deployable systems that wait to be answered and insights into their structural properties and response that remain to be gained. Perhaps one of the simplest representatives of this class is a two-dimensional pantographic column composed of several SLEs placed along a straight line and properly stabilized. The study of such a column may play the same role in understanding the behaviour of more complicated pantographic systems (three-dimensional columns, arches, slabs and domes) as the study of the conventional beam element does for analogous solid or reticulated structures.

In this thesis, the problem of finding the stiffness characteristics of two-dimensional pantographic columns in their deployed configurations will be addressed. An attempt will be made to answer the question of when the non-linear behaviour of these structures must be taken into account. Consequently, the problem of buckling analysis may become topical. The structural properties of two-dimensional columns can be related to, and used to obtain, the corresponding parameters for three-dimensional columns composed of three (middle column in Fig. 1.23) or four (first column in Fig. 1.20) planar structures.

Structural analysis formulations for pantographic systems have been developed by Escrig and Valcarcel (1986), Valcarcel et al. (1991), Shan (1992), Kwan and Pellegrino (1994), and Kaveh and Davaran (1996). Usually, this problem is approached from the point of view of a computerized matrix method. The stiffness or flexibility matrices are derived for the macro-elements which are either a single three-node bar in an SLE or a full scissor-like element. Some degrees of freedom are condensed in order to reduce the size of the final system of equations. Special care is taken with cable elements.

Gantes et al. (1994a) used an equivalent continuum model for deflection analysis of flat deployable slabs under lateral load. All radial and side SLEs of the square prismatic pantographic modules were substituted with equivalent uniform beam elements. The reticulated structure thus obtained was substituted with the equivalent continuous plate. The stiffness properties of the beam elements were defined by equating their deflections to those of the corresponding SLEs when both elements were subjected to the same loading. However, the support conditions of the loaded SLEs in this derivation resulted in the second order bending of bars only. In other words, if the axial deformations of bars are neglected, the structure becomes infinitely rigid. This, of course, is not the case for a separate pantographic column.

Although the results of numerical analyses are invaluable, it seems interesting and worthwhile to attempt, at least for cases of linear behaviour, the derivation of closed form analytical expressions for certain overall properties of deployable pantographic columns. These properties can then be compared with those of solid columns. Such comparison may indicate how much of the engineering intuition developed in the course of analysis of conventional structures can be applied to pantographic systems. Points of conceptual differences may also become more transparent by this approach.

The following Chapter contains the analysis of planar pantographic columns. Linear behaviour under moment, lateral and axial loadings is considered. It also includes problems of the non-linear response of the columns subjected to axial load, local and global buckling and a Section on non-uniform columns. Chapter 3 is devoted to the analysis of three-dimensional columns. Chapter 4 contains general conclusions and outlines some directions of future research.

Chapter 2

Planar Columns

2.1 Introduction

The basic unit of pantographic structures is a scissor-like element (SLE) formed of two beams, with hinges at the ends, connected at their intermediate points by a shear resisting pivot. If the bars in the SLE are of the same length and the pivot connection is at the midpoint of the bars, the pivot also becomes the centre of symmetry of the SLE. Placed along a straight line, several such SLEs form a uniform pantographic column. When the two bottom nodes of the column are hinged to the ground, the two-dimensional structure becomes geometrically stable in its plane and statically determinate. In this Chapter the behaviour of this column under different loads is investigated, and its stiffness characteristics are related to those of a uniform solid column. The parameters of the deployable column, as shown in Fig. 2.1, are: the half-length of the bars - a, their bending stiffness - EI, their axial stiffness - EA, the degree of deployment for the undeformed column - γ, the number of pantographic units in the column - n and the undeformed length of the column - $L = n\,2a\sin\gamma$. The equivalent solid column would have the same length L, with bending and axial stiffnesses $(EI)_e$ and $(EA)_e$, respectively.

We first consider linear behaviour of the structure subjected to several types of load applied at the top of the column, namely, lateral force, moment and axial compressive force. Under the assumptions of linearity and small displacements, internal forces can be found from the conditions of equilibrium for the undeformed column. The overall stiffness characteristics of the deployable column are derived from comparison of its response to the loads with that of a solid uniform column.

The relative rotation of bars in the column allowed by the end hinges and pivots gives rise to the phenomenon of geometric non-linearity, which greatly affects the behaviour of the axially loaded structure. This introduces the possibility of a local loss of stability - snap-through buckling of the top pantographic unit. If the pantographic column is restrained to improve its axial stiffness, another type of instability comes into view - overall column-type buckling. Finally, the behaviour of non-uniform tapered pantographic columns is investigated.

2.2 Linear Behaviour

2.2.1 Bending of a Uniform Column

2.2.1.1 Tip Displacements

Forces acting on a typical pantographic unit (unit number i) in the column subjected to a lateral force are shown in Fig. 2.2. The distribution of these forces along the deployable column resembles that of stresses along the solid column under the same loading: constant horizontal and linearly growing vertical forces correspond to constant shear and growing normal stresses, respectively. Bars in the pantographic units are beam elements and are

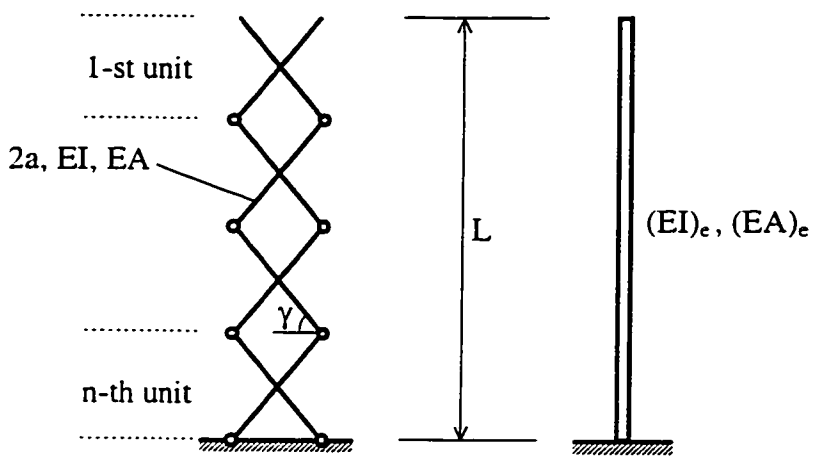

Figure 2.1: Uniform pantographic and solid columns with equivalent overall stiffness characteristics.

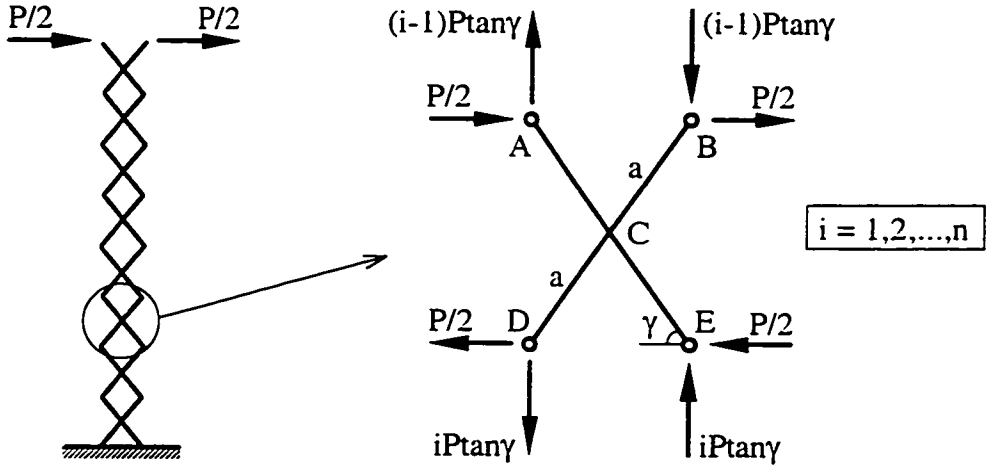

Figure 2.2: Pantographic column under lateral load and forces applied to a typical unit.

subject to bending and axial deformations. Axial forces are constant between the end of a bar and the pivot:

$$N_{AC} = -N_{BC} = -\frac{P}{2}\cos\gamma + (i-1)P\tan\gamma\sin\gamma = P\frac{(2i-1)\sin^2\gamma - 1}{2\cos\gamma}$$
$$N_{DC} = -N_{EC} = \frac{P}{2}\cos\gamma + iP\tan\gamma\sin\gamma = P\frac{(2i-1)\sin^2\gamma + 1}{2\cos\gamma} \tag{2.1}$$

Bending moments are zero at the end of a bar and grow linearly to the pivot:

$$M_C = \frac{P}{2}a\sin\gamma + (i-1)P\tan\gamma a\cos\gamma = \frac{Pa}{2}(2i-1)\sin\gamma \tag{2.2}$$

Knowing the internal forces and moments one can employ an energy method, e.g. Castigliano's second theorem, to calculate the horizontal displacement of the top of the column, h_p (subscript p stands for pantographic), due to the lateral force. The contribution of the i-th unit can be written as the sum of the terms corresponding to axial (h^a_i) and bending (h^b_i) deformations of bars in the unit. The total horizontal tip displacement is the sum of the contributions of all units:

$$h_p = \sum_{i=1}^{n}\left(h_i^a + h_i^b\right) = \sum_{i=1}^{n}\left(\frac{\partial}{\partial P}\int\frac{N_i^2 dx}{2EA} + \frac{\partial}{\partial P}\int\frac{M_i^2 dx}{2EI}\right) \tag{2.3}$$

After using the expressions for axial forces and moments from eqs 2.1 and 2.2, applying integration technique described in Appendix A and differentiating, we obtain the terms from eq. 2.3 in the following form:

$$h_i^a = P\frac{2a}{EA}\left[\left(\frac{(2i-1)\sin^2\gamma - 1}{2\cos\gamma}\right)^2 + \left(\frac{(2i-1)\sin^2\gamma + 1}{2\cos\gamma}\right)^2\right] = \frac{Pa}{EA}\frac{(2i-1)^2\sin^4\gamma + 1}{\cos^2\gamma}$$
$$h_i^b = \frac{4}{EI}\frac{Pa}{2}(2i-1)\sin\gamma\frac{a}{2}\frac{2}{3}\frac{a}{2}(2i-1)\sin\gamma = \frac{Pa^3}{3EI}(2i-1)^2\sin^2\gamma \tag{2.4}$$

In the process of calculating the sum of unit contributions for i from 1 to n, the following expression needs to be evaluated (eq. B.5):

$$\sum_{i=1}^{n}(2i-1)^2 = 4\sum_{i=1}^{n}i^2 - 4\sum_{i=1}^{n}i + \sum_{i=1}^{n}1 = 4\frac{n(n+1)(2n+1)}{6} - 4\frac{n(n+1)}{2} + n = \frac{4n^3}{3} - \frac{n}{3} \tag{2.5}$$

For sufficiently large n the second term on the right side of eq. 2.5 can be neglected; for n = 5 it will make difference of only one per cent. The summed axial and bending parts of the total horizontal displacement of the top of the pantographic column due to lateral loading are:

$$\sum_{i=1}^{n} h_i^a = \frac{Pa}{EA}\sum_{i=1}^{n}\frac{(2i-1)^2\sin^4\gamma+1}{\cos^2\gamma} = \frac{Pa}{EA}\frac{\frac{4}{3}n^3\sin^4\gamma+n}{\cos^2\gamma} \xrightarrow{\text{for large n}} \frac{Pa}{EA}\frac{4}{3}n^3\frac{\sin^4\gamma}{\cos^2\gamma}$$

$$\sum_{i=1}^{n} h_i^b = \frac{Pa^3}{3EI}\sum_{i=1}^{n}(2i-1)^2\sin^2\gamma = \frac{Pa^3}{3EI}\frac{4}{3}n^3\sin^2\gamma \qquad (2.6)$$

The term n in the numerator of the first of eqs 2.6 can be disregarded under the condition that the degree of deployment is not too small; however, a very small $\sin^4\gamma$ would make this assumption inaccurate. Finally, the resulting displacement is:

$$h_p = P\frac{4}{3}a n^3\sin^2\gamma\left(\frac{\tan^2\gamma}{EA}+\frac{a^2}{3EI}\right) \qquad (2.7)$$

The first term in the brackets corresponds to the axial deformations of the bars, while the second term corresponds to the bending deformations. The well-known formula for the deflection of a solid cantilever of uniform cross-section and the same height as the pantographic column, loaded at the tip with the lateral force is:

$$h_e = \frac{PL^3}{3(EI)_e} = \frac{P(n2a\sin\gamma)^3}{3(EI)_e} = P\frac{n^3 8a^3\sin^3\gamma}{3(EI)_e} \qquad (2.8)$$

To obtain the equivalent bending stiffness of the pantographic column we equate the right sides of eqs 2.7 and 2.8 and express $(EI)_e$ through other parameters. After simplifications:

$$(EI)_e = \frac{2a^2\sin\gamma}{\frac{\tan^2\gamma}{EA}+\frac{a^2}{3EI}} \qquad (2.9)$$

This bending stiffness does not depend on the number of units in the column, in the same manner as the bending stiffness of the solid column is only a characteristic of the cross-section, not of the length of the structure. It can be seen from the last equation that as the degree of deployment becomes close to a right angle the first term in the denominator

grows to infinity and the equivalent bending stiffness vanishes. This reflects the fact that at $\gamma = 90°$ the structure becomes geometrically unstable and, therefore, has zero bending stiffness. On the other hand, for moderate degrees of deployment, one could expect that deflections of the pantographic column would be primarily due to bending deformations of bars in the units, i.e. for finite $\tan\gamma$, we may consider EA to be infinite and neglect the first term in the denominator of eq. 2.9 in comparison with the second term. To show which parameter controls the situation here, we divide numerator and denominator by the second term of the denominator:

$$(EI)_e = \frac{6EI\sin\gamma}{\frac{3}{a^2}\frac{EI}{EA}\tan^2\gamma + 1} = \frac{6EI\sin\gamma}{3\left(\frac{r}{a}\right)^2\tan^2\gamma + 1} = \frac{6EI\sin\gamma}{3\frac{\tan^2\gamma}{\lambda^2} + 1} \quad , \tag{2.10}$$

where $r = (I/A)^{1/2}$ is the radius of gyration of the cross-section of bars in the pantographic units and $\lambda = a/r$ is a parameter similar to the slenderness ratio of the bars. Thus, if the bars are slender enough and γ is not very close to the right angle the denominator of eq. 2.10 is approximately equal to one, i.e.

$$(EI)_e = 6EI\sin\gamma \tag{2.11}$$

Let us once again list the assumptions that allowed us to arrive at the simple expression of eq. 2.11 for the equivalent bending stiffness of a uniform pantographic column:

- linear behaviour of the column under lateral load and small displacements
- sufficiently large number of pantographic units in the column
- degree of deployment is not too close to that of completely folded or completely deployed configurations
- axial deformations of bars in the pantographic units are negligible in comparison with bending deformations.

Another loading that could be used to determine the equivalent overall bending stiffness of the pantographic column is the moment applied at the top of the structure (Fig.

2.3). The moment is represented by two vertical forces (one upward and the other downward) applied to the two top nodes of the column. Again, the distribution of the internal forces along the column is similar to that of stresses in the uniform solid column subjected to the same load - constant along the structure. Axial forces in the bars of the i-th unit and the moment at its pivot are:

$$N_{AC} = N_{DC} = \frac{M}{2a\cos\gamma}\sin\gamma = \frac{M\tan\gamma}{2a} = -N_{BC} = -N_{EC}$$
$$M_C = \frac{M}{2a\cos\gamma}a\cos\gamma = \frac{M}{2} \qquad (2.12)$$

The angle of rotation of the top of the column can be calculated:

$$\varphi_p = \sum_{i=1}^{n}\left(\varphi_i^a + \varphi_i^b\right) = \sum_{i=1}^{n}\left(M\frac{\tan^2\gamma}{aEA} + M\frac{a}{3EI}\right) = M\frac{n}{a}\left(\frac{\tan^2\gamma}{EA} + \frac{a^2}{3EI}\right) \qquad (2.13)$$

and compared with that for the solid column:

$$\varphi_e = \frac{ML}{(EI)_e} = \frac{Mn2a\sin\gamma}{(EI)_e} \qquad (2.14)$$

Equating the right sides of eqs 2.13 and 2.14 yields the same expression for the equivalent stiffness as in eqs 2.9 and 2.10. Note that in this case we did not need the assumption about the large number of units in the column and did not impose any restrictions on the degree of deployment.

Fig. 2.4 presents the plots of the ratio of the equivalent bending stiffness from eq. 2.10 to the bending stiffness of bars in the pantographic units for four different values of the slenderness parameter λ. To see what the numerical values of this parameter might be, we can take as an example a bar of length a = 50 cm with a solid circular cross-section of diameter d = 4 cm. The slenderness parameter λ = 50. The second example is a member of the same length but with a thin-walled tubular cross-section of the same diameter. In this case λ = 35. Fig. 2.5 presents the plots of the ratio of the equivalent bending stiffness from eq. 2.10 to the equivalent bending stiffness of the column with bars in the units being infinitely rigid axially (eq. 2.11). The curves correspond to the same four values of λ. It

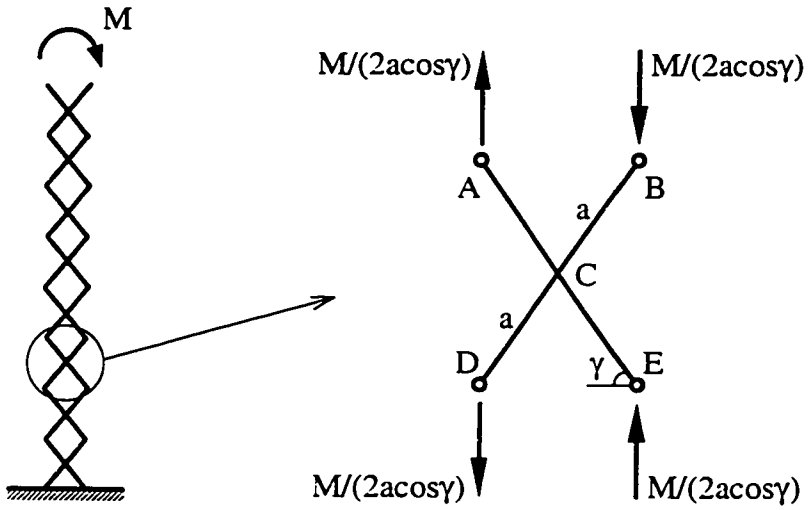

Figure 2.3: Pantographic column under moment load and forces applied to a typical unit.

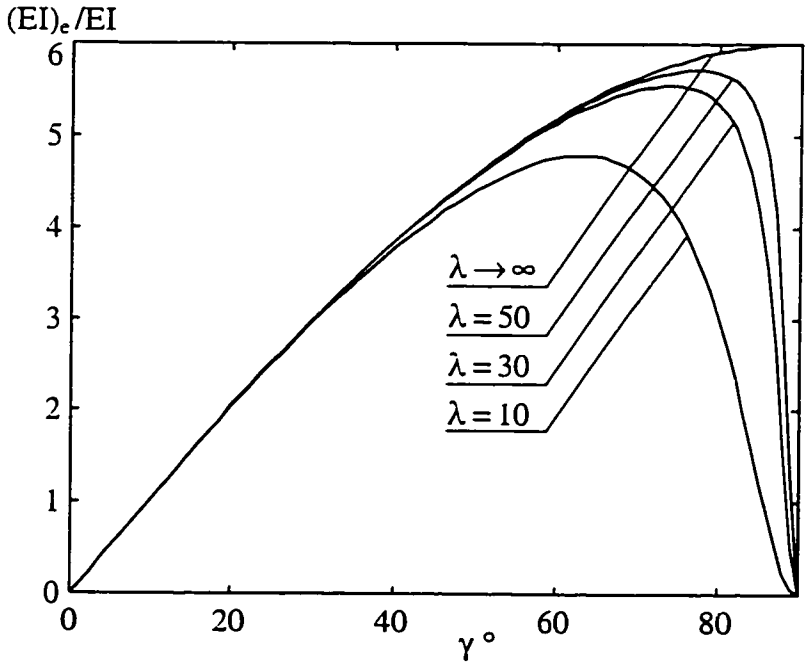

Figure 2.4: Plots of non-dimensional equivalent bending stiffness versus the degree of deployment for different values of bar slenderness.

can be seen that for a slenderness parameter greater than 30 the equivalent bending stiffness is very close to that for $\lambda \to \infty$ as long as the degree of deployment γ is not greater than 80°. This range of γ was, of course, already ruled out during the equivalent stiffness derivation above.

2.2.1.2 Deflections along the Column

The equivalent bending stiffness was derived from equality of the displacements of the pantographic and solid columns at a particular point. What happens to the rest of the structure? Is the shape of the deflected deployable column different from the elastic curve of a cantilever? Let us see how the unit interfaces move horizontally when the pantographic column is subjected to a lateral force. The internal force distribution for the column loaded at the top is available from Fig. 2.2 and eqs 2.1 and 2.2. To find the horizontal deflection of the bottom nodes of the k-th unit, we need to apply a unit virtual force at this level (Fig. 2.6). The virtual bending moments at the pivots are:

$$m_C = \frac{a\sin\gamma}{2}[2(i-k)-1], \quad i=(k+1)\ldots n \tag{2.15}$$

Using the principle of virtual work and neglecting axial deformations of bars in the pantographic units, the horizontal displacement at distance (n-k)2asinγ from the bottom can be found as:

$$h_k = \sum_{i=1}^{n}\int \frac{M_i m_i}{EI}dx = \sum_{i=1}^{n}\frac{Pa}{2}(2i-1)\sin\gamma\,\frac{a}{2}\,\frac{2}{3}\,\frac{a\sin\gamma}{2}[(2i-1)-2k]\cdot 4 = \\ = \frac{Pa^3}{3EI}\sin^2\gamma\sum_{i=k+1}^{n}\left[(2i-1)^2-2k(2i-1)\right] \tag{2.16}$$

The sum in the last equation can be rewritten as:

$$\sum_{i=k+1}^{n}[\cdots] = \sum_{i=1}^{n}[\cdots] - \sum_{i=1}^{k}[\cdots] \tag{2.17}$$

Each of the sums on the right side of eq. 2.17 can be evaluated using eqs 2.5, B.2 and the following:

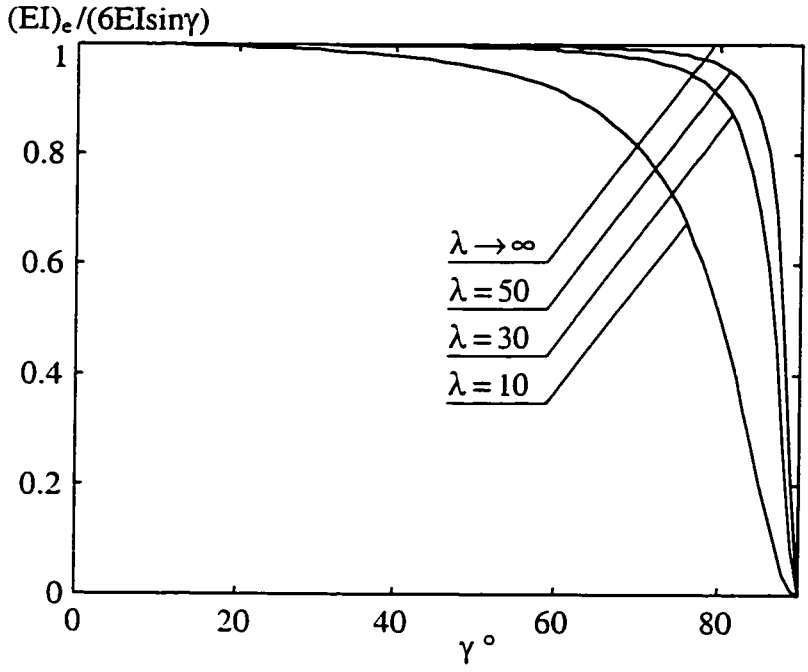

Figure 2.5: Plots of ratio of equivalent bending stiffness and that for column with axially rigid bars versus the degree of deployment for different values of bar slenderness.

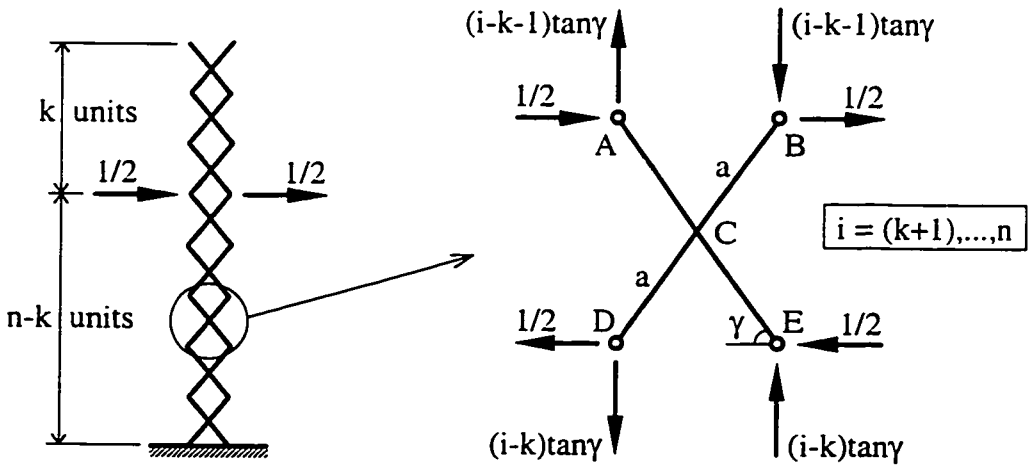

Figure 2.6: Pantographic column under virtual lateral unit load and forces applied to a typical unit below the load.

$$\sum_{i=1}^{n}(2i-1)=2\sum_{i=1}^{n}i-n=2\frac{n(n+1)}{2}-n=n^2 \tag{2.18}$$

With eqs 2.5, 2.17 and 2.18 the expression for h_k (eq. 2.16) can be transformed into:

$$h_k=\frac{Pa^3}{3EI}\sin^2\gamma\left\{\sum_{i=1}^{n}\left[(2i-1)^2-2k(2i-1)\right]-\sum_{i=1}^{k}\left[(2i-1)^2-2k(2i-1)\right]\right\}=$$

$$\frac{Pa^3}{3EI}\sin^2\gamma\left\{\left[\frac{4n^3}{3}-\frac{n}{3}-2kn^2\right]-\left[\frac{4k^3}{3}-\frac{k}{3}-2k^3\right]\right\}=\frac{Pa^3}{9EI}\sin^2\gamma\left\{4n^3-6kn^2+2k^3-n+k\right\} \tag{2.19}$$

Keeping, in the parentheses, only terms of the third degree (assuming a sufficiently large number of units):

$$h_k=\frac{Pa^3}{9EI}\sin^2\gamma(4n^3-6kn^2+2k^3)=\frac{2Pa^3}{9EI}\sin^2\gamma(n-k)^2(2n+k) \tag{2.20}$$

The deflected shape of a cantilever of uniform cross-section loaded with concentrated lateral force at the tip (Fig. 2.7) is a cubic polynomial:

$$y(x)=\frac{PL^3}{6(EI)_e}\left(\frac{x}{L}\right)^2\left[3-\frac{x}{L}\right], \tag{2.21}$$

where the origin of the x-axis is at the clamped end. The assumption of zero axial deformations of bars in the pantographic column used in the derivation of eq. 2.20 corresponds directly to the assumption from the beam theory about zero shear deformations in the solid column which is implied in eq. 2.21. Substituting in eq. 2.21 the expression for the bending stiffness from eq. 2.11, the length in terms of the parameters of the deployable column and x = (n-k)2asinγ, we obtain:

$$y(k)=\frac{P(n2a\sin\gamma)^3}{6(6EI\sin\gamma)}\left(\frac{(n-k)2a\sin\gamma}{n2a\sin\gamma}\right)^2\left[3-\frac{(n-k)2a\sin\gamma}{n2a\sin\gamma}\right]=$$
$$=\frac{2Pa^3}{9EI}\sin^2\gamma(n-k)^2(2n+k) \tag{2.22}$$

The right sides of eqs 2.20 and 2.22 are exactly the same. This means that under our assumptions the deployable column in bending behaves very much like a solid column with the appropriate bending stiffness.

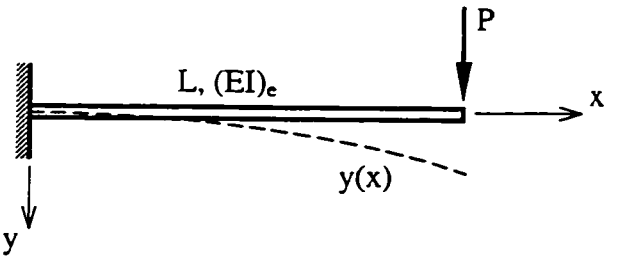

Figure 2.7: Uniform cantilever under lateral load.

2.2.2 Compression of a Uniform Column

The third loading to be considered is the axial force. Forces acting on a typical pantographic unit of the column subjected to this load are shown in Fig. 2.8. Here one may observe something distinct from the two previous cases. The horizontal forces applied to the unit grow linearly from top to bottom of the column; consequently, the internal axial forces and bending moments in the bars also are increasing linear functions of the unit number. This is quite different from the stress distribution in a solid column under axial loading, where the stress state is uniaxial and uniform throughout the column. Strictly speaking, there is the possibility of a two-dimensional stress state in the solid column also, for example, when the support conditions at the base are such that they prevent transverse expansion of the column. However, this effect is local and is present only in a small portion of the structure.

There are several ways to give the reader a feel for the increasing horizontal forces at unit interfaces of the pantographic column. One way is to remove the horizontal constraint at one of the hinge nodes at the bottom of unit number k and apply the corresponding equal and opposite horizontal reactive forces (Fig. 2.9a). Then we

introduce a virtual displacement Δ_1 in the direction of the removed constraint as shown in the figure. The k upper units of the column fold a little, and the vertical displacement Δ_2 of the top nodes, where load P is applied, will be proportional to the number of units k. The total virtual work done by P and T_k must be equal to zero:

$$P\Delta_2 - T_k\Delta_1 = 0 \quad \longrightarrow \quad T_k = P\frac{\Delta_2}{\Delta_1} \sim k \quad \text{for constant P and } \Delta_1 .$$

Thus, the more units there are above a certain pair of nodes at the unit interface the greater the horizontal forces at this level. Another way to look at the structure is to recognize that the top unit is a three-hinge frame supported by the rest of the column. It is easy to see that vertical loads on this three-hinge frame cause horizontal reactions, inward horizontal forces, in addition to vertical ones (Fig. 2.9b). Then the unit second from the top is loaded with the outward horizontal forces in addition to vertical ones. Its horizontal reactions are greater and so on.

Now let us calculate the vertical deflection of the top of the column. Axial forces and pivotal bending moments in the bars are:

$$\begin{aligned} N_{AC} &= N_{BC} = -\frac{P}{2}\sin\gamma + (i-1)P\cot\gamma\cos\gamma = P\frac{(2i-1)\cos^2\gamma - 1}{2\sin\gamma} \\ N_{DC} &= N_{EC} = -\left(\frac{P}{2}\sin\gamma + iP\cot\gamma\cos\gamma\right) = -P\frac{(2i-1)\cos^2\gamma + 1}{2\sin\gamma} \\ M_C &= \frac{P}{2}a\cos\gamma + (i-1)P\cot\gamma a\sin\gamma = \frac{Pa}{2}(2i-1)\cos\gamma \end{aligned} \tag{2.23}$$

The deflection is calculated in a similar manner as those before and under similar assumptions about the number of units and the restriction on the degree of deployment:

$$v_p = \sum_{i=1}^{n}\left(v_i^a + v_i^b\right) = \sum_{i=1}^{n}\left(\frac{Pa}{EA}\frac{(2i-1)^2\cos^4\gamma + 1}{\sin^2\gamma} + \frac{Pa^3}{3EI}(2i-1)^2\cos^2\gamma\right) \xrightarrow[\text{for large n}]{}$$

$$\rightarrow \frac{Pa}{EA}\frac{\frac{4}{3}n^3\cos^4\gamma + n}{\sin^2\gamma} + \frac{Pa^3}{3EI}\frac{4}{3}n^3\cos^2\gamma \tag{2.24}$$

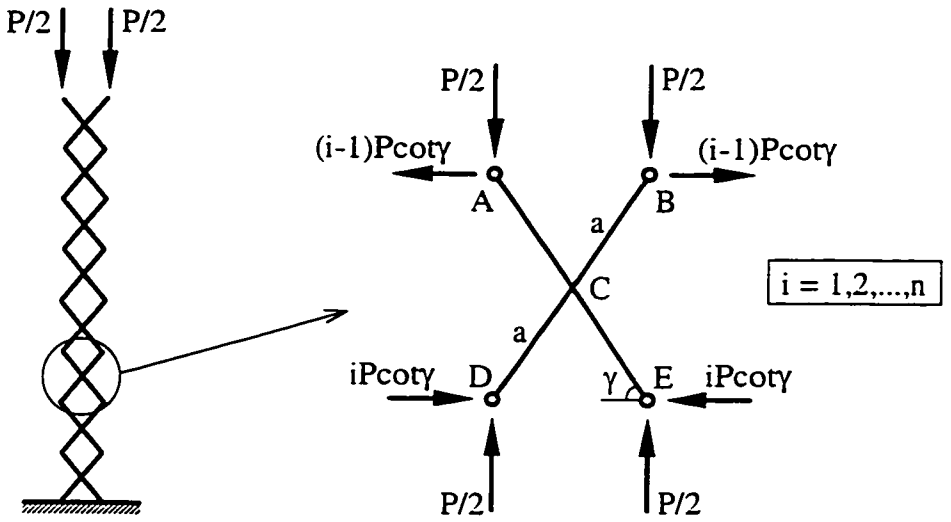

Figure 2.8: Pantographic column under axial load and forces applied to a typical unit.

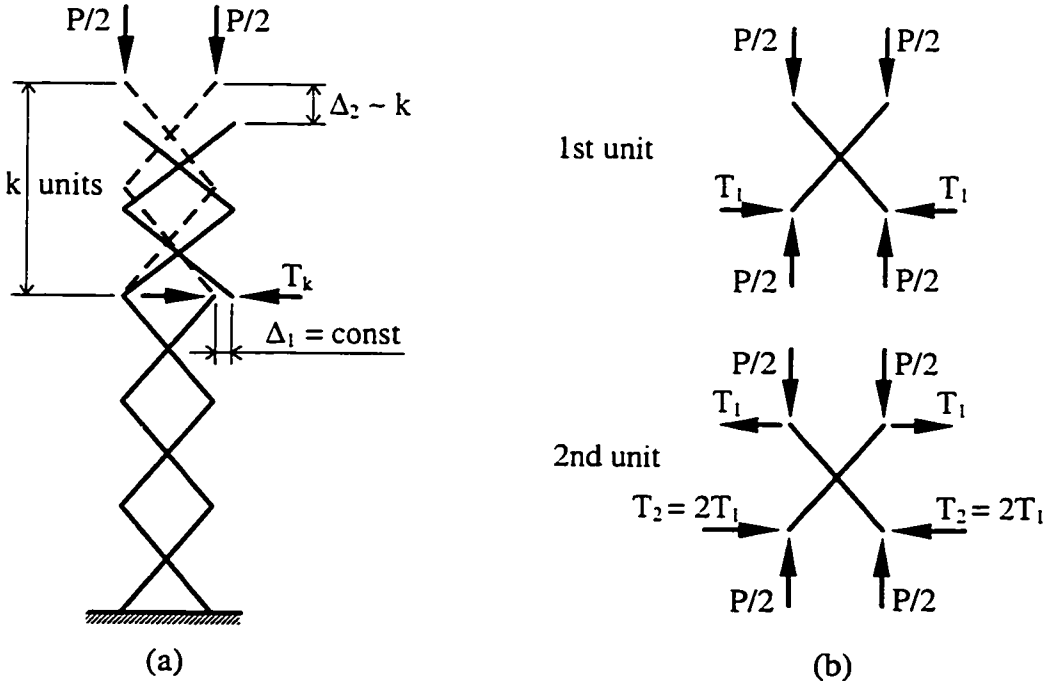

Figure 2.9: Increasing horizontal forces at unit interfaces: (a) from virtual work consideration; (b) unit by unit static equilibrium.

If cosγ is not very small, i.e. γ is not very close to the right angle, the constant n in the numerator of the first term in the last equation can be neglected in comparison with the value of $4/3\, n^3\cos^4\gamma$:

$$v_p = P\frac{4}{3}an^3\cos^2\gamma\left(\frac{\cot^2\gamma}{EA}+\frac{a^2}{3EI}\right) \tag{2.25}$$

Note that the expression for the vertical deflection (eq. 2.25) looks exactly the same as that for horizontal deflection (eq. 2.7), only sinγ is replaced by cosγ and vice versa. The vertical deflection of a compressed uniform solid member is:

$$v_e = \frac{PL}{(EA)_e} = \frac{P(n2a\sin\gamma)}{(EA)_e} \tag{2.26}$$

To obtain the equivalent axial stiffness we equate the right sides of the last two equations and express $(EA)_e$ through other parameters:

$$(EA)_e = \frac{3\sin\gamma}{2n^2\cos^2\gamma}\frac{1}{\frac{\cot^2\gamma}{EA}+\frac{a^2}{3EI}} = \frac{9EI\sin\gamma}{2a^2n^2\cos^2\gamma}\frac{1}{3\frac{\cot^2\gamma}{\lambda^2}+1} =$$
$$= \frac{18EI}{L^2}\sin\gamma\tan^2\gamma\frac{1}{3\frac{\cot^2\gamma}{\lambda^2}+1} \tag{2.27}$$

If the bars are slender and their axial deformations can be neglected:

$$(EA)_e = \frac{9EI\sin\gamma}{2a^2n^2\cos^2\gamma} = \frac{18EI}{L^2}\sin\gamma\tan^2\gamma \tag{2.28}$$

The equivalent axial stiffness of a pantographic column is inversely proportional to the square of column length. This means that, for constant degree of deployment, the more identical units are stacked on one another the softer the structure becomes axially. This result is the consequence of varying internal forces in the pantographic column under axial loading. Fig. 2.10 presents the plot of non-dimensional equivalent axial stiffness $(EA)_e L^2/EI$ calculated using eq. 2.27 versus the degree of deployment. For the scale of this plot there is practically no difference among the curves corresponding to the values of λ from 10 and up. This plot can be used for comparing the axial stiffness of columns of the same length and different degrees of deployment. Note that for constant length and

degree of deployment, the equivalent axial stiffness does not depend on the number of units in the column. Non-dimensionalizing the equivalent axial stiffness as in Fig. 2.11, $(EA)_e\, n^2a^2/EI$, shows the change in the axial stiffness of a particular column during the process of deployment.

Typical results for the overall bending and axial stiffnesses of pantographic columns are summarized in Fig. 2.12. It can be seen that, under the set of assumptions listed on p. 29, the stiffness properties of the columns with the same length are functions of the degree of deployment only. The fact that the first two columns in the figure have the same stiffnesses contradicts the intuitive feel that a member with greater overall width has greater bending stiffness. Such indifference of the stiffness to the width of a pantographic column is the direct consequence of the assumption of negligible axial deformations of bars in SLEs.

Eq. 2.28 indicates that the overall axial stiffness of a pantographic column depends on the length of the structure, which is quite different from the case of a uniform solid column. One may suspect that axial deformations (changes of unit heights), constant along the solid column, may vary along the deployable structure. To obtain the change of height of a pantographic unit, with undeformed height of $2a\sin\gamma$, we first find the vertical displacement of the bottom nodes of unit number k. A vertical unit virtual load applied at this level, along with the corresponding forces acting on a pantographic unit between this level and the bottom of the column, are shown in Fig. 2.13. The virtual bending moments at the pivots are:

$$m_c = \frac{a\cos\gamma}{2}[2(i-k)-1], \quad i=(k+1)\ldots n \tag{2.29}$$

Neglecting axial deformations of bars in the pantographic units, we obtain the following axial shortening of the lower (n-k) units of the axially loaded column:

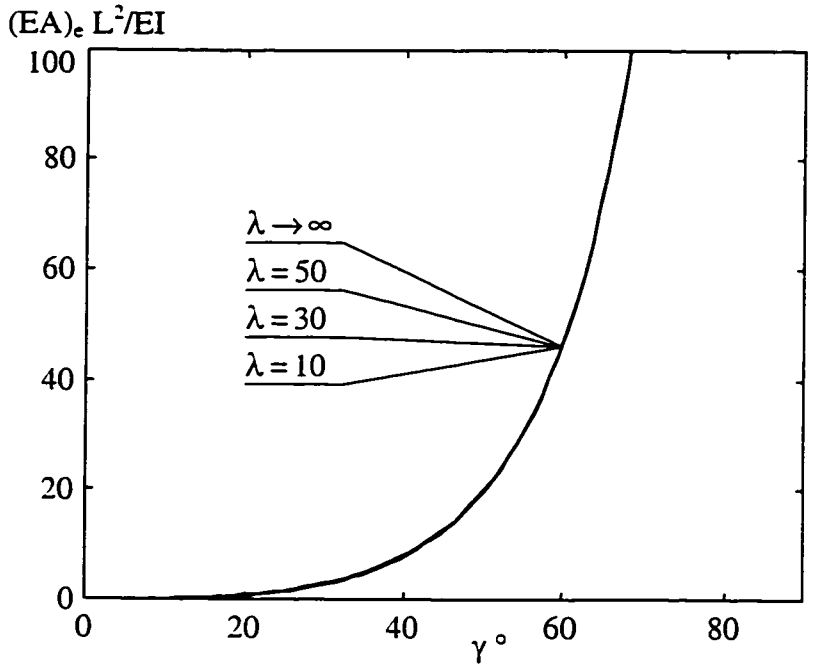

Figure 2.10: Plot of non-dimensional equivalent axial stiffness for pantographic columns of constant length versus the degree of deployment.

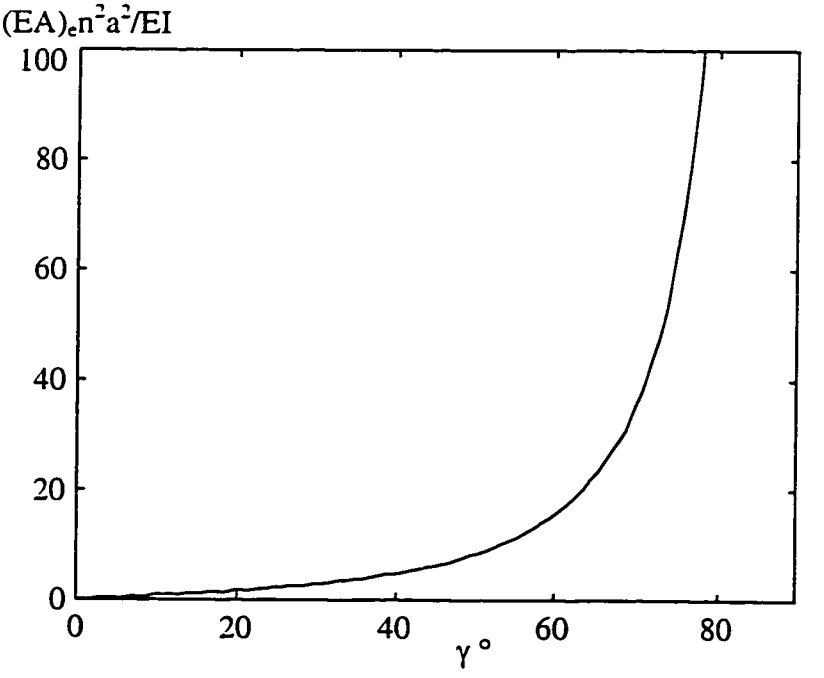

Figure 2.11: Plot of non-dimensional equivalent axial stiffness of a particular pantographic column during deployment.

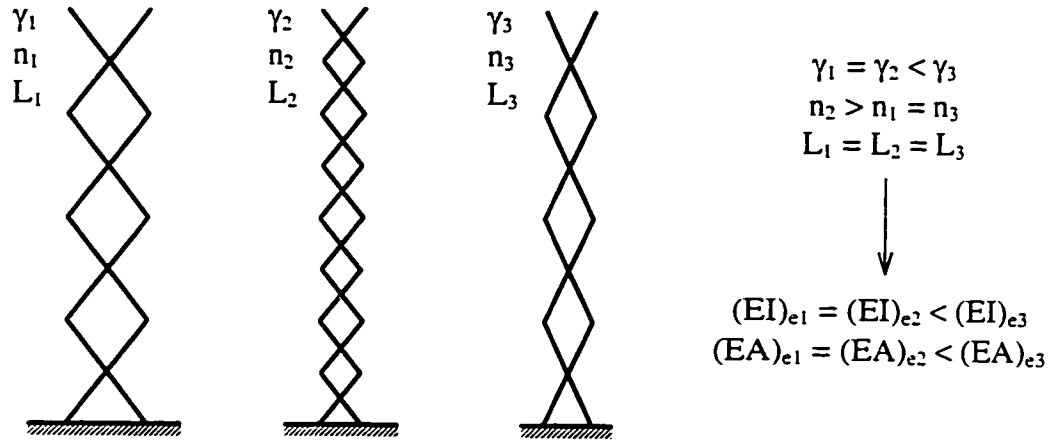

Figure 2.12: Overall equivalent stiffnesses of pantographic columns of the same length, with different numbers of units and degrees of deployment.

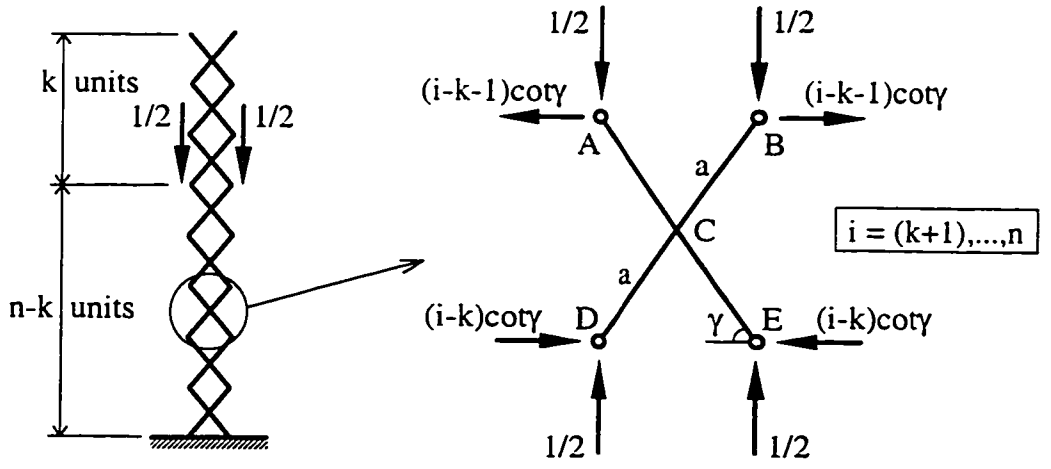

Figure 2.13: Pantographic column under virtual axial unit load and forces applied to a typical unit below the load.

$$v_k = \sum_{i=1}^{n} \int \frac{M_i m_i}{EI} dx = \frac{Pa^3}{3EI} \cos^2\gamma \sum_{i=k+1}^{n} \left[(2i-1)^2 - 2k(2i-1)\right] = \\ = \frac{Pa^3}{9EI} \cos^2\gamma \left[4n^3 - 6kn^2 + 2k^3 - n + k\right] \tag{2.30}$$

The top nodes of unit k move down by:

$$v_{k-1} = \frac{Pa^3}{9EI} \cos^2\gamma \left[4n^3 - 6(k-1)n^2 + 2(k-1)^3 - n + (k-1)\right] \tag{2.31}$$

The vertical deformation of unit k is found as:

$$\varepsilon_k^v = \frac{v_{k-1} - v_k}{2a\sin\gamma} = \frac{Pa^2 \cos^2\gamma}{6EI\sin\gamma} \left[2n^2 - 2k^2 + 2n - 1\right] \tag{2.32}$$

If the number of units in the column is increased infinitely, these deformations along the column become a continuous strain function of the distance from the ground x = (n-k)2asinγ :

$$\varepsilon^v(x) = \frac{PL^2 \cos^2\gamma}{12EI\sin^3\gamma} \frac{x}{L} \left(2 - \frac{x}{L}\right) \tag{2.33}$$

This function is plotted in Fig. 2.14 together with the constant strain which a solid column with axial stiffness equal to the corresponding equivalent axial stiffness would exhibit. Comparing the internal force and deformation distributions along the deployable pantographic column one may notice that they have opposite tendencies from top to bottom. While internal forces grow from top to bottom, making the bottom pantographic unit the most heavily loaded, vertical deformations of units are maximum at the top and minimum at the bottom. This happens because there are two parts in the height change of a unit. One is due to the bending of bars and the second is due to the increase of the distance between the bottom nodes of each unit except for the lowest one, which has its bottom nodes hinged to the ground. Let us find out how the distances between nodes at the unit interfaces change along the column length under axial load.

A pantographic column subjected to two horizontal virtual unit forces applied at the bottom nodes of unit k and forces acting on a typical pantographic unit located below that level are shown in Fig. 2.15. The virtual bending moments at the pivots are:

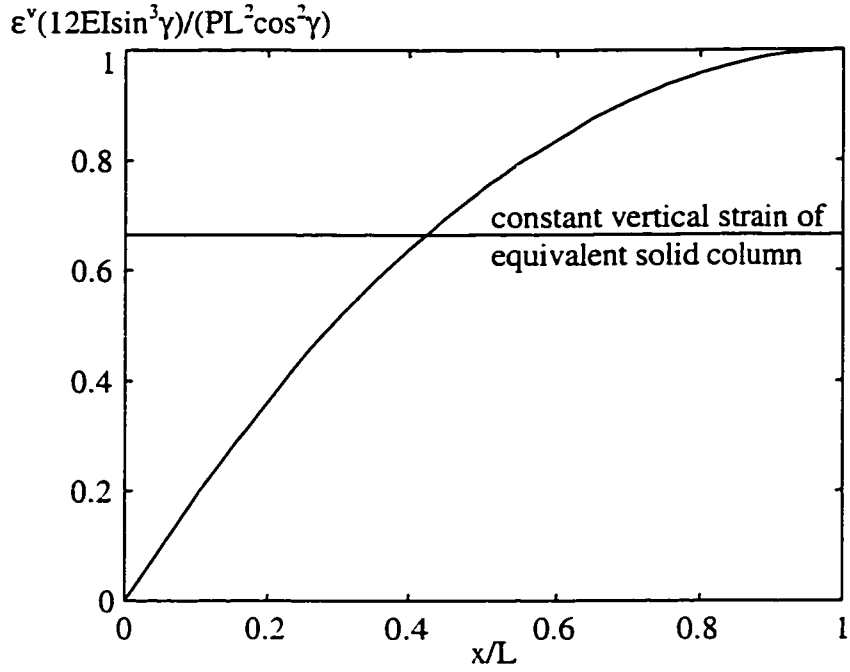

Figure 2.14: Vertical deformation distributions for pantographic and equivalent solid columns.

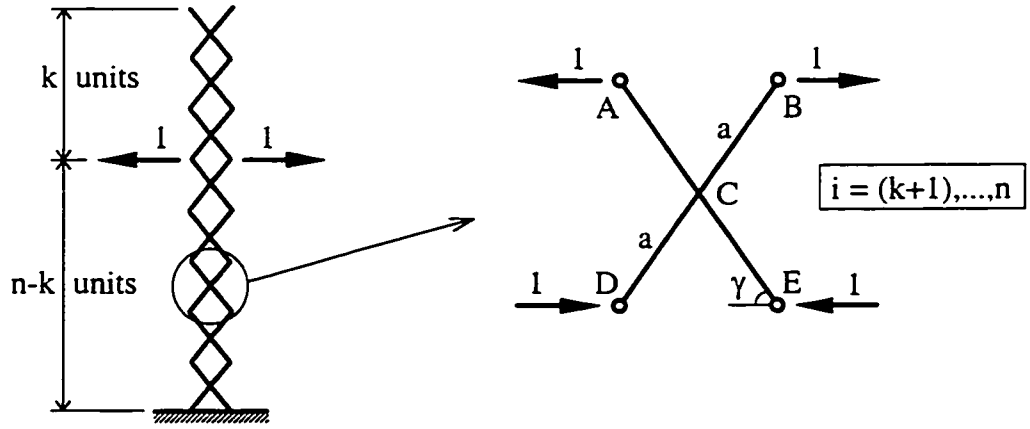

Figure 2.15: Pantographic column subjected to virtual horizontal unit forces and forces applied to a typical unit below the load.

$m_c = a\sin\gamma$, for units below the load. (2.34)

Due to the axial load at the top of the column, nodes at the interface between k and (k+1) units move apart by:

$$\Delta_k = \sum_{i=1}^{n}\int\frac{M_i m_i}{EI}dx = \frac{2Pa^3}{3EI}\sin\gamma\cos\gamma\sum_{i=k+1}^{n}(2i-1) = \frac{2Pa^3}{3EI}\sin\gamma\cos\gamma(n^2-k^2) \qquad (2.35)$$

Dividing the last equation by the original distance between the nodes, we obtain the horizontal "strain" at the same level:

$$\varepsilon_k^h = \frac{\Delta_k}{2a\cos\gamma} = \frac{Pa^2}{3EI}\sin\gamma(n^2-k^2) \qquad (2.36)$$

This may again be transformed into a continuous function of the distance from the ground:

$$\varepsilon^h(x) = \frac{PL^2}{12EI\sin\gamma}\frac{x}{L}\left(2-\frac{x}{L}\right) \qquad (2.37)$$

It can be seen that function in eq. 2.37 differs from that in eq. 2.33 only by the factor of $\tan^2\gamma$. This means that the greater part of the vertical unit deformations comes from a change of the unit base length, which is associated with the rotations of its bars.

In the light of the last derivations one note must be made about the assumption of linearity under which the behaviour of the pantographic columns was investigated so far. This assumption for the pantographic column in bending (under moment or lateral loads) is valid to the same extent as it would be for a solid column with the equivalent bending stiffness. In the case of axial loading, however, the proportionality between the vertical and horizontal "strains" in the deformed column suggests that finite rotations of bars in SLEs may considerably change the configuration of the structure and the internal force distribution. The phenomenon of geometric non-linearity in axially loaded pantographic columns is considered in Section 3 of this Chapter.

2.3 Non-Linear Behaviour under Axial Load

2.3.1 Source of Geometric Non-Linearity

It may be noticed that the equivalent axial stiffness of a deployable column (eq. 2.28) depends on the square of its length. If the number of units in the column is doubled, and the size of the bars in the units and the degree of deployment are kept the same, the new column, which is twice as long as the original one, would have the equivalent axial stiffness of one quarter of the original, and when subjected to the same axial load would exhibit a deflection eight times greater than the original. This can be explained by the fact that the main portion of the vertical deformation of the structure comes not directly from bending of bars in the units, but from the unit becoming more flat the closer to the top it is located. The schematic deformed shape of an axially loaded column is shown in Fig. 2.16. It can be expected that changes in the degrees of deployment of the upper units affect the internal force distribution in the column. Hence the geometric non-linearity becomes obvious. Let us look more closely at the mechanism of the pantographic column deformation under axial load.

When the column deforms, the top nodes of its bottom unit move down and apart due to bending of bars in the unit. Since the bottom nodes are hinged to the ground, the distance between them, i.e. the base of the bottom unit, as well as the degree of deployment of this unit, remain constant ($b_n = b$, $\gamma_n = \gamma$). The distance between its top nodes, i.e. the base of the unit number n-1, b_{n-1}, increases, while the degree of deployment, γ_{n-1}, decreases, and the configuration of the latter unit "before bending" becomes different from the original. Then, due to bending of the bars in unit number n-1, the base of the unit above it, b_{n-2}, becomes even greater and so on. This effect builds up from the bottom of the column to the top, and the higher the location of the unit the flatter it becomes. The internal force distribution in the column, therefore, becomes quite different from that found for its undeformed shape.

A note must be made about the sense of geometric non-linearity in this problem. The bending of bars in pantographic units is still regarded as linear and the corresponding deformations as small. The source of non-linearity is the finite relative rotations of bars at the pivotal hinges and at the hinges between the units.

2.3.2 Non-Linear Analysis

Three configurations of the i-th unit together with the forces acting on it are shown in Fig. 2.17. The configurations are: initial - in the undeformed column, intermediate - "after

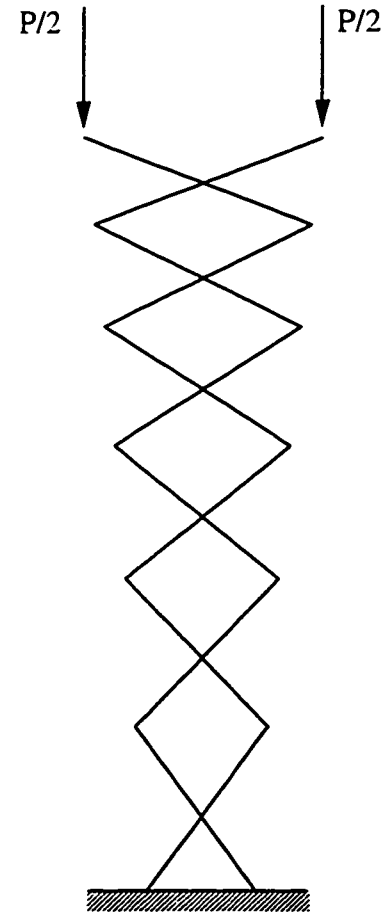

Figure 2.16: Source of geometric non-linearity under axial loading - schematic shape of the deformed column.

rotation" caused by deformation of the part of the column below the unit, and final - "after rotation and bending". Under the assumption stated at the end of the last section, the forces are applied to and the equilibrium conditions must be satisfied for the unit "after rotation". The vertical forces applied to the nodes of the unit are known and equal to the load on the column, whereas the horizontal forces at the bottom of the unit, T_i, base of the unit, b_i, and the degree of deployment, γ_i, are to be found for all units in the structure. From the condition of moment equilibrium about the pivot for each bar in the unit "after rotation":

$$T_{i-1}\, a\sin\gamma_i + \frac{P}{2} a\cos\gamma_i - T_i\, a\sin\gamma_i + \frac{P}{2} a\cos\gamma_i = 0, \quad i = 1,2,\ldots,n \tag{2.38}$$

the relation between horizontal forces applied to the bottom and top nodes can be obtained:

$$T_i = P\cot\gamma_i + T_{i-1}, \quad i = 1,2,\ldots,n, \tag{2.39}$$

where $T_0 = 0$ - no horizontal forces are applied to the top nodes of the column. To find the relative horizontal displacement of the top nodes of the unit when the bars bend, two horizontal opposite unit forces may be applied to the top nodes of the unit "after rotation". From the principle of virtual work:

$$b_{i-1} - b_i = \frac{2a^3 \sin^2\gamma_i}{3EI}\left(2T_i - P\cot\gamma_i\right), \quad i = 1,2,\ldots,n, \tag{2.40}$$

where $b_n = b$ - base of the bottom unit is fixed. This defines the degree of deployment of the unit above the one currently considered:

$$\cos\gamma_{i-1} = \frac{b_{i-1}}{2a} = \cos\gamma_i + \frac{a^2 \sin^2\gamma_i}{3EI}\left(2T_i - P\cot\gamma_i\right), \quad i = 1,2,\ldots,n, \tag{2.41}$$

where $\gamma_n = \gamma$ - the degree of deployment of the bottom unit is constant. The system of eqs 2.39 and 2.41 together with the boundary conditions can be solved iteratively for T_i and γ_i in the following manner. We start from the original configuration of the undeformed column, so that all γ_i are the same and equal to the initial degree of deployment γ. Using eqs 2.39, for i changing from 1 to n (i.e. moving from top to bottom), all T_i are calculated. These forces are equal to those obtained from linear analysis. With these forces we use

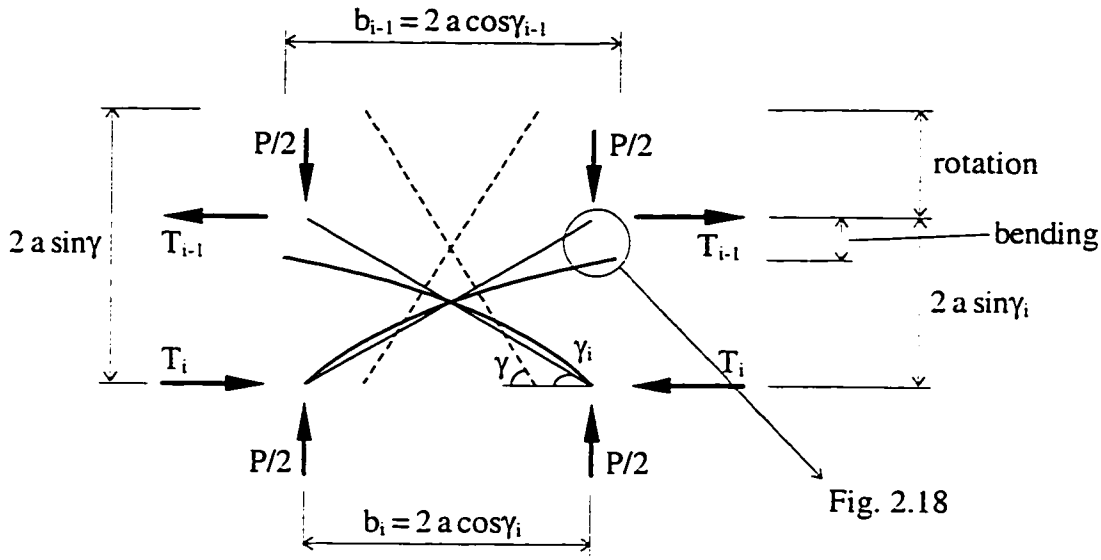

Figure 2.17: Configurations of the i-th pantographic unit in a non-linear column: initial - dashed line, "after rotation" - thin solid line and final - thick solid line.

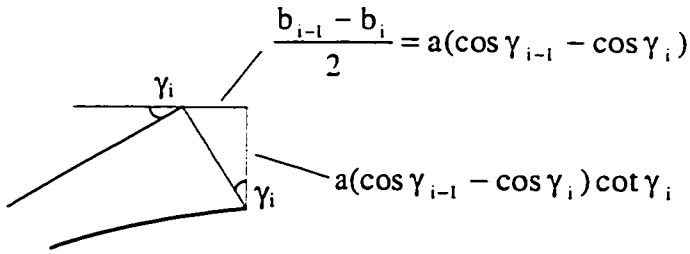

Figure 2.18: Bending deformations of bars in a pantographic unit.

eqs 2.41, for i changing from n to 1 (i.e. moving from bottom to top), to calculate new γ_i. For the new unit configurations the new forces are found, and so on, until the required accuracy is reached. These back and forth (or rather down and up) iterations are required because of the fact that the boundary conditions for forces and deformations are given at the opposite ends of the column. For the next step in load level, instead of starting again with the undeformed column shape, the final deployment angles from the previous load level can be used as the initial approximation to speed up the convergence.

After the analysis for the given load level is complete, the vertical deformation of the column can be found. The total vertical deflection of the top of the column, ΔL, is the sum of the height changes of all units in the column, Δl_i. In turn, Δl_i may be split in two parts: Δl^r_i - due to rotations of bars in an i-th unit and Δl^b_i - due to bending of bars (Figs 2.17 and 2.18). Therefore, the total deflection can be written as the sum of the rotational and bending components:

$$\Delta L = \sum_{i=1}^{n} \Delta l_i = \sum_{i=1}^{n} (\Delta l_i^r + \Delta l_i^b) = \sum_{i=1}^{n} \Delta l_i^r + \sum_{i=1}^{n} \Delta l_i^r = \Delta L^r + \Delta L^b \qquad (2.42)$$

The change of the height of an i-th unit may be expressed in terms of the available degrees of deployment:

$$\Delta l_i = \Delta l_i^r + \Delta l_i^b = 2a(\sin\gamma - \sin\gamma_i) + a\left(\cos\gamma_{i-1} - \cos\gamma_i\right)\cot\gamma_i \qquad (2.43)$$

Fig. 2.19 shows the load-deflection curves for a deployable column consisting of ten units, with the initial degree of deployment $\gamma = 45°$. The dotted line corresponds to the change of length of the column contributed only by bending deformations of the bars, the dashed line represents shortening due only to rotations, and the solid line gives the actual resulting deflection. It can be seen that deflection due to rotations is an order of magnitude greater than that due to bending. It should be noted, however, that separation of deformations and deflections into the rotational and bending parts (eq. 2.42), although having clear physical sense for a single unit (eq. 2.43), is somewhat artificial for the whole

structure. In the column, the rotational part of the vertical deformation of a particular unit is the result of both rotational and bending deformations of the units below it.

Linear and non-linear equilibrium paths for two axially loaded pantographic columns consisting of ten units with degrees of deployment of 45° and 60° are shown in Fig. 2.20. The straight linear equilibrium paths, with the slopes given by the equivalent axial stiffness from eq. 2.28,

$$\frac{PL^2}{EI} = 18\sin\gamma\tan^2\gamma\frac{\Delta L}{L} \tag{2.44}$$

are tangents to the non-linear ones at the origin. As the compressive axial load increases, the non-linear paths indicate softening of the structure which ultimately leads to a limit-point instability. The procedure for tracing the non-linear equilibrium path to its maximum and into the descending part is described in the next Section.

2.3.3 Local Snap-Through Buckling

As the compressive axial load grows the overall axial stiffness of the pantographic column diminishes and at some load level it vanishes (Figs 2.19 and 2.20). This can be thought of as a local buckling phenomenon happening at the top pantographic unit. This unit behaves somewhat similar to the von Mises truss, having finite support stiffness in the horizontal direction (Fig. 2.21). If the top nodes of this unit could slip through the bottom nodes with the forces still applied to the top nodes, the unit would snap through, invert and become stretched rather than compressed. In fact, after this, the axial stiffness of the column would increase, because now the top nodes of the second unit would be subjected, in addition to vertical compressive forces, to two horizontal forces tending to bring them together. In reality, only part of this snap-through would happen, since the top nodes of the first unit cannot go lower than its bottom nodes. The top unit would become practically flat and "lock" the column. We now describe how the complete equilibrium path between zero load and "locked" configurations can be traced.

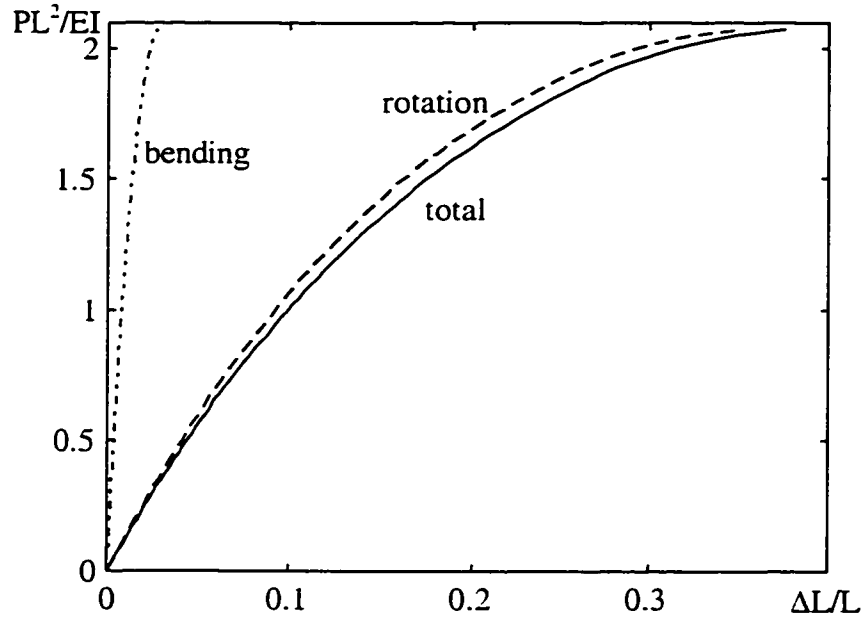

Figure 2.19: Load-deflection curves for axially loaded non-linear deployable column (n = 10, $\gamma = 45°$).

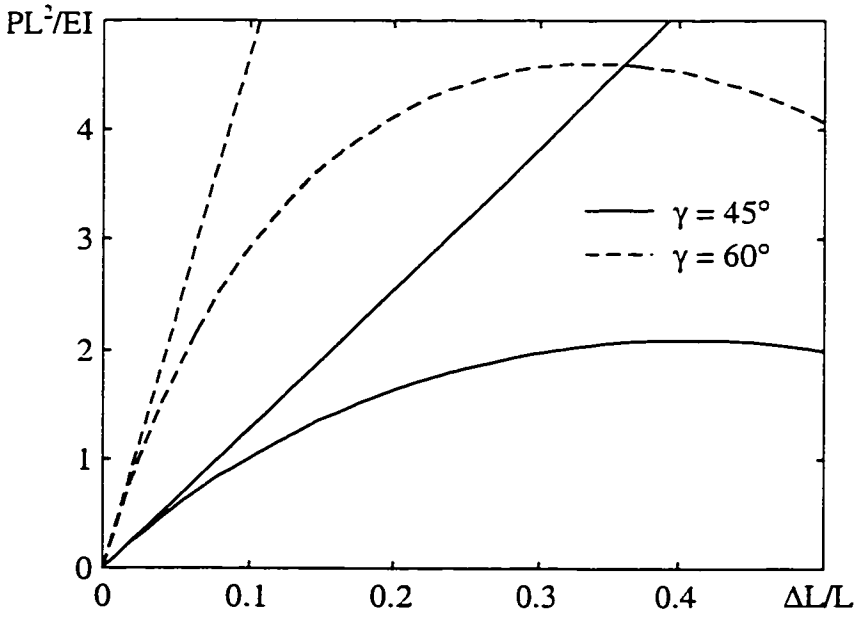

Figure 2.20: Linear and non-linear equilibrium paths for axially loaded pantographic columns (n = 10).

The graph in Fig. 2.19 was obtained from the "load-controlled" approach, i.e. the starting point of the analysis was the prescription of the load. Now the "displacement-controlled" approach will be employed. The distance between the bottom nodes of the top unit, b_1, or its degree of deployment, $\gamma_1 = \cos^{-1}(b_1/2a)$, becomes the independent parameter. The degrees of deployment for the rest of the units (except for the bottom one) and the load are to be found. Under the condition of $T_0 = 0$, eq. 2.39 can be transformed into:

$$T_i = P\sum_{j=1}^{i}\cot\gamma_j, \quad i = 1,2,\ldots,n \tag{2.45}$$

If T_i from the last equation is substituted in eq. 2.41, the axial force at unit number i can be expressed through the degrees of deployment of units from 1 to i:

$$P_i = \frac{3EI}{a^2\sin^2\gamma_i}\frac{\cos\gamma_{i-1}-\cos\gamma_i}{2\sum_{j=1}^{i}\cot\gamma_j-\cot\gamma_i}, \quad i = 2,\ldots,n \tag{2.46}$$

For an initially assumed distribution of γ_i, we generally have all P_i different. The goal is to obtain the correct distribution of degrees of deployment, with $\gamma_n = \gamma$ and γ_1 equal to the prescribed value, so that the axial forces in all units are the same. This is achieved in a way similar to the moment distribution method of frame analysis. Taking two adjacent units i-1 and i, we let γ_{i-1} change until P_{i-1} equals P_i. Then the same procedure is applied to units i and i+1, which, of course, will make P_i different from P_{i-1}, but equal to P_{i+1}. Nevertheless, we proceed to the bottom of the column, and after the first pass is finished, the maximum difference among P_i is smaller. These top to bottom iterations are repeated until the maximum difference is smaller than a specified tolerance. Once all degrees of deployment are known, the vertical deflection of the column can be calculated from eqs 2.42 and 2.43.

Fig. 2.22 shows the load-deflection curves for three columns of the same degree of deployment ($\gamma = 45°$), but different numbers of units. It can be seen that for relatively small values of the load, the three columns have practically the same relative deflections,

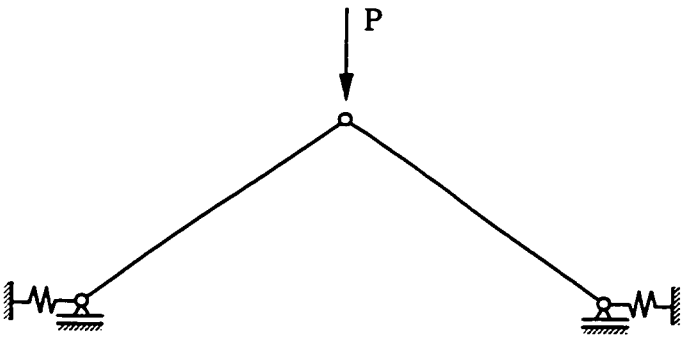

Figure 2.21: Von Mises truss with finite support stiffness in the horizontal direction.

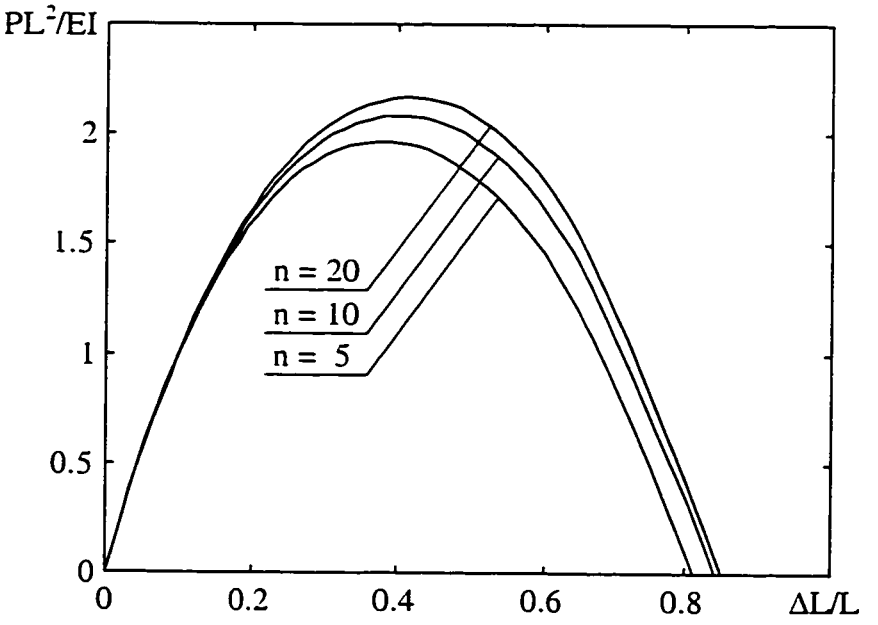

Figure 2.22: Load-deflection curves for columns of the same degree of deployment ($\gamma = 45°$) but different numbers of units.

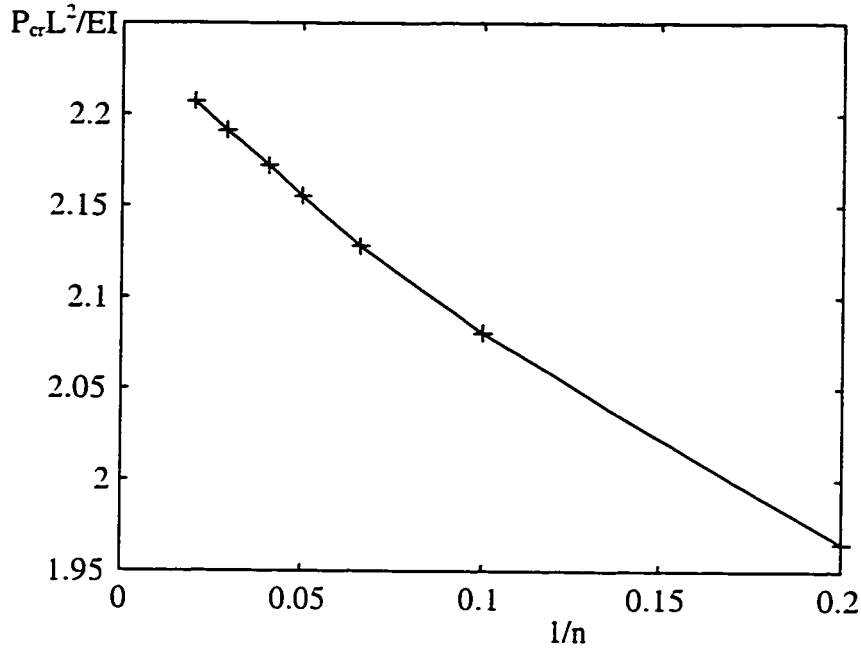

Figure 2.23: Snap-through buckling load versus the number of units under constant degree of deployment ($\gamma = 45°$).

which could be expected on the basis of the expression for the linear equivalent stiffness. The value of the snap-through buckling load and the corresponding deformation, however, slightly increase for greater number of units. This trend is shown in Fig. 2.23, from which the ultimate value of buckling load for an infinitely growing number of units can be predicted.

2.3.4 Restrained columns

The axial stiffness of the pantographic column could be greatly improved by the introduction of just one additional constraint, for example, a link between the top nodes. Although the structure becomes statically indeterminate, one may notice that as long as the number of the units in the column is even, the horizontal line of symmetry passes through the two nodes in the midheight of the column (Fig. 2.24a). Due to the symmetry

of loading there are no horizontal forces at the interface of the two units adjacent to the symmetry line. This means that each half of the column behaves as if it were a separate axially loaded structure and can be analyzed as outlined above.

The case of an odd number of units in the column (Fig. 2.24b) is slightly different, but still possible to deal with. Due to symmetry, the horizontal forces applied to the top and bottom nodes of the central unit are the same. From the moment equilibrium of bars in the unit:

$$T_k = \frac{P}{2}\cot\gamma_k, \quad \text{where} \quad k = \frac{n+1}{2} \tag{2.47}$$

This condition is then used in the analysis of the upper or lower portion of the rest of the column instead of $T_0 = 0$.

The initial amount of stiffening brought by the constraint at small load values is readily seen from the expression of linear equivalent axial stiffness $(EA)_e$ (eq. 2.28). Instead of the column of length L, we now have two columns of length L/2, each of them having axial stiffness four times greater than the original. The non-linear load-deflection curves for the statically determinate column with ten units and the same column with the link between the top nodes are shown in Fig. 2.25 (γ = 45°). The curve for the unrestrained column is the one from Fig. 2.22 for n = 10, whereas the curve for the restrained column is the curve from Fig. 2.22 for n = 5, whose ordinates are scaled by a factor of four to account for the presence of two such columns, one on top of the other. This figure indicates that the snap-through load for the restrained column is approximately four times greater than that for the unrestrained one. At the snap-through load level for the unrestrained column, the deformation of the restrained column is approximately ten percent of that of the unrestrained column.

When the additional constraint is put between the top nodes of the column, it produces a column with the initial equivalent axial stiffness four times greater than the

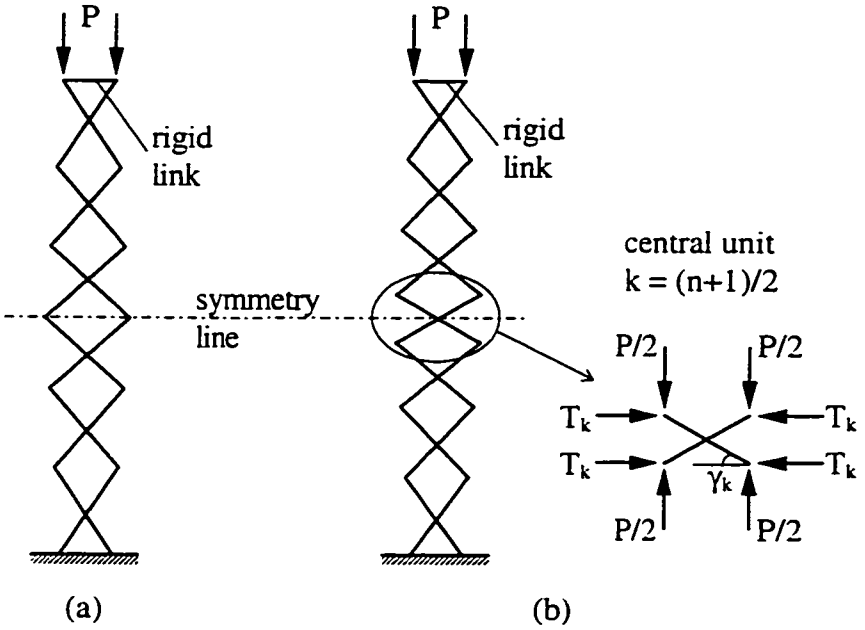

Figure 2.24: Restrained columns with even (a) and odd (b) number of units.

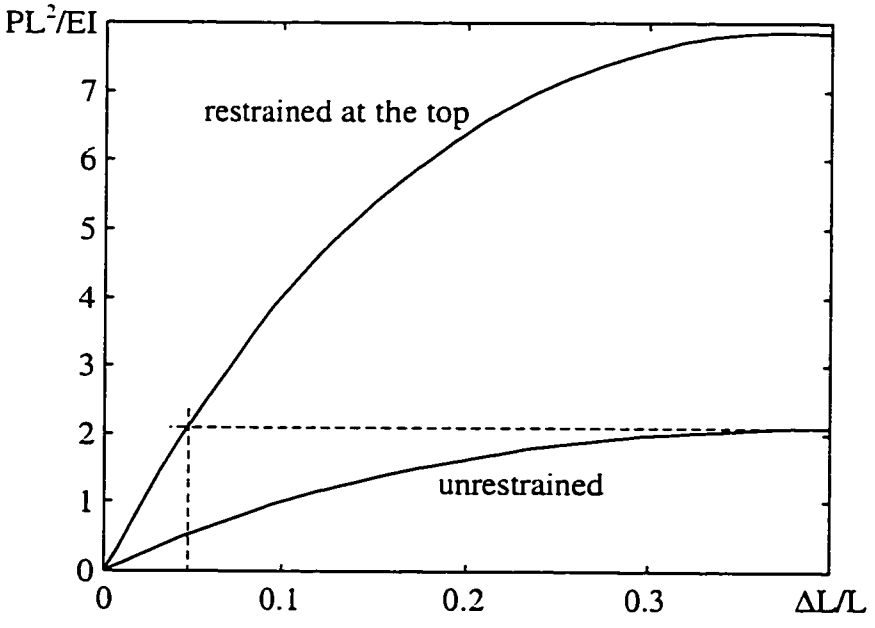

Figure 2.25: Load-deflection curves for the unrestrained column and the column with rigid link between the top nodes (n = 10, $\gamma = 45°$).

original. The question may be asked: is this the best result one link can give? If the link is placed at the distance L_1 from the top of the column, then the whole column is subdivided into three parts: one above the link, and the two halves of the portion of the column between the link and the ground. From linear analysis, the part of the column above the link yields a vertical deformation equal to:

$$\Delta L_1 = \frac{P L_1}{(EA)_{e1}} = \frac{P L_1^3}{B}, \quad \text{where} \quad B = 18EI \sin\gamma \tan^2\gamma \tag{2.48}$$

The rest of the column of length (L - L_1) is four times stiffer than a separate structure of this length but without an upper restraint:

$$\Delta L_2 = \frac{P (L - L_1)}{(EA)_{e2}} = \frac{P (L - L_1)^3}{4B} \tag{2.49}$$

The total vertical deflection is the sum of eqs 2.48 and 2.49:

$$\Delta L = \Delta L_1 + \Delta L_2 = \frac{P}{4B}[4L_1^3 + (L - L_1)^3] \tag{2.50}$$

The minimum ΔL in eq. 2.50 corresponds to $L_1 = L/3$, which gives an equivalent axial stiffness nine times greater than that of the unrestrained column. By introduction of the link at this location the whole column is subdivided into three roughly equal statically determinate parts (exactly equal if the total number of units is a multiple of three). This result is easily explained by thinking of these three parts as sequentially connected springs. The stiffness coefficient of a spring, which is a characteristic of the whole spring, is different from the axial stiffness, which is a characteristic of a cross-section. The stiffness coefficient of an unrestrained column of length L is B/L^3. The stiffness coefficient of the assembly, which equals the inverse of the sum of the inverses of the individual spring coefficients, is always less than the least of the coefficients. Making the three parts of the column equal we maximize the smallest of their stiffness coefficients, thus making the coefficient of the assembly $B/[3(L/3)^3] = 9B/L^3$.

2.4 Column-Type Buckling

The increase of the axial stiffness of the deployable column, caused by a link between the pair of nodes at a unit interface, brings about another type of instability, namely, the overall column-type buckling. For the purpose of buckling analysis, a composite model column is introduced.

2.4.1 Parameters of the Composite Model Column

We model the pantographic column as another structure that is stiffnesswise equivalent. The composite column shown in Fig. 2.26c consists of straight elements with infinite bending and finite axial stiffnesses. They are successively hinged to each other and to the base with rotational springs resisting relative rotations at hinges. The original length of each element in the composite model is equal to the height of the corresponding undeformed SLE in the deployable column. SLEs and elements in both columns are numbered from top to bottom. The parameters of each element - l_i, α_i, β_i - are its length, the stiffness coefficient of the rotational spring at its bottom and its axial stiffness coefficient, respectively. The equivalent bending and axial stiffnesses of such a structure, $(EI)_c$ and $(EA)_c$ (index "c" stands for "composite"), obtained in the same manner as those for the pantographic column, i.e. by equating the displacements of the composite model and a uniform solid column, are:

$$(EI)_c = \frac{L}{\sum_{i=1}^{n} 1/\alpha_i}, \quad (EA)_c = \frac{L}{\sum_{i=1}^{n} 1/\beta_i}, \quad \text{where} \quad L = \sum_{i=1}^{n} l_i \tag{2.51}$$

We start by defining the parameters of the composite column on the basis of a linear analysis of the pantographic structure. If all elements of the model have the same length, which corresponds to all SLEs in the uniform pantographic column having the

same height, and all rotational springs have the same stiffness, which corresponds to uniform equivalent bending stiffness along the pantographic column, then:

$$l_i = 2\,a\sin\gamma\,, \quad \alpha_i = \frac{3\,EI}{a} \tag{2.52}$$

The axial stiffness coefficient of each element can be obtained from eqs. 2.30 and 2.31 as the ratio of the load and vertical deformation of the unit:

$$\beta_i = \frac{P}{v_{i-1} - v_i} = \frac{3\,EI}{a^2\cos^2\gamma}\,\frac{1}{\left[2n^2 - 2\,i^2 + 2n - 1\right]} \tag{2.53}$$

2.4.2 Procedure of Buckling Analysis

A composite column, with all dimensions and stiffness parameters specified, subjected to axial compressive force P applied at the top, is shown in Fig 2.27. The potential energy of this system in a buckled configuration, V, equals the difference between the strain energy of the axially compressed elements and deformed rotational springs, U, and the work done by the load, W:

$$V = U - W = \sum_{i=1}^{n}\left[\frac{\alpha_i\,(\theta_i - \theta_{i+1})^2}{2} + \frac{\beta_i\,\delta_i^2}{2}\right] - P\sum_{i=1}^{n}\left[l_i\,(1-\cos\theta_i) + \delta_i\cos\theta_i\right] \tag{2.54}$$

where θ_i is the rotation of the i-th element ($\theta_{n+1} = 0$), and $\delta_i = P\cos\theta_i/\beta_i$ is the elemental compressive deformation. Substituting δ_i into eq. 2.54 and using the series expansion $\cos\theta_i \approx 1 - \theta_i^2/2$ for small θ_i yield:

$$V = \frac{1}{2}\sum_{i=1}^{n}\left[\alpha_i\,(\theta_i - \theta_{i+1})^2 + (P^2/\beta_i - P\,l_i)\,\theta_i^2 - P^2/\beta_i\right] \tag{2.55}$$

The stiffness matrix of the structure is obtained by differentiating eq. 2.55 two times with respect to the angles:

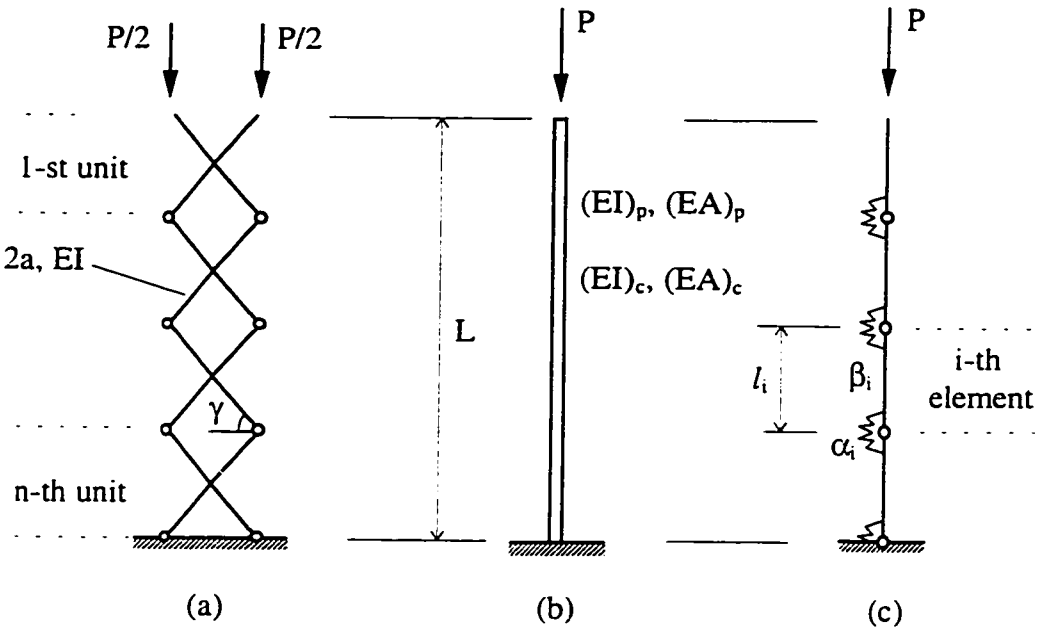

Figure 2.26: Pantographic (a), equivalent solid (b) and composite (c) columns.

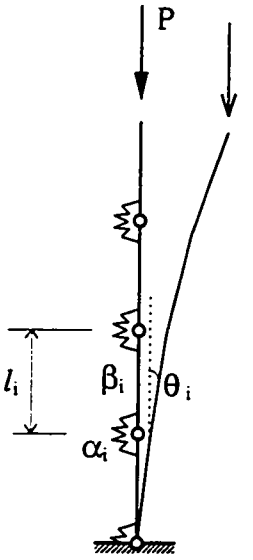

Figure 2.27: Initial and buckled configurations of the composite model column.

$$\frac{\partial^2 V}{\partial \theta_1^2} = \alpha_1 - P(l_1 - P/\beta_1), \quad \frac{\partial^2 V}{\partial \theta_i^2} = \alpha_{i-1} + \alpha_i - P(l_i - P/\beta_i), \quad \text{for} \quad i = 2,\ldots,n,$$
$$\frac{\partial^2 V}{\partial \theta_i \partial \theta_j} = -\alpha_i, \quad \text{if } j - i = 1; \qquad \frac{\partial^2 V}{\partial \theta_i \partial \theta_j} = 0, \quad \text{otherwise}. \tag{2.56}$$

Hence, the stiffness matrix is tri-diagonal with the entries on the main diagonal being quadratic functions of the load.

The vanishing of the determinant of the stiffness matrix gives the buckling load P_{cr}, which leads to a non-linear eigenvalue problem. One possible way to solve this problem is to employ a very robust algorithm suggested by Wittrick and Williams (1971) - the combination of bisection and sign counting. However, in assigning the parameters of the composite model the results of the linear analysis of a pantographic column under axial load were used (eq. 2.53), whereas the behaviour of the column subjected to such load is non-linear as was shown in Section 2.3. Although the stiffnesses of the rotational springs only depend on the bending stiffness and length of the bars in the SLEs and do not depend on their current degrees of deployment (eq. 2.52), the axial stiffness coefficients of the elements of the model corresponding to the non-linear pantographic column are non-linear functions of the load.

It may be noticed that the expressions in brackets in the load-dependent entries of the stiffness matrix (eq. 2.56), l_i - P/β_i, are the lengths of the elements of the composite model at the current load level. This leads to the following conclusion. The composite column with axially soft elements buckles at the same load as the column with axially rigid elements if the lengths of the rigid elements are the same as the lengths of the soft elements at the point of buckling. Since the current lengths of the elements can be obtained for any load by means of the non-linear analysis (eq. 2.43), we can find the critical force for the composite column with such elements considering them axially rigid. In this case the problem of finding the buckling load becomes a generalized linear eigenvalue problem. If this critical force is greater than the current load on the column the

structure is still stable. Then the load on the column is increased, new element lengths and new critical force are found. At some point, the load on the column and the critical force for the deformed structure will be equal. This load level is critical.

2.4.3 Results of Buckling Analyses

Fig. 2.28 shows the results of buckling analyses for columns of constant length and the same bending stiffness of bars in the pantographic units. All columns are restrained with a rigid link between the two top nodes. The three curves correspond to columns consisting of 10, 20 and 30 units, while the initial degree of deployment varies along each curve. The trend along each curve represents the change of the initial configuration from that of the first column in Fig. 2.12 to that of the third column in the same figure. Two points on different curves but with the same horizontal coordinate correspond to a change of the initial configuration from that of the first column to that of the second column in the same figure. For all values of the number of units (10, 20 or 30), snap-through occurs before overall buckling if the degree of deployment is less than 58°. For a constant degree of deployment the critical load grows as the number of units in the column increases. The reason for this is that with the greater number of units the effect of geometric non-linearity becomes more pronounced and the column shortens more (becomes more "stocky") before it buckles. For a column with constant length and number of units but varying degree of deployment there are two tendencies. As γ grows, the column becomes stiffer axially which reduces the buckling load. At the same time, since the bar length (2a) decreases, the bending stiffness increases and this contributes to the increase of the buckling load. It can be seen from the graph, that the former trend prevails at first and for some degree of deployment the buckling load reaches its minimum. After that the second trend overcomes the first and the buckling load slightly increases.

The buckling load versus the degree of deployment for a column consisting of 20 units is shown in Fig. 2.29. At each stage of deployment the length of the column is different since the size of the bars in the units is kept constant. Again, until γ reaches 58° snap-through occurs

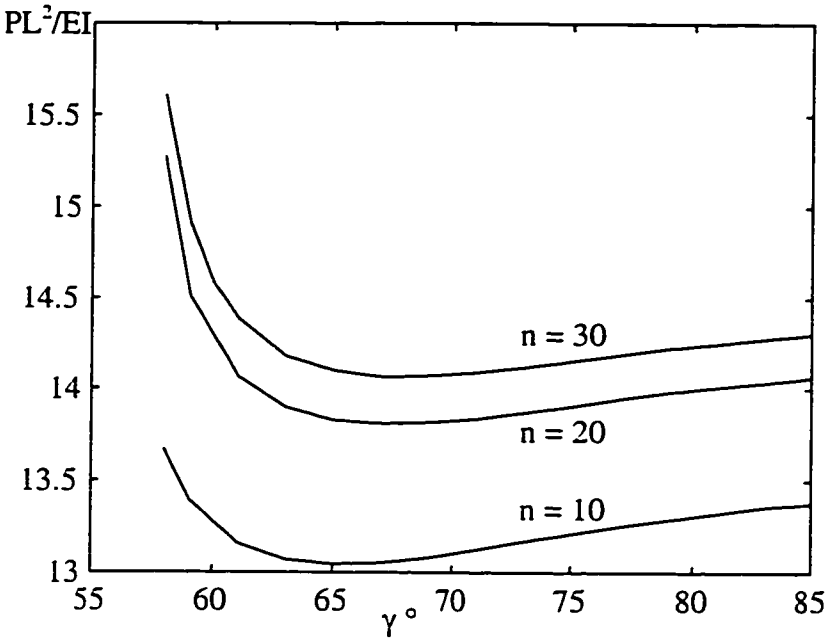

Figure 2.28: Buckling load for restrained pantographic columns of the same length and different number of units versus the degree of deployment.

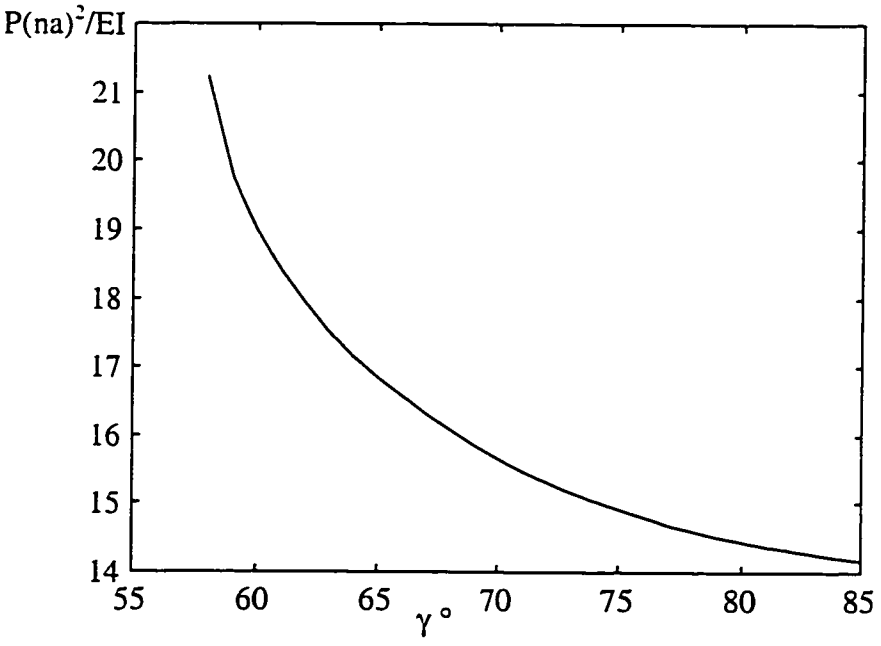

Figure 2.29: Buckling load for restrained pantographic column versus the degree of deployment (n = 20).

before column-type buckling. As the column deploys, its length and axial stiffness increase lowering the value of the buckling load in spite of the increasing bending stiffness.

2.5 Non-Uniform (Tapered) Columns

In this Section pantographic columns with the pivot connection in some or all SLEs shifted from the midpoint of bars (Fig. 2.30) will be examined. Such a shift immediately produces bars of different lengths in different units. As in the uniform column, the parts of the bars in the adjacent SLEs form rhombuses, only now these rhombuses are generally not equal. We will consider linear and non-linear behaviour of such non-uniform columns under different loads, deriving, where possible, the overall stiffness characteristics of these structures and comparing them with those of uniform columns. As before, the bars in all pantographic units are assumed to have the same bending stiffness EI; the contribution of axial deformations of bars to the overall deflections of the structure is assumed to be negligible compared to that of bending.

2.5.1 Linear Behaviour

2.5.1.1 Moment Loading

First we examine the linear behaviour of a non-uniform pantographic column. The first case of loading is a moment applied at the top of the column (Fig. 2.30). A typical pantographic unit (unit number i), together with forces acting on it, is also shown in Fig. 2.30. The structure under consideration is statically determinate, and therefore the forces acting at the interfaces of pantographic units can be obtained by considering the equilibrium of bars in each unit starting from the top of the column and moving down unit by unit. Alternatively, forces at a particular unit interface can be deduced from the

equilibrium of the part of the column above this level. For example, we can consider the equilibrium of the top portion of the column including the i-th unit. In general, there can be both vertical and horizontal force components acting at each of the two bottom nodes of the i-th unit. Since the structure is symmetrical and the moment load is anti-symmetrical, the vertical forces at the two nodes must have the same magnitude and opposite directions, and the two horizontal forces must have the same magnitude and direction. The value of the vertical forces is found from the moment equilibrium, about any point on the horizontal line connecting the two nodes, of all forces applied to the portion of the column above this line. This gives the vertical force value equal to $M/b_i = M/(2a_i\cos\gamma)$. The only way to satisfy the force equilibrium in the horizontal direction is to have both horizontal forces equal to zero.

The bending moments in the bars of the pantographic units are zero at the end hinges and increase linearly to the maximum value at the pivots. The maximum moment value is independent of the bar length and pivot location and equals M/2. Knowing the internal force distribution one can employ the principle of virtual work to find the rotation of the top of the column due to the applied moment. Applying a unit virtual moment at the top of the column and equating the external and internal virtual work we obtain:

$$\varphi = \frac{1}{EI}\sum_{i=1}^{n} 2\left(\frac{M}{2}\frac{a_{i-1}}{2}\frac{2}{3}\frac{1}{2} + \frac{M}{2}\frac{a_i}{2}\frac{2}{3}\frac{1}{2}\right) = \frac{M}{6EI}\sum_{i=1}^{n}\left(a_{i-1} + a_i\right) = \frac{M}{6EI}\frac{L}{\sin\gamma}, \qquad (2.57)$$

where the internal virtual work on the right is the sum of contributions of all n units. A uniform solid column of the same length subjected to the same load would produce the rotation $ML/(EI)_e$, where the familiar notation $(EI)_e$ is the equivalent bending stiffness of the solid column. Equating the two rotations yields the expression for the equivalent bending stiffness of the non-uniform pantographic column:

$$(EI)_e = 6EI\sin\gamma \qquad (2.58)$$

The last expression is exactly the same as that obtained for a uniform pantographic column. This shows that the equivalent bending stiffness of a pantographic column

depends only on the bending stiffness of bars in the SLEs and on the degree of deployment.

2.5.1.2 Lateral Force Loading

The pantographic column subjected to the lateral force applied at the top and a typical pantographic unit with forces acting on it are shown in Fig. 2.31. The horizontal forces acting at unit interfaces must ensure horizontal force equilibrium, hence they are the same throughout the column, and the vertical forces are responsible for moment equilibrium:

$$V_i b_i = PL_i = P\sum_{j=1}^{i} l_j = P\sin\gamma \sum_{j=1}^{i}\left(a_{j-1} + a_j\right), \tag{2.59}$$

where L_i is the length of the part of the column above the bottom level of the i-th SLE. The pivotal bending moments in the bars of the unit are:

$$M_{pi} = V_i \frac{b_i}{2} - \frac{P}{2} a_i \sin\gamma = \frac{P}{2}\sin\gamma\left[\sum_{j=1}^{i}\left(a_{j-1} + a_j\right) - a_i\right] = \frac{P}{2}\left(L_i - a_i \sin\gamma\right) \tag{2.60}$$

The horizontal deflection of the top of the column due to the lateral load is found as:

$$h = \frac{1}{EI}\sum_{i=1}^{n} 2\left(\frac{M_{pi} a_{i-1}}{2}\frac{2}{3}\frac{M_{pi}}{P} + \frac{M_{pi} a_i}{2}\frac{2}{3}\frac{M_{pi}}{P}\right) = \frac{P}{6EI\sin\gamma}\sum_{i=1}^{n}\left[\left(L_i - a_i \sin\gamma\right)^2 l_i\right] \tag{2.61}$$

Comparing the last equation with that for the deflection of a uniform solid column, $PL^3/3(EI)_e$, we obtain the following expression for the equivalent bending stiffness of the deployable column:

$$(EI)_e = \frac{2\,EI\,L^3 \sin\gamma}{\sum_{i=1}^{n}\left[\left(L_i - a_i \sin\gamma\right)^2 l_i\right]} \tag{2.62}$$

It can easily be shown that this expression simplifies to that of eq. 2.58 if the column is uniform and the number of units is sufficiently large.

Let us now consider the special case of a non-uniform pantographic column, in which the symmetric shape of the column is enveloped by two straight lines with opposite

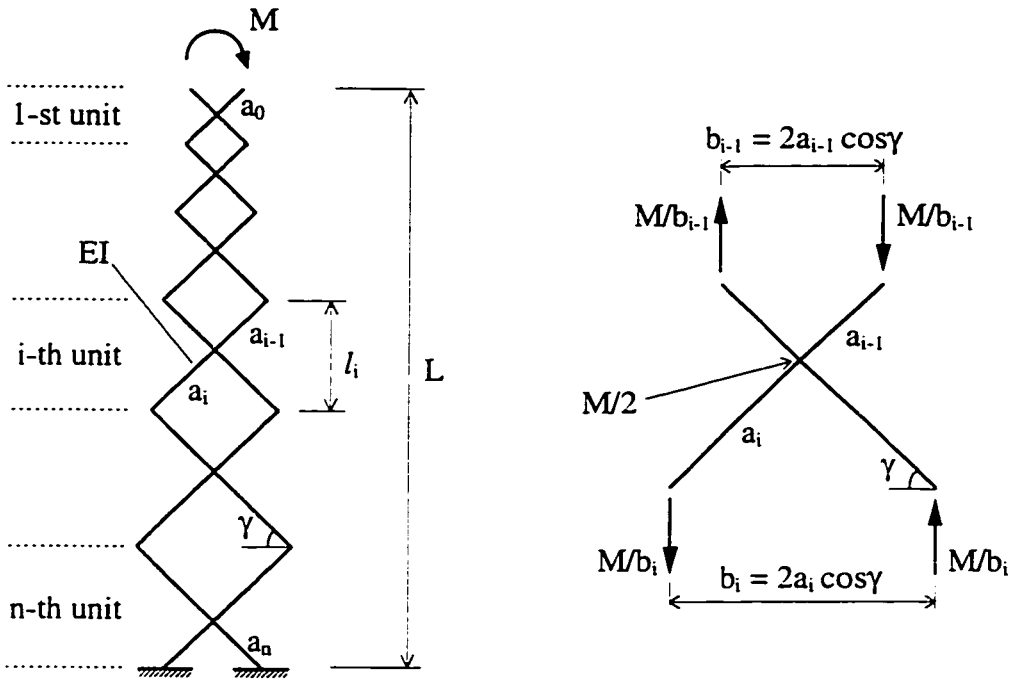

Figure 2.30: Non-uniform pantographic column under moment load and forces applied to a typical unit.

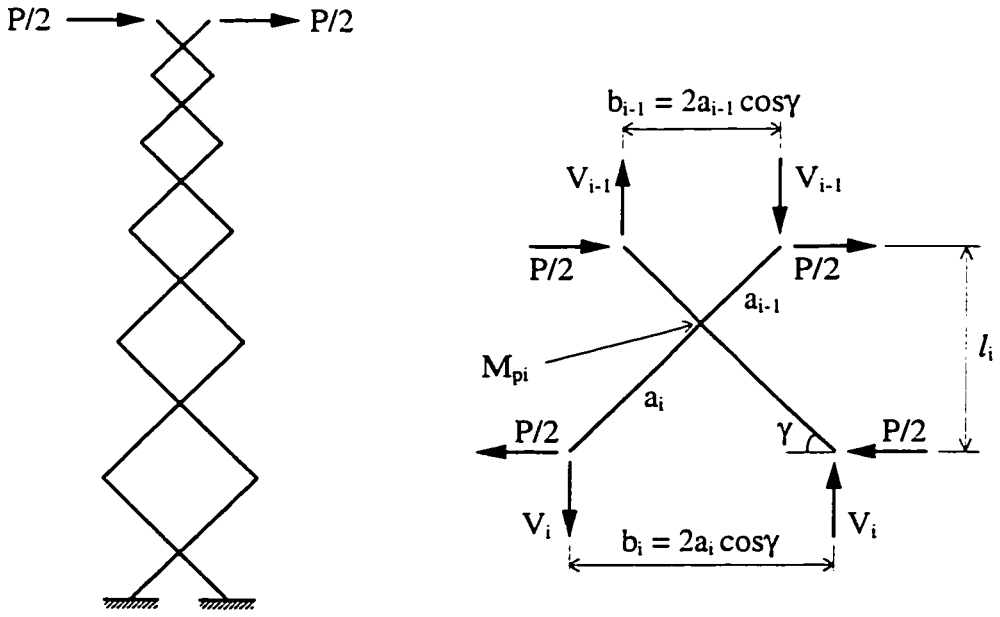

Figure 2.31: Non-uniform pantographic column under lateral load and forces applied to a typical unit.

slopes. In this case, all units of the column are inscribed in similar trapezoids (with the bars in the units being the diagonals of the trapezoids). For each bar in the column, the pivot divides it into two parts whose lengths are in the ratio $m = a_i / a_{i-1}$. Two such columns are shown in Fig. 2.33 for values of m less and greater than one on the left and on the right sides of the graph, respectively. Three additional parameters which, together with m, define the geometry of the structure, are the total length of the column, L, the number of SLEs, n, and the degree of deployment, γ. The lengths of bars in the units and the locations of the pivots are found as follows. The total column length can be written in terms of the bar lengths (in calculating the sum we use the fact that a_i, i = 0,...,n, form a geometric progression):

$$L = \sum_{i=1}^{n} l_i = \sin\gamma \sum_{i=1}^{n} (a_{i-1} + a_i) = \sin\gamma \sum_{i=1}^{n} a_{i-1}(1+m) = a_0 \sin\gamma (1+m) \sum_{i=1}^{n} \frac{a_{i-1}}{a_0} =$$
$$= a_0 \sin\gamma (1+m) \sum_{i=1}^{n} m^{i-1} = a_0 \sin\gamma (1+m) \frac{m^n - 1}{m-1} \qquad (2.63)$$

From eq. 2.63, a_0 and then a_i can be expressed through L, n, γ and m:

$$a_0 = \frac{L}{\sin\gamma} \frac{m-1}{(m+1)(m^n-1)}, \quad a_i = a_0 m^i = \frac{L}{\sin\gamma} \frac{(m-1)m^i}{(m+1)(m^n-1)} \qquad (2.64)$$

Extending the resulting expression of eq. 2.63 for L_i (note that $L = L_n$) we get:

$$L_i = a_0 \sin\gamma (1+m) \frac{m^i - 1}{m-1} = L \frac{m^i - 1}{m^n - 1} \quad \text{and} \qquad (2.65)$$

$$L_i - a_i \sin\gamma = L \frac{m^i - 1}{m^n - 1} - L \frac{(m-1)m^i}{(m+1)(m^n-1)} = \frac{L}{m^n - 1} \frac{2m^i - (m+1)}{m+1} \qquad (2.66)$$

With eq. 2.64, the undeformed height of an i-th unit becomes:

$$l_i = (a_{i-1} + a_i) \sin\gamma = L \frac{(m-1)m^i}{(m^n - 1)m} \qquad (2.67)$$

Now all the values under the summation sign in the denominator of eq. 2.62 are expressed in terms of the four basic parameters. With the use of eqs 2.66 and 2.67, the denominator of eq. 2.62 becomes:

$$\frac{L^3(m-1)}{(m^n-1)^3(m+1)^2 m}\sum_{i=1}^{n} m^i\left[2m^i-(m+1)\right]^2 \tag{2.68}$$

Expanding the expression under the summation sign in the last equation and using:

$$\sum_{i=1}^{n}\left(m^k\right)^i = m^k\frac{m^{kn}-1}{m^k-1}, \tag{2.69}$$

we can rewrite eq. 2.68 in the following form:

$$\frac{L^3(m-1)}{(m^n-1)^3(m+1)^2 m}\left[4m^3\frac{m^{3n}-1}{m^3-1}-4(m+1)m^2\frac{m^{2n}-1}{m^2-1}+(m+1)^2 m\frac{m^n-1}{m-1}\right]= \\ = L^3\frac{(m-1)^2\left(m^2+m+1\right)+4m\left(m^n m-1\right)\left(m^n-m\right)}{(m+1)^2\left(m^n-1\right)^2\left(m^2+m+1\right)} \tag{2.70}$$

Using the last result in eq. 2.62 we obtain the equivalent bending stiffness expression for the tapered pantographic column:

$$(EI)_e = 6EI\sin\gamma\left[\frac{1}{3}\frac{(m+1)^2\left(m^n-1\right)^2\left(m^2+m+1\right)}{(m-1)^2\left(m^2+m+1\right)+4m\left(m^n m-1\right)\left(m^n-m\right)}\right] \tag{2.71}$$

The change in the equivalent bending stiffness due to tapering is given by the bracketed term in the last equation.

2.5.1.3 Axial loading

The pantographic column subjected to axial load and a typical SLE with forces acting on it are shown in Fig. 2.32. From the condition of vertical equilibrium, the vertical forces acting at all unit interfaces are the same and equal to the load. The horizontal forces acting at the bottom nodes of an i-th SLE are found by application of the principle of virtual work to the portion of the column above this level:

$$T_i = \frac{P}{2}\cot\gamma\frac{L_i}{a_i\sin\gamma} \tag{2.72}$$

The pivotal bending moments in the bars of the unit are:

$$M_{pi} = T_i a_i \sin\gamma - \frac{P}{2} a_i \cos\gamma = \frac{P}{2}\cot\gamma\left(L_i - a_i \sin\gamma\right) \tag{2.73}$$

This expression for moment is similar to that from the case of lateral loading (eq. 2.60) except for the factor cotγ, which will appear squared in the expression for vertical deflection:

$$v = \frac{P\cot^2\gamma}{6EI\sin\gamma}\sum_{i=1}^{n}\left[\left(L_i - a_i \sin\gamma\right)^2 l_i\right] \tag{2.74}$$

Equating the above deflection to that of the equivalent solid column, $PL/(EA)_e$, we obtain the following equivalent axial stiffness:

$$(EA)_e = \frac{6EI\sin^3\gamma L}{\cos^2\gamma\sum_{i=1}^{n}\left[\left(L_i - a_i \sin\gamma\right)^2 l_i\right]} \tag{2.75}$$

For the linearly tapered column, using the transformations of eqs 2.63 through 2.70 we obtain:

$$(EA)_e = \frac{18EI\sin^3\gamma}{L^2\cos^2\gamma}\left[\frac{1}{3}\frac{(m+1)^2\left(m^n-1\right)^2\left(m^2+m+1\right)}{(m-1)^2\left(m^2+m+1\right)+4m\left(m^n m-1\right)\left(m^n-m\right)}\right] \tag{2.76}$$

One may notice that both the equivalent bending and the equivalent axial stiffnesses of the tapered column (eqs 2.71 and 2.76) differ from the corresponding characteristics of the uniform column (eqs. 2.11 and 2.28) by the same factor:

$$k = \frac{1}{3}\frac{(m+1)^2\left(m^n-1\right)^2\left(m^2+m+1\right)}{(m-1)^2\left(m^2+m+1\right)+4m\left(m^n m-1\right)\left(m^n-m\right)} \tag{2.77}$$

Fig. 2.33 shows the plot of the deflection ratio of tapered and uniform pantographic columns (solid line for linear behaviour) versus the value of m. This ratio is the inverse of k from eq. 2.77. For m less than one the top of the column is wider than the bottom, and deflections are greater than those of the uniform column. Ultimately, as m approaches zero, the deflection values reach that for a single bar, with the slope equal to

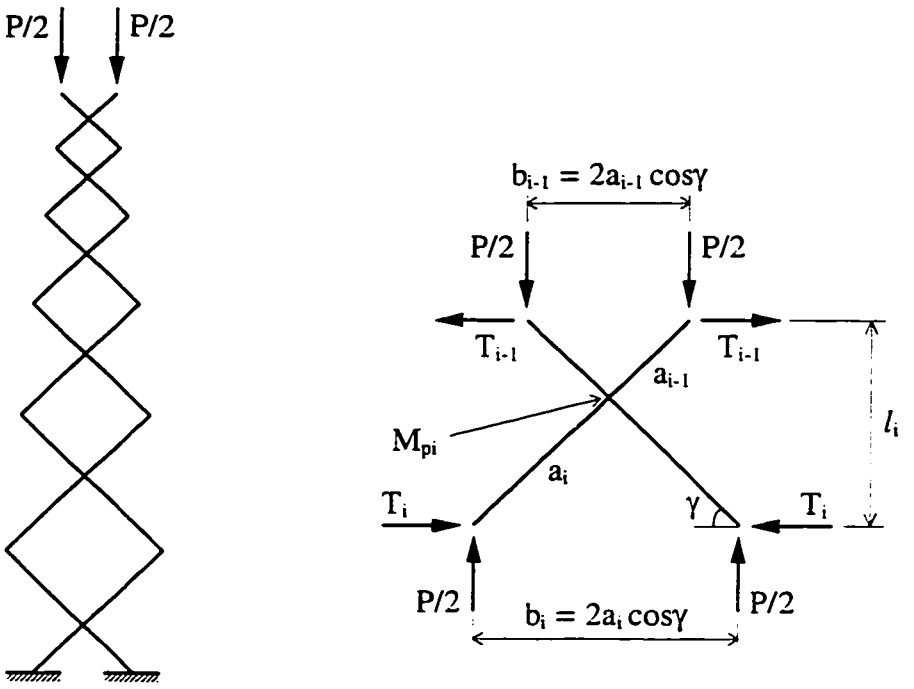

Figure 2.32: Non-uniform pantographic column under axial load and forces applied to a typical unit.

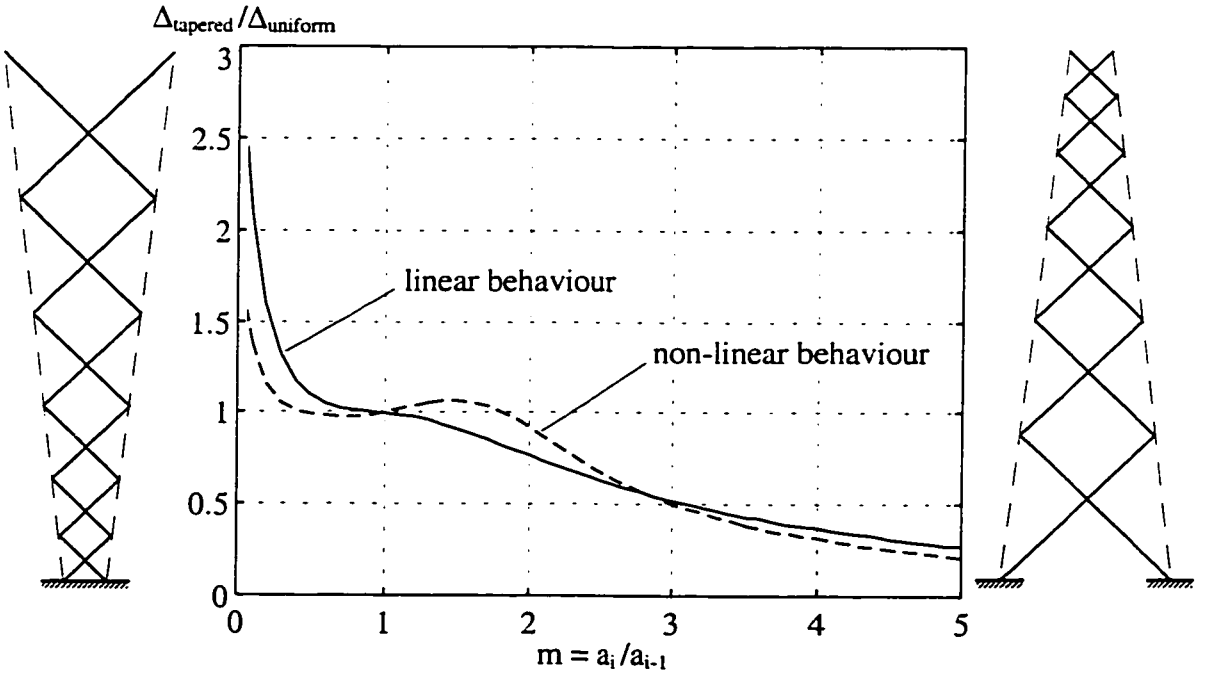

Figure 2.33: Relative deflections of linear (lateral and axial loads) and non-linear (axial load only) tapered pantographic columns versus the degree of tapering.

the degree of deployment, clamped at the ground level. For m greater than one, the column is more narrow at the top, and deflections decrease as m grows.

Let us look at what happens when m goes to infinity. The deflections of the tapered column approach zero, i.e. we get an infinitely stiff structure. What is the physical meaning of this? In a tapered column with a large value of m, the lower portion of the bottom unit would constitute the most of the structure's length regardless of the number of units in the column. As m grows, quite soon the pantographic column is transformed essentially into a two member truss. Since the assumption of zero axial deformation of bars in pantographic units was used in the problem formulation, this truss is, of course, infinitely rigid.

2.5.2 Non-Linear Behaviour; Axial Loading

The source of geometric non-linearity in the behaviour of a uniform pantographic column under axial loading was described in detail in Section 2.3.1. In the case of a non-uniform column the origin of this phenomenon is the same: it is caused by the finite rotations of bars in a unit due to the deformations of the part of the column below it. The internal forces are to be found for a deformed configuration of the structure, when the degrees of deployment for all units are different. A typical unit from the axially loaded non-linear deployable column is shown in Fig. 2.34. The degree of deployment of this unit after rotation of bars and the horizontal forces applied to the nodes are unknown. The change in the unit height consists of the part due to rotation of bars caused by change in the unit base (the distance between the bottom nodes) and the part due to bending of bars, which further multiplies the effect of the bar rotations for the units above. Eqs 2.39 and 2.41 modified for the non-uniform column system:

$$T_i = T_{i-1}\frac{a_{i-1}}{a_i} + \frac{P}{2}\cot\gamma_i\left(1+\frac{a_{i-1}}{a_i}\right)$$

$$\cos\gamma_{i-1} = \cos\gamma_i + \sin^2\gamma_i \frac{a_{i-1}(a_{i-1}+a_i)}{3EI}\left(T_{i-1}+\frac{P}{2}\cot\gamma_i\right) \quad , \quad i = 1, 2, ..., n, \qquad (2.78)$$

together with the boundary conditions, $T_0 = 0$ and $\gamma_n = \gamma$, after being solved iteratively, yield the forces and deformations in the non-linear column with the prescribed accuracy. The possibility of a snap-through buckling of the top unit is also present here.

The dashed line in the plot of Fig. 2.33 shows the deflection ratio versus the degree of tapering for non-linear columns at a load level of 90% of the snap-through load for the uniform column. Qualitatively, this dependence is similar to that for the linear case (solid line) with marginal gain in stiffness for the values of m between 0.6 and 1. Again, for large values of m, the internal forces become primarily axial ones in the lower portion of the bottom unit, and deflection approaches zero.

Fig. 2.35 shows the m-dependence of the snap-through buckling axial load and the corresponding deflection of tapered columns relative to those of a uniform column. For m less than one (column is wider at the top), both the buckling load and the deflection grow as m decreases. For m greater than one (column is wider at the bottom), the snap-through load reaches its minimum at m = 1.8. The trend for snap-through deflection resembles that seen in Fig. 2.33 for large values of m.

2.6 Conclusions

The behaviour of a uniform pantographic column subjected to lateral, moment and axial loadings is considered in this Chapter. Assuming linear behaviour, the deflection for each load type is obtained as a function of the geometric parameters of the structure and the stiffness parameters of its components. The overall bending and axial stiffnesses of the

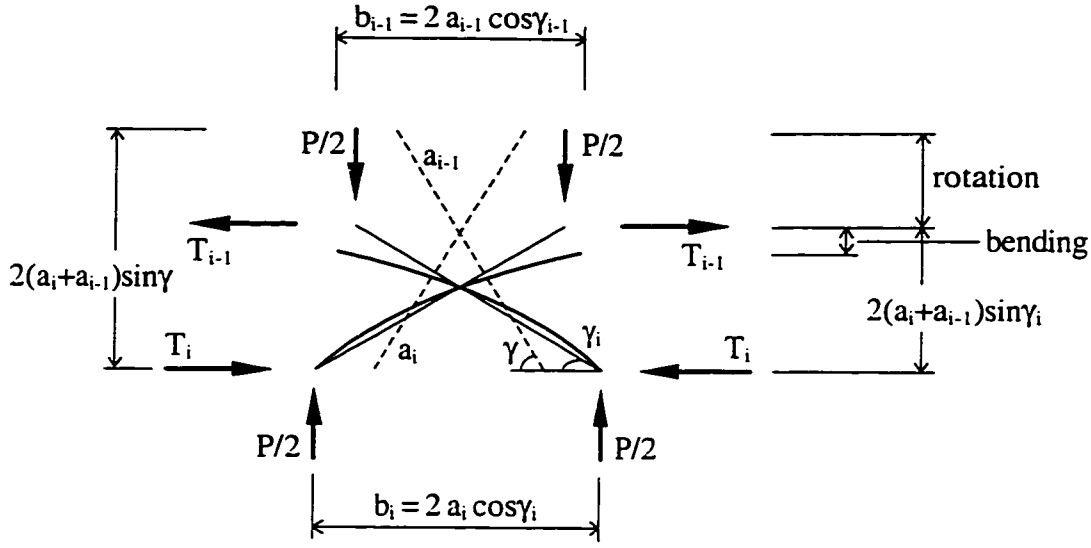

Figure 2.34: Three configurations of pantographic unit in non-uniform non-linear column under axial loading: initial - dashed line, "after rotation" - thin solid line, final - thick solid line.

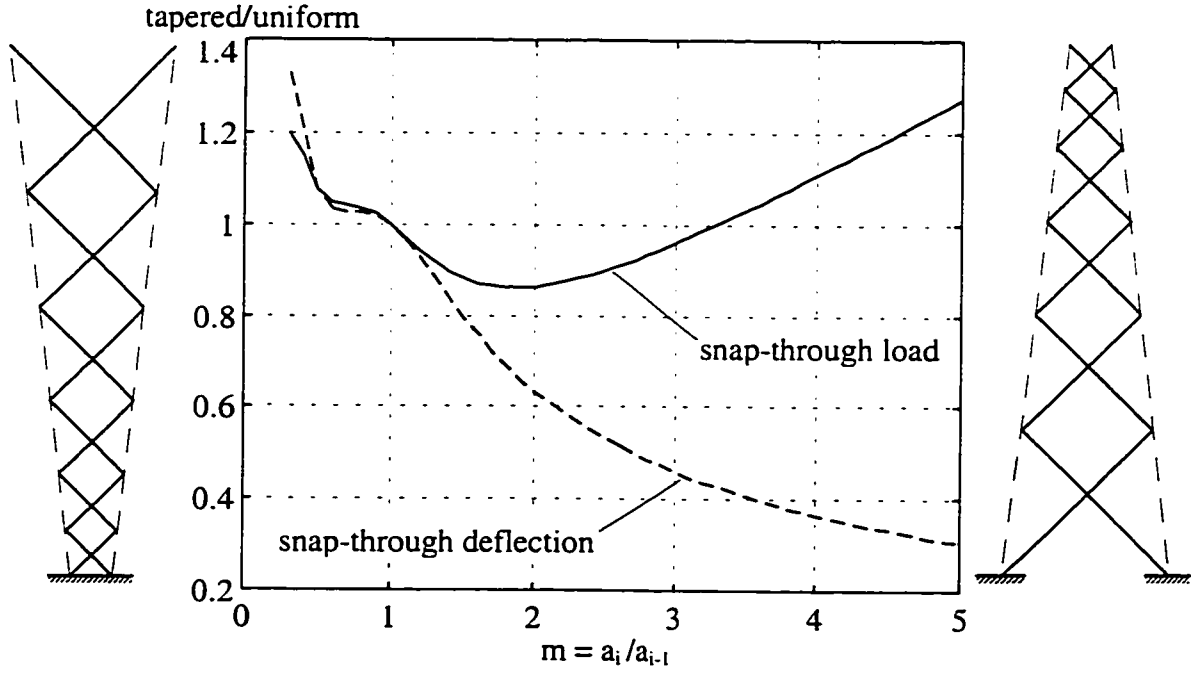

Figure 2.35: Relative snap-through load and deflection of tapered non-linear column subjected to axial load versus the degree of tapering.

deployable column are derived by equating its deflections to those of a uniform solid column of the same length. It is found that under certain assumptions the behaviour of the pantographic column in bending resembles very closely that of the solid column. However, under axial load, the distribution of internal forces and deformations along the deployable structure differs qualitatively from the distribution of stresses and strains in its solid counterpart.

The results of linear analyses of pantographic deployable columns under axial load suggest that, even for small bending deformations of bars in pantographic units, finite rotations of bars about the pivotal connections in the units and hinges at unit interfaces cause the phenomenon of geometric non-linearity to play a significant part in the column behaviour. For the purpose of non-linear analysis, the equilibrium equations are written for each unit in its intermediate configuration and supplemented with the compatibility equations and boundary conditions for forces and deformations. This highly non-linear system of equations is solved iteratively for a specified value of the load. The results of the non-linear analyses show that the bulk of the unit height change, and therefore bulk of the overall vertical deformation of a column, indeed comes from the rotations of bars in the units, not from their bending. The equilibrium paths for axially loaded columns, obtained by the "load-controlled" approach, reveal the possibility of stability loss in the form of snap-through buckling of the top unit. To trace both the ascending and the descending parts of the equilibrium path a "displacement-controlled" approach is used.

Columns with an additional constraint between the two nodes at a particular unit interface are also considered. It is shown that the analysis of a restrained column comes down to analyzing the various parts of the structure by the above procedures, with slight modifications depending on the number of pantographic units (even or odd) between the link and the ground. The constraint location that yields the greatest increase of the axial stiffness is found to be at one third of the column length from the top.

The procedure for calculating the buckling load of a uniform pantographic column is presented. This procedure incorporates the effect of geometric non-linearity exhibited by the column under axial loading. For stability analysis the pantographic structure is substituted by a stiffnesswise equivalent composite model having fewer degrees of freedom. The parameters of the model are determined on the basis of the deformed configuration of the original structure. Orthogonality of rotations and vertical deformations of the elements of the composite column at the point of buckling is employed in calculating the buckling load.

The columns analyzed for the buckling load are restrained, i.e. a rigid link is introduced between the top nodes. This does not affect the procedure, but it increases the axial stiffness and postpones the phenomenon of the local snap through buckling. For constant height and degree of deployment, the buckling load increases with the number of units in the column. For constant height and number of units, it is found that for a certain degree of deployment the buckling load is minimized. When the number of units and dimensions of the bars are constant the buckling load decreases as the column deploys.

The behaviour of non-uniform pantographic columns under moment, lateral and axial loads is also considered. Closed form expressions for equivalent bending and axial stiffnesses are obtained for linearly behaving columns whose shapes are tapered uniformly. The corresponding non-linear results for axially loaded tapered columns are obtained numerically. The results indicate that in the practical range of the degree of tapering the stiffness properties of the pantographic column are not very sensitive to changes in the value of this parameter.

Chapter 3

Three-Dimensional Columns

3.1 Introduction

In the previous Chapter a planar pantographic column was analyzed for different load conditions. However, structures in our three-dimensional world are usually also three-dimensional. This Chapter discusses the behaviour of spatial pantographic columns. The columns considered here have square and triangular "cross-sections". A column consists of a number of three-dimensional pantographic units, stacked on top of each other (Fig. 3.1). The sides of a unit are identical SLEs with a pivot connection at the midpoint of the bars. Hence, the top view ("cross-section") of the unit and of the column is a square or an equilateral triangle. The ends of the bars are assumed to be connected through spherical hinges that allow free relative rotations about three axes. The pivot connections between the bars in SLEs are revolute joints allowing free relative rotation of the bars only in the plane of SLEs. The bottom nodes of the column are hinged to the ground. The bending stiffness of the bars is taken the same in plane and out of plane of the SLEs, and axial deformations of the bars are neglected. As before, the length of each bar is denoted by 2a, its bending stiffness is EI, the degree of deployment is given by angle γ between the axis of the bar and the horizontal plane, and the total number of units in the column is n.

The analysis of the response of the columns to the load is limited to their linear behaviour in this Chapter. It can be expected that the stiffness characteristics of three-dimensional columns are very closely related to those of planar columns. Because of the four-fold symmetry of square columns and the three-fold symmetry of triangular columns under the axial load equally distributed between the top nodes of a column, their linear response is the direct superposition of that of the four, or three, two-dimensional columns which form the sides of the spatial structure. In bending, however, the manner in which the planar columns contribute to the response of the structure is not quite obvious. The cases presented here are: square and triangular columns in bending and square columns subjected to lateral load. Remarks on some possible arrangements of three-dimensional columns into deployable slabs are given in a separate Section.

3.2 Pantographic Column of Square Cross-Section under Moment Load

In this Section, a three-dimensional pantographic deployable column with square cross-section and subjected to a moment load at the top is considered (Fig. 3.1). The moment load is represented by two force couples applied to the top nodes of the column. The goal is to obtain the overall equivalent bending stiffness of the structure, i.e. the bending stiffness of a solid column of the same length which would exhibit the same displacement under the same loading. This characteristic was derived for a two-dimensional pantographic column in the previous Chapter and was found to be $6EI\sin\gamma$.

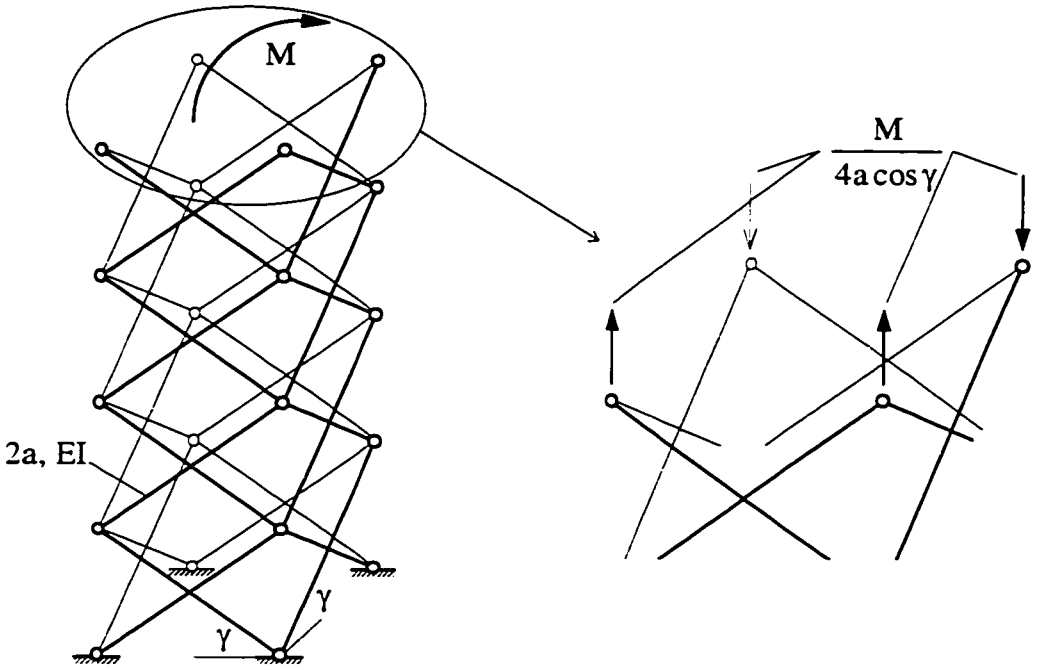

(a) - 3d view

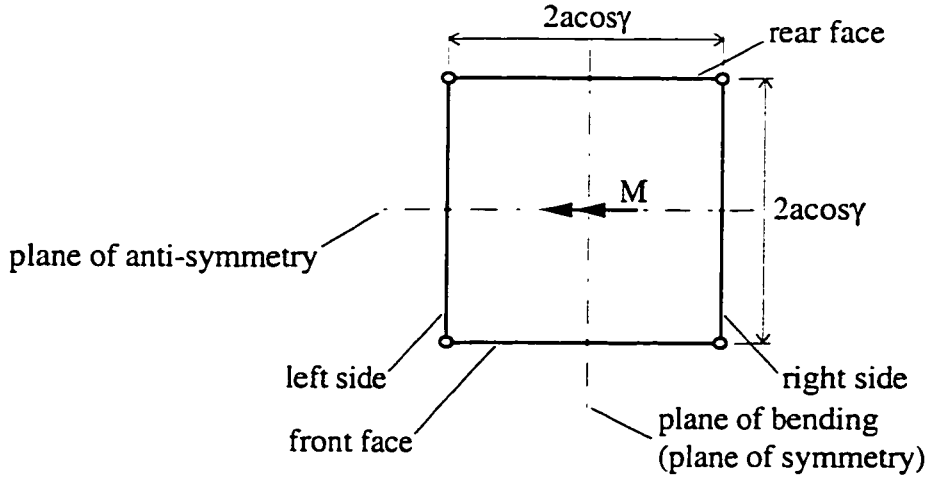

(b) - top view

Figure 3.1: Three-dimensional pantographic column of square cross-section subjected to moment loading.

3.2.1 Analysis of a Single Unit by the Force Method

3.2.1.1 Load and Support Conditions, Symmetry Considerations

We start by considering a single three-dimensional square pantographic unit taken out of the column subjected to moment load (Fig. 3.2). The portion of the column above this unit transfers the load applied to the top of the structure to the top nodes of the unit by means of forces applied to the four top nodes of the unit. Each of these forces has, in general, three components parallel to the coordinate axes. The unit, as well as the whole structure and the load, has certain symmetry properties that can be utilized in the analysis to reduce the number of unknowns. The vertical plane of bending (xOz) is the plane of symmetry and the vertical plane perpendicular to it (yOz) is the plane of anti-symmetry (skew-symmetry). Now, instead of twelve unknown forces acting on the top nodes of the unit there are only three.

The four vertical forces all have the same magnitude. The two vertical forces acting on the front nodes are both upward in this case, and the two vertical forces acting on the rear nodes are downward. The opposites of these four forces, applied to the bottom nodes of the portion of the column above the unit, are the only forces that could resist the external moment applied at the top of the column. Therefore their values must be $M/4a\cos\gamma$ each as shown in Fig. 3.2a. Hence, the vertical forces at all unit interfaces are the same as those at the top of the column.

The x-components of all four forces must have the same magnitude and direction due to the two-fold symmetry described above. Then, their opposites applied to the upper portion of the column should sum up to a horizontal force in the x-direction which is not balanced by anything else. The only way to avoid this violation of force equilibrium in the

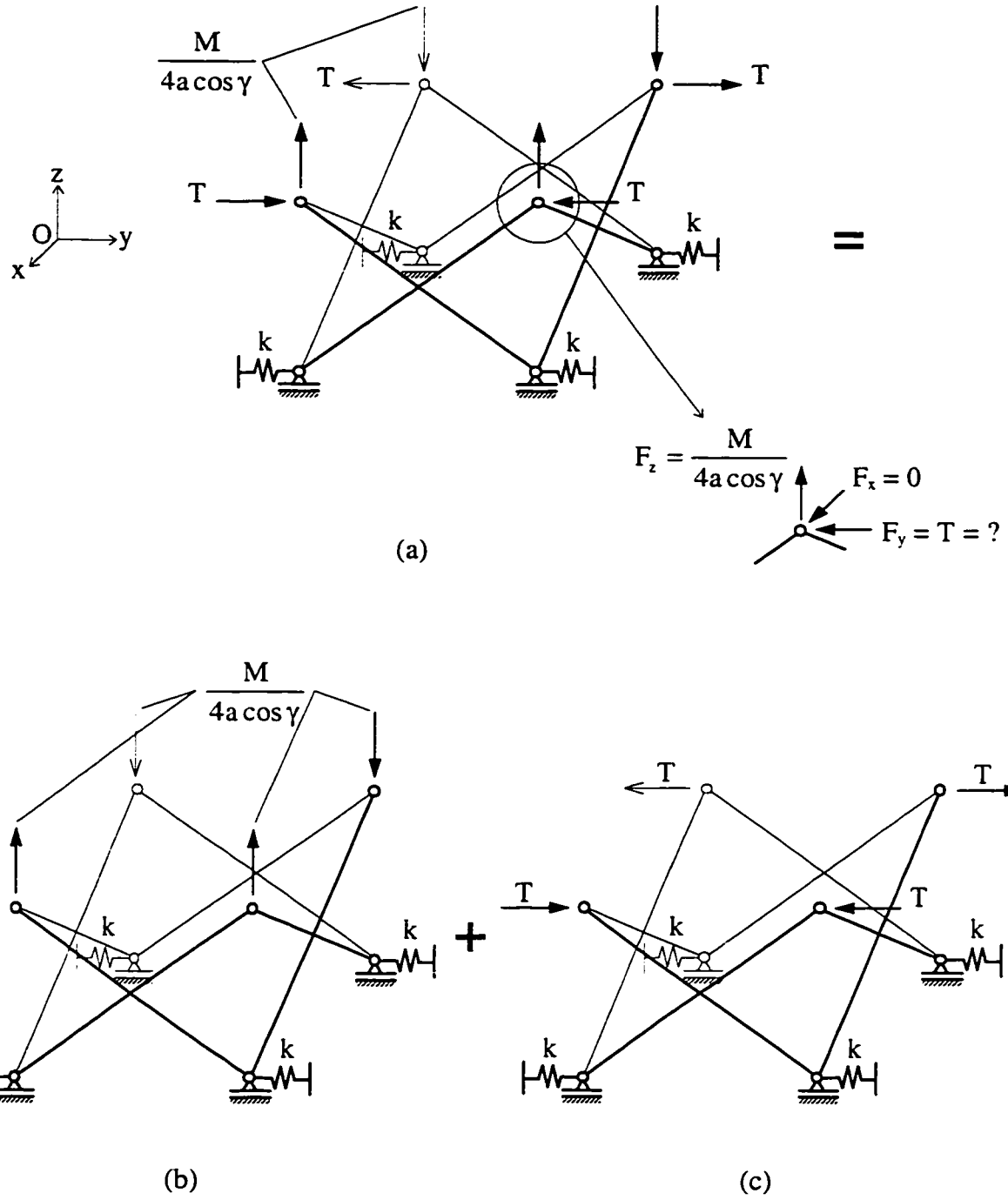

Figure 3.2: Single three-dimensional square pantographic unit from the column subjected to moment loading (a) under vertical (b) and horizontal (c) forces applied at the top nodes and the bottom node supports with finite stiffness in horizontal direction.

x-direction is to have each of these four forces equal to zero. Hence, there are no horizontal forces in the x-direction at any unit interface.

The y-components of the forces at the nodes again all have the same magnitude, and their directions must be as shown in Fig. 3.2a up to the sign of all of them. The value of T, however, is unknown at the moment.

The unit is supported by the portion of the column below it. The bottom nodes of the unit cannot be considered hinged to a rigid foundation (except for the lowest unit in the column) since the lower portion of the column provides only finite resistance. To account for this, we support the bottom nodes of the unit with four horizontal springs of equal but yet unknown stiffness k in the direction perpendicular to the plane of bending (in the y-direction). After the analysis of the unit with springs is done, all possible situations can be obtained by varying the spring stiffnesses between zero and infinity. Strictly speaking, the stiffness of the supports in the vertical direction is also finite. However, the vertical reactions are known for all units and are the same as the external forces at the top of the column, and the vertical displacements of the two front nodes are the same as, but opposite to, the vertical displacements of the two rear nodes. Therefore, the finite vertical stiffness of the supports would only produce a rigid body motion of the unit. Thus, making the supports rigid in the vertical direction we simply eliminate this displacement component and do not affect the state of internal forces in the bars of the unit. A similar argument can be applied for the supports in the direction parallel to the plane of bending (in the x-direction).

Since the behaviour of the pantographic column is assumed to be linear, we can consider separately the effects of vertical and horizontal forces applied to the unit (Fig. 3.2b and c), and superimpose the internal forces in the bars of the unit afterwards.

3.2.1.2 Primary Structure, Compatibility Equations

A square pantographic unit includes eight bars. In three dimensional space each of these bars has six degrees of freedom as a rigid body. Therefore, there are a total of 48 degrees of freedom for eight unconstrained bars "floating" in space. Each spherical hinge connection between two bars as well as each hinge support eliminates three degrees of freedom. There are eight such connections and four such supports; the number of constraints introduced is 36. Four pivot connections (revolute joints) in scissor-like elements impose five constraints each. The total number of constraints is, therefore, 56. The pantographic unit is $56 - 48 = 8$ times statically indeterminate.

It is relatively easy to analyze a two-dimensional SLE if the forces applied to its nodes are known. The four sides of the three-dimensional square pantographic unit are such two-dimensional elements. The two SLEs perpendicular to the plane of bending will be called "front and rear faces"; the two SLEs parallel to the plane of bending will be called "left and right sides". We will cut these four SLEs apart at the top nodes of the unit and use the procedure of the force method to find the forces acting at the cuts (Fig. 3.3). The four cuts at the hinges introduce twelve translational releases in the eight times indeterminate structure. Therefore, the primary structure must be four times underconstrained. The four degrees of freedom introduced are the rotations of the four planar SLEs about the axes through their bottom nodes. Thus, we are going to use a geometrically unstable primary structure in the force method of analysis of the pantographic unit, which is somewhat unconventional but still possible with carefully chosen redundant forces.

The twelve unknown force components corresponding to the releases are reduced to three unknowns in this twice symmetrical system. The unknown forces are denoted by x_1, x_2 and x_3 in the directions of the z-, y- and x-axes, respectively. The symmetry of the problem allows us to make one more conclusion at this point. It can be seen from Fig.

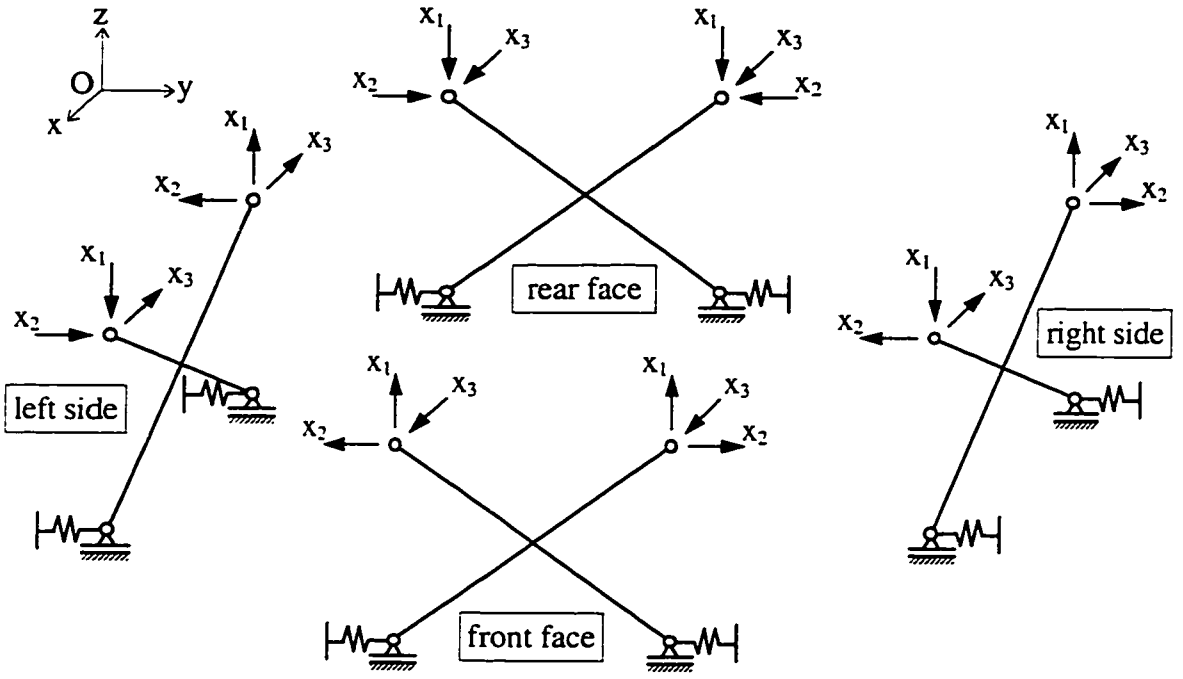

Figure 3.3: Unknown forces at SLE connections of three-dimensional square unit with two-fold symmetry: symmetric about xOz plane and anti-symmetric about yOz plane; ($x_3 = 0$).

3.3, that for the equilibrium of the front and rear faces of the unit the unknown x_3 has to be zero. Hence, only two unknowns x_1 and x_2 are left, and they can be found from the compatibility equations of the force method:

$$\begin{aligned} \delta_{11}x_1 + \delta_{12}x_2 + \Delta_1 = 0 \\ \delta_{21}x_1 + \delta_{22}x_2 + \Delta_2 = 0 \end{aligned} \qquad (3.1)$$

Fig. 3.4 shows the internal forces in the separated SLEs and the supporting springs due to the two unknowns. Only the front face and right side SLEs are shown. The flexibility coefficients of the force method can be found through the principle of virtual work. The bending moment diagrams along the bars are triangular, with zeros at the bar

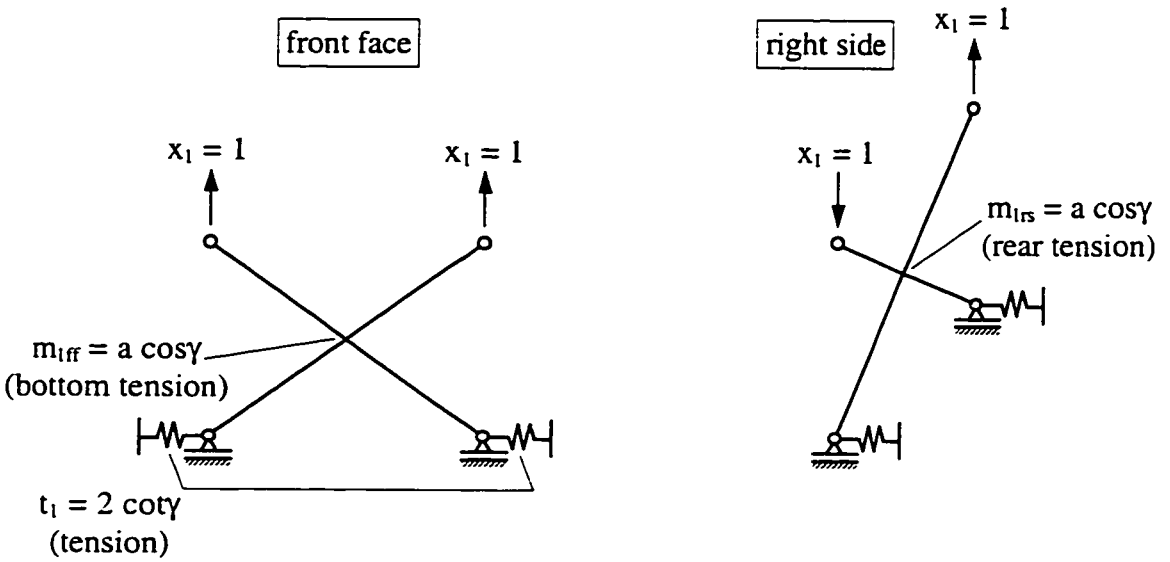

(a)

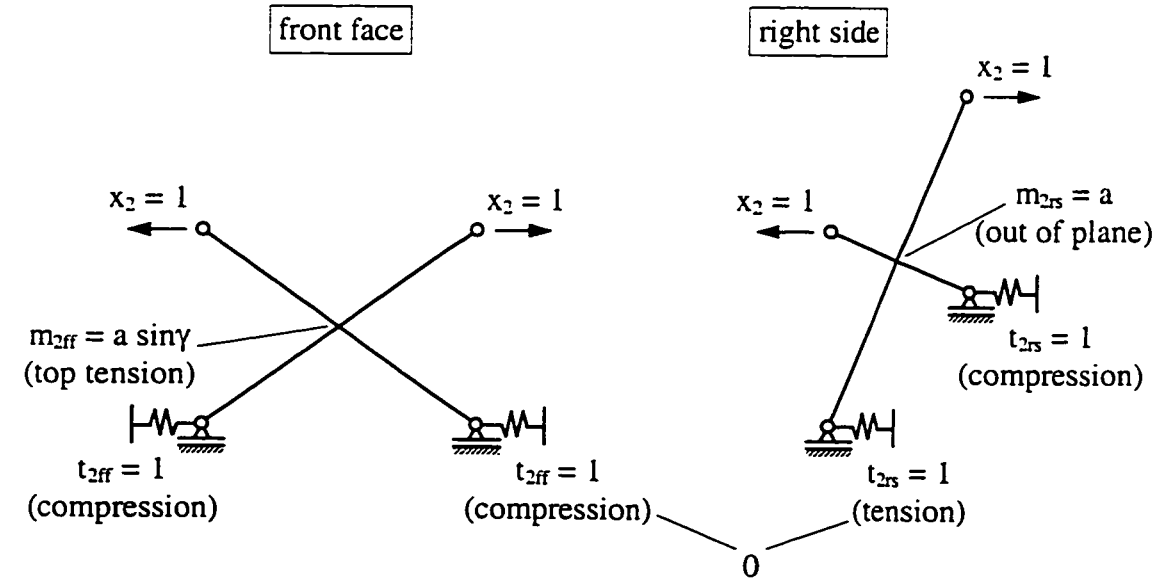

(b)

Figure 3.4: Internal forces in the primary structure of a single three-dimensional square pantographic unit due to $x_1 = 1$ (a) and $x_2 = 1$ (b).

ends and maxima at the pivots. These maximum moments are shown in Fig. 3.4. For such moment functions, the virtual work of bending moments on bending deformations can be readily calculated as described in Appendix A. The virtual work due to spring forces and spring deformations must also be included.

The total relative vertical displacement of the cut hinges due to $x_1 = 1$:

$$\delta_{11} = \frac{1}{EI}\frac{a\cos\gamma}{2}\frac{a}{3}\frac{2}{3}a\cos\gamma\cdot 4\cdot 4 + 2\cot\gamma\frac{2\cot\gamma}{k}\cdot 4 = \frac{16\,a^3\cos^2\gamma}{3\,EI} + \frac{16}{k}\frac{\cos^2\gamma}{\sin^2\gamma} \tag{3.2}$$

The total relative horizontal displacement of the cut hinges due to $x_2 = 1$:

$$\delta_{22} = \frac{1}{EI}\left(\frac{a\sin\gamma}{2}\frac{a}{3}\frac{2}{3}a\sin\gamma\cdot 4\cdot 2 + \frac{a\cdot a}{2}\frac{2}{3}a\cdot 4\cdot 2\right) = \frac{8\,a^3}{3\,EI}\left(1+\sin^2\gamma\right) \tag{3.3}$$

The cross-coefficients are:

$$\delta_{12} = \delta_{21} = -\frac{1}{EI}\frac{a\cos\gamma}{2}\frac{a}{3}\frac{2}{3}a\sin\gamma\cdot 4\cdot 2 = -\frac{8\,a^3\sin\gamma\cos\gamma}{3\,EI} \tag{3.4}$$

3.2.1.3 Moment Loading of a Single Unit (Vertical Forces)

The first external load applied to the unit are the four vertical forces corresponding to the moment loading. The internal forces in the primary structure are shown in Fig. 3.5. Since in the original unit the external forces are applied at the nodes which are cut, we are free to apply the forces to either side of the cuts in the primary structure. This would affect the values of x_1 and x_2, but would change neither the final bending moments in the bars nor the spring forces. In this analysis it was chosen to load the side SLEs of the primary structure of the unit and leave the faces unstressed.

The load coefficients, i.e. the displacements in the primary structure in the direction of unknown forces due to the external load, are:

$$\Delta_1 = -\frac{1}{EI}\frac{a\cos\gamma}{2}\frac{a}{3}\frac{2}{4}\frac{M}{}\cdot 4\cdot 2 = -\frac{2\,M\,a^2\cos\gamma}{3\,EI}, \quad \Delta_2 = 0 \tag{3.5}$$

The compatibility equations now become:

$$\begin{aligned}\left(\frac{16\,a^3\cos^2\gamma}{3\,EI}+\frac{16}{k}\frac{\cos^2\gamma}{\sin^2\gamma}\right)x_1-\frac{8\,a^3\sin\gamma\cos\gamma}{3\,EI}x_2&=\frac{2\,M\,a^2\cos\gamma}{3\,EI}\\ -\frac{8\,a^3\sin\gamma\cos\gamma}{3\,EI}x_1+\frac{8\,a^3}{3\,EI}\left(1+\sin^2\gamma\right)x_2&=0\end{aligned}\quad, \tag{3.6}$$

from which x_1 and x_2 are found:

$$\begin{aligned}x_1&=\frac{M}{4\,a\cos\gamma}\frac{K\sin^2\gamma\left(1+\sin^2\gamma\right)}{K\sin^2\gamma\left(2+\sin^2\gamma\right)+2\left(1+\sin^2\gamma\right)}\\ x_2&=\frac{M}{4\,a}\frac{K\sin^3\gamma}{K\sin^2\gamma\left(2+\sin^2\gamma\right)+2\left(1+\sin^2\gamma\right)}\end{aligned}\quad, \tag{3.7}$$

where $K = k\,a^3/(3\,EI)$ is the non-dimensional spring stiffness. The bending moments at the pivots of the bars in the front face are:

$$M_{ff}=m_{1ff}x_1+m_{2ff}x_2=\frac{M}{4}\frac{K\sin^2\gamma}{K\sin^2\gamma\left(2+\sin^2\gamma\right)+2\left(1+\sin^2\gamma\right)}\,(\text{bottom tension}), \tag{3.8}$$

the in-plane bending moments at the pivots of the bars in the side are:

$$M_{rs}^{in}=m_{0rs}+m_{1rs}x_1=\frac{M}{4}\frac{K\sin^2\gamma+2\left(1+\sin^2\gamma\right)}{K\sin^2\gamma\left(2+\sin^2\gamma\right)+2\left(1+\sin^2\gamma\right)}\,(\text{front tension}), \tag{3.9}$$

the out-of-plane bending moments at the pivots of the bars in the side are:

$$M_{rs}^{out}=m_{2rs}x_2=\frac{M}{4}\frac{K\sin^3\gamma}{K\sin^2\gamma\left(2+\sin^2\gamma\right)+2\left(1+\sin^2\gamma\right)} \tag{3.10}$$

The force in the right front spring is:

$$t=t_1x_1=\frac{M}{2a}\frac{K\sin\gamma\left(1+\sin^2\gamma\right)}{K\sin^2\gamma\left(2+\sin^2\gamma\right)+2\left(1+\sin^2\gamma\right)}\,(\text{tension}) \tag{3.11}$$

From the last six equations it is shown that when the bottom nodes of the unit are hinged to the ground, i.e. the springs are infinitely rigid, the values of the unknown forces become:

$$x_1 = \frac{M}{4\,a\cos\gamma}\,\frac{1+\sin^2\gamma}{2+\sin^2\gamma}, \quad x_2 = \frac{M}{4\,a}\,\frac{\sin\gamma}{2+\sin^2\gamma}, \tag{3.12}$$

and the bending moments and spring force are:

$$M_{rs}^{in} = \frac{M}{4}\,\frac{1}{2+\sin^2\gamma}, \quad M_{rs}^{out} = \frac{M}{4}\,\frac{\sin\gamma}{2+\sin^2\gamma},$$
$$M_{ff} = \frac{M}{4}\,\frac{1}{2+\sin^2\gamma}, \quad t = \frac{M}{2a\sin\gamma}\,\frac{1+\sin^2\gamma}{2+\sin^2\gamma} \tag{3.13}$$

If the bottom nodes are not supported in the horizontal direction, i.e. the spring stiffness is zero, both x_1 and x_2 are equal to zero as well as bending moments in the face bars, out-of-plane bending moments in the side bars and the spring forces. The load is therefore entirely resisted by the in-plane bending of the sides, with the pivotal moments in their bars equal to M/4. The bars in the SLEs of the faces rotate about the pivots without bending to fit the new location of the nodes.

3.2.1.4 Unit Loaded with Two Self-Balanced Horizontal Couples

The next case of loading of a single pantographic unit consists of the four horizontal forces shown in Figs 3.2c and 3.6. The load coefficients in this case are:

$$\Delta_1 = \frac{T}{k}2\cot\gamma\cdot 4 = \frac{8\,T}{k}\cot\gamma, \quad \Delta_2 = \frac{1}{EI}\,\frac{a\,T\,a}{2}\,\frac{2}{3}a\cdot 4\cdot 2 = \frac{8\,T\,a^3}{3\,EI} \tag{3.14}$$

The compatibility equations with the corresponding right sides:

$$\left(\frac{16\,a^3\cos^2\gamma}{3\,EI} + \frac{16}{k}\,\frac{\cos^2\gamma}{\sin^2\gamma}\right)x_1 - \frac{8\,a^3\sin\gamma\cos\gamma}{3\,EI}x_2 = -\frac{8\,T}{k}\,\frac{\cos\gamma}{\sin\gamma}$$
$$-\frac{8\,a^3\sin\gamma\cos\gamma}{3\,EI}x_1 + \frac{8\,a^3}{3\,EI}\left(1+\sin^2\gamma\right)x_2 = -\frac{8\,T\,a^3}{3\,EI} \tag{3.15}$$

yield the following expressions for the unknowns:

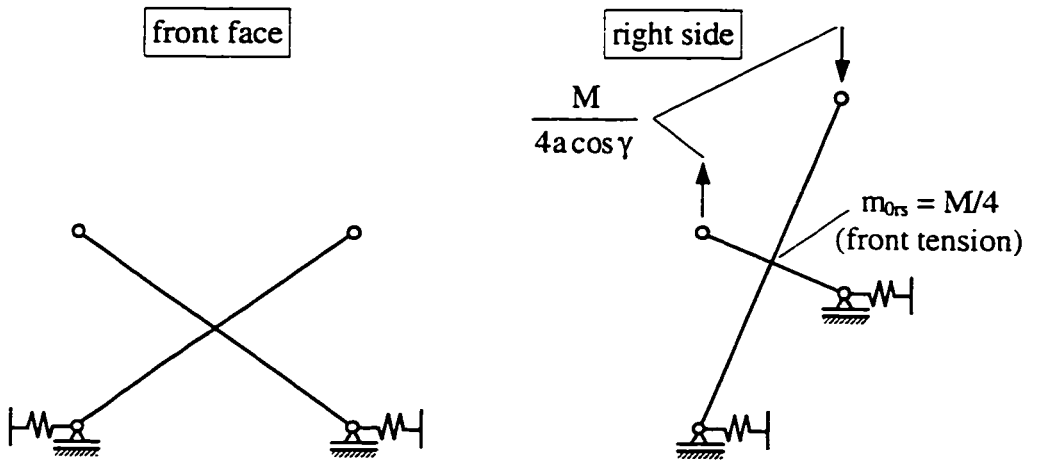

Figure 3.5: Internal forces in the primary structure of a single three-dimensional square pantographic unit due to vertical forces corresponding to moment loading.

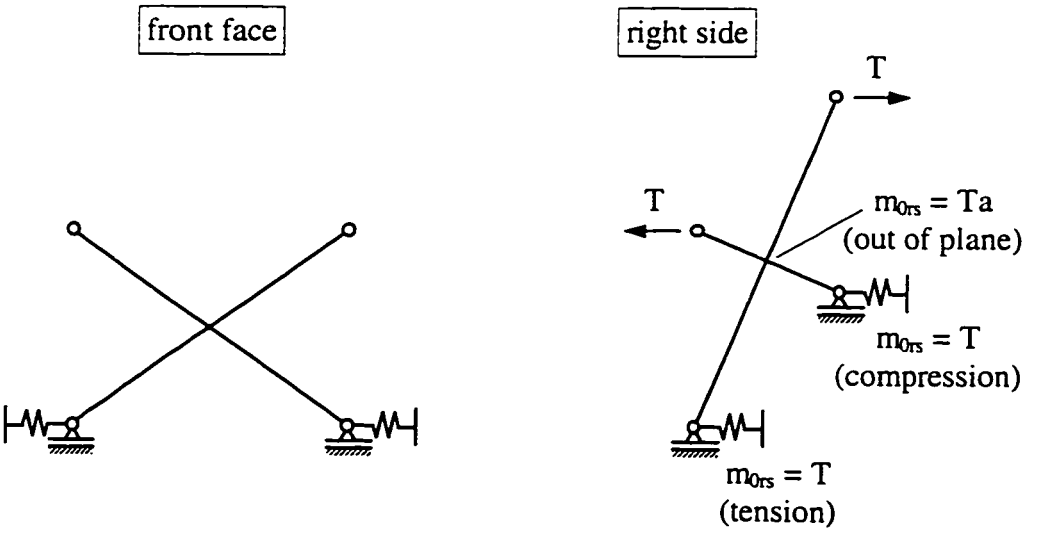

Figure 3.6: Internal forces in the primary structure of a single three-dimensional square pantographic unit due to horizontal forces corresponding to moment loading.

$$x_1 = -T\frac{\sin\gamma}{\cos\gamma}\frac{K\sin^2\gamma+\left(1+\sin^2\gamma\right)}{K\sin^2\gamma\left(2+\sin^2\gamma\right)+2\left(1+\sin^2\gamma\right)}$$
$$x_2 = -T\frac{K\,2\sin^2\gamma+\left(2+\sin^2\gamma\right)}{K\sin^2\gamma\left(2+\sin^2\gamma\right)+2\left(1+\sin^2\gamma\right)} \qquad (3.16)$$

For these values of x_1 and x_2 the pivotal bending moments and the spring force can be found:

$$M_{ff} = T\,a\sin\gamma\,\frac{K\sin^2\gamma+1}{K\sin^2\gamma\left(2+\sin^2\gamma\right)+2\left(1+\sin^2\gamma\right)}\ (\text{bottom tension}) \qquad (3.17)$$

$$M_{rs}^{in} = T\,a\sin\gamma\,\frac{K\sin^2\gamma+\left(1+\sin^2\gamma\right)}{K\sin^2\gamma\left(2+\sin^2\gamma\right)+2\left(1+\sin^2\gamma\right)}\ (\text{front tension}) \qquad (3.18)$$

$$M_{rs}^{out} = T\,a\sin^2\gamma\,\frac{K\sin^2\gamma+1}{K\sin^2\gamma\left(2+\sin^2\gamma\right)+2\left(1+\sin^2\gamma\right)} \qquad (3.19)$$

$$t = T\,\frac{K\sin^4\gamma}{K\sin^2\gamma\left(2+\sin^2\gamma\right)+2\left(1+\sin^2\gamma\right)}\ (\text{tension}) \qquad (3.20)$$

When K goes to infinity (rigid supports instead of springs):

$$x_1 = -\frac{T\tan\gamma}{2+\sin^2\gamma},\quad x_2 = -\frac{2\,T}{2+\sin^2\gamma} \qquad (3.21)$$

$$M_{ff} = \frac{T\,a\sin\gamma}{2+\sin^2\gamma},\quad M_{rs}^{in} = \frac{T\,a\sin\gamma}{2+\sin^2\gamma},\quad M_{rs}^{out} = \frac{T\,a\sin^2\gamma}{2+\sin^2\gamma},\quad t = \frac{T\sin^2\gamma}{2+\sin^2\gamma}, \qquad (3.22)$$

and if K is zero (no support in horizontal direction):

$$x_1 = -\frac{T\tan\gamma}{2},\quad x_2 = -T\frac{2+\sin^2\gamma}{2\left(1+\sin^2\gamma\right)} \qquad (3.23)$$

$$M_{ff} = \frac{T\,a\sin\gamma}{2\left(1+\sin^2\gamma\right)},\quad M_{rs}^{in} = \frac{T\,a\sin\gamma}{2},\quad M_{rs}^{out} = \frac{T\,a\sin^2\gamma}{2\left(1+\sin^2\gamma\right)},\quad t = 0 \qquad (3.24)$$

3.2.2 Constrained Pantographic Unit

3.2.2.1 External Loading

Knowing the internal force distribution in the pantographic unit one can find the horizontal displacements of its top nodes in both load cases studied in the previous two Sections. A virtual unit load can be applied to the primary structure. This virtual load will be four unit forces in the directions of T in Fig. 3.6. The total horizontal displacement of the four top nodes due to the loading of Fig. 3.2b is (the first term is the part of the virtual work due to out-of-plane bending of bars in the side SLEs, the second term is the virtual work due to deformation of the springs):

$$h_M = \frac{1}{EI}\frac{M}{4}\frac{K\sin^3\gamma}{K\sin^2\gamma\left(2+\sin^2\gamma\right)+2\left(1+\sin^2\gamma\right)}\frac{a}{2}\frac{2}{3}a\cdot 4\cdot 2 + \frac{M}{2a}\frac{K\sin\gamma\left(1+\sin^2\gamma\right)}{K\sin^2\gamma\left(2+\sin^2\gamma\right)+2\left(1+\sin^2\gamma\right)}\frac{1}{k}\cdot 1\cdot 4 = \frac{2M\sin\gamma}{a}\frac{a^3}{3EI}\frac{K\sin^2\gamma+1+\sin^2\gamma}{K\sin^2\gamma\left(2+\sin^2\gamma\right)+2\left(1+\sin^2\gamma\right)} \tag{3.25}$$

The total horizontal displacement caused by the four horizontal forces in Fig. 3.2c is:

$$h_T = \frac{1}{EI}T\,a\sin^2\gamma\frac{K\sin^2\gamma+1}{K\sin^2\gamma\left(2+\sin^2\gamma\right)+2\left(1+\sin^2\gamma\right)}\frac{a}{2}\frac{2}{3}a\cdot 4\cdot 2 + T\frac{K\sin^4\gamma}{K\sin^2\gamma\left(2+\sin^2\gamma\right)+2\left(1+\sin^2\gamma\right)}\frac{1}{k}\cdot 1\cdot 4 = 4\,T\sin^2\gamma\frac{a^3}{3EI}\frac{2K\sin^2\gamma+2+\sin^2\gamma}{K\sin^2\gamma\left(2+\sin^2\gamma\right)+2\left(1+\sin^2\gamma\right)} \tag{3.26}$$

Now it is possible to find the horizontal forces (Fig. 3.2c) that are needed to eliminate the horizontal displacements of the top nodes of the unit caused by the vertical forces (Fig. 3.2b):

$$h_T = -h_M \quad \rightarrow \quad T = -\frac{M}{2\,a\sin\gamma}\frac{K\sin^2\gamma+1+\sin^2\gamma}{2K\sin^2\gamma+2+\sin^2\gamma} \tag{3.27}$$

If the bottom nodes of the unit are hinged to the foundation (rigid supports in the horizontal direction instead of springs):

$$T = -\frac{M}{4\,a \sin\gamma} \tag{3.28}$$

The latter situation represents a unit with all nodes restricted against horizontal movement and subjected to the four vertical forces corresponding to the moment loading (Fig. 3.7a). In this case, because of symmetry, the horizontal reactions of the bottom supports are expected to be of the same value as the horizontal forces applied to the top nodes, which can be verified by combining the expressions for t from eqs 3.13 and 3.22:

$$t = \frac{M}{2a\sin\gamma}\frac{1+\sin^2\gamma}{2+\sin^2\gamma} - \frac{M}{4a\sin\gamma}\frac{\sin^2\gamma}{2+\sin^2\gamma} = \frac{M}{4a\sin\gamma} \text{ (tension in the right front "spring")} \tag{3.29}$$

The pivotal bending moments in a such unit can also be obtained from eqs 3.13 and 3.22. All moments are equal to zero, therefore there are only axial forces in the bars of SLEs of the constrained pantographic unit under moment loading.

3.2.2.2 Stiffness in the Direction of Constraints

The stiffness of the unit in Fig. 3.7a in the direction of horizontal constraints can be found from eq. 3.26. If K goes to infinity, then for unit displacement of each of the top nodes we have:

$$1 = T\frac{a^3}{3\,EI}\frac{2\sin^2\gamma}{2+\sin^2\gamma} \quad \rightarrow \quad T = \frac{3\,EI}{a^3}\frac{2+\sin^2\gamma}{2\sin^2\gamma} \tag{3.30}$$

The pivotal bending moments as well as the reactions at the bottom nodes in this case can be found from eqs 3.22 and 3.30:

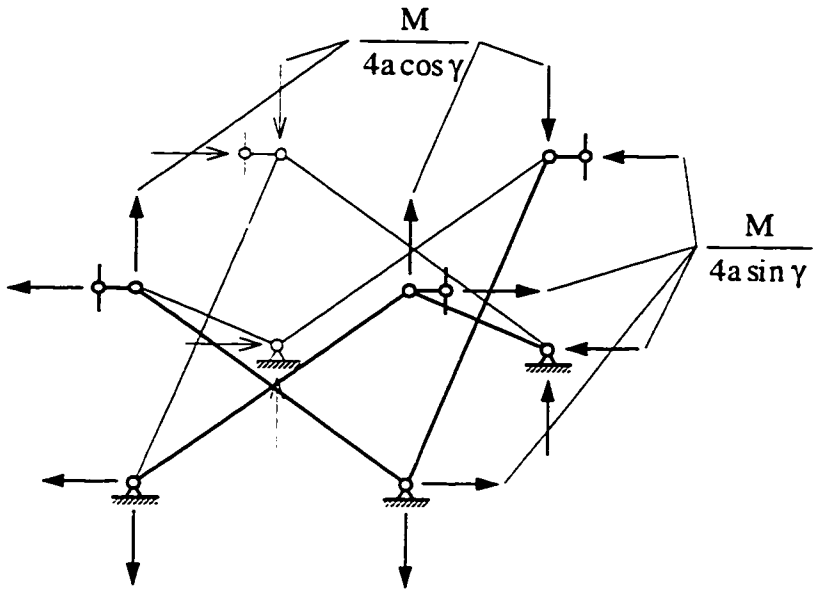

(a)

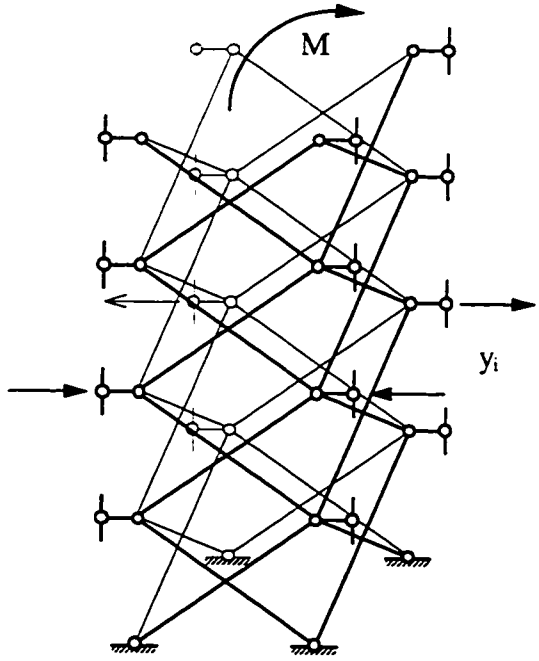

(b)

Figure 3.7: Constrained pantographic unit (a) and primary structure of the column (b) for the analysis by the displacement method.

$$M_{ff} = T\frac{a\sin\gamma}{2+\sin^2\gamma} = \frac{3EI}{a^3}\frac{2+\sin^2\gamma}{2\sin^2\gamma}\frac{a\sin\gamma}{2+\sin^2\gamma} = \frac{3EI}{2a^2\sin\gamma} \text{ (bottom tension)}$$

$$M_{rs}^{in} = T\frac{a\sin\gamma}{2+\sin^2\gamma} = \frac{3EI}{a^3}\frac{2+\sin^2\gamma}{2\sin^2\gamma}\frac{a\sin\gamma}{2+\sin^2\gamma} = \frac{3EI}{2a^2\sin\gamma} \text{ (front tension)} \qquad (3.31)$$

$$M_{rs}^{out} = T\frac{a\sin^2\gamma}{2+\sin^2\gamma} = \frac{3EI}{a^3}\frac{2+\sin^2\gamma}{2\sin^2\gamma}\frac{a\sin^2\gamma}{2+\sin^2\gamma} = \frac{3EI}{2a^2}$$

$$t = T\frac{\sin^2\gamma}{2+\sin^2\gamma} = \frac{3EI}{a^3}\frac{2+\sin^2\gamma}{2\sin^2\gamma}\frac{\sin^2\gamma}{2+\sin^2\gamma} = \frac{3EI}{2a^3} \text{ (direction opposite to T)}$$

3.2.3 Analysis of the Column by the Displacement Method

3.2.3.1 Stiffness Matrix and Load Vector

The pantographic unit that has been considered so far can now be used in the displacement analysis of the whole column. The constrained primary structure of the pantographic column used in the displacement method is shown in Fig. 3.7b. The constraints against horizontal displacements are introduced at the top of the structure and at each unit interface. The four links at each level are considered as one constraint since the relative values and directions of the displacements they prevent are known from the symmetry conditions. The total number of constraints and unknown displacements is equal to the number of units in the column, n, and they are numbered from the top to the bottom of the column. The positive directions of the displacements y_i and the reactions in the constraints are as shown in Fig. 3.7b. To solve the system of equilibrium equations

$$\mathbf{K}\,\mathbf{y} + \mathbf{P} = \mathbf{0} \qquad (3.32)$$

we need to obtain the stiffness matrix **K** and the load vector **P**.

The entries of the stiffness matrix k_{ij} are the reactions in the constraint number i due to unit displacement number j. Since the four links at a particular level are treated as a single constraint, the value of k_{ij} is equal to the sum of the four forces in the links. As is

often the case for the structures with one dimension much larger than the other two, the stiffness matrix in this problem is narrow banded. In fact, it is tri-diagonal, because the displacement of any constraint causes reactions only at the two neighbouring ones. From eq. 3.30, the reaction at the constraint at the top of the column due to its unit displacement is

$$k_{11} = \frac{6\,EI}{a^3}\,\frac{2+\sin^2\gamma}{\sin^2\gamma} \tag{3.33}$$

The reactions at the rest of the constraints, due to their own unit displacements, are twice this value because the resistance at the unit interfaces is provided by the two units above and below the displaced constraint:

$$k_{ii} = \frac{12\,EI}{a^3}\,\frac{2+\sin^2\gamma}{\sin^2\gamma}, \quad i = 2,\ldots,n \tag{3.34}$$

The entries of the stiffness matrix located off the main diagonal are found from eq. 3.31:

$$k_{ij} = -\frac{6\,EI}{a^3}, \quad |i-j| = 1 \tag{3.35}$$

The entries in the load vector, which are the reactions in the constraints due to the external load, are found from eqs 3.28 and 3.29. In the constrained structure subjected to moment loading all pantographic units behave identically as shown in Fig. 3.7a. The reaction in the first constraint at the top of the structure is:

$$p_1 = -\frac{M}{a\sin\gamma} \tag{3.36}$$

The reactions in the rest of the constraints are twice this value:

$$p_i = -\frac{2\,M}{a\sin\gamma}, \quad i = 2,\ldots,n \tag{3.37}$$

With the entries of the stiffness matrix and the load vector from eqs 3.33 through 3.37, eq. 3.32 becomes:

$$\begin{bmatrix} \frac{6\,EI}{a^3}\frac{2+\sin^2\gamma}{\sin^2\gamma} & -\frac{6\,EI}{a^3} & & \\ -\frac{6\,EI}{a^3} & \frac{12\,EI}{a^3}\frac{2+\sin^2\gamma}{\sin^2\gamma} & -\frac{6\,EI}{a^3} & \\ & \cdots & & \\ & -\frac{6\,EI}{a^3} & \frac{12\,EI}{a^3}\frac{2+\sin^2\gamma}{\sin^2\gamma} & \end{bmatrix} y = \begin{bmatrix} \frac{M}{a\sin\gamma} \\ \frac{2\,M}{a\sin\gamma} \\ \cdots \\ \frac{2\,M}{a\sin\gamma} \end{bmatrix} \tag{3.38}$$

Using the following notations:

$$A = \frac{2+\sin^2\gamma}{\sin^2\gamma}, \quad B = \frac{M}{a\sin\gamma}\frac{a^3}{6\,EI} = \frac{M\,a^2}{6\,EI\sin\gamma}, \tag{3.39}$$

system of equations 3.38 can be rewritten in a more compact form:

$$\begin{bmatrix} A & -1 & & & 0 \\ -1 & 2A & -1 & & \\ & & \cdots & & \\ & & -1 & 2A & -1 \\ 0 & & & -1 & 2A \end{bmatrix} y = \begin{bmatrix} B \\ 2B \\ \cdots \\ 2B \\ 2B \end{bmatrix} \tag{3.40}$$

If the modified stiffness matrix and right-side vector are denoted $\mathbf{K_m}$ and $\mathbf{P_m}$, respectively, system 3.40 becomes:

$$\mathbf{K_m}\, y = \mathbf{P_m} \tag{3.41}$$

3.2.3.2 Solution of the System of Equilibrium Equations

3.2.3.2.1 Uniform Solution

Upon inspection of system 3.40, one may notice that it would be very easy to solve if it was just a little different. Namely, if there was A instead of 2A in the lower right corner of matrix $\mathbf{K_m}$ and B instead of 2B for the last entry of vector $\mathbf{P_m}$, then the system would look like:

$$\begin{bmatrix} A & -1 & & & 0 \\ -1 & 2A & -1 & & \\ & & \cdots & & \\ & & -1 & 2A & -1 \\ 0 & & & -1 & A \end{bmatrix} \mathbf{y} = \begin{bmatrix} B \\ 2B \\ \cdots \\ 2B \\ B \end{bmatrix}, \tag{3.42}$$

and the almost obvious solution vector would have all entries the same and equal to:

$$y_i^u = \frac{B}{A-1} = \frac{M a^2 \sin\gamma}{12\,EI}, \quad i = 1,\ldots,n \tag{3.43}$$

We will call this solution "uniform", hence the superscript. Also, the matrix and the right-side vector in eq. 3.42 will be called $\mathbf{K}_m^u$ and $\mathbf{P}_m^u$, respectively. Let us discuss the physical meaning of system 3.42, the displacement vector $\mathbf{y}^u$ and the internal forces corresponding to them.

Suppose we had a column with the bottom nodes supported by rollers, not by hinges, in the direction perpendicular to the plane of bending (Fig. 3.8). Then at the beginning of the procedure of the displacement method we would put the horizontal constraints at the top of the structure, at each unit interface *and* at the bottom. The stiffness coefficient of the bottom constraint and the reaction in this constraint due to the external load on the restrained primary structure would be exactly the same as those for the top constraint. The last of the equilibrium equations would be similar to the first. Of course, the number of unknown displacements would increase by one, so would the dimensions of the stiffness matrix and the load vector, but this is not of great importance because in all previous derivations we operated with an arbitrary dimension of the problem. The resulting system of equations would look exactly as eq. 3.42, the solution of which (eq. 3.43) we already found. Thus, we had the solution, and we were able to formulate the structural problem corresponding to it.

The internal forces acting in the bars of pantographic units of such a deformed column can be found from eqs 3.31 and 3.43. The pivotal bending moments in the bars

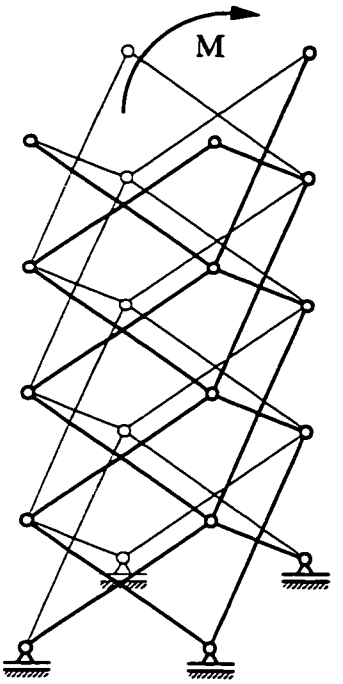

Figure 3.8: Uniformly bent pantographic column - bottom nodes are free to move in the horizontal direction normal to the plane of bending.

due to the external load on the constrained primary structure are zero. These moments due to the displacement of the top nodes y_i^u are:

$$M_{ff} = \frac{3\,EI}{2\,a^2 \sin\gamma}\,\frac{M\,a^2 \sin\gamma}{12\,EI} = \frac{M}{8}, \quad M_{rs}^{in-plane} = \frac{M}{8}, \quad M_{rs}^{out-of-plane} = \frac{M}{8}\sin\gamma \tag{3.44}$$

For the same displacement of the bottom nodes of the unit, y_{i+1}^u, because of the mirror symmetry of the top and bottom nodal displacements about the horizontal plane through the pivots of four SLEs, the pivotal bending moments have the same magnitudes, but the moments in the face bars and out-of-plane moments in the sides are opposite to those in eq. 3.44, and therefore sum up to zero. For the same reason of symmetry, the in-plane moments in the bars of side SLEs due to y_i^u and y_{i+1}^u act in the same direction, making the resulting bending moment equal to M/4. One may notice that all units in the pantographic

column, which is "unconstrained" at the bottom and subjected to moment load, behave in exactly the same manner as a single unit which has supports at the bottom nodes with zero stiffness in the direction normal to the plane of bending (Section 3.2.1.3).

This result indicates the following. In a square cross-section pantographic column in bending, when its bottom nodes are free to move in the direction perpendicular to the plane of bending, the external load is distributed equally between the two-dimensional columns that form the sides of the three-dimensional column parallel to the plane of bending. The two sides perpendicular to the plane of bending are free of stress. The equivalent bending stiffness of the three-dimensional column therefore is twice the equivalent bending stiffness of one of its sides in the plane of this side: $2(6EI\sin\gamma) = 12EI\sin\gamma$. This is true for the case when the plane of bending is parallel to a pair of the sides of the square cross-section.

The above conclusion can also be justified intuitively if we try to distribute the load among the two-dimensional pantographic columns, that form the sides of the three-dimensional structure in Fig. 3.8, and consider them separately. Again, the sides parallel to the plane of bending have a certain stiffness against the moment load. The two sides perpendicular to the plane of bending (which we called front and rear faces) would have to resist tension (front face) and compression (rear face). However, if the bottom nodes of a two-dimensional pantographic column are supported by rollers in the plane of the column, such plane structure is essentially a mechanism with regard to axial loading and offers no resistance to it. Moreover, when the sides parallel to the plane of bending deform, the distances between the front nodes of all SLEs in these sides increase and the distances between the rear nodes decrease by the same amount. The faces will readily comply with these displacements by opening (front face) or closing (rear face) all SLEs in them without inducing any deformations (bending or axial) in the bars.

3.2.3.2.2 Local Solution

Now, let us remind the reader that the solution obtained and discussed in the previous section is not the complete solution of the original system 3.40, but only satisfies the system 3.42. We will call the difference between the actual solution vector $\mathbf{y}$ and the uniform solution $\mathbf{y}^u$ the "local" solution $\mathbf{y}^{loc}$; the meaning of the name will become clear shortly. Similar differences for the matrix and the right-side vector are denoted by $\mathbf{K}_m^{loc}$ and $\mathbf{P}_m^{loc}$, respectively:

$$\mathbf{y} = \mathbf{y}^u + \mathbf{y}^{loc}, \quad \mathbf{K}_m = \mathbf{K}_m^u + \mathbf{K}_m^{loc}, \quad \mathbf{P}_m = \mathbf{P}_m^u + \mathbf{P}_m^{loc} \tag{3.45}$$

Eq. 3.41 may now be written in the following form:

$$\left(\mathbf{K}_m^u + \mathbf{K}_m^{loc}\right)\left(\mathbf{y}^u + \mathbf{y}^{loc}\right) = \mathbf{P}_m^u + \mathbf{P}_m^{loc} \tag{3.46}$$

Partially expanding the left side of the last equation we obtain:

$$\mathbf{K}_m^u\,\mathbf{y}^u + \mathbf{K}_m^{loc}\,\mathbf{y}^u + \mathbf{K}_m\,\mathbf{y}^{loc} = \mathbf{P}_m^u + \mathbf{P}_m^{loc} \tag{3.47}$$

The first terms on the left and right sides of eq. 3.47 constitute eq. 3.42 and can be taken out. Eq. 3.47 becomes:

$\mathbf{K}_m^{loc}\,\mathbf{y}^u + \mathbf{K}_m\,\mathbf{y}^{loc} = \mathbf{P}_m^{loc}$, or

$$\begin{bmatrix} 0 & 0 & & & 0 \\ 0 & 0 & 0 & & \\ & & \cdots & & \\ & & 0 & 0 & 0 \\ 0 & & & 0 & A \end{bmatrix} \mathbf{y}^u + \begin{bmatrix} A & -1 & & & 0 \\ -1 & 2A & -1 & & \\ & & \cdots & & \\ & & -1 & 2A & -1 \\ 0 & & & -1 & 2A \end{bmatrix} \mathbf{y}^{loc} = \begin{bmatrix} 0 \\ 0 \\ \cdots \\ 0 \\ B \end{bmatrix} \tag{3.48}$$

Since vector $\mathbf{y}^u$ is already known (eq. 3.43), the first term on the left of eq. 3.48 can be moved to the right:

$$\begin{bmatrix} A & -1 & & & 0 \\ -1 & 2A & -1 & & \\ & & \cdots & & \\ & & -1 & 2A & -1 \\ 0 & & & -1 & 2A \end{bmatrix} \mathbf{y}^{loc} = \begin{bmatrix} 0 \\ 0 \\ \cdots \\ 0 \\ -B/(A-1) \end{bmatrix} \tag{3.49}$$

The question now is what structural problem is described by the last system. The matrix on the left side is the same as the one in the original equation (eqs 3.40 and 3.41), therefore the structure is the original pantographic column with the bottom nodes hinged to the ground. The right vector consists of zeros except for the last entry, therefore the external load only causes a reaction in the lowest constraint (the constraint between the first and second units from the bottom of the column - units number n and n-1). Such external load may be represented by four horizontal forces as shown in Fig. 3.9.

Since all but the last entries of the right side vector are equal to zero, we can try to eliminate the unknowns y_i^{loc} from the system starting from the first equation and proceeding down. Using the first equation we express the first component of the vector through the second:

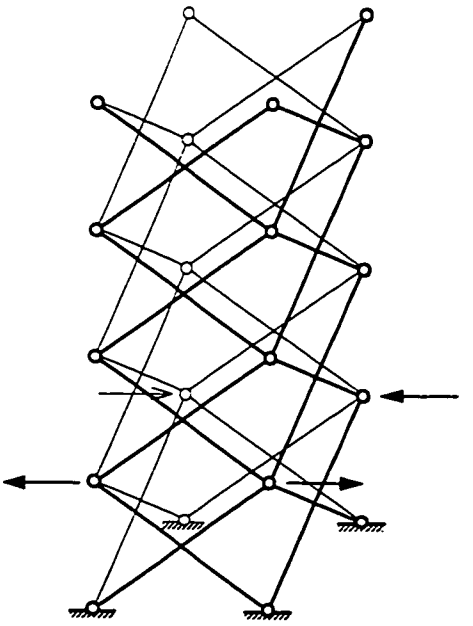

Figure 3.9: Pantographic column subjected to local load - two self-balanced horizontal couples.

$$y_1^{loc} = \frac{y_2^{loc}}{A} \; ; \tag{3.50}$$

then using this result in the second equation we express the second component through the third:

$$-\frac{y_2^{loc}}{A} + 2Ay_2^{loc} - y_3^{loc} = 0 \quad \rightarrow \quad y_2^{loc} = \frac{1}{2A - \frac{1}{A}} y_3^{loc} \; ; \tag{3.51}$$

and after the next step:

$$-\frac{1}{2A - \frac{1}{A}} y_3^{loc} + 2Ay_3^{loc} - y_4^{loc} = 0 \quad \rightarrow \quad y_3^{loc} = \frac{1}{2A - \frac{1}{2A - \frac{1}{A}}} y_4^{loc} \tag{3.52}$$

the pattern becomes clear. As soon as it is recognized, the relation between any two successive components of the yet unknown solution vector can be written in the following form:

$$y_i^{loc} = C_i y_{i+1}^{loc}, \quad \text{where} \quad C_i = \frac{1}{2A - \frac{1}{2A - \cdots}} \quad \text{or} \quad C_i = \frac{1}{2A - C_{i-1}} \tag{3.53}$$

One may notice that the first expression for C_i in eq. 3.53 is a type of *continued fraction*. It was shown by Olds (1963), that such a continued fraction is convergent for i going to infinity as long as we can find the limit. Suppose that the limit exists, then for large i it can be assumed that $C_i = C_{i-1}$. Using this condition in the last expression of eq. 3.53 and dropping the subscript we obtain:

$$C = \frac{1}{2A - C} \quad \rightarrow \quad C^2 - 2AC + 1 = 0 \quad \rightarrow \quad C = A \pm \sqrt{A^2 - 1} \tag{3.54}$$

The only condition for the existence of this limit is that the absolute value of A must be greater than one, which is guaranteed, since the lowest value A can take is three (eq. 3.39). It can be seen from eqs 3.50 through 3.52 that in this case the relevant root is the one with a minus in front of the square root. The value of C, therefore, is a positive number less than unity. If the expression for A from eq. 3.39 is substituted into the last equation, the expression for C in terms of degree of deployment is obtained:

$$C = A - \sqrt{A^2 - 1} = \frac{\left(\sqrt{1+\sin^2\gamma} - 1\right)^2}{\sin^2\gamma}, \tag{3.55}$$

and plotted in Fig. 3.10.

The existence, far enough from the top of the vector, of a practically constant proportionality between the neighbouring vector entries, means that when, in the process of eliminating unknowns, we arrive at the last equation with the non-zero right side, the last two entries of the solution vector are related by $y_{n-1}^{loc} = C\, y_n^{loc}$, and the value of y_n^{loc} is readily obtained:

$$-C\, y_n^{loc} + 2A y_n^{loc} = -\frac{B}{A-1} \quad \rightarrow \quad y_n^{loc} = -\frac{B}{(A-1)(2A-C)} \tag{3.56}$$

To get an idea of how long the column should be (or rather how many pantographic units it should have) for C_i to settle down to C, let us consider for example a column with degree of deployment equal to 45°. Then A is equal to 5, and as i grows C_i approaches C which is equal to 0.10102. The first several values of C_i are:

$$C_1 = 0.2, \quad C_2 = 0.10204, \quad C_3 = 0.10103, \quad C_4 = 0.10102, \quad \ldots \tag{3.57}$$

The difference between the exact C_2 and C is only one per cent, therefore even for a column consisting of only three units eq. 3.56 is valid.

The expression for y_n^{loc} in terms of the parameters of the structure and the load may be obtained by combining eqs 3.39, 3.55 and 3.56:

$$y_n^{loc} = -B\frac{A - \sqrt{A^2-1}}{A-1} = -\frac{M a^2}{12\, EI \sin\gamma}\left(\sqrt{1+\sin^2\gamma} - 1\right)^2 \tag{3.58}$$

The rest of the solution vector entries can be found one by one using eq. 3.53. For the most part of the column, where C_i equals C, these entries form a decreasing geometric progression. For the above example of $\gamma = 45°$ their values decrease very rapidly. Thus it is safe to say that units only a few unit heights above the load would feel practically

nothing. This is the reason why we called this solution "local". This result is reminiscent of Saint Venant's principle. The load shown in Fig. 3.9 consists of four self-equilibrated forces applied locally; therefore it is statically equivalent to a zero load. According to the principle, such loading affects the stress distribution only in its local neighbourhood, leaving the stresses in the rest of the structure practically unchanged. In our case, the local solution will introduce noticeable changes in the internal force distribution only in the pantographic unit at the bottom of the column and in one or two units above it. In the rest of the units the uniform solution found before will solely describe the column response to the load.

The greatest pivotal bending moments corresponding to the local solution alone occur in the bars of the lowest unit. They are found from eqs 3.31 and 3.58

$$M_{ff} = \frac{3\,EI}{2\,a^2 \sin\gamma}\,\frac{M\,a^2}{12\,EI\sin\gamma}\left(\sqrt{1+\sin^2\gamma}-1\right)^2 = \frac{M}{8\sin^2\gamma}\left(\sqrt{1+\sin^2\gamma}-1\right)^2$$

$$M_{rs}^{in} = \frac{M}{8\sin^2\gamma}\left(\sqrt{1+\sin^2\gamma}-1\right)^2 \qquad (3.59)$$

$$M_{rs}^{out} = \frac{M}{8\sin\gamma}\left(\sqrt{1+\sin^2\gamma}-1\right)^2$$

For $\gamma = 45°$ these moments constitute approximately five per cent of the pivotal moments in the bars of side SLEs from the uniform solution.

3.2.3.2.3 Superposition of Uniform and Local Solutions

The general expression for an element of the final solution vector **y** is the sum of the corresponding entries from uniform $\mathbf{y}^u$ and local $\mathbf{y}^{loc}$ solution vectors (eqs 3.43 and 3.56):

$$y_i = y_i^u + y_n^{loc}\,C^{n-i} = \frac{B}{A-1}\left(1-\frac{C^{n-i}}{2A-C}\right), \quad i = 1,\ldots,n \qquad (3.60)$$

The bending moments in the bars of pantographic unit number i are defined by y_i and y_{i+1}, with $y_{n+1} = 0$. The in-plane moments in the bars of side SLEs in terms of these displacements are (eqs 3.31, 3.39 and 3.60):

$$M^{in}_{rs,i} = \frac{3\,EI}{2\,a^2 \sin\gamma}(y_i + y_{i+1}) = \frac{M}{4}\left[1 - \frac{(1+C)C^{n-i}}{2(2A-C)C}\right], \quad i = 1,\ldots,n-1$$
$$M^{in}_{rs,n} = \frac{3\,EI}{2\,a^2 \sin\gamma}\,y_n = \frac{M}{8}\left[1 - \frac{1}{2A-C}\right] \tag{3.61}$$

If a unit virtual moment is applied to the primary structure of the column, obtained by separating the four planar columns, in such way that the moment is equally divided between the left and right sides, then the pivotal bending moments in all side SLEs are 1/4. The total rotation of the top column can be calculated as:

$$\varphi = \frac{1}{EI}\sum_{i=1}^{n} M^{in}_{rs,i}\,\frac{a}{2}\,\frac{2}{3}\,\frac{1}{4}\cdot 4\cdot 2 = \frac{Ma}{6EI}\left[n - \frac{1}{2} - \frac{1}{2(2A-C)} - \frac{1+C}{2(2A-C)C}\sum_{i=1}^{n-1} C^{n-i}\right] \tag{3.62}$$

The first term in brackets in the last equation corresponds to the uniform solution. As was pointed out before, the equivalent bending stiffness, calculated on the basis of this part of the resulting rotation, is twice that of the side planar columns. The sum in the last term of eq. 3.62 is practically constant for n greater than three. Therefore the second, third and fourth terms do not depend on the number of units in the column. If A is expressed through C from eq. 3.54, eq. 3.62 can be simplified to the form:

$$\varphi = \frac{Ma}{6EI}\left[n - \frac{1}{2}\,\frac{1+C}{1-C}\right] \tag{3.63}$$

Comparison of the value of the second term in brackets in the last equation (Fig. 3.11) with the number of units in the column gives a good indication of the overall stiffening effect of the hinge supports at the bottom of the column.

For columns with a sufficiently large number of units the local effect near the bottom of the column can be neglected and the uniform solution alone can be used to describe the behaviour of the structure. The equivalent bending stiffness of a three-dimensional column of square cross-section therefore equals $12EI\sin\gamma$.

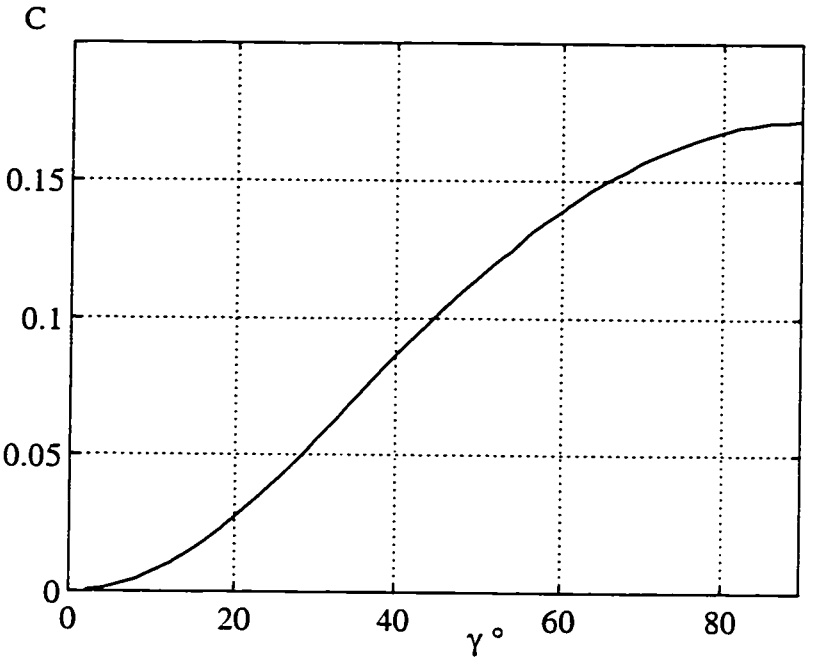

Figure 3.10: Proportionality coefficient between the neighbouring entries of the local solution vector for a square pantographic column versus the degree of deployment.

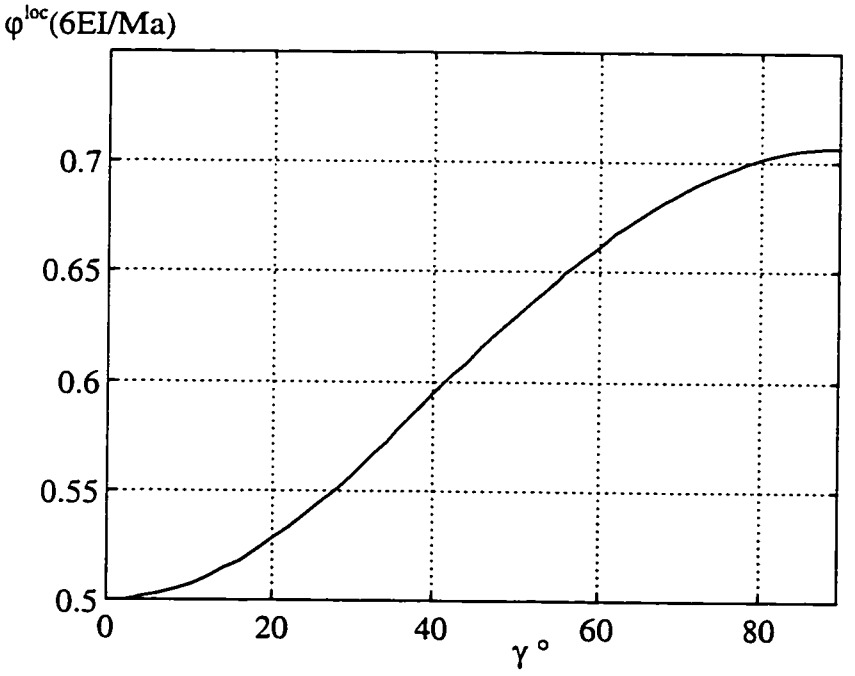

Figure 3.11: Local part of the tip rotation of a square pantographic column subjected to moment load versus degree of deployment (compare with n).

The reason for the relatively small difference between the column behaviour described by the uniform solution alone and the sum of the uniform and local solutions becomes more apparent once the stiffness characteristics of a two-dimensional pantographic column are known. If a solid column of hollow square section is subjected to bending, its sides parallel to the plane of bending would be bent in their plane, and the sides perpendicular to the plane of bending would primarily be stretched and compressed, thus contributing their axial stiffness to the bending stiffness of the column. The two-dimensional pantographic column, while having a fixed equivalent bending stiffness, $(EI)_e = 6EI\sin\gamma$, similar to a solid column, has an equivalent axial stiffness which is inversely proportional to the squared length, $(EA)_e = 18EI\sin\gamma\tan^2\gamma/L^2$, for sufficiently large number of units. Therefore, for a long column, the contribution of the stretched and compressed faces to the overall bending stiffness ultimately becomes negligible.

3.3 Pantographic Column of Triangular Cross-Section under Moment Load

The subject of this Section is a pantographic column consisting of three-dimensional triangular pantographic units and subjected to a moment load applied at the top. Each unit is composed of three identical two-dimensional SLEs forming a prism with the base of an equilateral triangle which is regarded as the "cross-section" of the column. The plane of bending is perpendicular to one of the sides of the three-dimensional column. This side is called "rear face" of the column, or a single pantographic unit, and the other two sides are called "left side" and "right side" of the cross-section as shown in Fig. 3.12. The plane of bending is at the same time the plane of symmetry of the system. The moment load is represented by three statically equivalent vertical forces applied at the top nodes of the column.

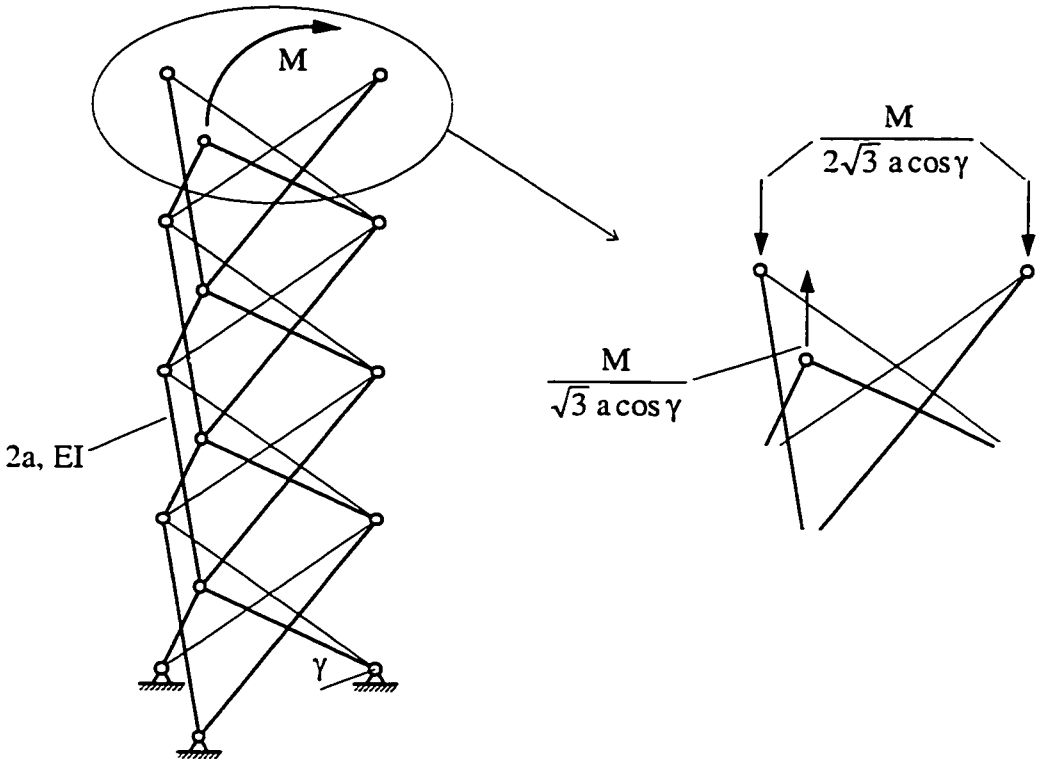

(a) - 3d view

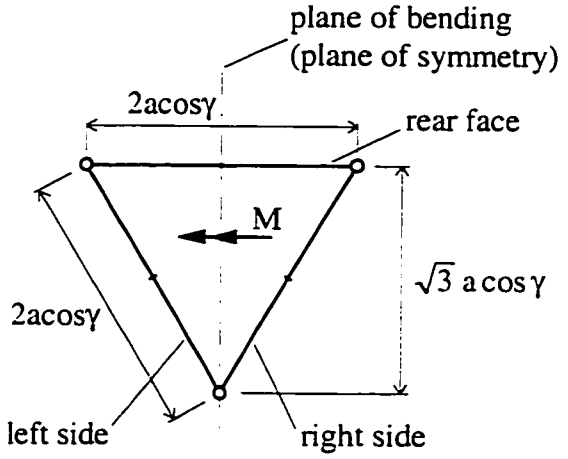

(b) - top view

Figure 3.12: Three-dimensional pantographic column of equilateral triangular cross-section subjected to moment loading.

The analysis will be similar to that employed in the case of the pantographic column with square cross-section. The main steps are the following:
1) use the force method to analyze a single pantographic unit, with the bottom nodes hinged to the ground, subjected to moment load;
2) use the force method to analyze the same unit subjected to horizontal forces similar to the horizontal reactions at the bottom nodes from 1) applied to the top nodes of the unit;
3) using the results of 1) and 2) compose a basic element (a constrained unit) for a displacement method of analysis of the pantographic column subjected to moment load;
4) use the displacement method to analyze the column subjected to moment load, and separate the solution into uniform and local parts.

3.3.1 Analysis of a Single Triangular Unit by the Force Method

3.3.1.1 Statical Determinacy, Primary Structure and Redundant Forces

Consider a single triangular pantographic unit with bottom nodes hinged to the ground. This unit includes six bars which have the total of 36 degrees of freedom. Six hinge connections, three pivotal connections and three hinge supports introduce the total of 42 constraints. The triangular pantographic unit is therefore $42 - 36 = 6$ times statically indeterminate.

The primary structure of the pantographic unit is obtained by releasing the translational constraints at the three top hinges (Fig. 3.13), i.e. nine constraints are released in a six times statically indeterminate structure. Therefore, the primary structure is three times underconstrained. The three degrees of freedom introduced are the rotations of the three plane SLEs about the axis through their bottom nodes. The redundant forces, at each of the three points where the constraints are released, are shown in Fig. 3.13. The three force components, x_1, x_2 and x_3, at the two top nodes of the rear

face must be the same because of symmetry. Equal and opposite forces are applied to the rear top nodes of the left and right sides. It can be clearly seen that the only possibility for the rear face not to exercise its degree of freedom is to have x_3 equal to zero. Component x_1 can be resisted by all three SLEs through bending of bars in the planes of SLEs. However, component x_2, while acting in the plane of the rear face, creates out-of-plane action for the left and right sides. To ensure equilibrium of these sides opposite forces in the y-direction must be applied at their front top nodes. The action-reaction pairs in the x- and z-directions are absent at this location since it lies on the symmetry plane.

3.3.1.2 Flexibility Coefficients; Compatibility Equations

Since there are only two unknown redundant forces, x_1 and x_2 in Fig. 3.13, there will be two equations of compatibility in the force method, similar to the case of the pantographic column with square cross-section:

$$\begin{aligned} \delta_{11}x_1 + \delta_{12}x_2 + \Delta_1 = 0 \\ \delta_{21}x_1 + \delta_{22}x_2 + \Delta_2 = 0 \end{aligned} \tag{3.64}$$

The primary structure subjected to x_1 equal to one is shown in Fig. 3.14. The left side SLE is not shown since it is symmetrical with the right side. The pivotal bending moments in the bars and the reactions at the bottom nodes of SLEs are indicated in the figure. This redundant force causes only in-plane bending in all SLEs of the pantographic unit. The total work done by all $x_1 = 1$ forces equals the total corresponding displacement:

$$\delta_{11} = \frac{1}{EI}\frac{a\cos\gamma\, a}{2}\frac{2}{3}a\cos\gamma\cdot(4+2\cdot 2) = \frac{8\,a^3\cos^2\gamma}{3\,EI} \tag{3.65}$$

Two views of the primary structure loaded with $x_2 = 1$ are shown in Fig. 3.15. While there is only in-plane bending of the rear face SLE, the bars in the left and right sides are bent both in- and out-of-plane of these SLEs. The total displacement corresponding to this load is the sum of three terms:

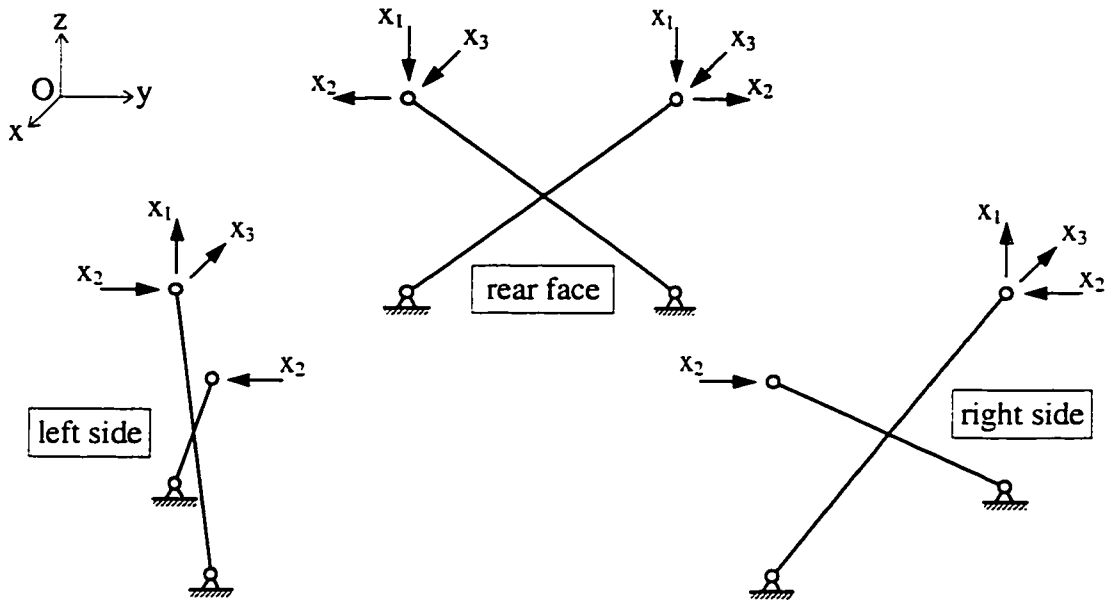

Figure 3.13: Unknown forces at SLE connections of a three-dimensional triangular unit symmetrical about xOz plane ($x_3 = 0$).

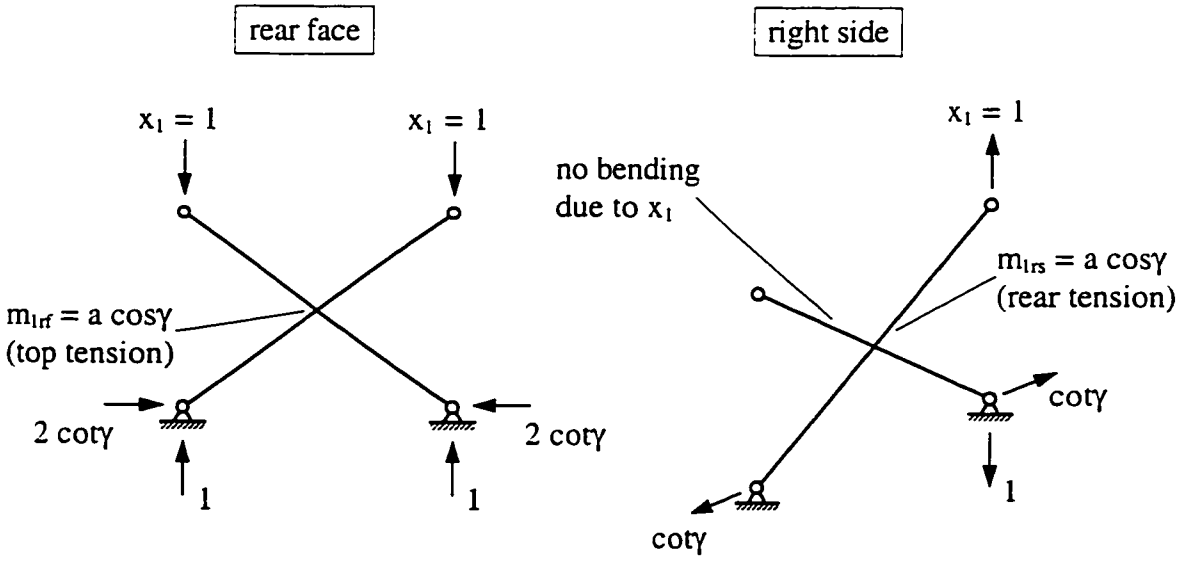

Figure 3.14: Internal forces in the primary structure of a three-dimensional triangular pantographic unit due to $x_1 = 1$.

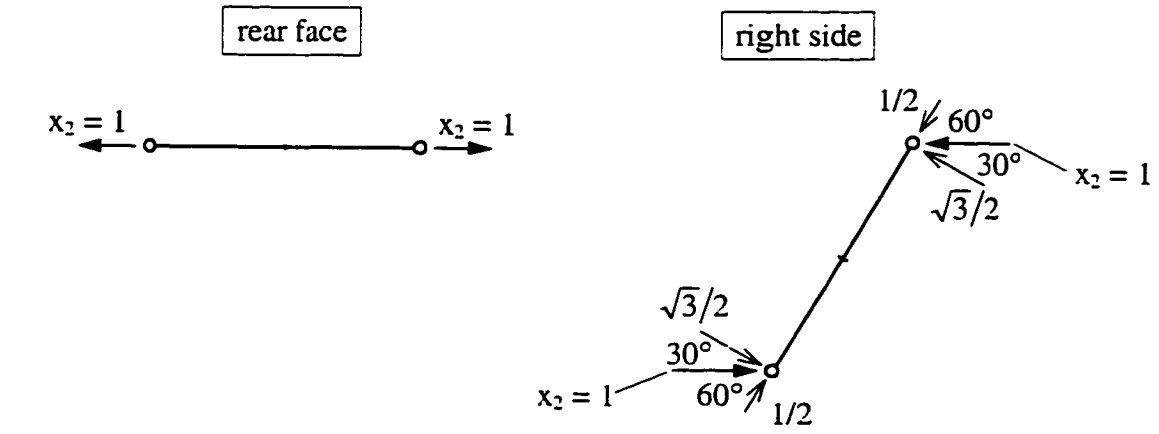

(a) - top view

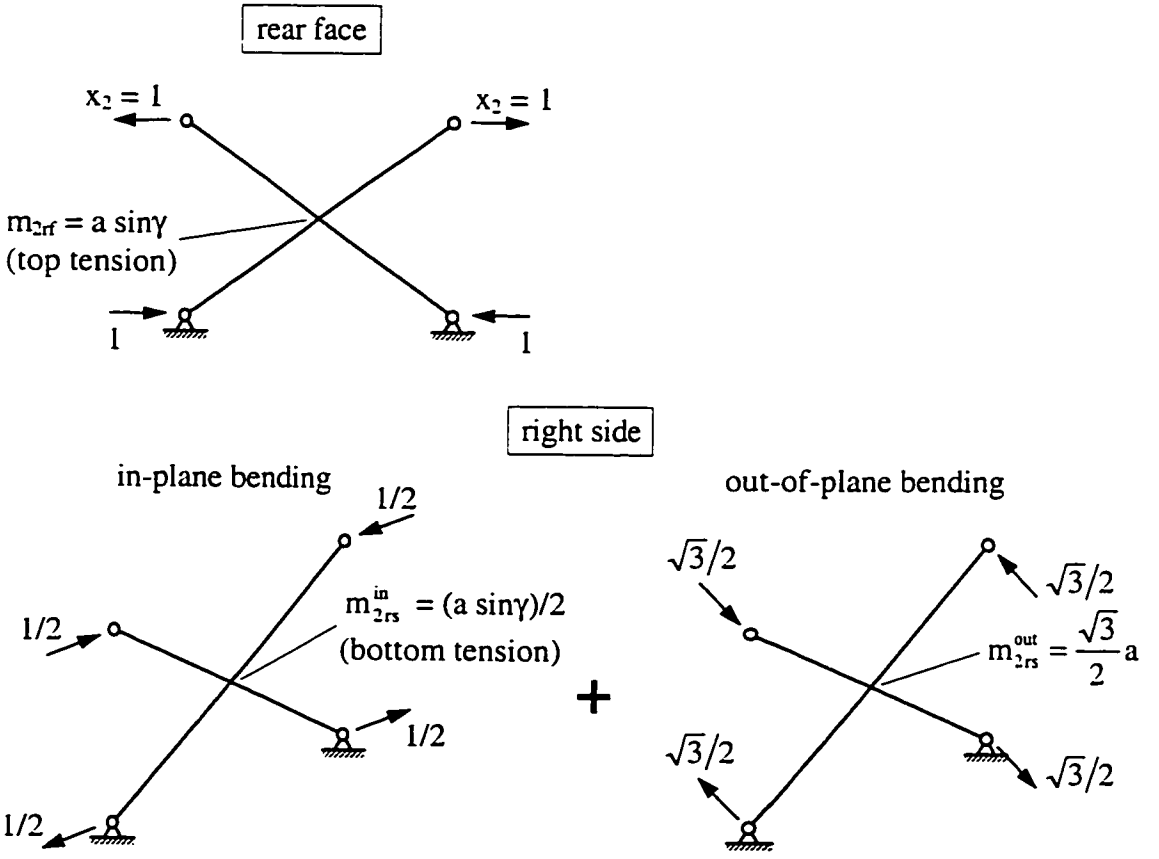

(b) - 3d view

Figure 3.15: Internal forces in the primary structure of a three-dimensional triangular pantographic unit due to $x_2 = 1$.

$$\delta_{22} = \frac{1}{EI}\left(\frac{a\sin\gamma\, a}{2}\frac{2}{3}\, a\sin\gamma\cdot 4 + \frac{a\sin\gamma}{2}\frac{a}{2}\frac{2}{3}\frac{a\sin\gamma}{2}\cdot 4\cdot 2 + \right.$$
$$\left. + \frac{\sqrt{3}}{2}a\frac{a}{2}\frac{2}{3}\frac{\sqrt{3}}{2}a\cdot 4\cdot 2 \right) = \frac{2a^3\left(1+\sin^2\gamma\right)}{EI} \qquad (3.66)$$

The cross-coefficients only include terms associated with the in-plane bending of bars in all three sides:

$$\delta_{12} = \delta_{21} = \frac{1}{EI}\left(\frac{a\cos\gamma\, a}{2}\frac{2}{3}a\sin\gamma\cdot 4 + \frac{a\cos\gamma\, a}{2}\frac{2}{3}\frac{a}{2}\sin\gamma\cdot 2\cdot 2 \right) = \frac{2a^3\sin\gamma\cos\gamma}{EI} \qquad (3.67)$$

3.3.1.3 Moment Loading

The moment load is represented by three vertical forces applied to the top nodes of the unit as shown in Fig. 3.12a. The primary structure subjected to this load is shown in Fig. 3.16 together with the pivotal bending moments and reactions. By arbitrary choice the forces are applied to the top nodes of the side SLEs and the rear face is left unstressed. The displacements at the releases corresponding to x_1 and x_2 are found using the values of bending moments in Figs 3.14, 3.15 and 3.16:

$$\Delta_1 = -\frac{1}{EI}\frac{a\cos\gamma\, a}{2}\frac{2}{3}\frac{M}{2\sqrt{3}}\cdot 2\cdot 2 = -\frac{2Ma^2\cos\gamma}{3\sqrt{3}\,EI}, \qquad \Delta_2 = 0 \qquad (3.68)$$

The compatibility equations become:

$$\frac{8a^3\cos^2\gamma}{3EI}x_1 + \frac{2a^3\sin\gamma\cos\gamma}{EI}x_2 = \frac{2Ma^2\cos\gamma}{3\sqrt{3}\,EI}$$
$$\frac{2a^3\sin\gamma\cos\gamma}{EI}x_1 + \frac{2a^3}{EI}\left(1+\sin^2\gamma\right)x_2 = 0 \qquad (3.69)$$

which yield the following expressions for x_1 and x_2:

$$x_1 = \frac{M\left(1+\sin^2\gamma\right)}{\sqrt{3}\,a\cos\gamma\left(4+\sin^2\gamma\right)}, \qquad x_2 = \frac{M\sin\gamma}{\sqrt{3}\,a\left(4+\sin^2\gamma\right)} \qquad (3.70)$$

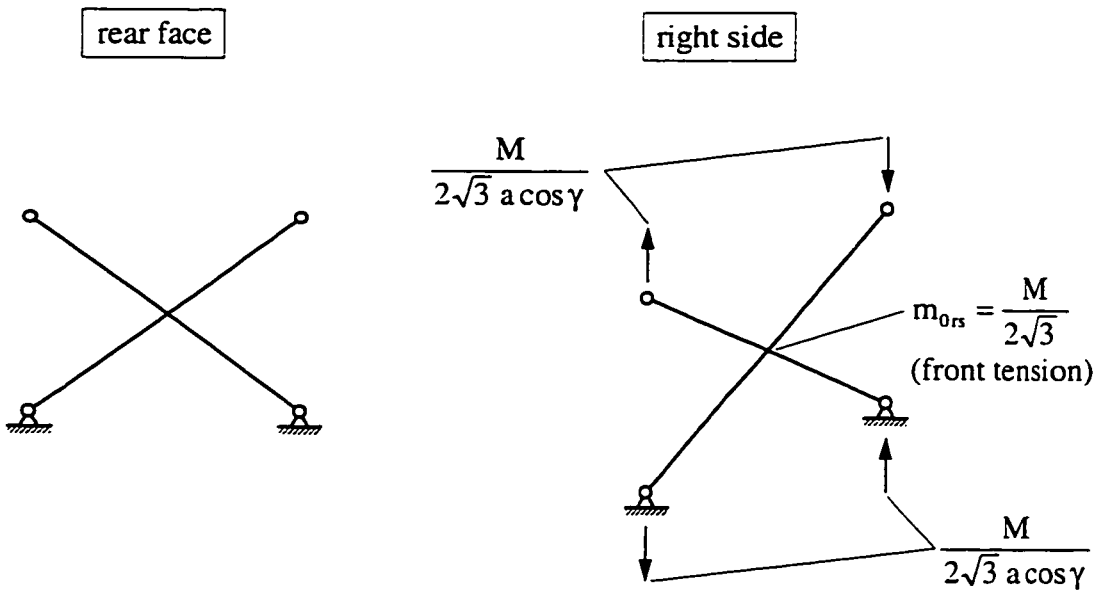

Figure 3.16: Internal forces in the primary structure of a three-dimensional triangular pantographic unit due to moment loading.

The resulting pivotal bending moments and horizontal reactions at the bottom nodes of the rear face and the right side SLEs are shown in Fig. 3.17. If the sums of all horizontal reactions at each bottom node (Fig. 3.18a) are found, there will be three equal horizontal forces at 120° to each other (Fig. 3.18b). This self-equilibrated force pattern will be used in the next analysis as an external load applied to the top nodes of the unit.

3.3.1.4 Self-Balanced Load in Horizontal Plane

The three equal horizontal forces applied at the top nodes of the unit are shown in Fig. 3.19. The force that acts at the node lying in the plane of symmetry can be represented as the sum of two equal forces acting in the directions normal to the planes of the side SLEs. Then the situation becomes very similar to that of the unit from the pantographic column with square cross-section, which was also subjected to two self-equilibrated horizontal

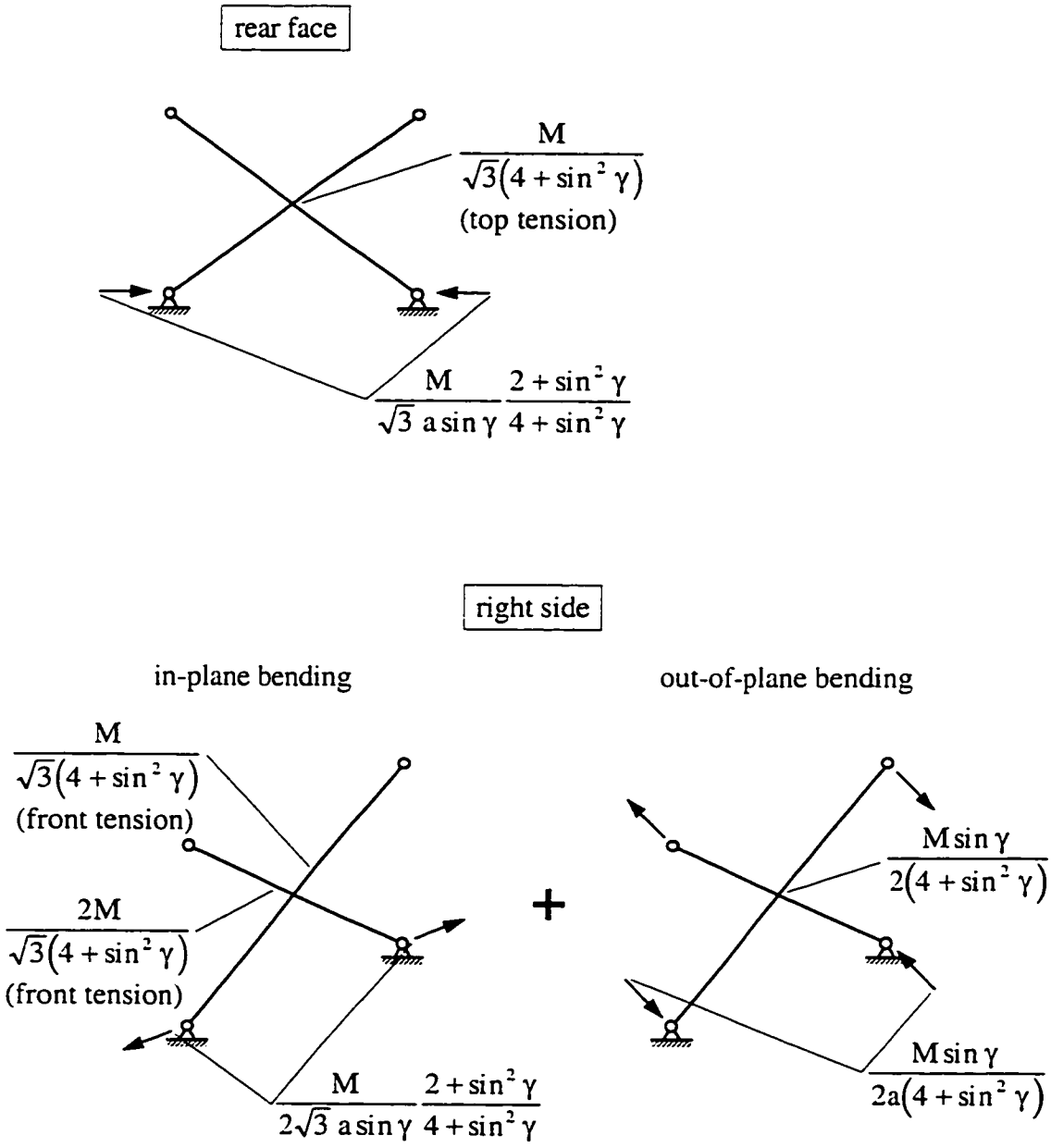

Figure 3.17: Pivotal bending moments and horizontal reactions at bottom nodes of three-dimensional triangular pantographic unit under moment load.

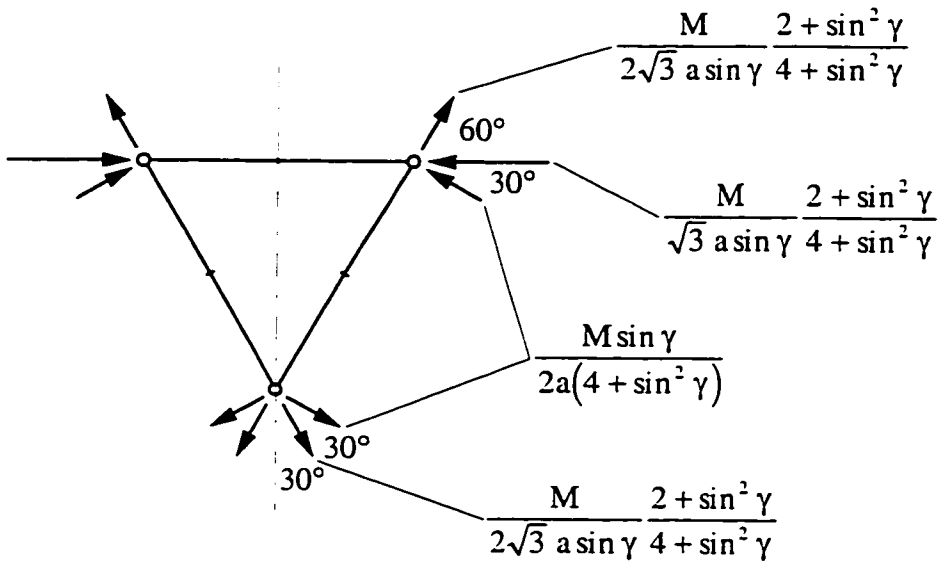

(a) - reactions in, and perpendicular to, the planes of two-dimensional side SLEs

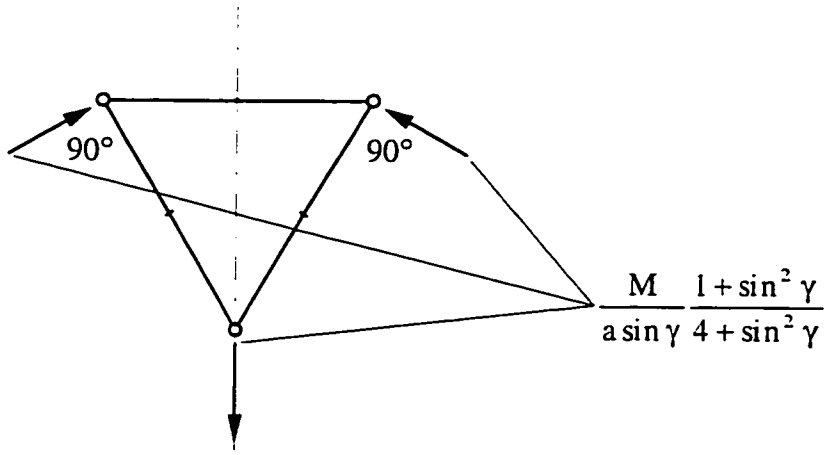

(b) - resultant reactions at the bottom nodes

Figure 3.18: Horizontal reactions at bottom nodes of triangular pantographic unit under moment load.

couples. With this load arrangement, the primary structure will only experience out-of-plane bending of the side SLEs (Fig. 3.20). The free terms in the equations of compatibility for this load case are:

$$\Delta_1 = 0, \qquad \Delta_2 = -\frac{1}{EI}\frac{Ta}{2}\frac{2}{3}\frac{\sqrt{3}}{2}a\cdot 4\cdot 2 = -\frac{4\sqrt{3}}{3\,EI}Ta^3, \tag{3.71}$$

and the equations themselves become:

$$\begin{aligned} &\frac{8\,a^3\cos^2\gamma}{3\,EI}x_1 + \frac{2\,a^3\sin\gamma\cos\gamma}{EI}x_2 = 0 \\ &\frac{2\,a^3\sin\gamma\cos\gamma}{EI}x_1 + \frac{2\,a^3}{EI}\left(1+\sin^2\gamma\right)x_2 = \frac{4\sqrt{3}}{3\,EI}Ta^3 \end{aligned} \tag{3.72}$$

with the solution:

$$x_1 = -\frac{2\sqrt{3}\sin\gamma}{\cos\gamma\left(4+\sin^2\gamma\right)}T, \qquad x_2 = \frac{8\sqrt{3}}{3\left(4+\sin^2\gamma\right)}T \tag{3.73}$$

Figs 3.21 and 3.22 show the final pivotal bending moments and horizontal reactions at the bottom nodes of the unit. Interestingly, the reaction forces have the same direction as the applied load.

3.3.2 Constrained Triangular Unit

3.3.2.1 Reactions and Internal Bending Moments due to External Moment Load

A single triangular pantographic unit has been considered for two load cases: moment load and self-balanced horizontal load. In both cases there are certain horizontal displacements of the top nodes in the directions of the horizontal forces shown in Fig. 3.19. Let us find the total (generalized) displacement corresponding to this generalized load due to the moment applied to the unit. The final bending moments in the bars of the pantographic unit due to moment loading are shown in Fig. 3.17. The virtual horizontal unit forces are applied in the same manner as those in Fig. 3.19. Moreover, they can be applied to the

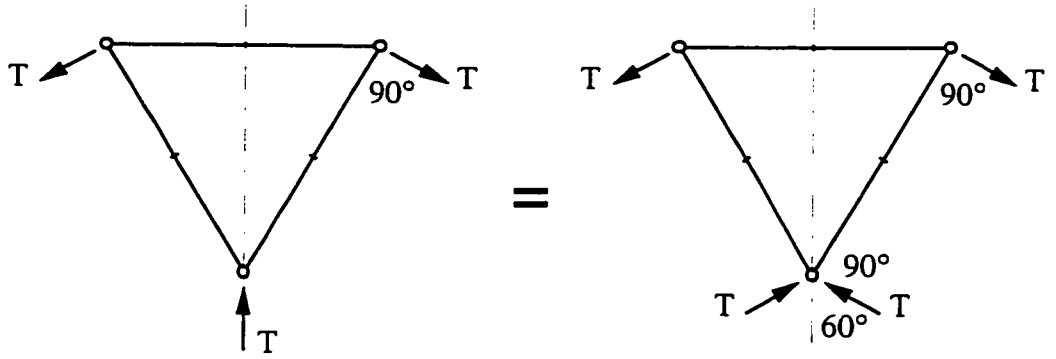

Figure 3.19: Horizontal forces applied to the top nodes of triangular unit (top view).

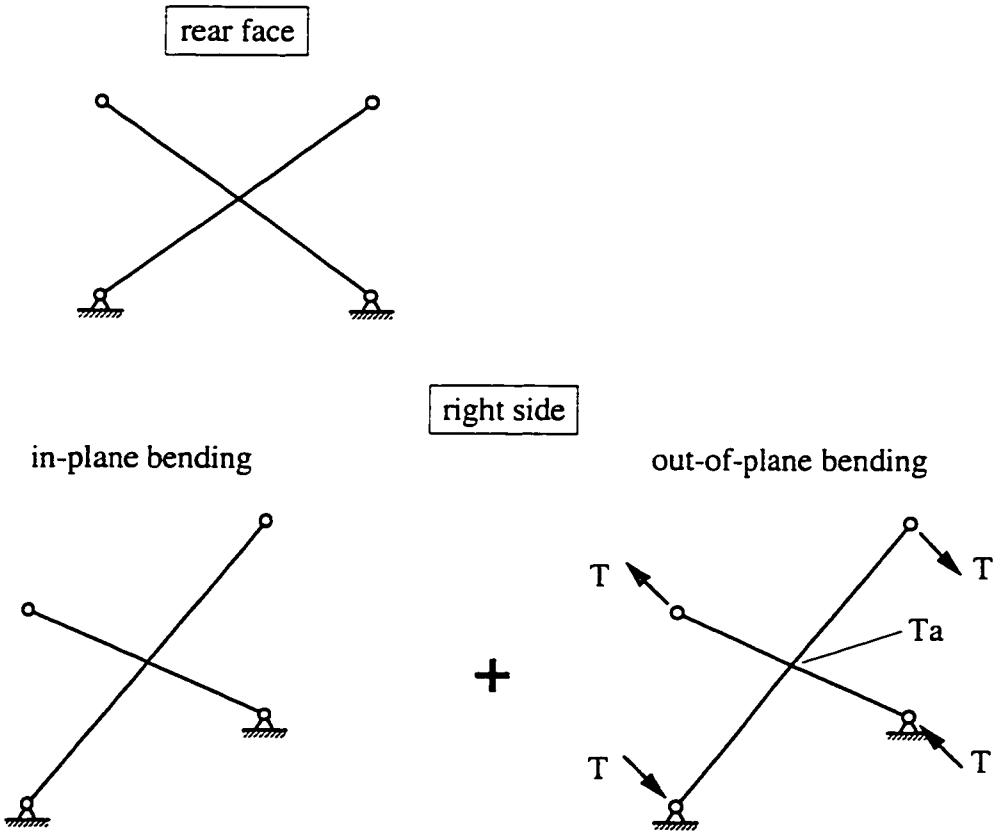

Figure 3.20: Primary structure of triangular unit loaded with horizontal forces at the top nodes.

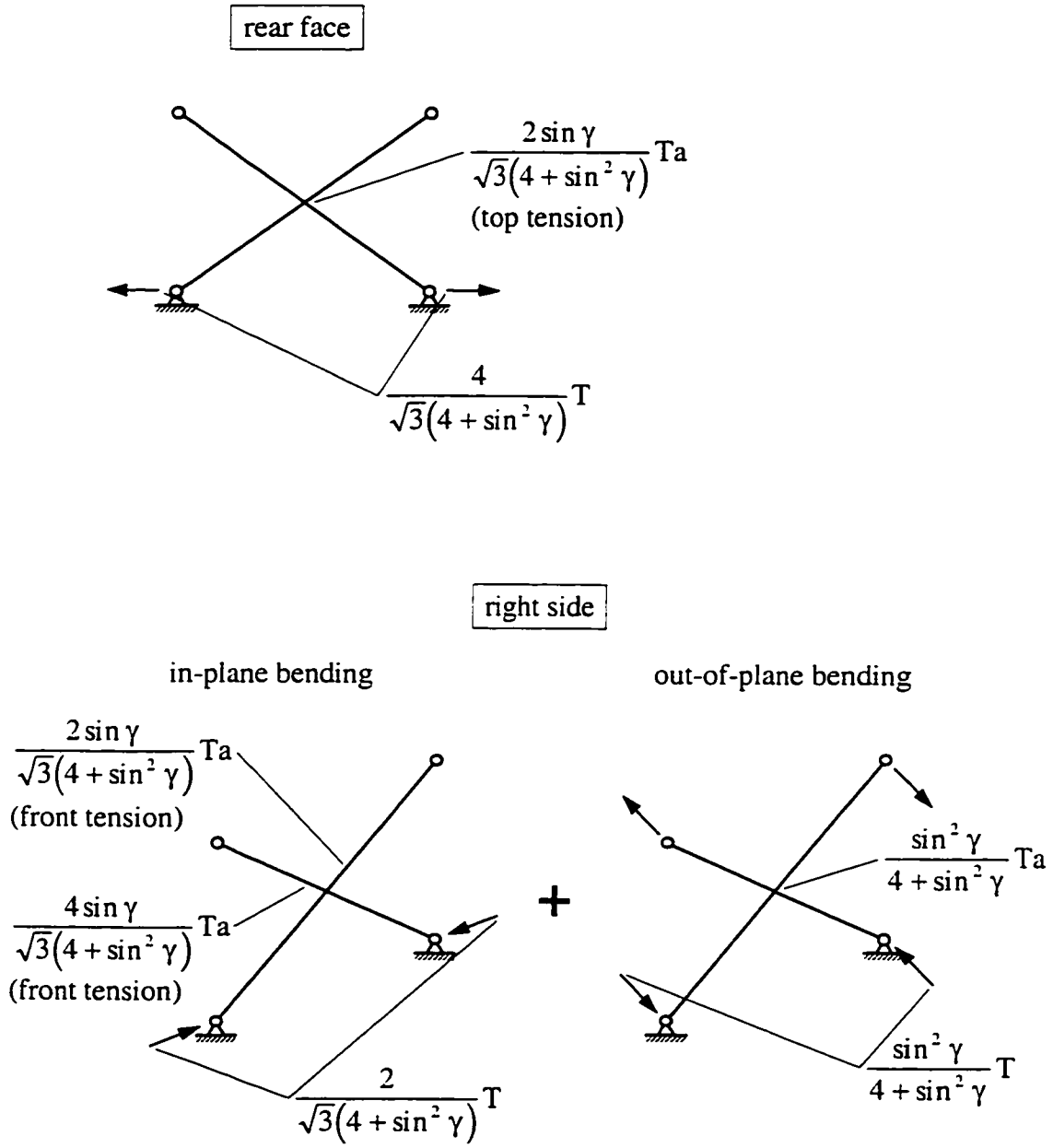

Figure 3.21: Pivotal bending moments and horizontal reactions at bottom nodes of triangular unit subjected to horizontal forces at the top nodes.

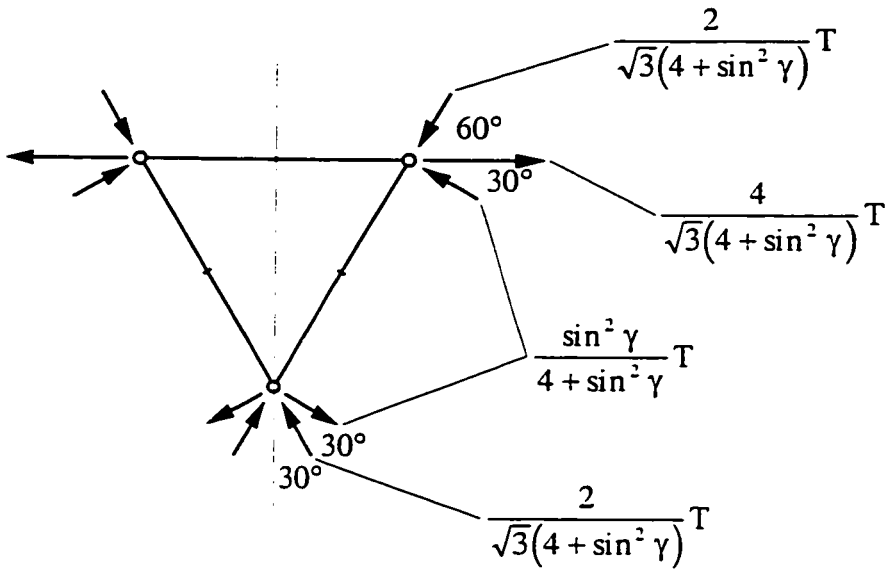

(a) - reactions in, and perpendicular to, the planes of two-dimensional side SLEs

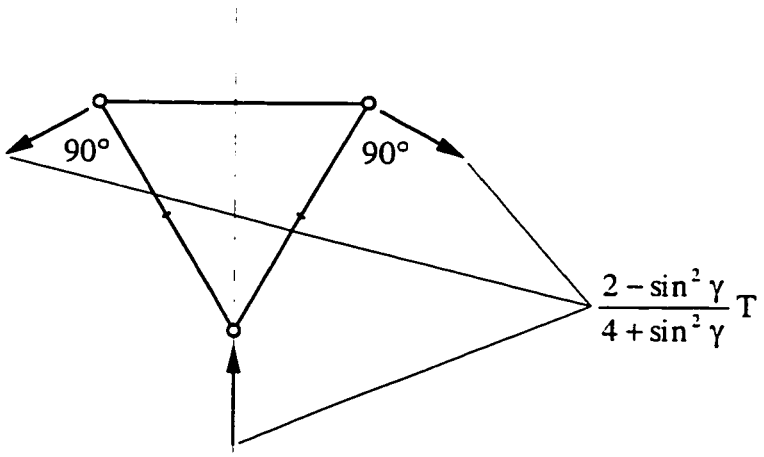

(b) - resultant reactions at the bottom nodes

Figure 3.22: Horizontal reactions at the bottom nodes of triangular pantographic unit subjected to horizontal forces at the top nodes.

primary structure so that they only cause out-of-plane bending in the side SLEs (Fig. 3.20). Although the final bending moments for such load on the statically indeterminate unit are already available (Fig 3.21), the application of the virtual load to the primary structure will considerably simplify calculation of the displacement:

$$h_M = \frac{1}{EI}\frac{M\sin\gamma}{2\left(4+\sin^2\gamma\right)}\frac{a}{2}\frac{2}{3}a\cdot 4\cdot 2 = \frac{4\,M\,a^2\sin\gamma}{3\,EI\left(4+\sin^2\gamma\right)} \tag{3.74}$$

The same displacement due to the three horizontal forces T in Fig. 3.19 can be obtained by calculating the "product" of the moment diagrams from Figs 3.20 and 3.21:

$$h_T = \frac{1}{EI}\frac{T a\sin^2\gamma}{4+\sin^2\gamma}\frac{a}{2}\frac{2}{3}a\cdot 4\cdot 2 = \frac{8\,T\,a^3\sin^2\gamma}{3\,EI\left(4+\sin^2\gamma\right)} \tag{3.75}$$

If the horizontal translational constraints are introduced at the top nodes of the unit instead of forces, the reactions at these constraints in the case of moment load would be such that the sum of displacements from eqs 3.74 and 3.75 equals zero:

$$h_M + h_T = \frac{4\,M\,a^2\sin\gamma}{3\,EI\left(4+\sin^2\gamma\right)} + \frac{8\,T\,a^3\sin^2\gamma}{3\,EI\left(4+\sin^2\gamma\right)} = 0\ , \tag{3.76}$$

which yields the reactions in the constraints:

$$T = -\frac{M}{2\,a\sin\gamma} \tag{3.77}$$

Superposition of the reaction forces at the bottom nodes from Fig. 3.18b and 3.22b (with T from eq. 3.77 substituted in the latter) gives these reactions in the constrained unit under the moment load (Fig. 3.23a). The reactions at the bottom nodes are the same as those in the constraints at the top nodes (eq. 3.77), which could be expected since the constrained unit (Fig. 3.23a) is symmetric about the horizontal plane through the pivots of its SLEs. After similar superposition is performed for the pivotal bending moments, we obtain zero bending in all bars of the constrained unit.

3.3.2.2 Reactions and Bending Moments due to Unit Constraint Displacement

To find the stiffness of the triangular pantographic unit in the direction of the generalized horizontal constraint, the deflection h_T in eq. 3.75 is assigned the value of one. The forces T that cause such a deflection are:

$$T\Big|_{h_T=1} = \frac{3\,EI\left(4+\sin^2\gamma\right)}{8\,a^3\sin^2\gamma} \tag{3.78}$$

The bending moments and the reactions at the bottom nodes corresponding to the unit horizontal displacement of the top nodes are obtained from Figs 3.21 and 3.22 when T from the last equation is substituted into the moment and force expressions.

3.3.3 Analysis of the Triangular Column by the Displacement Method

3.3.3.1 Stiffness Matrix and Load Vector

The constrained primary structure of the triangular pantographic column subjected to moment load is shown in Fig. 3.23b. The three horizontal links constituting a single constraint are placed at the top of the column and at each unit interface. The assumed positive directions of the horizontal nodal displacements are also shown in the figure. The entries of the stiffness matrix and the load vector in the system of equilibrium equations:

$$\mathbf{K\,y + P = 0} \tag{3.79}$$

are readily obtained from eqs 3.77 and 3.78. The reactions in the constraint at the top of the column due its unit displacement and the external moment are:

$$k_{11} = \frac{3\,EI\left(4+\sin^2\gamma\right)}{8\,a^3\sin^2\gamma} \quad \text{and} \quad p_1 = -\frac{M}{2\,a\sin\gamma}\,, \tag{3.80}$$

respectively. The reactions in the rest of the constraints due to the same factors are twice as much:

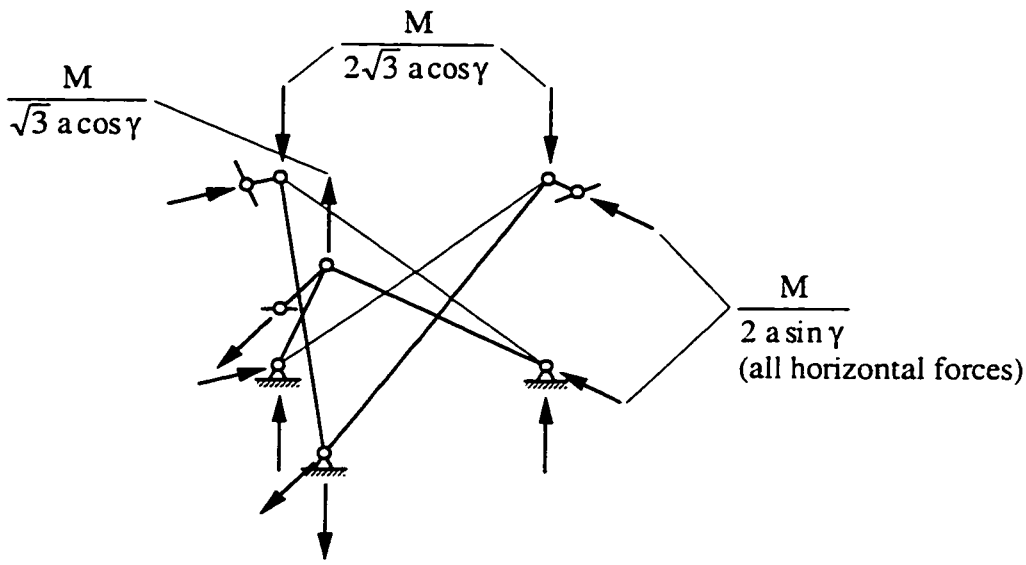

(a)

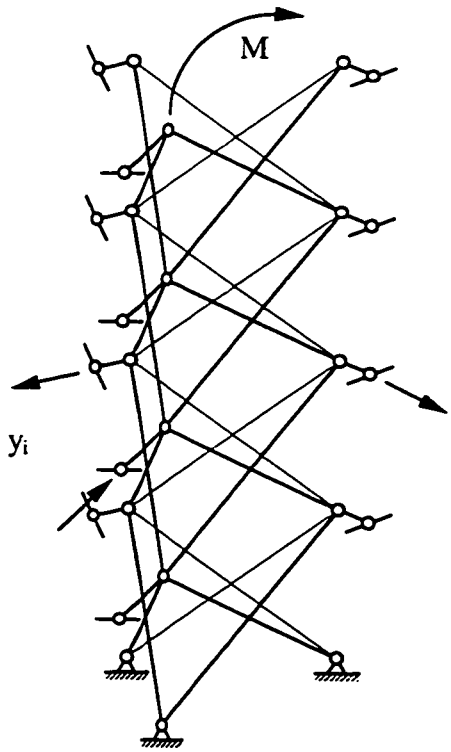

(b)

Figure 3.23: Constrained triangular pantographic unit subjected to moment load (a) and primary structure of the column for the analysis by the displacement method (b).

$$k_{ii} = \frac{3\,EI\left(4+\sin^2\gamma\right)}{4\,a^3\sin^2\gamma} \quad \text{and} \quad p_i = -\frac{M}{a\sin\gamma}, \quad i = 2,\ldots,n \tag{3.81}$$

The entries of the stiffness matrix above and below the main diagonal, i.e. the reactions in a constraint due to unit displacement of the adjacent one, are:

$$k_{ij} = \frac{3\,EI\left(2-\sin^2\gamma\right)}{8\,a^3\sin^2\gamma}, \quad |i-j| = 1 \tag{3.82}$$

Now, the system of equilibrium equations can be written in the following form:

$$\begin{bmatrix} A & 1 & & & 0 \\ 1 & 2A & 1 & & \\ & \cdots & & & \\ & & 1 & 2A & 1 \\ 0 & & & 1 & 2A \end{bmatrix} \mathbf{y} = \begin{bmatrix} B \\ 2B \\ \cdots \\ 2B \\ 2B \end{bmatrix} \quad \text{or} \quad \mathbf{K_m}\,\mathbf{y} = \mathbf{P_m}\,, \tag{3.83}$$

where $\mathbf{K_m}$ and $\mathbf{P_m}$ are the modified stiffness matrix and right side vector:

$$\mathbf{K_m} = \frac{8\,a^3\sin^2\gamma}{3\,EI\left(2-\sin^2\gamma\right)}\mathbf{K}, \quad \mathbf{P_m} = -\frac{8\,a^3\sin^2\gamma}{3\,EI\left(2-\sin^2\gamma\right)}\mathbf{P} \tag{3.84}$$

and

$$A = \frac{4+\sin^2\gamma}{2-\sin^2\gamma}, \quad B = \frac{4\,M\,a^2\sin\gamma}{3\,EI\sin\gamma\left(2-\sin^2\gamma\right)} \tag{3.85}$$

3.3.3.2 Solution of the System

In solving the system of equations 3.83 we will, as in the case of the column with a square cross-section, separate the solution into two parts - uniform and local - but it will be done in a slightly different way which has a more transparent physical meaning. Under the assumption of linear behaviour, the response of the column, with the bottom nodes hinged to the ground, to the moment load can be obtained as the superposition of two effects. First, the horizontal constraint at the bottom nodes is released (Fig. 3.24) and the behaviour of such a column subjected to the same moment load is considered. In this

case, the bottom nodes will have a certain displacement in the direction of the constraint. In fact, this displacement will be the outcome of the solution of the system of equations of the displacement method for this structure. To return to the original situation, we will apply the three horizontal unit forces to the bottom nodes (Fig. 3.25) and find the corresponding displacement. Next, the latter solution will be scaled to make this displacement equal and opposite to that from the moment loading. After that, the superposition of the solution for the moment load and the scaled solution for the horizontal load at the bottom nodes will describe the behaviour of the original system.

3.3.3.2.1 Uniform Solution

The column in Fig. 3.24, that has its bottom nodes free to move in the horizontal plane, requires one additional constraint at the ground level. The size of the system of equations increases by one and the system becomes:

$$\begin{bmatrix} A & 1 & & & 0 \\ 1 & 2A & 1 & & \\ & & \cdots & & \\ & & 1 & 2A & 1 \\ 0 & & & 1 & A \end{bmatrix} \mathbf{y}^u = \begin{bmatrix} B \\ 2B \\ \cdots \\ 2B \\ B \end{bmatrix} \quad \text{or} \quad \mathbf{K}_m^u \, \mathbf{y}^u = \mathbf{P}_m^u \tag{3.86}$$

The vector $\mathbf{y}^u$ satisfying this system has all entries the same and equal to:

$$y_i^u = \frac{B}{A+1} = \frac{2\,M\,a^2 \sin\gamma}{9\,EI}, \quad i = 1,\ldots,n+1 \tag{3.87}$$

For a particular pantographic unit the horizontal displacement of its top nodes and that of its bottom nodes reflect the symmetrical effects about the horizontal plane through the pivots of the three SLEs in this unit. These effects cancel each other's contribution to the in-plane bending of the rear face SLE and to the out-of-plane bending of the side SLEs. The in-plane bending moments in the side SLEs are additive and can be found from Fig. 3.21 and eqs 3.78 and 3.87:

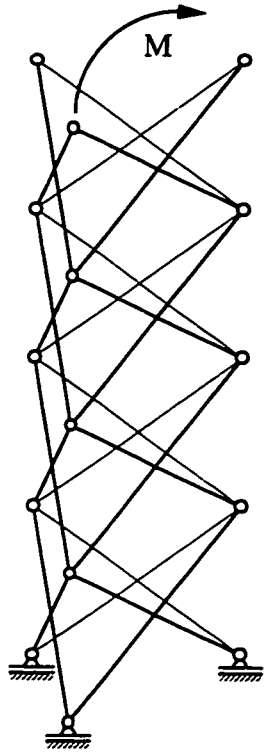

Figure 3.24: Uniformly bent triangular column - bottom nodes free in horizontal plane.

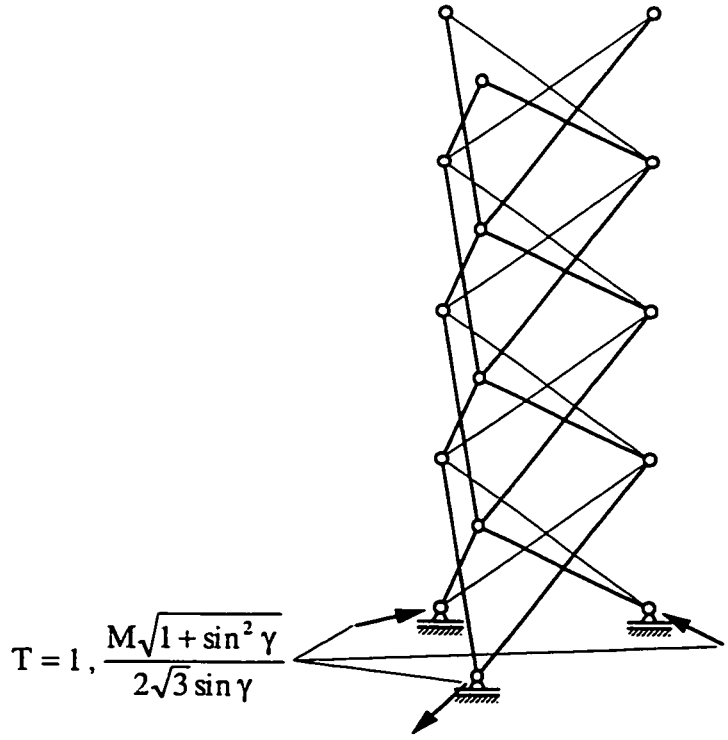

Figure 3.25: Triangular pantographic column subjected to self-balanced local load.

$$\frac{4\,a\sin\gamma}{\sqrt{3}\left(4+\sin^2\gamma\right)}\,\frac{3\,EI\left(4+\sin^2\gamma\right)}{8\,a^3\sin^2\gamma}\,\frac{2\,M\,a^2\sin\gamma}{9\,EI}\,\frac{3}{2}=\frac{\sqrt{3}}{6}M \tag{3.88}$$

3.3.3.2.2 Local Solution

The pantographic column with the bottom nodes free to move the in horizontal plane and subjected to horizontal forces (each equal to one) is shown in Fig. 3.25. The system of equilibrium equations for this structure and loading is:

$$\begin{bmatrix} A & 1 & & & 0 \\ 1 & 2A & 1 & & \\ & & \cdots & & \\ & & 1 & 2A & 1 \\ 0 & & & 1 & A \end{bmatrix} \bar{y}^{loc} = \begin{bmatrix} 0 \\ 0 \\ \cdots \\ 0 \\ D \end{bmatrix} \quad \text{or} \quad \mathbf{K}_m^u\,\bar{y}^{loc} = \bar{\mathbf{P}}_m^{loc}\,, \tag{3.89}$$

where $D=(-1)\dfrac{8\,a^3\sin^2\gamma}{3\,EI\left(2-\sin^2\gamma\right)}$ and the bar indicates the fact that the column is subjected to unit forces. Starting from the first equation, we can express an arbitrary component of the solution vector through the next one as:

$$\bar{y}_i^{loc}=C_i\,\bar{y}_{i+1}^{loc}\,,\quad i=1\ldots n \tag{3.90}$$

From equation number (i + 1):

$$\bar{y}_{i+1}^{loc}=-\frac{1}{2A+C_i}\,\bar{y}_{i+2}^{loc}=C_{i+1}\,\bar{y}_{i+2}^{loc}\quad\rightarrow\quad C_{i+1}=-\frac{1}{2A+C_i} \tag{3.91}$$

Recognizing in the recursive formula of eq. 3.91 a continued fraction and assuming that it converges for growing i, one can try to calculate the limit for C_i:

$$C=-\frac{1}{2A+C}\quad\rightarrow\quad C^2+2AC+1=0\quad\rightarrow\quad C=-A+\sqrt{A^2-1} \tag{3.92}$$

The only condition for the existence of C is that A be greater than one, which is always satisfied since the lowest possible value of A is two (eq. 3.85). Having established the relationship between the elements of the solution vector $\bar{y}_i^{loc}=C\,\bar{y}_{i+1}^{loc}$ $(i=1\ldots n)$ far enough from the top of the column, from the last equation of system 3.89 we obtain:

$$C\,\bar{y}^{loc}_{n+1} + A\bar{y}^{loc}_{n+1} = -1 \quad \rightarrow \quad \bar{y}^{loc}_{n+1} = \frac{D}{A+C} = \frac{D}{\sqrt{A^2-1}} = -\frac{4\,a^3 \sin^2\gamma}{3\sqrt{3}\,EI\,\sqrt{1+\sin^2\gamma}} \tag{3.93}$$

The rest of $\bar{y}^{loc}_i$ form a decreasing geometric series as i changes from n to one. How fast this series decreases for columns with different degrees of deployment can be seen from Fig. 3.26 that shows the plot of C(γ) dependence.

The magnitude of the horizontal forces required to bring the bottom nodes of the column back to their original position, after they have moved by the amount from eq. 24 due to the moment load, can now be found:

$$\frac{2\,M\,a^2 \sin\gamma}{9\,EI} - \frac{4\,a^3 \sin^2\gamma}{3\sqrt{3}\,EI\,\sqrt{1+\sin^2\gamma}}\,T = 0 \quad \rightarrow \quad T = \frac{M\sqrt{1+\sin^2\gamma}}{2\sqrt{3}\,a \sin\gamma} \tag{3.94}$$

in the direction shown in Fig. 3.25. The local solution vector corresponding to this load is a multiple of that obtained for the unit forces:

$$\mathbf{y}^{loc} = T\,\bar{\mathbf{y}}^{loc}, \quad i = 1,\ldots,n+1, \tag{3.95}$$

with the last entry of this vector, $\bar{y}^{loc}_{n+1}$, of course, being equal to the displacement opposite to that from eq. 3.87.

3.3.3.2.3 Superposition of Uniform and Local Solutions

The sum of uniform, $\mathbf{y}^u$, and local, $\mathbf{y}^{loc}$, solution vectors yields the resulting displacement vector, **y**, for original column in bending:

$$y_i = y^u_i + y^{loc}_{n+1}\,C^{n+1-i} = \frac{B}{A+1}\left(1 - C^{n+1-i}\right) = \frac{2\,M\,a^2 \sin\gamma}{9\,EI}\left(1 - C^{n+1-i}\right), \; i = 1,\ldots,n+1 \tag{3.96}$$

The in-plane pivotal bending moment in the bar connecting the bottom front node with the top right rear node of the right side SLE in unit number i, can be found from Fig. 3.21 and eq. 3.78:

$$M_{rs,i}^{in\,1} = \frac{2\,a\sin\gamma}{\sqrt{3}\left(4+\sin^2\gamma\right)} \frac{3\,EI\left(4+\sin^2\gamma\right)}{8\,a^3\sin^2\gamma}\left(y_i + 2\,y_{i+1}\right) = \\ = \frac{\sqrt{3}\,EI}{4\,a^2\sin\gamma} \frac{2\,M\,a^2\sin\gamma}{9\,EI}\left[1 - C^{n+1-i} + 2\left(1 - C^{n+1-(i+1)}\right)\right] = \frac{\sqrt{3}}{18} M\left[3 - (2+C)\,C^{n-i}\right] \tag{3.97}$$

Similarly, the moment in the bar connecting the top front node with the bottom right rear node is:

$$M_{rs,i}^{in\,2} = \frac{\sqrt{3}}{18} M\left[3 - (2\,C+1)\,C^{n-i}\right] \tag{3.98}$$

If the primary structure of the triangular column is obtained by separating three planar pantographic columns and subjected to unit virtual moment load, distributed equally between left and right sides, then the pivotal bending moments in all SLEs of the side columns are equal to $\sqrt{3}/6$ (Fig. 3.16). Using such virtual moments and the real moments from eqs 3.97 and 3.98, one can calculate the tip rotation of the three-dimensional column due to moment load:

$$\varphi = \frac{1}{EI}\sum_{i=1}^{n}\left(\frac{M_{rs,i}^{in\,1}\,a}{2}\frac{2}{3}\frac{\sqrt{3}}{6} + \frac{M_{rs,i}^{in\,2}\,a}{2}\frac{2}{3}\frac{\sqrt{3}}{6}\right)\cdot 2\cdot 2 = \frac{2\,M\,a}{9\,EI}\left[n - \frac{1+C}{2}\sum_{i=1}^{n} C^{n-i}\right] \tag{3.99}$$

The sum in the last equation can be considered independent of n even for a relatively small number of units in the column. Therefore the expression for rotation becomes:

$$\varphi = \frac{2\,M\,a}{9\,EI}\left[n - \frac{1}{2}\frac{1+C}{1-C}\right] \tag{3.100}$$

The last equation is almost identical with eq. 3.63 which describes the tip rotation for a square pantographic column. The first term in brackets corresponds to the rotation given by uniform solution, which applies to the column with unconstrained bottom nodes. The second term reflects the stiffening contribution of the bottom constraint (Fig. 3.27) and has exactly the same form for square and triangular columns.

As in the case of the square pantographic column, for the triangular column in pure bending the uniform solution describes the behaviour of most of the structure, and the effects of the support conditions are confined to one or two pantographic units near the

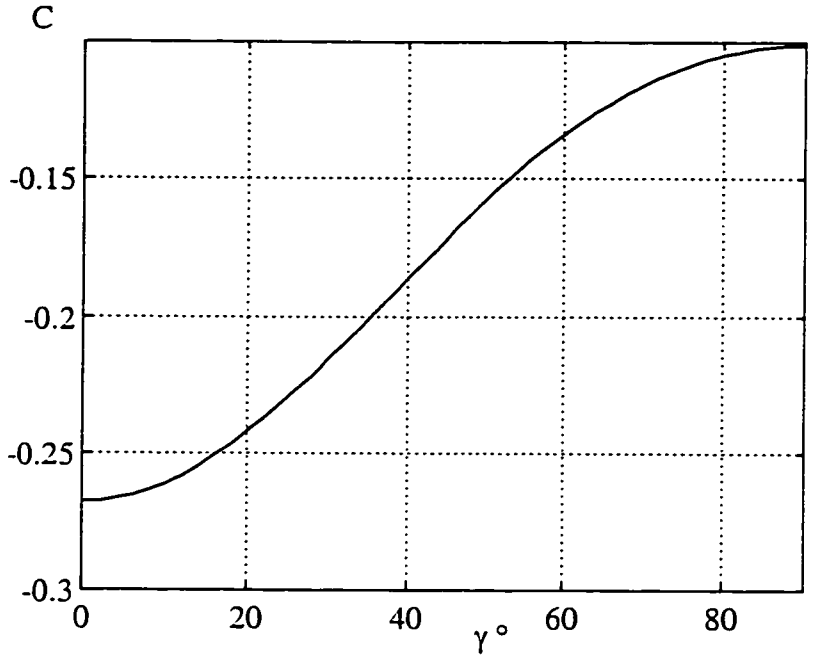

Figure 3.26: Proportionality coefficient between the neighbouring entries of the local solution vector for a triangular column versus the degree of deployment.

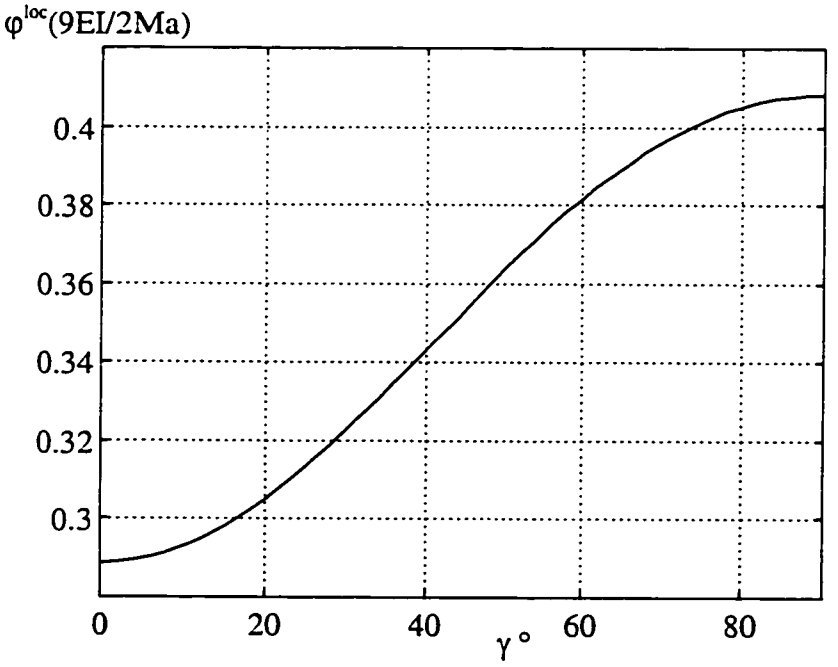

Figure 3.27: Local part of the tip rotation of a triangular pantographic column subjected to moment load versus the degree of deployment (compare with n).

base. The overall bending stiffness of the column is obtained by equating its end rotation to that of a solid column of the same length. If the number of pantographic units in the column is large, the second term in eq. 3.100 can be neglected:

$$\frac{2}{9}\frac{M\,a\,n}{EI}=\frac{M\,L}{(EI)_e},\quad \text{where}\quad L=2a\sin\gamma\; n\;\rightarrow$$
$$(EI)_e=9\,EI\sin\gamma=\frac{3}{2}(6\,EI\sin\gamma) \tag{3.101}$$

Thus, the equivalent bending stiffness of a triangular column is 1.5 times that of a single planar column which forms the sides of the three-dimensional structure. The implications of this result will be discussed in the next Section.

3.4 Bending of Three-Dimensional Columns in Arbitrary Plane

So far three-dimensional pantographic columns of square and triangular cross-sections subjected to bending in the plane perpendicular to one or two of their sides were analyzed. These sides are planar pantographic columns which, linked together, form the three-dimensional structures. The plane of bending was also the symmetry plane for these systems. The logical question, that should be asked after the previous analyses, is how these columns would respond if the direction of the plane of bending were arbitrary. In this Section we consider this question. Only the uniform parts of the solutions from Sections 3.2 and 3.3 are taken into account.

One could expect that pantographic columns with the units made of identical SLEs would have cross-sectional properties for arbitrarily oriented sets of perpendicular axes similar to those of the solid columns having the cross-sections with high degree of symmetry. We will perform the derivation of the stiffness of pantographic columns for the bending in arbitrary direction, to emphasize the differences and similarities between pantographic and solid structures.

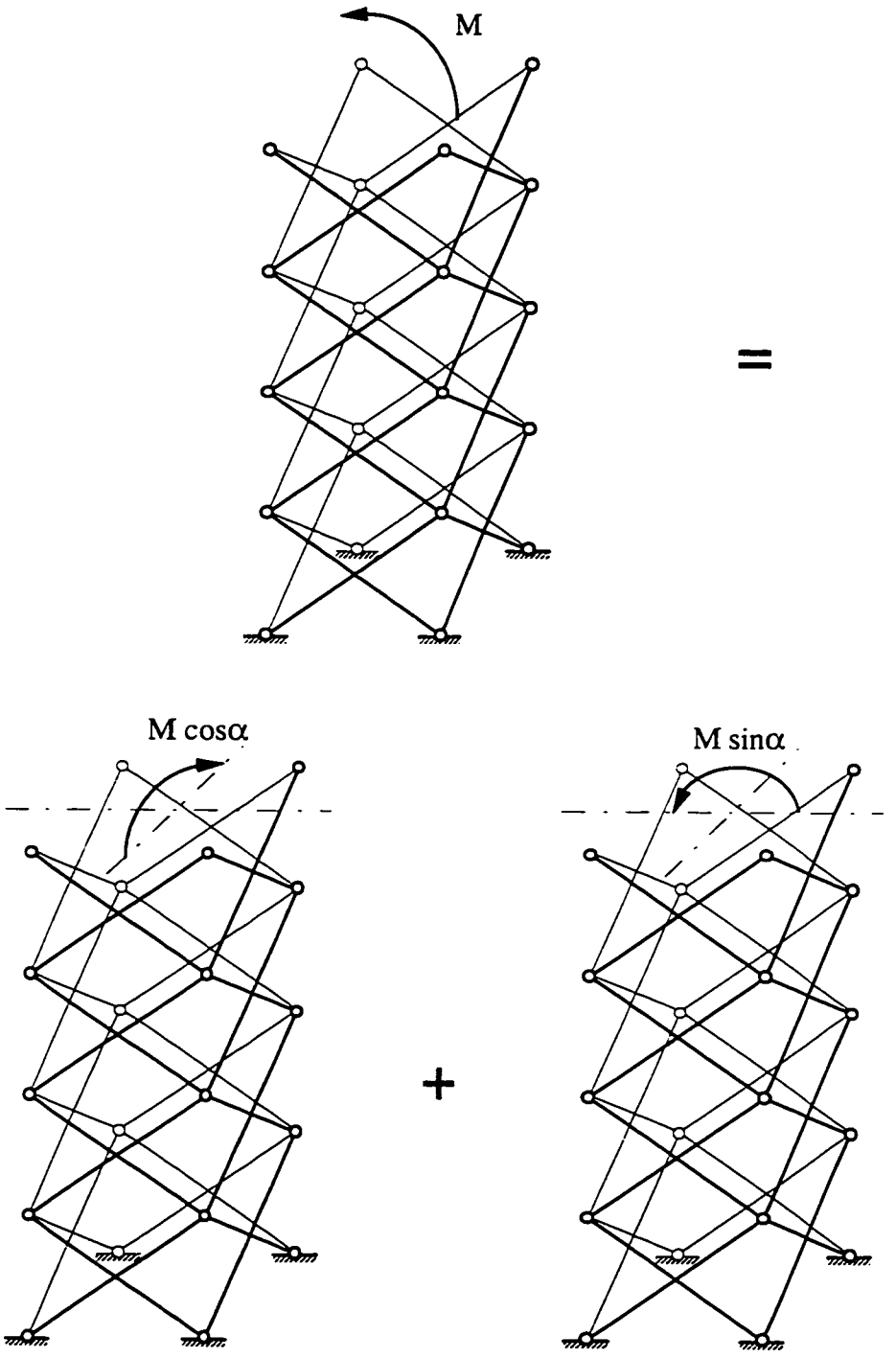

(a) - 3d view

Figure 3.28: Bending of a square pantographic column in an arbitrary plane.

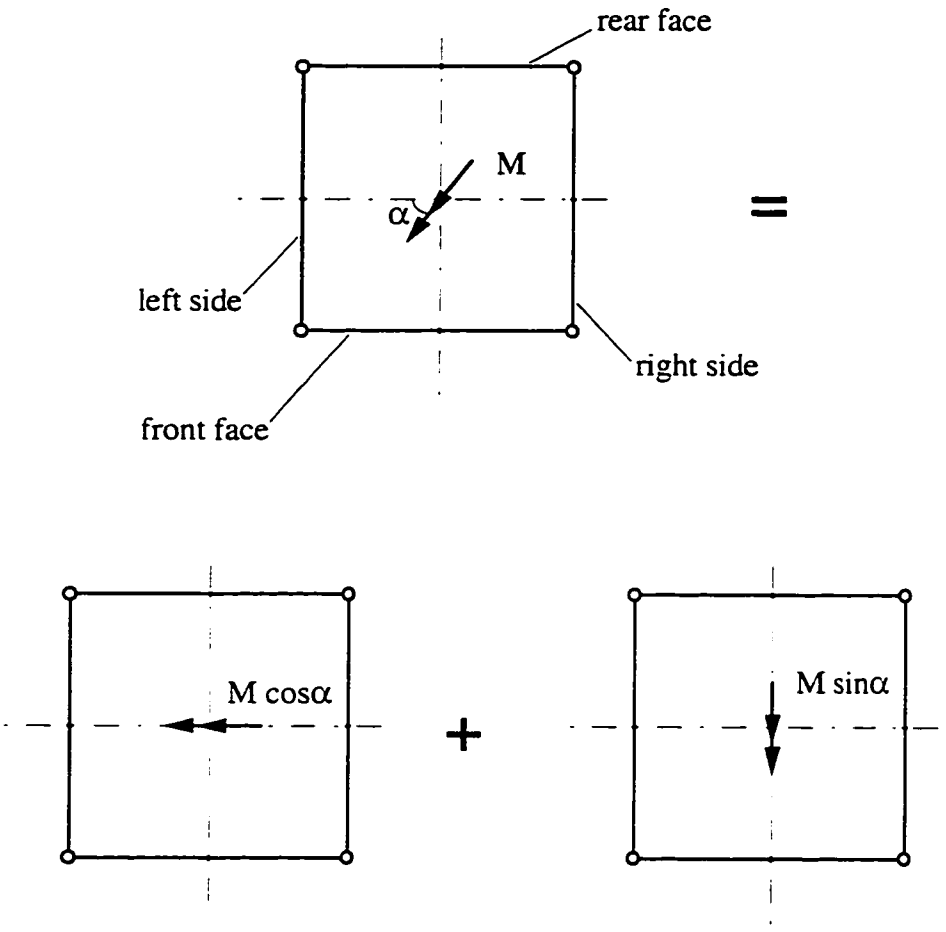

(b) - top view

Figure 3.28: Bending of a square pantographic column in an arbitrary plane (cont.)

Let us consider a square pantographic column subjected to bending in a plane of arbitrary orientation. The moment applied to the column shown in Fig. 3.28 acts in a plane at angle α to one of the symmetry planes of the structure. The vector of the moment load can be represented as a sum of two moment vectors acting in the two planes orthogonal to the two pairs of parallel sides of the column. In this case, each of the two moment loads represents the situation of a square pantographic column bent in one of its

symmetry planes. Under the assumption of linear behaviour, the internal forces for these loads can be superimposed and will yield the internal forces acting in the column under the original moment load.

If the contribution of the local solution caused by the support conditions at the bottom of the column is neglected, the pivotal bending moments in the bars of the front and rear faces, and the left and right sides can be written as:

$$M_{faces} = \frac{M}{4}\sin\alpha\,, \quad M_{sides} = \frac{M}{4}\cos\alpha \tag{3.102}$$

Each of the two orthogonal moment load components causes bending moments only in the two opposite sides of the square cross-section and leaves the other pair of sides free of stress. Thus, the superposition of the moments from eq. 3.102 immediately gives the internal forces in the pantographic column due to the original loading.

To find the rotation of the top of the column caused by moment M, one can use the same distribution of internal forces but now due to the virtual load M = 1:

$$\varphi = \frac{1}{EI}\left(\frac{M}{4}\sin\alpha\,\frac{a}{2}\,\frac{2}{3}\,\frac{1}{4}\sin\alpha + \frac{M}{4}\cos\alpha\,\frac{a}{2}\,\frac{2}{3}\,\frac{1}{4}\cos\alpha\right) 4\cdot 2\,n = \frac{M\,a\,n}{6\,EI} \tag{3.103}$$

The equivalent bending stiffness of the column is found by equating the rotation in eq. 3.103 to that of the equivalent solid column of the same length:

$$\frac{M\,a\,n}{6\,EI} = \frac{M\,L}{(EI)_e}, \quad \text{where} \quad L = 2\,a\sin\gamma\,n \;\rightarrow$$
$$(EI)_e = 12\,EI\sin\gamma = 2\,(6\,EI\sin\gamma) \tag{3.104}$$

The equivalent bending stiffness in the case of arbitrary orientation of the moment load (eq. 3.104) is the same as the stiffness found in the case when the direction of bending coincides with one of the planes of symmetry of the structure. This is one more situation in which the behaviour of pantographic columns can be related to that of their solid counterparts. Let us take a closer look at the bending stiffness of a solid column

with a tubular square cross-section (Fig. 3.29a). Each of the four solid plates forming the sides of this column can be related to the corresponding planar pantographic column in the deployable structure. The bending stiffness of such a plate in its own plane is $Eb^3t/12$, whereas the bending stiffness of the planar pantograph in its plane is $6EI\sin\gamma$. The bending stiffnesses of both the thin solid plate and the pantograph out of their planes can be taken equal to zero. The qualitative difference between the two lies in their axial stiffnesses, which is Ebt for the plate but can be effectively ignored for the long pantograph.

The moment of inertia of a thin plate about an axis x′-x′ through its midpoint and at angle α to its principal axis x-x (Fig. 3.29b) is the same as the moment inertia about the axis x′-x′ of the plate with thickness $t/\cos\alpha$ and width $b\cos\alpha$ (axis x′-x′ is the principal axis for the latter plate):

$$I_{x'}^{plate} = \frac{(b\cos\alpha)^3\, t/\cos\alpha}{12} = \frac{b^3 t}{12}\cos^2\alpha = I_x^{plate}\cos^2\alpha \tag{3.105}$$

The bending stiffness of the solid tubular column consists of two parts. One part is contributed by the in-plane bending stiffness of each side about its own principal axis multiplied by the squared cosine of the angle between the plane of this side and the plane of bending. The other part is due to the axial stiffness of each side multiplied by the squared distance between the centre of gravity of this side and the neutral axis:

$$\begin{aligned} EI_{x'} &= 2EI^{plate}\cos^2\alpha + 2EI^{plate}\cos^2(\pi-\alpha) + 2EA^{plate}\left(\frac{b}{2}\cos\alpha\right)^2 + \\ &2EA^{plate}\left(\frac{b}{2}\cos(\pi-\alpha)\right)^2 = 2EI^{plate} + 2EA^{plate}\frac{b^2}{4} = EI_x \end{aligned} \tag{3.106}$$

It can be seen from the last equation that the bending stiffness of the square tubular cross-section is the same about any axis through the centre of the square, which is a known result for shapes with more than two axes of symmetry. Moreover, the relative contributions of bending stiffnesses of the plates in their planes and their axial stiffnesses also stay constant as the plane of bending rotates. The result shown in eq. 3.104 reveals a

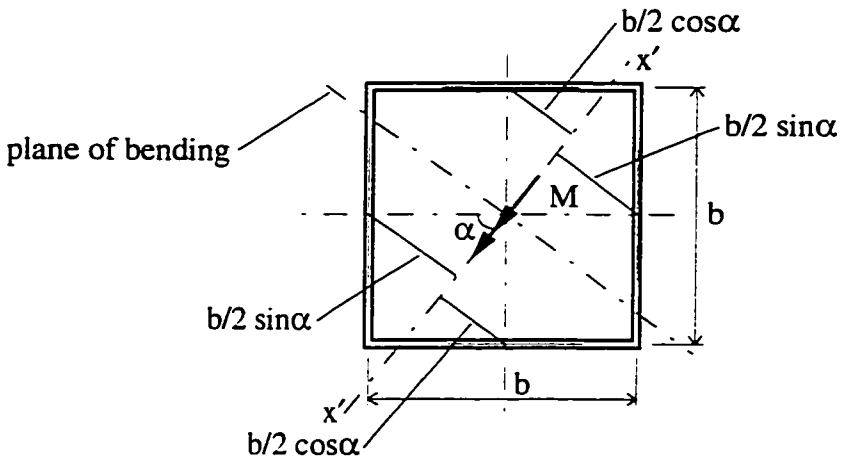

(a)

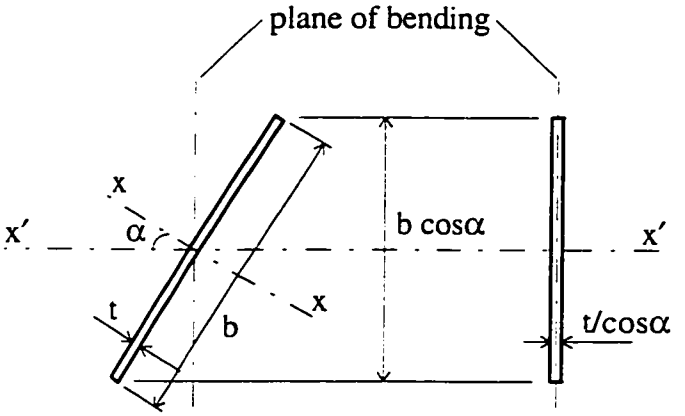

(b)

Figure 3.29: Bending of a solid tubular square cross-section (a) and thin plate (b) in an arbitrary plane.

similar situation in the case of square pantographic column. Its equivalent bending stiffness is the same for any direction of bending and equals twice the value of the equivalent bending stiffness of a single planar pantographic column in its own plane. This suggests that the same formula can be applied to calculate the bending stiffness of the planar column for bending about an arbitrary axis as that on the right side of eq. 3.105; i.e. the equivalent bending stiffness $6EI\sin\gamma$ has to be multiplied by the squared cosine of the angle between the plane of the two-dimensional column and the plane of bending.

Let us see if the last conclusion is valid for the triangular column. The equivalent bending stiffness for such a column in the situation when the plane of bending is perpendicular to one of the sides of the triangle was found in the last Section and equals $1.5(EI)_e^{planar}$. Based on the last conclusion one can calculate this stiffness by adding the contributions of the three sides of the triangle, one of which is perpendicular to the plane of bending and the other two form the angles of 30° with this plane (Fig. 3.30a):

$$(EI)_e = (EI)_e^{planar}\cos^2 90° + 2(EI)_e^{planar}\cos^2 30° = \frac{3}{2}(EI)_e^{planar} \tag{3.107}$$

If the plane of bending is parallel to one of the sides, the other two sides form the angles of 60° with this plane (Fig. 3.30b):

$$(EI)_e = (EI)_e^{planar}\cos^2 0° + 2(EI)_e^{planar}\cos^2 60° = \frac{3}{2}(EI)_e^{planar} \tag{3.108}$$

And finally, for arbitrary orientation of the plane of bending (Fig. 3.30c):

$$(EI)_e = (EI)_e^{planar}\cos^2\alpha + (EI)_e^{planar}\cos^2(\alpha - 60°) + (EI)_e^{planar}\cos^2(\alpha + 60°) =$$

$$(EI)_e^{planar}\left[\cos^2\alpha + (\cos\alpha\cos 60° + \sin\alpha\sin 60°)^2 + (\cos\alpha\cos 60° - \sin\alpha\sin 60°)^2\right] = \tag{3.109}$$

$$(EI)_e^{planar}\left[\cos^2\alpha + \frac{1}{4}\cos^2\alpha + \frac{3}{4}\sin^2\alpha + \frac{1}{4}\cos^2\alpha + \frac{3}{4}\sin^2\alpha\right] = \frac{3}{2}(EI)_e^{planar}$$

The bending stiffness of a triangular column is therefore also independent of orientation of the plane of bending.

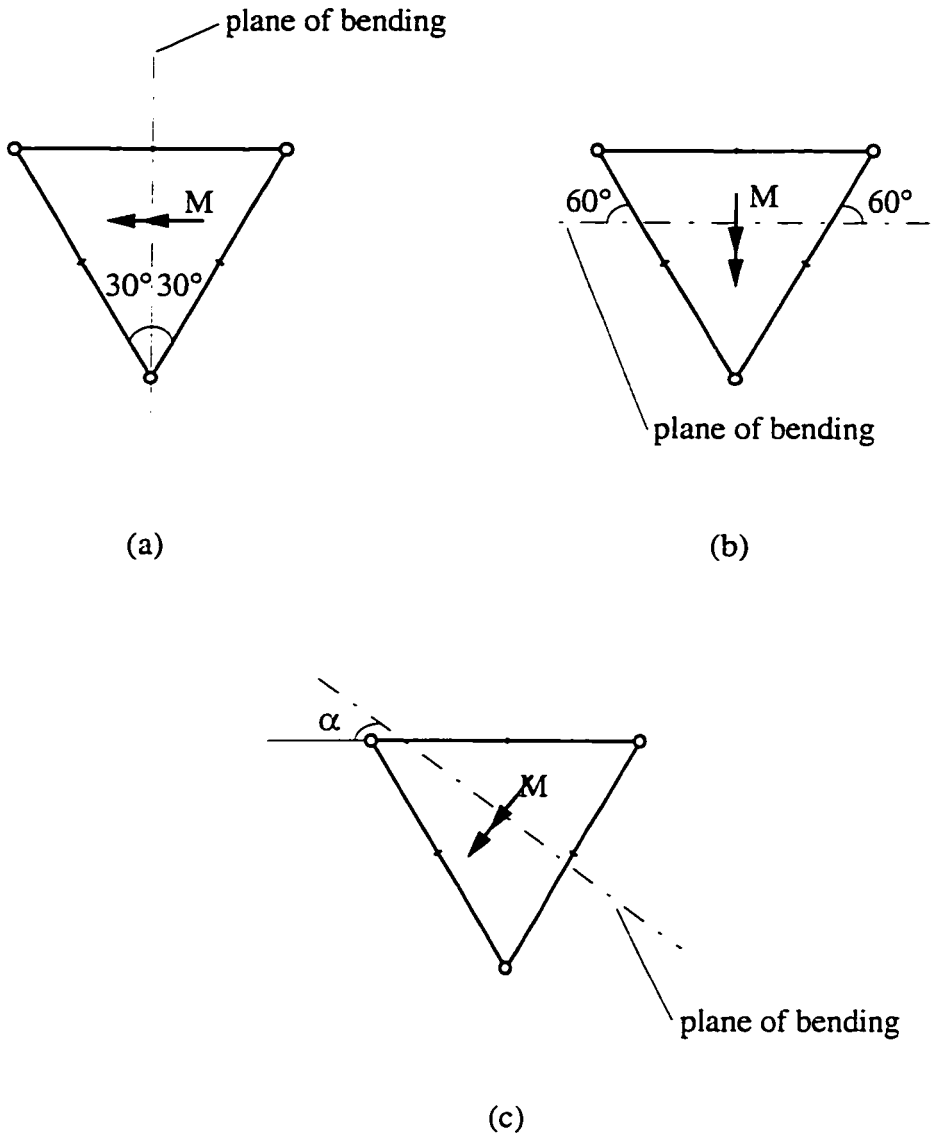

Figure 3.30: Bending of a triangular column: in the plane normal to one of the sides (a), in the plane parallel to one of the sides (b), in an arbitrary plane (c).

The general expression for calculating the equivalent bending stiffness of pantographic columns can be written in the following form:

$$(EI)_e = \sum_{i=1}^{k} (EI)_{ei}^{planar} \cos^2 \alpha_i \ , \qquad (3.110)$$

where k is the number of sides in the column cross-section. The similarity between solid columns with hollow cross-section and pantographic columns lies in the fact that the contribution of each side of the cross-section due to its own bending stiffness to the stiffness of the whole section is calculated in the same fashion. In the solid columns, however, the bending stiffness of a side, as well as its axial stiffness, is an integral effect of the axial stiffness of the fibres. Each fibre contributes axial stiffness regardless of its location: it can be located in a side of the column which undergoes only bending, in a side which experiences only axial deformation (tension or compression), or in a side subjected to a combination of the two. The farther a particular fibre (and the side of the cross-section it belongs to) is from the neutral axis the higher its contribution to overall bending stiffness will be. In pantographic columns, where the axial stiffness of the sides is negligible, the distance between the side and the neutral axis does not matter. In fact, the concept of a neutral axis hardly has meaning in this type of structures. The contribution of each side of the pantographic column to the overall stiffness depends only on the orientation of the side with respect to the plane of bending.

3.5 Pantographic Column Subjected to Lateral Load

The next system to be considered is the three-dimensional pantographic column of square cross-section subjected to a horizontal lateral load (Fig. 3.31). The load acts in the direction parallel to two sides of the cross-section. Therefore all symmetry considerations discussed for the same column in bending are valid. The stiffness matrix of this structure was derived earlier. Hence, only the new load vector has to be derived.

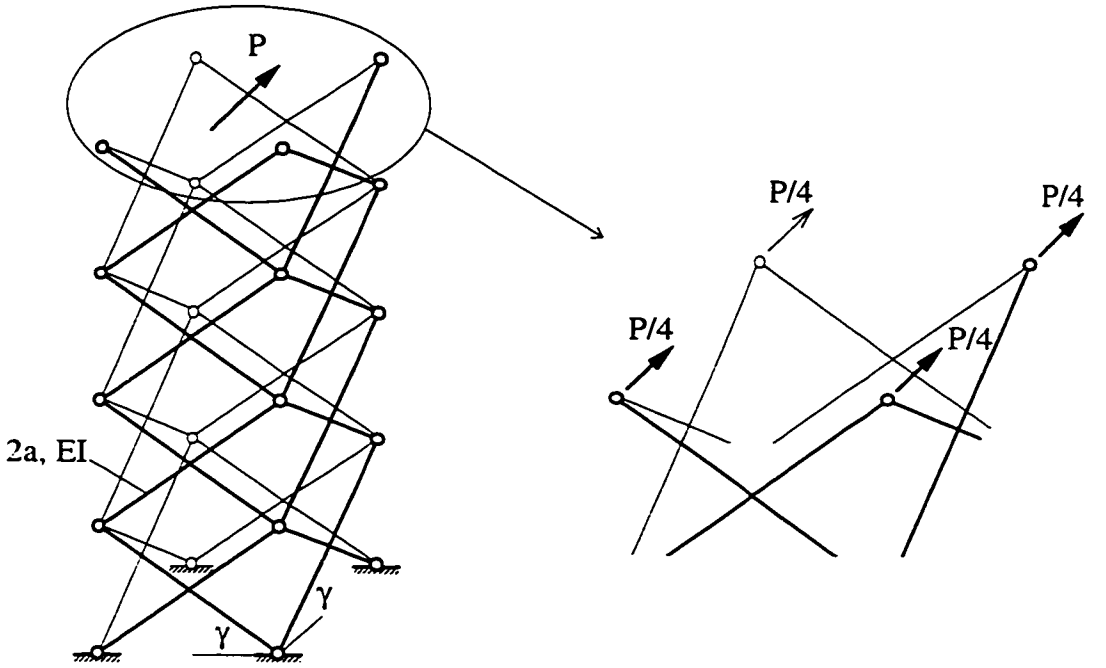

(a) - 3d view

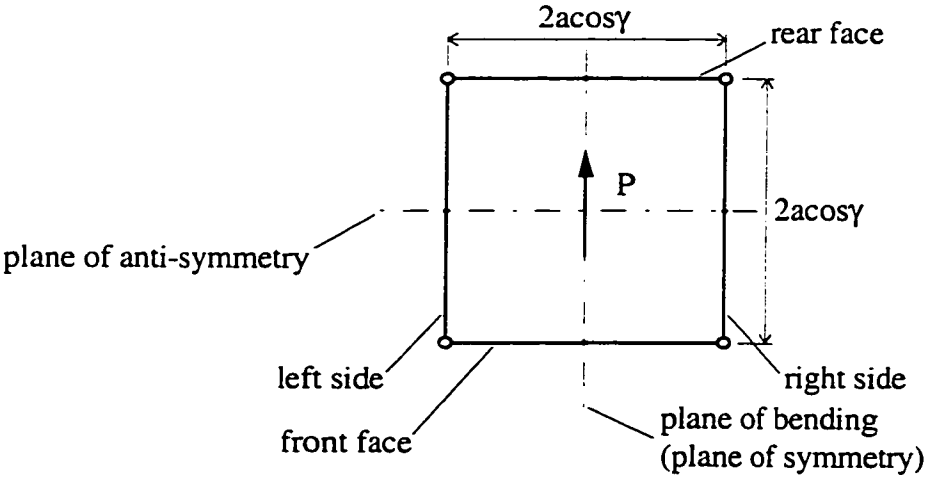

(b) - top view

Figure 3.31: Three-dimensional pantographic column of square cross-section subjected to lateral loading.

3.5.1 Analysis of a Single Square Unit by the Force Method

The top nodes of a single square pantographic unit are subjected to four horizontal forces, similar to those applied at the top of the column in Fig. 3.31. The bottom nodes of the unit are hinged to the ground. The primary structure and the redundant forces are the same as those shown in Fig. 3.3 with only this difference, that the springs at the bottom nodes are infinitely rigid. The flexibility coefficients from eqs 3.2 to 3.4 can be used without the terms containing k in the denominator. The primary structure subjected to the external lateral load is shown in Fig. 3.32 - the forces are applied to the side SLEs only. The load coefficients:

$$\Delta_1 = -\frac{1}{EI}\frac{a\cos\gamma\, a}{2}\frac{2}{3}\frac{P}{4}a\sin\gamma\cdot 4\cdot 2 = -\frac{2Pa^3\sin\gamma\cos\gamma}{3EI}, \quad \Delta_2 = 0 \tag{3.111}$$

and the compatibility equations:

$$\begin{aligned}\frac{16a^3\cos^2\gamma}{3EI}x_1 - \frac{8a^3\sin\gamma\cos\gamma}{3EI}x_2 &= \frac{2Pa^3\sin\gamma\cos\gamma}{3EI}\\ -\frac{8a^3\sin\gamma\cos\gamma}{3EI}x_1 + \frac{8a^3}{3EI}\left(1+\sin^2\gamma\right)x_2 &= 0\end{aligned} \tag{3.112}$$

yield the following expressions for the redundant forces:

$$x_1 = \frac{P}{4}\frac{\sin\gamma}{\cos\gamma}\frac{1+\sin^2\gamma}{2+\sin^2\gamma}, \qquad x_2 = \frac{P}{4}\frac{\sin^2\gamma}{2+\sin^2\gamma} \tag{3.113}$$

The pivotal bending moments and horizontal reactions at the bottom nodes normal to the plane of bending are shown in Fig. 3.33. The total horizontal displacement of the top nodes in the same direction can be found based on these moments and those caused by horizontal virtual unit forces applied to the primary structure as shown in Fig. 3.6 (T = 1):

$$h_P = \frac{1}{EI}\frac{Pa}{4}\frac{\sin^2\gamma}{2+\sin^2\gamma}\frac{a}{2}\frac{2}{3}a\cdot 4\cdot 2 = \frac{2Pa^3}{3EI}\frac{\sin^2\gamma}{2+\sin^2\gamma} \tag{3.114}$$

If the top nodes are constrained from such horizontal displacement, the reactions in the constraints can be obtained by superimposing the effects given by eqs 3.26 and 3.114:

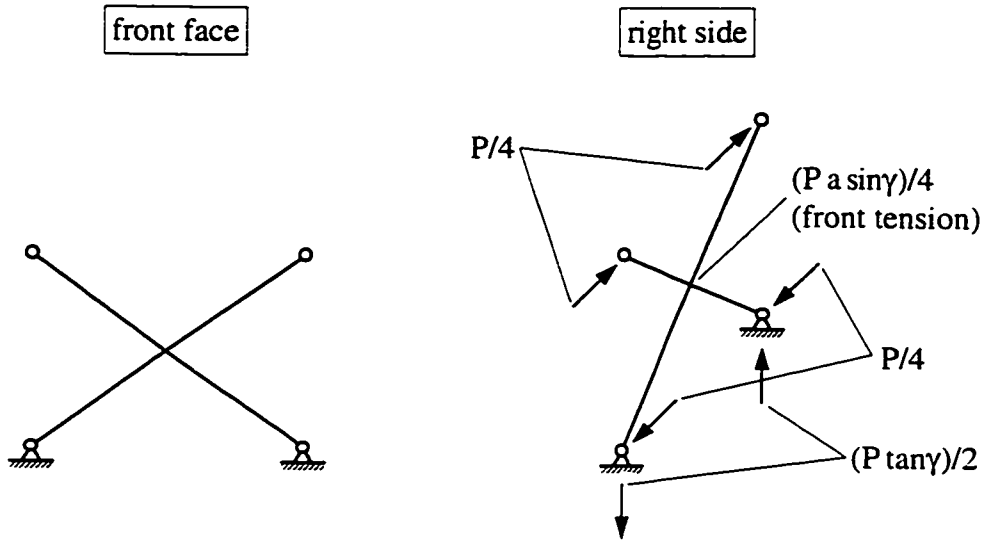

Figure 3.32: Pivotal moments and reactions for the primary structure of a square pantographic unit subjected to lateral load.

$$h_T = -h_P \quad \rightarrow \quad T = -\frac{P}{4} \tag{3.115}$$

The reactions at the bottom nodes, found from eq. 3.22, eq. 3.115 and Fig. 3.33, have the same direction and magnitude. There is no bending in the bars of the constrained unit under the lateral load.

3.5.2 Load Vector for the Displacement Method Analysis of Square Column

To avoid the local effects near the bottom of the column because of the support conditions there, we will first analyze the structure shown in Fig. 3.34a with the bottom nodes free to move in the direction normal to the plane of bending. Therefore, a constraint against such a displacement has to be placed at this level as well as at every unit interface and the top of

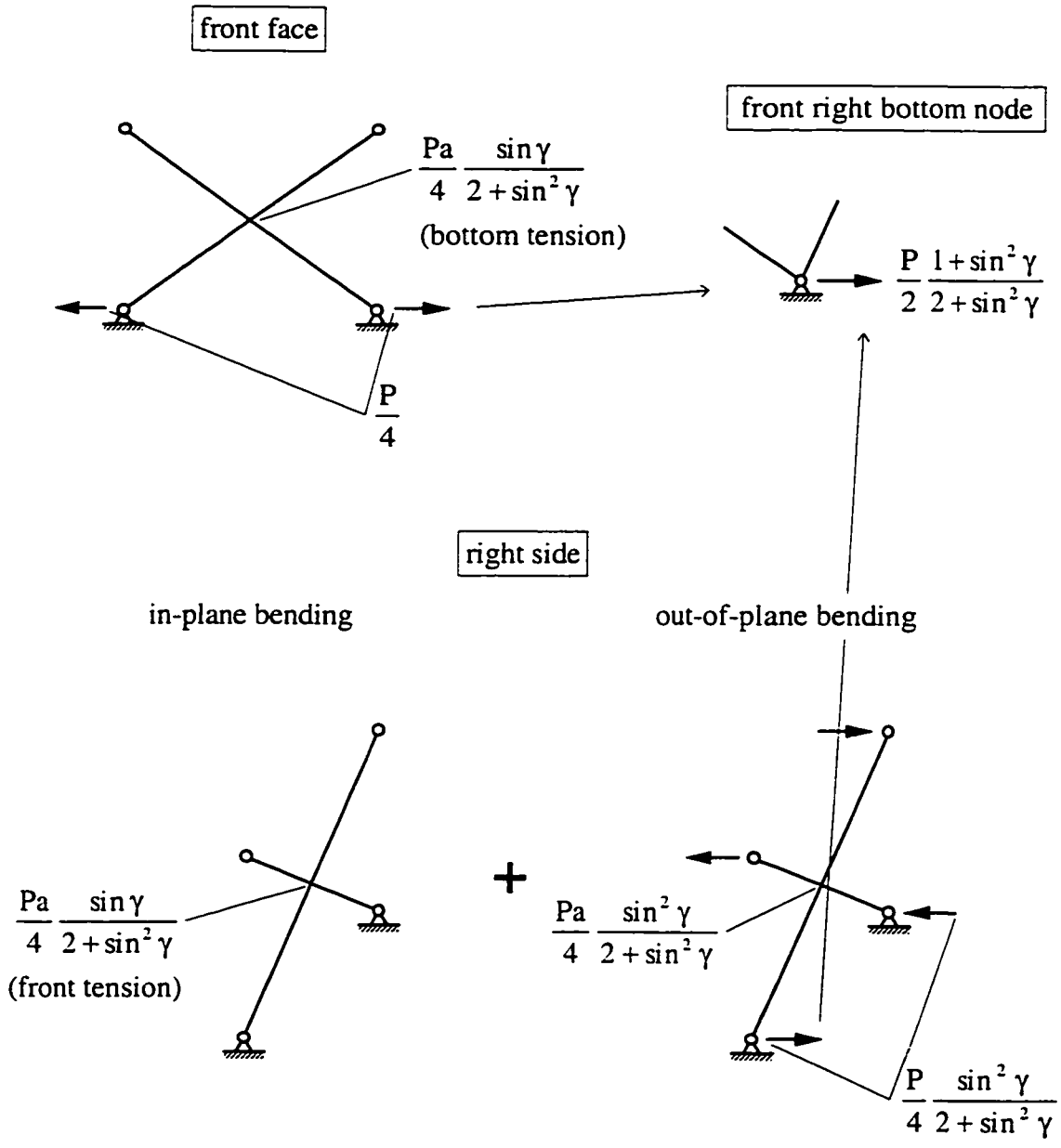

Figure 3.33: Pivotal moments and horizontal reactions (normal to the plane of bending) at bottom nodes of a square pantographic unit subjected to lateral load.

the column to obtain the primary structure of the displacement method (Fig. 3.34b). The entries of the load vector are the reactions in (n+1) constraints of the primary structure due to lateral load; these entries are the sums of reactions in the four links at each level since these four links constitute a single constraint. A typical square pantographic unit, unit number i, from the constrained column subjected to lateral load is shown in Fig. 3.35. The contribution of this unit to the constraint reactions at its top and bottom nodes is the superposition of the constraint forces due to lateral load P applied to this unit (eq. 3.115) and the constraint forces due to moment M_i = P 2a sinγ (i-1) at the top of this unit (Fig. 3.7a). The first and last entries of the load vector **P** are:

$$p_1 = -P\,, \qquad p_{n+1} = \left[-\frac{P}{4} - \frac{P}{2}(n-1)\right]\cdot 4 = -P\,(2n-1) \tag{3.116}$$

The constraints at unit interfaces serve for the units above and below each interface. Hence the intermediate entries of the load vector are:

$$p_i = \left[-\frac{P}{4} - \frac{P}{2}(i-2) - \frac{P}{4} - \frac{P}{2}(i-1)\right]\cdot 4 = -4P\,(i-1)\,, \quad i = 2,\ldots,n \tag{3.117}$$

The system of (n+1) equilibrium equations can now be written:

$$\begin{bmatrix} \frac{6\,EI}{a^3}\frac{2+\sin^2\gamma}{\sin^2\gamma} & -\frac{6\,EI}{a^3} & & & & 0 \\ & \cdots & & & & \\ & -\frac{6\,EI}{a^3} & \frac{12\,EI}{a^3}\frac{2+\sin^2\gamma}{\sin^2\gamma} & -\frac{6\,EI}{a^3} & & \\ & & \cdots & & & \\ 0 & & & -\frac{6\,EI}{a^3} & \frac{6\,EI}{a^3}\frac{2+\sin^2\gamma}{\sin^2\gamma} & \end{bmatrix} \mathbf{y} = \begin{bmatrix} P \\ \cdots \\ 4P(i-1) \\ \cdots \\ P(2n-1) \end{bmatrix} \tag{3.118}$$

If each equation in the above system is divided by $6EI/a^3$ throughout and the following notations are introduced:

$$A = \frac{2+\sin^2\gamma}{\sin^2\gamma}, \quad B = \frac{P\,a^3}{6\,EI}\,, \tag{3.119}$$

the system becomes

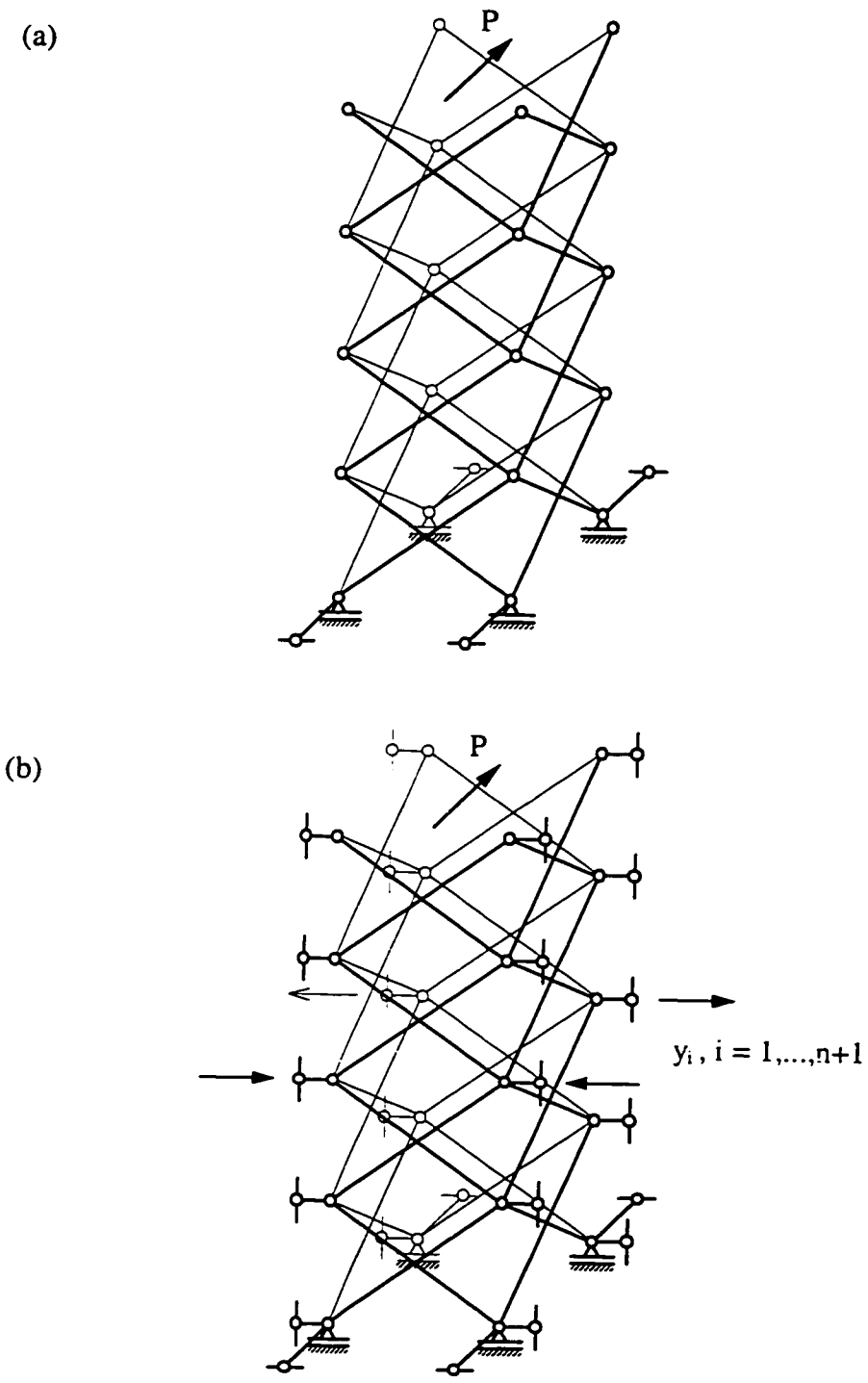

Figure 3.34: Pantographic column with the bottom nodes free in the direction normal to the plane of bending subjected to lateral load (a), its primary structure of the displacement method (b).

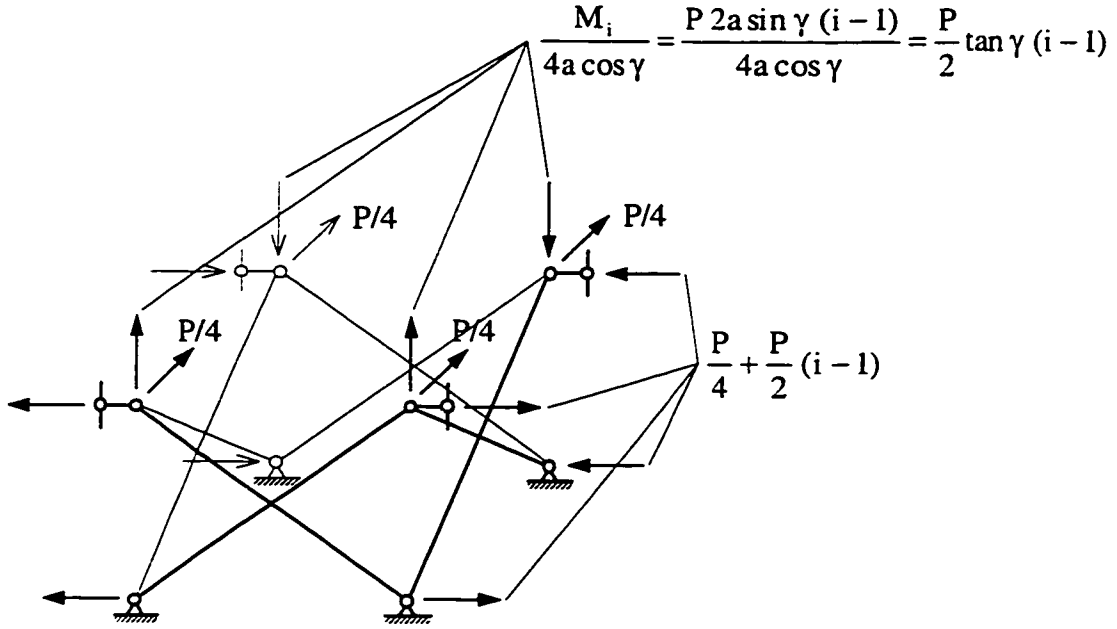

Figure 3.35: Pantographic unit number i from the constrained column under lateral load and reactions in horizontal constraints.

$$\begin{bmatrix} A & -1 & & & 0 \\ & \cdots & & & \\ & -1 & 2A & -1 & \\ & & \cdots & & \\ 0 & & & -1 & A \end{bmatrix} \mathbf{y} = \begin{bmatrix} B \\ \cdots \\ 4B(i-1) \\ \cdots \\ B(2n-1) \end{bmatrix} \quad \text{or} \quad \mathbf{K}_m^u\,\mathbf{y} = \mathbf{P}_m \tag{3.120}$$

3.5.3 Linear and Local Solutions

Matrix $\mathbf{K}_m^u$ is the same as that used to find the uniform solution in the case of square column in bending (eq. 3.42). Let us inspect the right side vector to see whether its pattern suggests any particular form of solution. In the main portion of the right side vector, for i = 2,...,n, every two successive entries differ by the constant 4B. If it can be

assumed that the entries of the solution vector also have a similar pattern of linear growth, i.e. $y_{i+1}^{lin} = y_i^{lin} + \Delta_y$, then the i-th equation of the system can be written as:

$$-y_{i-1}^{lin} + 2Ay_i^{lin} - y_{i+1}^{lin} = 4B(i-1) \quad \rightarrow \quad -(y_i^{lin} - \Delta_y) + 2Ay_i^{lin} - (y_i^{lin} + \Delta_y) = 4B(i-1)$$

$$\rightarrow \quad y_i^{lin} = \frac{2B(i-1)}{A-1} = \frac{P\,a^3 \sin^2\gamma}{6\,EI}(i-1), \quad i = 1,\ldots,n+1 \tag{3.121}$$

The last expression of eq. 3.121 must hold for all elements of the solution vector including the first and the last, otherwise the equations number two and n of system 3.120 would not be satisfied. The first and the last entries of the right-side vector which comply with this solution vector can now be found by substitution of y_1^{lin} and y_2^{lin} in the first equation, and y_n^{lin} and y_{n+1}^{lin} in the last equation of system 3.120:

$$\begin{aligned} A\cdot 0 - \frac{2B}{A-1} &= B - B\frac{A+1}{A-1} = p_{m,1}^{lin} \\ -\frac{2B(n-1)}{A-1} + A\frac{2B[(n+1)-1]}{A-1} &= B(2n-1) + B\frac{A+1}{A-1} = p_{m,n+1}^{lin} \end{aligned} \tag{3.122}$$

System 3.120 can now be written in the following form:

$$\mathbf{K}_m^u\,(\mathbf{y}^{lin} + \mathbf{y}^{loc}) = \mathbf{P}_m^{lin} + \mathbf{P}_m^{loc}, \quad \text{where} \quad \mathbf{P}_m^{loc} = \mathbf{P}_m - \mathbf{P}_m^{lin} = \begin{bmatrix} B\frac{A+1}{A-1} \\ 0 \\ \cdots \\ 0 \\ -B\frac{A+1}{A-1} \end{bmatrix} \tag{3.123}$$

If the "local" right-side vector is separated into two parts:

$$\mathbf{P}_m^{loc} = \mathbf{P}_m^{loc\,1} + \mathbf{P}_m^{loc\,2} = \begin{bmatrix} B\frac{A+1}{A-1} \\ 0 \\ \cdots \\ 0 \end{bmatrix} + \begin{bmatrix} 0 \\ \cdots \\ 0 \\ -B\frac{A+1}{A-1} \end{bmatrix}, \tag{3.124}$$

the two local solutions can be obtained in the manner described in Section 3.2.3.2.2 and superimposed to form vector $\mathbf{y}^{loc}$. The first of these solution vectors has the first element equal to:

$$y_1^{loc} = \frac{B}{A-C}\frac{A+1}{A-1}, \quad \text{where} \quad C = A - \sqrt{A^2-1} < 1 \tag{3.125}$$

and the rest of the entries down the vector quickly diminish. The second of the local solution vectors has its last element equal to:

$$y_{n+1}^{loc} = -\frac{B}{A-C}\frac{A+1}{A-1} \tag{3.126}$$

and the rest of the entries up the vector also quickly approach zero. Hence, for a sufficiently large number of pantographic units in the column, the resulting local solution vector will have zeros in much of its middle portion, with a few non-zero elements near the top and bottom. The general expression for an element of vector $\mathbf{y}^{loc}$ is:

$$y_i^{loc} = y_1^{loc}C^{i-1} + y_{n+1}^{loc}C^{n+1-i} = \frac{B}{A-C}\frac{A+1}{A-1}\left(C^{i-1} - C^{n+1-i}\right) \tag{3.127}$$

The total horizontal displacement of the bottom nodes of the column is the sum of the last entries of the linear and local solution vectors:

$$y_{n+1}^{lin} + y_{n+1}^{loc} = \frac{2B}{A-1}n - \frac{B}{A-C}\frac{A+1}{A-1} = \frac{B}{A-1}\left(2n - \frac{A+1}{A-C}\right) \tag{3.128}$$

If the bottom nodes are hinged to the ground, then the value $-\left(y_{n+1}^{lin} + y_{n+1}^{loc}\right)$ is the last entry of an additional $\mathbf{y}^{sup}$ vector corresponding to the local horizontal support reaction load, at the ground level, which would bring these nodes to their original position (Fig. 3.36). Again, this additional solution is localized and affects mostly the internal forces in the bottom unit. Nevertheless, we will include this displacement in the final displacement vector, whose typical element can be now written as:

$$\begin{aligned} y_i = y_i^{lin} + y_i^{loc} + y_i^{sup} &= \frac{2B(i-1)}{A-1} + \frac{B}{A-1}\frac{A+1}{A-C}\left(C^{i-1} - C^{n+1-i}\right) - \\ &- \frac{B}{A-1}\left(2n - \frac{A+1}{A-C}\right)C^{n+1-i} = \frac{B}{A-1}\left[2(i-1) + \frac{A+1}{A-C}C^{i-1} - 2n\,C^{n+1-i}\right] \end{aligned} \tag{3.129}$$

From eq. 3.54 and eq. 3.119 one can obtain:

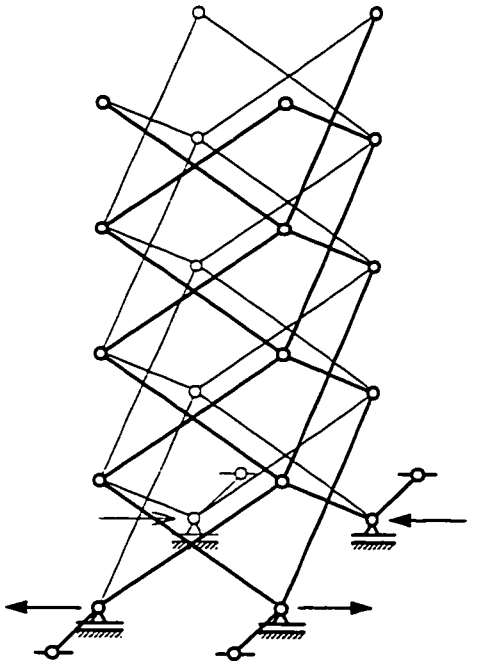

Figure 3.36: Local self-balanced load compensating horizontal displacement of the bottom nodes.

$$\frac{A+1}{A-C}=\frac{1+C}{1-C} \quad \text{and} \quad \frac{B}{A-1}=\frac{P\,a^3\sin^2\gamma}{12\,EI}, \quad \text{respectively} \tag{3.130}$$

The pivotal bending moments in the plane of the side SLEs can be found in the same fashion as was done in eq. 3.61. Using eqs 3.129 and 3.130 we obtain:

$$\begin{aligned} M^{in}_{rs,i} &= \frac{3\,EI}{2\,a^2\sin\gamma}(y_i+y_{i+1})= \\ &= \frac{P\,a\sin\gamma}{8}\left[2(i-1)+\frac{1+C}{1-C}C^{i-1}-2nC^{n+1-i}+2i+\frac{1+C}{1-C}C^{i}-2nC^{n-i}\right] \\ &= \frac{P\,a\sin\gamma}{8}\left[2(2i-1)+\frac{(1+C)^2}{(1-C)C}C^{i}-2n(1+C)C^{n-i}\right] \end{aligned} \tag{3.131}$$

To find the horizontal displacement of the top of the column, a unit virtual lateral load can be applied to the primary structure obtained by completely separating the four

planar pantographic columns forming faces and sides of the three-dimensional structure. The unit force, distributed in halves between the left and right sides, produces the in-plane pivotal bending moments in the side SLEs equal to (a sinγ)(2i-1)/4. The horizontal displacement is, therefore:

$$h = \sum_{i=1}^{n} \frac{1}{EI} \frac{M_{rs,i}^{in}}{2} a \frac{2}{3} \frac{a \sin\gamma}{4} (2i-1) \cdot 4 \cdot 2 = \\ = \frac{P a^3 \sin^2\gamma}{12\,EI} \sum_{i=1}^{n} \left[2(2i-1) + \frac{(1+C)^2}{(1-C)C} C^i - 2n(1+C)C^{n-i} \right] (2i-1) \tag{3.132}$$

The first term under the summation sign in the last equation corresponds to the deflection given by the linear solution alone:

$$h^{lin} = \frac{P a^3 \sin^2\gamma}{6\,EI} \sum_{i=1}^{n} (2i-1)^2 = \frac{2\,P a^3 \sin^2\gamma}{9\,EI} \left(n^3 - \frac{n}{4} \right) \tag{3.133}$$

This displacement is half of that of a planar column subjected to the same lateral load, which indicates the familiar fact that the stiffness of the square pantographic column is twice as much as that of the planar one. The reduction of the deflection due to the other two terms in eq. 3.132 is:

$$\Delta h = -\frac{P a^3 \sin^2\gamma}{12\,EI} \sum_{i=1}^{n} \left[2n(1+C)C^{n-i} - \frac{(1+C)^2}{(1-C)C} C^i \right] (2i-1) = -\frac{P a^3 \sin^2\gamma}{12\,EI} \cdot \\ \cdot \left[4n(1+C) \sum_{i=1}^{n} iC^{n-i} - 2n(1+C) \sum_{i=1}^{n} C^{n-i} - \frac{2(1+C)^2}{C(1-C)} \sum_{i=1}^{n} iC^i + \frac{(1+C)^2}{C(1-C)} \sum_{i=1}^{n} C^i \right] \tag{3.134}$$

The sums in the first and third terms in brackets in eq. 3.134 are calculated through the formulae of eqs B.13 and B.10; the sums in the second and fourth terms are those of standard geometric progressions:

$$\Delta h = -\frac{P a^3 \sin^2\gamma}{12\,EI} \left[\begin{array}{l} 4n(1+C) \left(\frac{n}{1-C} - C \frac{1-C^n}{(1-C)^2} \right) - 2n(1+C) \frac{1-C^n}{1-C} - \\ -2 \frac{(1+C)^2}{(1-C)} \frac{1-(1+n-nC)\,C^n}{(1-C)^2} + \frac{(1+C)^2}{(1-C)} \frac{1-C^n}{1-C} \end{array} \right] \tag{3.135}$$

If all terms containing C^n in the last equation are neglected (recall: C is small, n is large) and the coefficient in front of the brackets is made the same as that in eq. 3.133:

$$\Delta h = -\frac{P\,a^3 \sin^2\gamma}{12\,EI}\left[4n^2\frac{1+C}{1-C} - 2n\left(\frac{1+C}{1-C}\right)^2 - \left(\frac{1+C}{1-C}\right)^3\right] =$$
$$= -\frac{2\,P\,a^3 \sin^2\gamma}{9\,EI}\left[\frac{3}{2}n^2\frac{1+C}{1-C} - \frac{3}{4}n\left(\frac{1+C}{1-C}\right)^2 - \frac{3}{8}\left(\frac{1+C}{1-C}\right)^3\right] \tag{3.136}$$

The ratio of Δh from eq. 3.136 and h^{lin} from eq. 3.133 is plotted in Fig. 3.37 versus degree of deployment for two columns consisting of five and ten units. Even for the column with five units the difference for the ratios calculated with Δh from eq. 3.135 and 3.136 cannot be seen on the scale of this graph. The linear solution, proportional to n^3, becomes more and more predominant as the number of units in the column increases. The important part of the sum of all local solutions Δh is, of course, the term of order n^2 which also can be seen in the graphs of Fig. 3.37. This term is present here due to the hinge supports at the bottom of the column. Comparing this result and those from eqs. 3.63 and 3.100, one can conclude that such support conditions introduce a displacement reduction one power of n smaller than the displacement given by the dominant solution, i.e. the uniform solution in the case of pure bending and the linear solution in the case of lateral load. If the bottom nodes were free to move in the direction normal to the plane of bending, the highest power of n in Δh would be one - resulting from in-plane bending of bars in the face SLEs and out-of-plane bending of bars in the side SLEs. These bending moments are uniform along most of the column because of the constant difference between the successive elements of the linear solution vector.

3.5.4 Triangular Column Subjected to Lateral Load

Observing eqs. 3.63 and 3.100 and noticing that the displacement reduction due to the support conditions has exactly the same form for square and triangular columns in pure bending, one may expect such a sameness of form in the case of lateral load. Scaling eqs. 3.133 and 3.136 to transform the equivalent bending stiffness from $12EI\sin\gamma$ for square column to $9EI\sin\gamma$ for triangular column, we therefore write, without further proof:

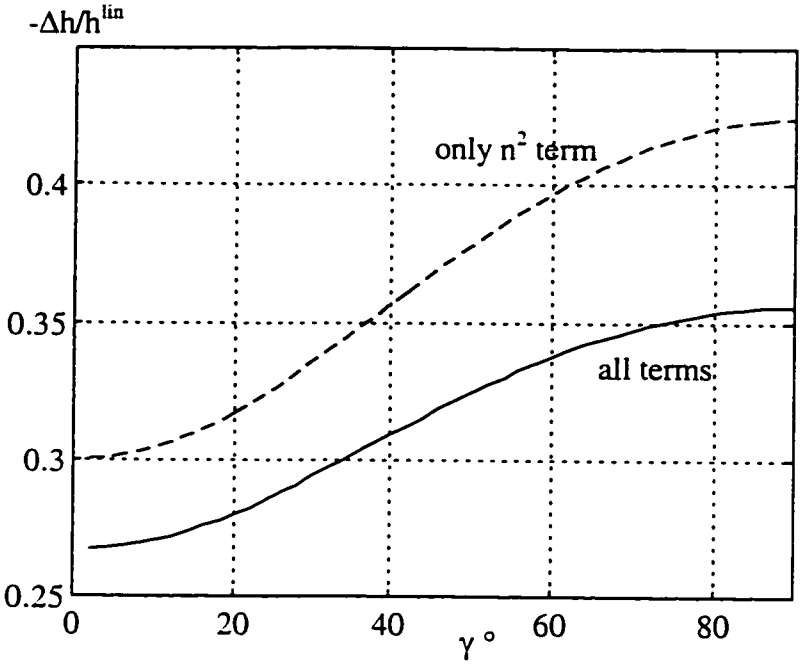

(a) - n = 5

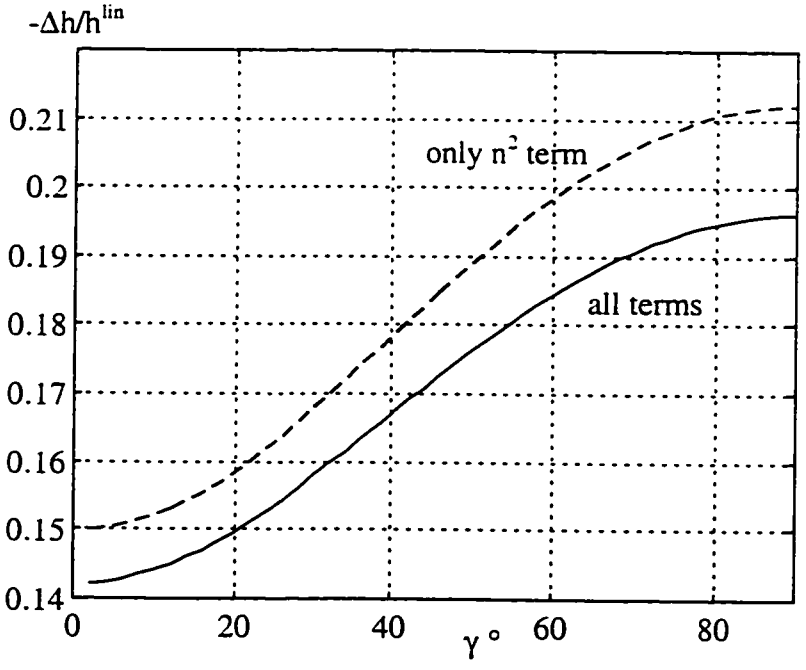

(b) - n = 10

Figure 3.37: Stiffening of a square pantographic column under lateral load compared to two separate planar columns versus the degree of deployment.

$$h = h^{lin} + \Delta h = \frac{8\,P\,a^3 \sin^2\gamma}{27\,EI}\left\{\left[n^3 - \frac{n}{4}\right] - \left[\frac{3}{2}n^2\frac{1+C}{1-C} - \frac{3}{4}n\left(\frac{1+C}{1-C}\right)^2 - \frac{3}{8}\left(\frac{1+C}{1-C}\right)^3\right]\right\}, \quad (3.137)$$

where C is given by eq. 3.92. The ratio of the two terms in the figure brackets in eq. 3.137 is plotted in Fig. 3.38 for n = 5.

Fortunately, there exists a reference that allows a check on this result. A five-unit triangular pantographic column (Fig. 3.39a) was analyzed and tested by You and Pellegrino (1996b). Although the subject of the paper is a cable-stiffened deployable structure, some results for the column without prestressing are also provided. Fig. 3.39b reproduces the response of the column (deflections of one of the top nodes) to the lateral load equally divided among the three top nodes and acting in the direction parallel to the plane of symmetry of the system.

The experimental model had the following parameters. The bars were made of Aluminum alloy with Young's modulus 69 GPa, they all had a circular tubular cross-section with inside and outside radii 3.86 mm and 4.77 mm, respectively. The length of each bar was 400 mm, and therefore the length of the column at $\gamma = 45°$ was 1.410 m. With this information the equivalent bending stiffness of the column can be readily calculated: $(EI)_e = 103 \cdot 10^6$ N/mm^2. The deflection of the equivalent cantilever is $h = PL^3/3(EI)_e = 8.9$ P, which yields deflection in millimeters if the load is in Newtons. If the support conditions at the bottom nodes are assumed to be similar to hinges, this deflection has to be reduced by approximately one fifth (Fig. 3.38): h = 7.15 P. For P equal to 4 N, the deflection is 28.6 mm, compared to roughly 25 mm that can be read from the diagram in Fig. 3.39b. The reason for the calculated deflection being higher than that of the model may be attributed to the type of connections between the bar ends in the model. These connections were revolute, not spherical, joints which introduce torsion in the bars and therefore additional stiffness. The question of whether the active cable contributes to the stiffness of the structure without prestress is also open.

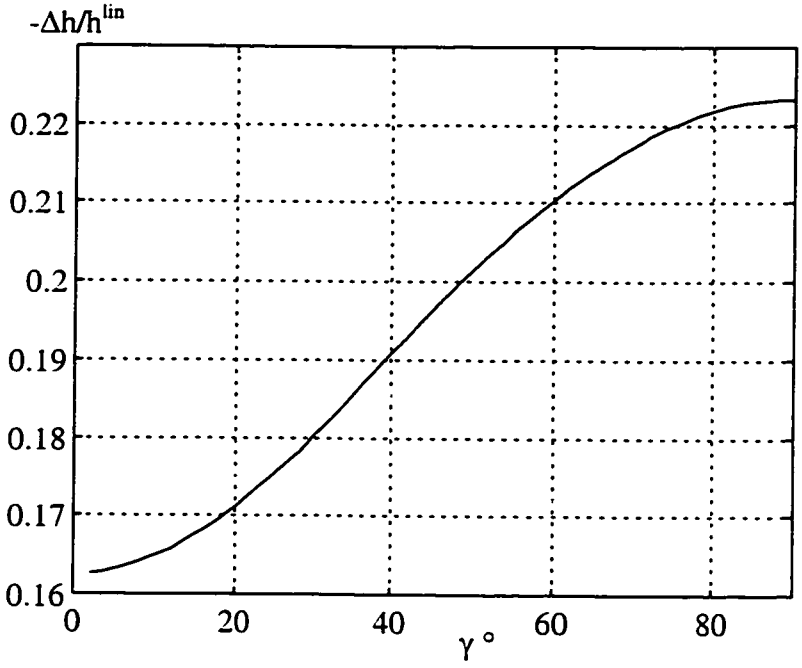

Figure 3.38: Ratio of the deflections from all local and linear solutions for a triangular pantographic column under lateral load (n = 5) versus the degree of deployment.

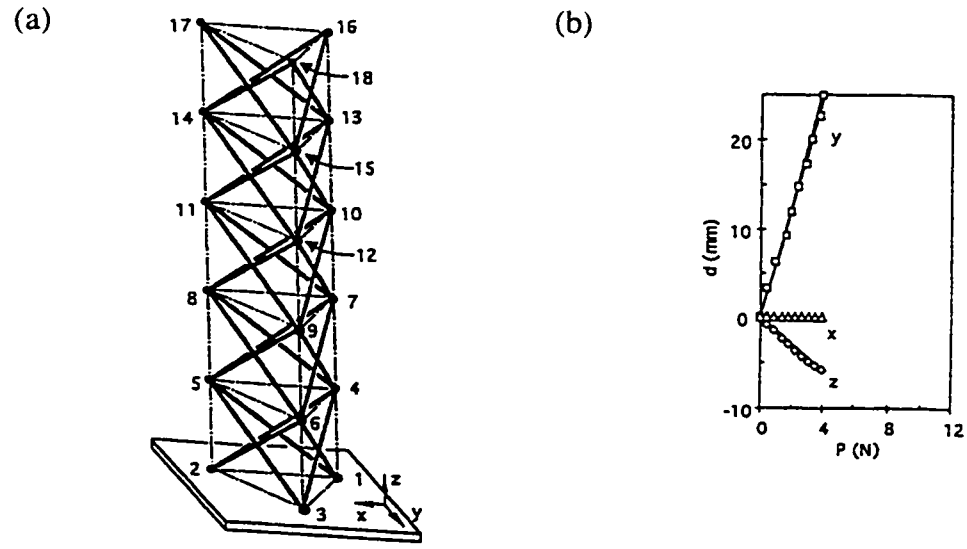

Figure 3.39: Triangular mast - n = 5, γ = 45° (a); displacement components of joint 18 due to load P in the y-direction (b) (You and Pellegrino, 1996b).

3.6 Pantographic Slabs

Most of the pantographic slabs seen in the literature have a layout similar to that shown in Fig. 3.40a (the planes of all two-dimensional SLEs are made opaque to unload the figure). They consist of two sets of planar pantographic beams running in orthogonal directions. The planes of all two-dimensional columns are perpendicular to the "midsurface" of the slab. Another way to imagine how such slabs are formed is to take a number of three-dimensional identical square pantographic units made of four vertical SLEs each, such as those analyzed in the previous Sections, and put them on a horizontal plane side by side, with common faces shared between adjoining units. When folded, every unit, as well as the whole slab, becomes a one-dimensional segment of length 2a, which is the length of bars in all two-dimensional SLEs. This, of course, is true in the ideal case when bars have only length and no thickness, and joints are points with zero size. The other extreme state of such slabs is a completely unfolded two-dimensional configuration - the rectangle 2am×2an, where m and n are the numbers of square units in the two directions in the plane of the slab (m = n = 3 in Fig. 3.40a). The deployed three-dimensional configuration of the structure lies between these two extremes. The bending stiffness of such slabs is the same in both directions of the two families of planar beams and is defined by the bending stiffness of a single two-dimensional pantographic beam in its own plane. The advantage of these structures, being a compact bundle in the folded state, is therefore paired with a relatively low bending stiffness of their working configuration.

Another possibility for creating a deployable pantographic slab is illustrated in Fig. 3.40b. The slab can be formed from a number of single units put side by side, but now each unit has two SLEs horizontal and the other two - vertical. Thinking in terms of planar pantographic columns, one can say that there are three sets of them: columns in one set lie in planes perpendicular to the "midsurface" of the slab; columns in the other two sets are parallel to the "midsurface" and form the top and bottom "skins" of the slab. Finally, the same result is obtained if a number of three-dimensional columns considered

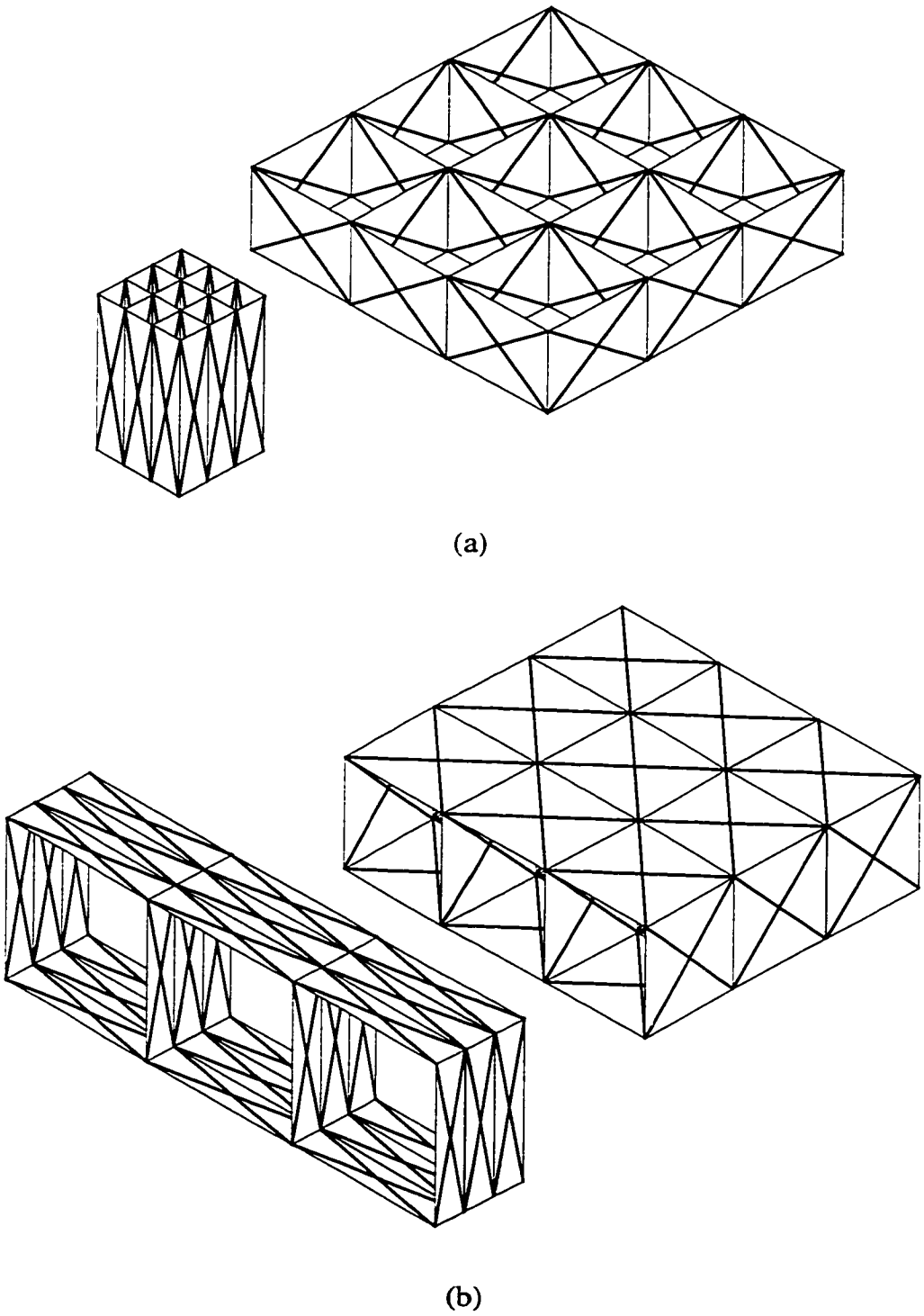

Figure 3.40: Pantographic slabs: with two sets of planar columns normal to the "midsurface" of the slab (a), with one set of planar columns normal and two sets of planar columns parallel to the "midsurface" of the slab (b).

before are laid horizontally side by side. One extreme configuration of such an arrangement is obtained if each unit is folded into a two-dimensional square. The structure, therefore, becomes a rectangle 2a×2am, where m is the number of three-dimensional columns put together to form the slab (m = 3 in Fig. 3.40b). The almost folded configuration of the slab is shown in Fig. 3.40b. In the completely unfolded state, the slab becomes a straight line of length 2an, where n is the number of square units in each column (n = 3 in Fig. 3.40b). It can be seen that this type of pantographic slab looses in the compactness of the folded configuration to the one described earlier.

The behaviour of a slab of the second type under certain loads is qualitatively different from that of the first type and even from the behaviour of a separate three-dimensional pantographic column. A long slab bent in the short direction is shown in Fig. 3.41. If one were to estimate the bending stiffness of this structure, the first impulse would probably be to relate this characteristic to that of a single three-dimensional column, which is a function of the equivalent bending stiffness of the planar columns parallel to the plane of bending. The latter stiffness, in turn, is proportional to the bending stiffness of bars in the SLEs.

It is a known fact that, due to the Poisson's effect, the stiffness of a one-way solid slab is greater than that of a number of separate beams of the same thickness. A similar but much more crucial effect is present here. If a long slab is subjected to a load causing one-way bending, the vertical sections of such a slab, if they are located far enough away from the edges, are in a state of plane strain. In the long pantographic slab the vertical planes through the interfaces of the three-dimensional columns that form the slab can be considered planes of symmetry of the system, if these planes have large enough portions of the structure on both sides (Fig. 3.41). Joints lying in such a plane will not have any displacements in the direction normal to it. A typical three-dimensional pantographic column in the middle portion of the long deployable slab is confined between the two vertical symmetry planes. The rest of the slab prevents displacements of the nodes of this

column in the direction normal to the plane of bending. The column, therefore, behaves as the constrained structure from Fig. 3.7b. The bars in such a column do not experience any bending. For pure moment load there are only axial forces in the bars of the SLEs perpendicular to the plane of bending. For a transverse load the corresponding bending moment will also induce axial forces in these bars, and shear will be resisted by the axial forces in the bars of the vertical SLEs. Thus, the moment bearing function is shifted from bending of bars in the SLEs parallel to the plane of bending (in a separate column) to axial action of bars in the SLEs perpendicular to the plane of bending (if the column is a part of a slab assembly). The bending stiffness of the slab is therefore greatly increased since it is defined by the axial rather than bending stiffness of the bars.

The above reasoning can also be applied to pantographic slabs made of three-dimensional columns with triangular cross-section (Fig. 3.42).

3.7 Conclusions

In this Chapter three-dimensional pantographic columns subjected to two types of load are considered. Columns with both square and triangular cross-sections subjected to moment load are analyzed first. The column with a square cross-section subjected to lateral load is then investigated, and the results are extended to the column with triangular cross-section. The common procedure starts from the analysis of the basic three-dimensional pantographic unit by the force method. Square and triangular units are both statically indeterminate structures for which the primary structure is obtained by separating the two-dimensional SLEs that form the sides of a unit. The symmetry properties of the structure and its loading are extensively utilized to reduce the number of unknowns. The outcome of the single unit analysis allows one to arrive at the displacement method formulation for the whole column.

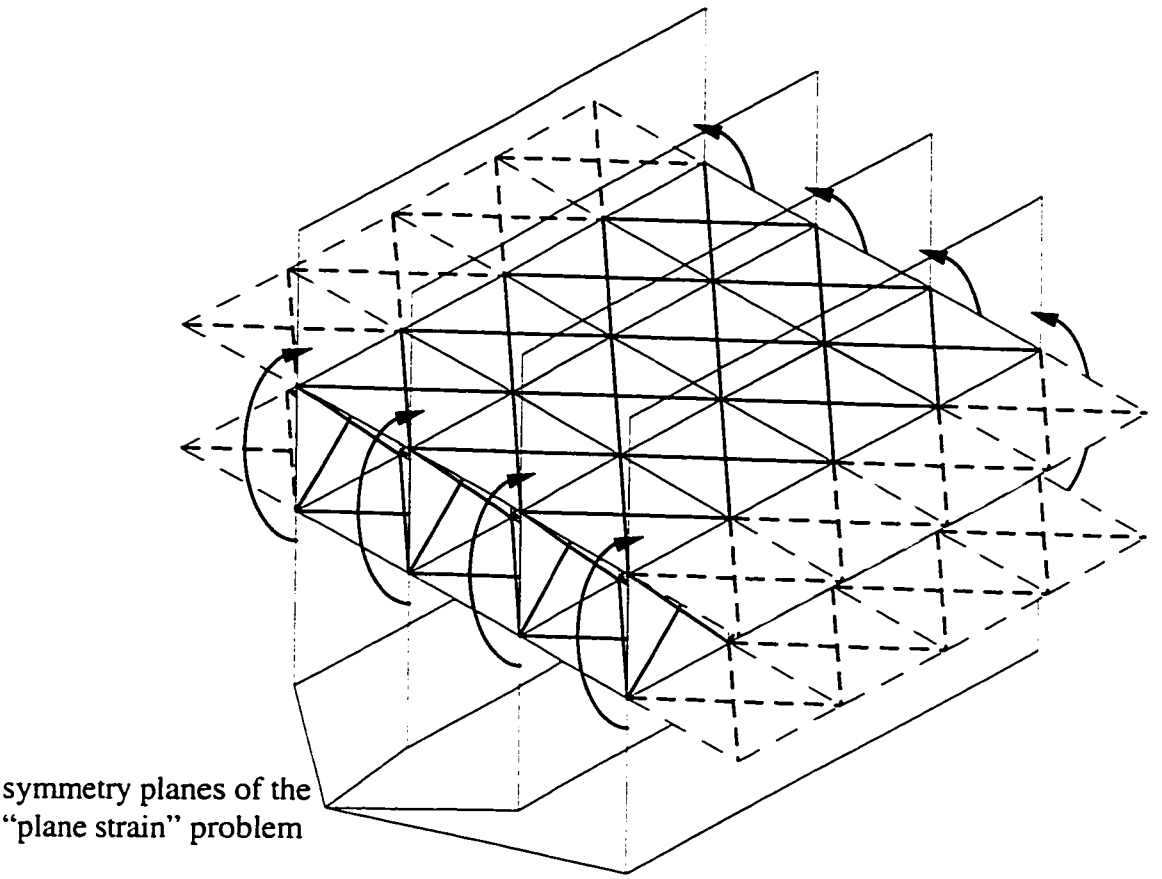

Figure 3.41: Long pantographic slab in bending.

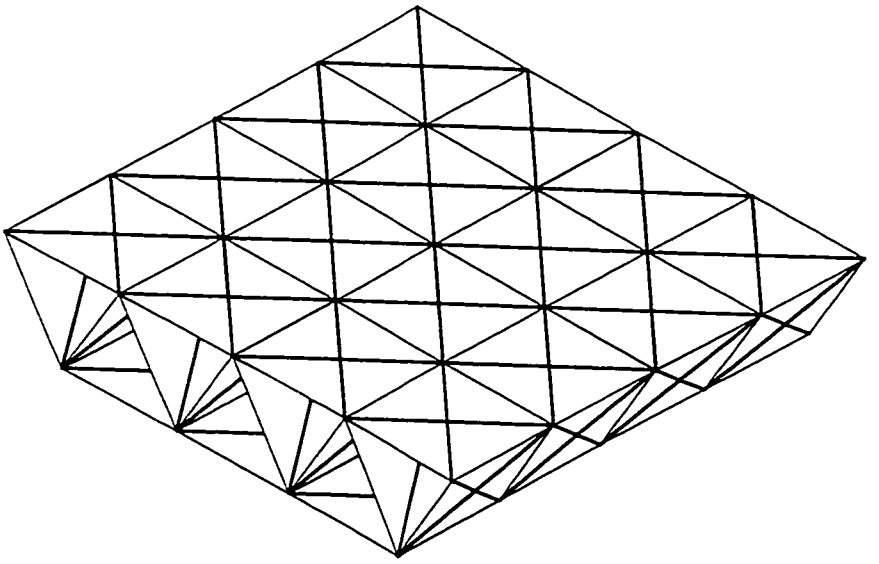

Figure 3.42: Pantographic slab formed by triangular columns.

The primary structure of the column for the displacement method is obtained by preventing relative horizontal displacements of nodes at unit interfaces. It is noted that the external load does not cause any bending in the bars of the constrained primary structure. The narrow-banded stiffness matrix and the load vector are obtained for each particular structure and loading. An analytical solution of the system of equilibrium equations is obtained in each case. This solution consists of two parts: the primary solution, which describes the behaviour of the most of the column, and the local solution, which is caused by the end conditions at the top and the bottom of the column and is confined to a few units near the corresponding ends of the structure. The influence of the local part of the solution on the overall behaviour of the column becomes small compared to that of the primary part, as the number of units in the structure increases. If the number of units in the column is constant and the degree of deployment increases, e.g. when a particular column deploys, the relative stiffening due to the local part of the solution increases, although the order of magnitude of this stiffening stays the same.

The displacement vector, obtained by superposition of the above solutions, is used to calculate the internal bending moments in the loaded column, which in turn are used to derive the expressions for the displacements corresponding to a particular type of loading. On the basis of these displacements the equivalent bending stiffness of a three-dimensional column is obtained. When the local effects are neglected, this characteristic is closely related to the equivalent bending stiffness of the planar pantographic column derived in the previous Chapter. It is shown that the contribution of each side of the three-dimensional column to the overall bending stiffness equals the bending stiffness of this side multiplied by the squared cosine of the angle between the plane of the side and the plane of bending.

Local effects due to support conditions at the bottom of the column - bottom nodes hinged to the ground - are found to introduce subtractive terms in the expressions for displacements. The highest order of magnitude of these terms is one power of the number of units in the column smaller than that of the term given by the primary part of

the solution. Therefore, for columns with a relatively small number of units, the contribution of the local solution to the deflections and stiffness should be taken into account.

Chapter 4

Closure

4.1 Summary of the Results

1. The equivalent bending stiffness of a two-dimensional uniform pantographic column in its own plane, when the axial deformations of bars are taken into account, is found to be $(EI)_e = \dfrac{2a^2 \sin\gamma}{\dfrac{\tan^2\gamma}{EA} + \dfrac{a^2}{3EI}}$, where a is the half-length of the bars in the scissor-like elements, EA and EI are the axial and bending stiffnesses of the bars, respectively, γ is the degree of deployment - the angle between the axis of a bar and the ground. The expression for the same stiffness when axial deformations of the bars are neglected is $(EI)_e = 6EI\sin\gamma$.

2. The equivalent axial stiffness of a planar uniform pantographic column, if the axial deformations of the bars are accounted for, is $(EA)_e = \dfrac{3\sin\gamma}{2n^2\cos^2\gamma} \dfrac{1}{\dfrac{\cot^2\gamma}{EA} + \dfrac{a^2}{3EI}}$, where

n is the number of SLEs in the column. If the axial deformations of the bars are neglected, $(EA)_e = \frac{9EI\sin\gamma}{2a^2n^2\cos^2\gamma} = \frac{18EI}{L^2}\frac{\sin^3\gamma}{\cos^2\gamma}$, where $L = 2an\sin\gamma$ - the length of the column.

3. The equivalent stiffnesses of a planar, uniformly tapered column are: $(EI)_e = k\,6EI\sin\gamma$ and $(EA)_e = k\frac{18EI}{L^2}\frac{\sin^3\gamma}{\cos^2\gamma}$, where k is a function of the degree of tapering m - the size ratio of the two neighbouring SLEs: $k = \frac{1}{3}\frac{(m+1)^2(m^n-1)^2(m^2+m+1)}{(m-1)^2(m^2+m+1)+4m(m^nm-1)(m^n-m)}$.

4. Geometric non-linearity, due to finite rotations of bars allowed by the pivotal connections, exhibited by pantographic columns under axial loading leads to a limit-point type of instability. The snap-through of the top SLE occurs at large (more than 30%) overall vertical deformations of the columns.

5. The introduction of a constraint against the relative horizontal displacement of the two top nodes of a column gives an axial stiffness four times greater than the original. The location of such constraint that yields the maximum stiffness increase (nine times) is at one third of the column length from the top.

6. Constrained columns are more rigid axially, and may buckle globally. The transition from the local snap-through (at lower degrees of deployment) to the global column-type buckling (at higher degrees of deployment) for the columns with the constraint between the top nodes occurs at a degree of deployment of 58°.

7. The equivalent bending stiffness of a three-dimensional pantographic column can be calculated using the following expression: $(EI)_e = \sum_{i=1}^{k} (EI)_{ei}^{planar} \cos^2 \alpha_i$, where k is the number of planar pantographic columns forming the sides of the three-dimensional structure, each having the equivalent bending stiffness $(EI)_{ei}^{planar}$ found as shown in 1, and α_i is the angle between the plane of a particular two-dimensional column and the plane of bending.

8. The rotation of the top of a three-dimensional column subjected to a moment load is $\varphi = M \frac{2a \sin\gamma}{(EI)_e} \left[n - \frac{1}{2} \frac{1+C}{1-C} \right]$, where $(EI)_e$ is found as shown in 7; $C = -A + \sqrt{A^2 - 1}$ and $A = \frac{4 + \sin^2\gamma}{2 - \sin^2\gamma}$ for a triangular column; $C = A - \sqrt{A^2 - 1}$ and $A = \frac{2 + \sin^2\gamma}{\sin^2\gamma}$ for a square column.

9. The lateral deflection of the top of a three-dimensional column subjected to a lateral force equally distributed among the top nodes is given by $h = P \frac{8a^3 \sin^3\gamma}{3(EI)_e} \left\{ \left[n^3 - \frac{n}{4} \right] - 3 \left[n^2 \frac{1}{2} \frac{1+C}{1-C} - n \left(\frac{1}{2} \frac{1+C}{1-C} \right)^2 - \left(\frac{1}{2} \frac{1+C}{1-C} \right)^3 \right] \right\}$; the parameters in this expression are the same as those in 8.

4.2 Concluding Remarks

Straight or curved planar pantographic columns are an integral part of three-dimensional deployable structures made of scissor-like elements. Understanding the behaviour of these columns is important in developing the necessary structural "feel" by designers of this

class of systems. In this thesis, straight planar and spatial pantographic columns subjected to bending and axial load are studied.

The closed form analytical expressions for the equivalent bending and axial stiffnesses of the uniform planar columns are obtained by comparing the response of the pantographic structure with that of a uniform solid column. These expressions become fairly compact under the following assumptions about the behaviour of the deployable columns. The response is assumed to be linear, axial deformations of bars in the SLEs are neglected, the number of SLEs in the column is large, and the degree of deployment is not very close to zero or the right angle. It is found that the internal force distribution and the deflections of pantographic columns subjected to bending in their plane (caused by the moment or lateral force loadings) are very similar to those of the conventional uniform beam.

The equivalent bending stiffness, which corresponds to the cross-sectional bending stiffness of the solid column, is a function of the degree of deployment and the bending stiffness of bars only. This parameter depends neither on the number of units in the column nor on the bar lengths. This fact has an important consequence. In conventional structural analysis a member having wider cross-section is usually associated with higher bending stiffness. A pantographic column with fewer SLEs (but still sufficiently many of them to satisfy one of the above assumptions) can be much wider then the column of the same length and degree of deployment but with more SLEs. Yet these two structures have the same lateral deflections. As long as two pantographic columns are made of bars with the same cross-sectional properties and have the same degree of deployment, their equivalent bending stiffnesses are the same.

The following paragraphs describe the important role played by the pivotal connections between the two bars forming an SLE in the behaviour of the pantographic columns subjected to axial load. In bending, however, the freedom of relative rotation of

bars about the pivots is of no importance. This rotation, being a symmetrical displacement in a symmetrical structure subjected to an anti-symmetrical load (moment or lateral force), is equal to zero. In fact, the bars in the SLEs could be rigidly connected at their intersections and this would not change the behaviour of the column in bending.

The distribution of internal forces in the pantographic column subjected to axial load differs qualitatively from that in the solid column subjected to the same load. The internal bending moments and axial forces grow from the top of the column to the bottom, but the vertical deformations of SLEs have the opposite trend. The equivalent axial stiffness for different columns of constant height again depends only on the bending stiffness of bars and the degree of deployment. However, for columns made of the same bars and having the same degree of deployment but different heights, the longer the column the softer its "cross-section" becomes. The reason for this lies in the mechanism of the axial deformation of the pantographic column. The change of height of each SLE includes two components. One of them is due to the bending of bars of a particular scissor-like element. The other is due to the deformation of the portion of the column below this SLE. The latter deformation causes the bottom nodes of the SLE to move apart, which causes relative rotation of the bars allowed by the pivotal connection. Therefore, even if the column is axially loaded at some level (not at the top), the part of the column below the load will be deformed and stressed, but the part of the column above the load, although stress-free, will also change its configuration.

The finite rotations of bars in the pantographic column under axial load make linear analysis applicable only for small loads. The procedure for non-linear analysis accounting for the changes in the degree of deployment in the SLEs along the column was developed. The equilibrium paths obtained by the "load-controlled" approach indicated softening of the structure under increasing load. The "displacement-controlled" approach allowed the column response to be traced up to and beyond the limit point on the equilibrium path. It was found that this limit point is closely related to the snap-through

buckling of the top SLE. If a rigid horizontal link is placed between the two nodes at a particular SLE interface, it increases the axial stiffness of the structure and postpones the local snap-through buckling, but makes the structure more susceptible to the overall column-type buckling. A stiffness-equivalent analytical model with fewer degrees of freedom is introduced for the purpose of the global buckling analysis. The obtained buckling loads depend on the bending as well as the axial stiffness distributions along the deformed columns.

Three-dimensional triangular and square pantographic columns in bending were studied. The force method was used to analyze single units of these types of columns. The results of these analyses were employed in the displacement method formulation for a full structure. Closed form analytical solutions of the resulting systems of equilibrium equations were obtained by taking advantage of certain properties of the stiffness matrices and load vectors. The typical solution consists of primary and local parts, the latter originating from the support conditions at the bottom of the column. The relative negative contribution of the local part of the solution to column deflections diminishes as the number of units in the column increases. The overall bending stiffness of a three-dimensional column is closely related to the bending stiffness of the planar columns that form the sides of the spatial structure. The contribution of the planar column of a particular side to the overall bending stiffness depends on the orientation of that side with respect to the plane of bending. This is similar to the way the solid walls of a hollow cross-section contribute their own bending stiffnesses to the stiffness of the whole cross-section. That part of the overall bending stiffness which is due to the axial stiffness of the planar columns (important for solid walls) has a secondary effect in pantographic structures and is included in the local solution. It was shown that deployable columns with square and equilateral-triangular cross-sections have the same stiffness for bending in any direction.

4.2 Directions of Future Research

In this Section we list some aspects of the structural behaviour of pantographic columns that were not addressed in this thesis and require further investigation. Possible applications of the results obtained are also outlined.

In calculating the deflections of the deployable columns, in both linear and non-linear analyses, the influence of the elemental axial forces on the bar bending stiffness was not taken into account. This effect may considerably soften the bottom portion of the column where the axial forces are the highest in the cases of lateral and axial loadings.

In the case of a three-dimensional column subjected to axial load the linear stiffness of the column is the direct sum of the axial stiffnesses of the sides. If the non-linear behaviour of such a column is considered, there exists another type of instability in addition to the snap-through buckling of the SLEs in the top unit. This instability is also of the local snap-through nature and corresponds to a "folding out" of the top three-dimensional pantographic unit. To capture this phenomenon, the equilibrium equations must be written for the units in their final configurations - "after rotation and bending".

The joints connecting the bar ends in spatial pantographic structures usually include additional hub element with slots and pins. These are revolute rather than spherical joints which may introduce torsion in the bars. Columns with such connections are more statically indeterminate and stiffer than the columns analyzed in this thesis.

It would be interesting to see whether the behaviour of curved pantographic beams and arches can be predicted on the basis of the stiffness characteristics obtained for planar and spatial straight columns. The general description of the idea of the pantographic slabs in which bending of bars is eliminated also requires further detailed development.

Appendix A

Integration Rule

When the principle of virtual work is used to find displacements in frames, the procedure involves the calculation of the internal virtual work done by internal virtual forces on real deformations. This work is expressed in the form of the following integral:

$$I.V.W. = \sum_i \int_{L_i} \frac{M_i(x)\, m_i(x)}{(EI)_i} dx \ , \qquad (A.1)$$

where $M_i(x)$ and $m_i(x)$ are the functions of real and virtual bending moments in a frame member number i, L_i and $(EI)_i$ are the length and the bending stiffness of the member, and the summation is done for all bars in the structure. For a straight bar with constant bending stiffness the calculation of such an integral can be simplified, mostly due to the fact that, since the virtual load is usually a set of concentrated moments or forces, the virtual bending moment diagram is a set of straight lines. This means that any bar in the structure can be divided into a number of parts for which the virtual bending moment, $m_i(x)$, is a linear function.

The problem now becomes:

$$I = \int_a^b f(x)\, g(x)\, dx \ , \qquad (A.2)$$

where f(x) is a general function of x, g(x) is a linear function of x, a and b are the limits of integration, i.e. (b-a) is the length of the bar or its segment (Fig. A.1). If the origin of the coordinate system is chosen at the point where the straight line of function g(x) crosses the horizontal axis, then this function becomes simply g(x) = k x. Substitution of such linear function in the integral in eq. A.2 yields:

$$I = \int_a^b f(x)\, k\, x\, dx = k \int_a^b x\, f(x)\, dx = k\, A_f\, x_{f.c.g.} = A_f\, k\, x_{f.c.g.} = A_f\, g(x_{f.c.g.}) \qquad (A.3)$$

The following steps were performed in eq. A.3. When constant k is factored out of the integral, the remaining expression constitutes the first moment of the area below function f(x) about the y-axis. If the area and the location of the centre of gravity of this shape are known, the first moment can be written as the product of the area, A_f, and the distance between the vertical axis and the centre of gravity, $x_{f.c.g.}$, instead of the integral. However, constant k multiplied by this coordinate yields the value of function g(x) at this point. Therefore, the rule:

The integral from a to b of the product of two functions, one of which is a general function and the other is a linear function, equals the area under the first function between a and b multiplied by the value of the second function at the location of the centre of gravity of that area.

In Russian textbooks this rule is called *Vereshchagin's* method for integration; the legend says that the technique was introduced in 1925 by a student of Moscow Railway Institute A. K. Vereshchagin.

The above derivation may be regarded as the geometrical sense of the rule. The physical sense can also be readily provided. If one thinks of function f(x) as weight distribution along a rigid bar running from a to b, then the integral in eq. A.2 may be seen as the work done by gravity field when the displacement of such a bar is described by function g(x). In this case, instead of integration, the total weight of the bar (area A_f) can

be multiplied by the displacement of its centre of gravity ($g(x_{f.\,c.g.})$), which corresponds to the final result of eq. A.3.

In cases when both functions under the integral (eq. A.2) are linear the rule has commutative property. In such cases it is immaterial whether the area under the first diagram be multiplied by the ordinate of the second diagram or the area under the second diagram be multiplied by the ordinate of the first diagram. In this thesis the bending moment diagrams, the product of which has to be integrated, are always linear; moreover, they are triangles with zero and maximum values at the same locations (hinged ends of the bars in SLEs and their pivots, respectively). The integral under the sum in eq. A.1 for such moment diagrams can be expressed in terms of the real and virtual pivotal moments, M_p and m_p, and the distance between the end of the bar and its pivot, a:

$$\int_0^a \frac{M(x)\,m(x)}{EI}dx = \frac{M_p\,a}{2}\frac{2}{3}m_p = M_p m_p \frac{a}{3} \qquad (A.4)$$

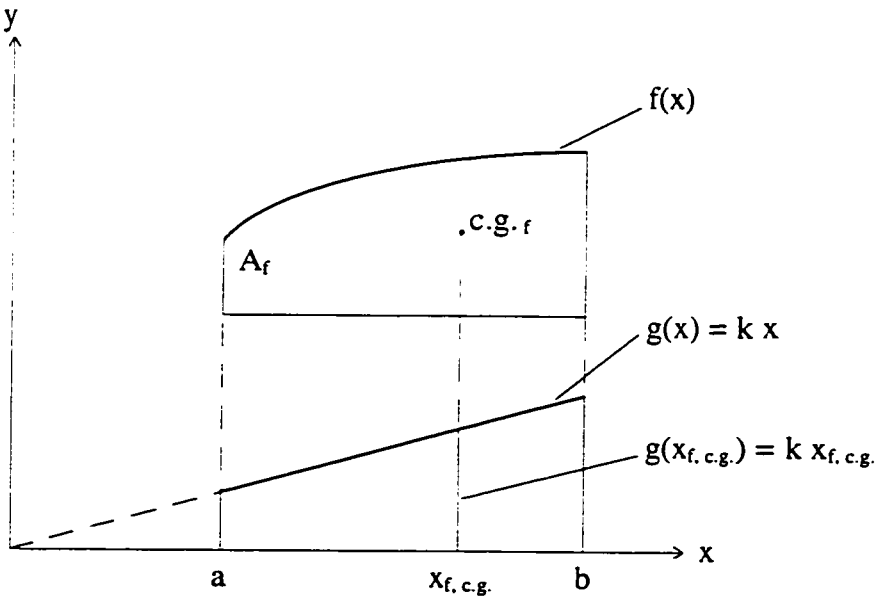

Figure A.1: Integration of the product of a general and a linear functions.

Appendix B

Summation Formulae

B.1 Standard Sums

Since pantographic columns, the subject of this thesis, are repetitive structures, many derivations contain sums of terms which need to be calculated over all pantographic units in a column. Sometimes these series are arithmetic or geometric progressions, for which well known analytical expressions are available. A simple arithmetic progression has the following expressions for its i-th term and the sum of the first n terms:

$$a_i = a_1 + (i-1)\,d\,, \quad S_n = \sum_{i=1}^{n} a_i = n\frac{a_1 + a_n}{2} = n\,a_1 + \frac{n(n-1)}{2}\,d\,, \tag{B.1}$$

where $d = a_{i+1}-a_i$ is the difference between the two successive terms. This arithmetic progression is an arithmetic progression of the first order. An example of such a progression is the series of natural numbers, for which:

$$a_i = i \quad (\text{therefore} \quad d = 1)\,, \quad S_n = \sum_{i=1}^{n} i = \frac{n(n+1)}{2} \tag{B.2}$$

The series of squares of natural numbers is an arithmetic progression of the second order. One of the possible ways to obtain the sum of the first n terms of this series is shown below (Hall and Knight, 1932):

$$\begin{aligned} n^3-(n-1)^3 &= n^3-\left(n^3-3n^2+3n-1\right)=3n^2-3n+1 \\ (n-1)^3-(n-2)^3 &= 3(n-1)^2-3(n-1)+1 \\ &\cdots \\ 2^3-1^3 &= 3(2)^2-3\cdot 2+1 \\ 1^3-0^3 &= 3(1)^2-3\cdot 1+1 \end{aligned} \qquad \text{(B.3)}$$

Adding the right and left sides of n equations in B.3 results in:

$$n^3=3\sum_{i=1}^{n} i^2-3\sum_{i=1}^{n} i+n\ , \qquad \text{(B.4)}$$

from which, with the use of eq. B.2, the sum of squares can be expressed as:

$$\sum_{i=1}^{n} i^2=\frac{2n^3+3n^2+n}{6}=\frac{n(n+1)(2n+1)}{6} \qquad \text{(B.5)}$$

The general forms of the i-th term and the sum of a geometric progression are:

$$a_i=a_1\,q^{i-1}\ ,\quad S_n=\sum_{i=1}^{n} a_i=\sum_{i=1}^{n} a_1 q^{i-1}=a_1\left(1+q+\ldots+q^{n-1}\right)=a_1\frac{1-q^n}{1-q}\ , \qquad \text{(B.6)}$$

where $q = a_{i+1}/a_i$ is the ratio between the two successive terms. If the absolute value of q is less than one and the number of terms in the sum is sufficiently large, the numerator on the right side of eq. B.6 is very close to unity.

B.2 Arithmetico-Geometric Series

In this Section the formulae for the sums of two series are derived. These sums are required in the process of calculating the deflection of a three-dimensional pantographic column under lateral load. The first sum has the form:

$$S_n=\sum_{i=1}^{n} i\,q^i=q+2q^2+3q^3+\ldots+nq^n\ , \qquad \text{(B.7)}$$

which is similar to a geometric progression, but has each term multiplied by its number. We factor q out of the sum and split each term into the part corresponding to the term of the standard geometric progression and the remaining part:

$$= q\left(1 + q + q + q^2 + 2q^2 + q^3 + 3q^3 + \ldots + q^{n-1} + (n-1)q^{n-1}\right) \tag{B.8}$$

The sum of the powers of q from zero to (n-1) is given by eq. B.6. The sum of the rest of the terms is S_{n-1}, so we add and subtract the last term of the original series:

$$= q\left(\frac{1-q^n}{1-q} + S_{n-1} + nq^n - nq^n\right) = q\left(\frac{1-q^n}{1-q} + S_n - nq^n\right) \tag{B.9}$$

All terms containing S_n are grouped on the left side, which gives the following expression for the sum:

$$S_n = q\frac{1-(n+1)q^n + nq^{n+1}}{(1-q)^2} = q\frac{1-(1+n-nq)q^n}{(1-q)^2} \tag{B.10}$$

For an absolute value of q less than one and an infinite number of terms the exponential decrease of q^n overcomes linearly growing n and the sum becomes:

$$S_n = \frac{q}{(1-q)^2} \tag{B.11}$$

The second sum to be calculated is:

$$S_n = \sum_{i=1}^{n} i\, q^{n-i} = q^{n-1} + 2q^{n-2} + 3q^{n-3} + \ldots + (n-1)q + n \tag{B.12}$$

Proceeding along the same lines as in the previous derivation we obtain the final expression for the sum:

$$S_n = \frac{n}{1-q} - q\frac{1-q^n}{(1-q)^2}\ , \tag{B.13}$$

which, for $|q| < 1$ and $n \to \infty$, becomes:

$$S_n = \frac{n}{1-q} \tag{B.14}$$

Bibliography

Becchi, P. and Dell'Amico, S. (1989). "Design and Testing of a Deployable, Retrievable Boom for Space Applications", Proceedings of the 23rd Aerospace Mechanisms Symposium, NASA-CP-3032, pp. 101-112.

Belda, E.P. (1996). "Constructive Problems in the Deployable Structures of Emilio Pérez Pinero", Proceedings of the 2nd International Conference MARAS 96 (Mobile and Rapidly Assembled Structures), edited by Escrig, F. and Brebbia, C.A., June 17-19, Seville, Spain, pp. 23-34.

Bulson, P.S. (1991). "The Efficiency of Rapidly Assembled Structures", Proceedings of the International Conference MARAS 91 (Mobile and Rapidly Assembled Structures), edited by Bulson, P.S., April, Southampton, UK, pp. 3-14.

Chew, M. and Kumar, P. (1993). "Conceptual Design of Deployable Space Structures from the Viewpoint of Symmetry", International Journal of Space Structures, Vol. 8, nos. 1-2, pp. 17-27.

Clarke, R.C. (1984). "The Kinematics of a Novel Deployable Space Structure System", Proceedings of the Third International Conference on Space Structures, edited by Nooshin, H., Sep. 11-14, 1984, Guildford, UK, pp. 820-822.

Clevett, M.L., Lowdermilk, R.H., Bright, J.K., Coulter, C.S. and Melton. T.W. (1986). "Expandable portable bridge structure", US Patent No. 4,628,560 (filed Feb. 27, 1984).

Escrig, F. (1984). "Expandable Space Frame Structures", Proceedings of the Third International Conference on Space Structures, edited by Nooshin, H., Sep. 11-14, 1984, Guildford, UK, pp. 845-850.

Escrig, F. (1985). "Expandable Space Structures", International Journal of Space Structures, Vol. 1, pp. 79-91.

Escrig, F. (1996). "General Survey of Deployability in Architecture", Proceedings of the 2nd International Conference MARAS 96 (Mobile and Rapidly Assembled Structures), edited by Escrig, F. and Brebbia, C.A., June 17-19, Seville, Spain, pp. 3-22.

Escrig, F. and Valcarcel, J.P. (1986). "Analysis of Expandable Space Bar Structures", *Shells, Membranes and Space Frames*, Proceedings of the IAAS Symposium on Membranes and Space Frames, edited by Heki, K., Sep. 15-19, 1986, Osaka, Japan, Vol. 3, pp. 269-276.

Escrig, F. and Valcarcel, J.P. (1991). "To Cover a Swimming Pool with an Expandable Structure", Proceedings of the International Conference MARAS 91 (Mobile and Rapidly Assembled Structures), edited by Bulson, P.S., April, Southampton, UK, pp. 273-282.

Fanning, P. and Hollaway, L. (1993). "The Deployment Analysis of a Large Space Antenna", International Journal of Space Structures, Vol. 8, no. 3, pp. 209-220.

Funabashi, H., Horie, M., Tachiya, H. and Tanio, S. (1991). "A Synthesis of Robotic Pantograph Mechanisms Based on Working Spaces and Static Characteristic Charts", JSME International Journal, Series III, Vol. 34, no. 2, pp. 239-244.

Furuya, H. and Isomichi, B. (1992). "Optimal Configurations of Actively Controlled Space Truss Antennas", Third International Conference on Adaptive Structures, editors: Wada, B.K., Natori, M. and Breitbach, E., Nov. 9-11, 1992, San Diego, California, USA, pp. 207-215.

Gantes, C. (1991). "A Design Methodology for Deployable Structures", Ph.D. Thesis, Department of Civil Engineering, Massachusetts Institute of Technology, Cambridge, Mass., USA.

Gantes, C. (1993). "Geometric Constraints in Assembling Polygonal Deployable Units to Form Multi-Unit Structural Systems", Proceedings of the 4th International Conference on Space Structures, edited by Parke, G.A.R. and Howard, C.M., Sep. 6-10, Surrey, UK, pp. 793-803.

Gantes, C. (1996). "Analytical Predictions of the Snap-Through Characteristics of Deployable Structures", Proceedings of the 2nd International Conference MARAS 96 (Mobile and Rapidly Assembled Structures), edited by Escrig, F. and Brebbia, C.A., June 17-19, Seville, Spain, pp. 83-92.

Gantes, C., Connor, J.J., Logcher, R.D. and Rosenfeld, Y. (1989). "Structural Analysis and Design of Deployable Structures", Computers and Structures, Vol. 32, nos. 3-4, pp. 661-669.

Gantes, C., Connor, J.J. and Logcher, R.D. (1991a). "Combining Numerical Analysis and Engineering Judgement to Design Deployable Structures", Computers and Structures, Vol. 40, no. 2, pp. 431-440.

Gantes, C., Connor, J.J. and Logcher, R.D. (1991b). "Geometric and Structural Design Considerations for Deployable Space Frames", Proceedings of the International Conference MARAS 91 (Mobile and Rapidly Assembled Structures), edited by Bulson, P.S., April, Southampton, UK, pp. 250-260.

Gantes, C., Connor, J.J. and Logcher, R.D. (1993a). "Simple Friction Model for Scissor-Type Mobile Structures", Journal of Engineering Mechanics, Vol. 119, no. 3, pp. 456-475.

Gantes, C., Logcher, R.D., Connor, J.J. and Rosenfeld, Y. (1993b). "Geometric Design of Deployable Structures with Discrete Joint Size", International Journal of Space Structures, Vol. 8, nos. 1-2, pp. 107-117.

Gantes, C., Logcher, R.D., Connor, J.J. and Rosenfeld, Y. (1993c). "Deployability Conditions for Curved and Flat, Polygonal and Trapezoidal Deployable Structures", International Journal of Space Structures, Vol. 8, nos. 1-2, pp. 97-106.

Gantes, C., Connor, J.J. and Logcher, R.D. (1994a). "Equivalent Continuum Model for Deployable Flat Lattice Structures", Journal of Aerospace Engineering, Vol. 7, no. 1, pp. 72-91.

Gantes, C., Connor, J.J. and Logcher, R.D., (1994b). "A Systematic Design Methodology for Deployable Structures", International Journal of Space Structures, Vol. 9, nos. 2, pp. 67-86.

Guest, S.D. and Pellegrino, S. (1994a). "The Folding of Triangulated Cylinders, Part I: Geometric Considerations", Journal of Applied Mechanics, Vol. 61, no. 4, pp. 773-777.

Guest, S.D. and Pellegrino, S. (1994b). "The Folding of Triangulated Cylinders, Part II: The Folding Process", Journal of Applied Mechanics, Vol. 61, no. 4, pp. 778-783.

Guidetti, S. and Silvestri, G. (1996). "Puff", Proceedings of the 2nd International Conference MARAS 96 (Mobile and Rapidly Assembled Structures), edited by Escrig, F. and Brebbia, C.A., June 17-19, Seville, Spain, pp. 155-164.

Hall, H.S. and Knight, S.R. (1932). Higher Algebra, 4th edition, Macmillan and Co., London.

Hardin, G.L. (1978). "Expandable Beam Structure", US Patent No. 4,126,974 (filed Nov. 17, 1977).

Hegedus, I. (1993). "Branching of Equilibrium Paths in a Deployable Column", International Journal of Space Structures, Vol. 8, nos. 1-2, pp. 119-125.

Hernandes, M. and Carlos, H. (1991). "Deployable Structures", Proceedings of the International Conference MARAS 91 (Mobile and Rapidly Assembled Structures), edited by Bulson, P.S., April, Southampton, UK, pp. 237-248.

Hernandez, C.H. (1996). "New Ideas on Deployable Structures", Proceedings of the 2nd International Conference MARAS 96 (Mobile and Rapidly Assembled Structures), edited by Escrig, F. and Brebbia, C.A., June 17-19, Seville, Spain, pp. 63-72.

Hoberman, C. (1990). "Reversibly Expandable Doubly-Curved Truss Structure", US Patent No. 4,942,700 (filed Oct. 27, 1988).

Ichikawa, H., Nakayama, M. and Nakamura, H. (1990). "Pantograph Type Robot Arm", US Patent No. 4,933,531 (filed June 27, 1989).

Kaveh, A. and Davaran, A. (1996). "Analysis of Pantograph Foldable Structures", Computers and Structures, Vol. 59, no. 1, pp. 131-140.

Kitamura, T., Natori, M.C., Okazaki, K. and Yamashiro, K. (1993). "Developments of Extendible Beams for Space Applications", Proceedings of the AIAA/AHS/ASEE Aerospace Conference, (AIAA Paper 93-0977), pp. 1-5.

Krishnapillai, A. (1992). "Deployable structures", US Patent No. 5,167,100 (filed May 13, 1988).

Kumar, P. and S. Pellegrino, S. (1996). "Deployment and Retraction of a Cable-Driven Rigid Panel Solar Array", Journal of Spacecraft and Rockets, Vol. 33, no. 6, pp. 836-842.

Kwan, A.S.K. and Pellegrino, S. (1991). "The Pantographic Deployable Mast: Design, Structural Performance, and Deployment Tests", Proceedings of the International Conference MARAS 91 (Mobile and Rapidly Assembled Structures), edited by Bulson, P.S., April, Southampton, UK, pp. 213-224.

Kwan, A.S.K. and Pellegrino, S. (1993). "Prestressing a Space Structure", AIAA Journal, Vol. 31, no. 10, pp. 1961-1963.

Kwan, A.S.K., You, Z. and Pellegrino, S. (1993). "Active and Passive Cable Elements in Deployable/Retractable Masts", International Journal of Space Structures, Vol. 8, nos. 1-2, pp. 29-40.

Kwan, A.S.K. and Pellegrino, S. (1994). "Matrix Formulation of Macro-Elements for Deployable Structures", Computers and Structures, Vol. 50, no. 2, pp. 237-254.

LeBlond, M. (1986). "Adjustable Staircase", US Patent No. 4,615,160 (filed Sep. 30, 1985).

Makowski, Z.S. (1966). "Space Structures", Proceedings of the 1st International Conference on Space Structures, edited by Davies, R.M., Sep., 1966, Guildford, UK, pp. 1-8.

McCollum, F.H. (1975). "Stress Balanced Extendible Boom Structure", US Patent No. 3,877,544 (filed July 13, 1973).

McNulty, O. (1986). "Foldable Space Structures", *Shells, Membranes and Space Frames*, Proceedings of the IAAS Symposium on Membranes and Space Frames, edited by Heki, K., Sep. 15-19, 1986, Osaka, Japan, Vol. 3, pp. 277-284.

Mikulas, M.M. Jr., Wada, B.K., Farhat, C., Thorwald, G. and Withnell, P. (1992). "Initially Deformed Truss Geometry for Improving the Adaptivity Performance of Truss Structures", Third International Conference on Adaptive Structures, editors: Wada, B.K., Natori, M. and Breitbach, E., Nov. 9-11, 1992, San Diego, California, USA, pp. 305-319.

Miura, K. (1989). "Studies of Intelligent Adaptive Structures", AD-Vol. 15, Adaptive Structures, presented at the Winter Annual Meeting of the American Society of Mechanical Engineers, edited by Wada, B.K., Dec. 10-15, 1989, San Francisco, California, USA, pp. 89-94.

Miura, K. (1993). "Concepts of Deployable Space Structures", International Journal of Space Structures, Vol. 8, nos. 1-2, pp. 3-16.

Miura, K. and Furuya, H. (1988). "Adaptive Structure Concept for Future Space Applications", AIAA Journal, Vol. 26, no. 8, pp. 995-1002.

Mollaert, M. (1996). "Retractable Membrane Roofs", Proceedings of the 2nd International Conference MARAS 96 (Mobile and Rapidly Assembled Structures), edited by Escrig, F. and Brebbia, C.A., June 17-19, Seville, Spain, pp. 407-417.

Morales, J., Sanchez, F. and Escrig, F. (1996). "Geometry of Deployable Structures Generated by Computer-Aided Design", Proceedings of the 2nd International Conference MARAS 96 (Mobile and Rapidly Assembled Structures), edited by F. Escrig and C.A. Brebbia, June 17-19, Seville, Spain, pp. 253-258.

Murray, C.J. (1990). "Pantograph-Type Structure Forms Semicircular Arch", Design News, Vol. 46, no. 3, pp. 188-189.

Natori, M., Miura, K. and Furuya, H. (1986). "Deployable Truss Concepts in Space Technology", *Shells, Membranes and Space Frames*, Proceedings of the IAAS Symposium on Membranes and Space Frames, edited by Heki, K., Sep. 15-19, Osaka, Japan, Vol. 3, pp. 261-268.

Nodskov, P. and Thelander, F. (1986). "Collapsible Exhibit Panel", US Patent No. 4,580,375 (filed May 18, 1984).

O'Connor, D.N., Eppinger, S.D., Seering, W.P. and Wormley, D.N. (1997). "Active Control of High-Speed Pantograph", Journal of Dynamic Systems, Measurement and Control, ASME, Vol. 119, no. 1, pp. 1-4.

Olds, C.D. (1963). *Continued Fractions*, 9th series of The Mathematical Association of America, Washington, DC.

Onoda, J. (1988). "Two-Dimensional Deployable Truss Structures for Space Applications", Journal of Spacecraft and Rockets, Vol. 25, no. 2, pp. 109-116.

Onoda, J., Fu, D.-Y. and Minesugi, K., (1996). "Two-Dimensional Deployable Hexapod Truss", Journal of Spacecraft and Rockets, Vol. 33, no. 3, pp. 416-421.

Oral, H.A. (1996). "Kinematics of Parallel Platforms: Pantograph Mechanism Based Transmission", Proceedings of the 1996 3rd Biennial Joint Conference on Engineering Systems Design and Analysis, edited by Ovunc, B.A., Tichkiewich, S. and Ankara, A.O., July 1-4, Montpellier, France, Vol. 8, pp. 9-16.

Pellegrino, S. (1995). "Large Retractable Appendages in Spacecraft", Journal of Spacecraft and Rockets, Vol. 32, no. 6, pp. 1006-1014.

Pinero, E.P. (1961). "Project for a Mobile Theatre", Architectural Design, Vol. 31, no. 12, p. 570.

Pinero, E.P. (1962). "Expandable Space Framing", Progressive Architecture, Vol. 43, no. 6, pp. 154-155.

Ramesh, A.V., Utku, S., Wada, B.K. and Chen, G.S. (1989). "Effect of Imperfections on Static Control of Adaptive Structures as a Space Crane", AD-Vol. 15, *Adaptive Structures*, presented at the Winter Annual Meeting of the American Society of Mechanical Engineers, edited by Wada, B.K., Dec. 10-15, 1989, San Francisco, California, USA, pp. 95-101.

Ramesh, A.V., Utku, S. and Wada, B.K. (1991). "Real-Time Control of Geometry and Stiffness in Adaptive Structures", Computer Methods in Applied Mechanics and Engineering, Vol. 90, pp. 761-779.

Raskin, I. and Roorda, J. (1996). "Buckling Force for Deployable Pantographic Columns", Proceedings of the 2nd International Conference MARAS 96 (Mobile and Rapidly Assembled Structures), edited by Escrig, F. and Brebbia, C.A., June 17-19, Seville, Spain, pp. 305-314.

Raskin, I. and Roorda, J. (1997a). "Stiffness of Geometrically Non-Linear Pantographic Column", Proceedings of the 16th Canadian Congress of Applied Mechanics (CANCAM 97), edited by Cloutier, L. and Rancourt, D., June 1 - 5, 1997, Sainte-Foy, Quebec, Canada, Vol. 1, pp. 27-28.

Raskin, I. and Roorda, J. (1997b). "Stability of Non-Linear Pantographic Column", Proceedings of the 25th CSCE Annual Conference, edited by Neale, K.W. and Proulx, J., May 27 - 30, 1997, Sherbrooke, Quebec, Canada, Vol. 4, pp. 49-57.

Raskin, I. and Roorda, J. (1998a). "Bending of Three-Dimensional Pantographic Column", Symposium on Deployable Structures: Theory and Applications, IUTAM-IASS, September 6 - 9, 1998, (abstract accepted).

Raskin, I. and Roorda, J. (1998b). "Non-Uniform Pantographic Column in Bending and Compression", Proceedings of the 2nd Structural Specialty Conference, CSCE, edited by Newhook, J.P. and Jaeger, L.G., June 10-13, 1998, Halifax, NS, Canada, Vol. 3b, pp. 501-510.

Raskin, I. and Roorda, J. (1998c). "Linear Behaviour of a Uniform Pantographic Column in Bending and Compression", International Journal of Space Structures, (submitted).

Raskin, I. and Roorda, J. (1998d). "Non-Linear Uniform Pantographic Column in Compression", Journal of Engineering Mechanics, ASCE, (submitted).

Rauschenbach, H.S. (1980). *Solar Cell Array Design Handbook* (The Principles and Technology of Photovoltaic Energy Conversion), Van Nostrand Reinhold Company, New York.

Renner, W. (1996). "Variable Roofing-System for the Step-by-Step Covering of the Industrial Waste Deposite Plant at Bielefeld-Herford", Proceedings of the 2nd International Conference MARAS 96 (Mobile and Rapidly Assembled Structures), edited by Escrig, F. and Brebbia, C.A., June 17-19, Seville, Spain, pp. 165-174.

Sanchez, J., Escrig, F. and Valcarcel, J.P. (1996a). "Analysis of Reduced Scale Models of X-Frame Structures", Proceedings of the 2nd International Conference MARAS 96 (Mobile and Rapidly Assembled Structures), edited by Escrig, F. and Brebbia, C.A., June 17-19, Seville, Spain, pp. 55-62.

Sanchez, J., Escrig, F. and Valcarcel, J.P. (1996b). "The Adventure of Covering a Swimming Pool with an X-Frame Structure", Proceedings of the 2nd International Conference MARAS 96 (Mobile and Rapidly Assembled Structures), edited by Escrig, F. and Brebbia, C.A., June 17-19, Seville, Spain, pp. 113-122.

Sanchez-Cuenca, L. (1996). "Geometric Models for Expandable Structures", Proceedings of the 2nd International Conference MARAS 96 (Mobile and Rapidly Assembled Structures), edited by Escrig, F. and Brebbia, C.A., June 17-19, Seville, Spain, pp. 93-102.

Sastre, R. (1996). "Expandable Arches", Proceedings of the 2nd International Conference MARAS 96 (Mobile and Rapidly Assembled Structures), edited by Escrig, F. and Brebbia, C.A., June 17-19, Seville, Spain, pp. 123-131.

Schmidt, L.C. and Li, H. (1995). "Geometric Models of Deployable Domes", Journal of Architectural Engineering, Vol. 1, no. 3, pp. 115-120.

Shahinpoor, M. (1993). "Deployable Fractal Mechanisms as Smart Structures", AMD-Vol. 167, *Recent Developments in Stability, Vibration, and Control of Structural Systems*, presented at the 1st Joint Mechanics Meeting of ASME/ASCE/SES - MEET'N'93, edited by Guran, A., June 6-9, 1993, Charlottesville, Virginia, USA, pp. 119-126.

Shan, W. (1992). "Computer Analysis of Foldable Structures", Computers and Structures, Vol. 42, no. 6, pp. 903-912.

Smola, J.F., Radford, W.E. and Reitz, M.H. (1980). "The Magsat Magnetometer Boom", Proceedings of the 14th Aerospace Mechanisms Symposium, NASA-CP-2127, pp. 267-278.

Sorenson, G.R. and Gerberding, P.C. (1994). "Collapsible Modular Display Tower Assembly", US Patent No. 5,327,700 (filed Dec. 5, 1991).

Stern, T.G., Cornwall, M., Lawrence, J.F. and Peterson, D.M. (1992). "Deployable Retractable Photovoltaic Concentrator Solar Array Assembly for Space Applications", US Patent No. 5,131,955 (filed Jan. 14, 1991).

Takamatsu, K.A. and Onoda, J. (1991). "New Deployable Truss Concepts for Large Antenna Structures or Solar Concentrators", Journal of Spacecraft and Rockets, Vol. 28, no. 3, pp. 330-338.

Valcarcel, J.P., Escrig, F., Martin, E. and Freire, M. (1991). "Expandable Space Structures with Self-Folding Textile Cover", Proceedings of the International Conference MARAS 91 (Mobile and Rapidly Assembled Structures), edited by Bulson, P.S., April, Southampton, UK, pp. 283-295.

Valcarcel, J.P., Escrig, F., Estevez, J. and Martin, E. (1992). "Large Span Expandable Domes", *Innovative Large Span Structures*, IASS-CSCE International Congress 1992, edited by Srivastava, N.K., Sherbourne, A.N. and Roorda, J., Vol. 2, pp. 619-630.

Valcarcel, J.P. and Escrig, F. (1996). "Recent Advances in the Analysis of Expandable Structures", Proceedings of the 2nd International Conference MARAS 96 (Mobile and Rapidly Assembled Structures), edited by Escrig, F. and Brebbia, C.A., June 17-19, Seville, Spain, pp. 45-54.

Wada, B.K. (1990). "Adaptive Structures: an Overview", Journal of Spacecraft And Rockets, Vol. 27, no. 3, pp. 330-337.

Wada, B.K., Fanson, J.L. and Crawley, E.F. (1989). "Adaptive Structures", AD-Vol. 15, *Adaptive Structures*, presented at the Winter Annual Meeting of the American Society of Mechanical Engineers, edited by Wada, B.K., Dec. 10-15, 1989, San Francisco, California, USA, pp. 1-8.

Warnaar, D.B. (1992). "Evaluation Criteria for Conceptual Designs of Deployable-Foldable Truss Structures", DE-Vol. 46, *Mechanism Design and Synthesis*, presented at the 22nd Biennial Mechanisms Conference, edited by Kinzel, G. et al., Sep. 13-16, 1992, Scottsdale, Arizona, USA, pp. 167-174.

Warnaar, D.B. and Chew, M. (1990a). "Conceptual Design Of Deployable-Foldable Truss Structures Using Graph Theory - Part 1: Graph Generation", DE-Vol. 26, *Cams, Gears, Robot and Mechanism Design*, presented at the 21st Biennial Mechanisms Conference, edited by Pisano, A., McCarthy, M. and Derby, S., Sep. 16-19, 1990, Chicago, Illinois, USA, pp. 107-113.

Warnaar, D.B. and Chew, M. (1990b). "Conceptual Design Of Deployable-Foldable Truss Structures Using Graph Theory - Part 2: Generation of Deployable Truss Module Design Concepts", DE-Vol. 26, *Cams, Gears, Robot and Mechanism Design*, presented at the 21st Biennial Mechanisms Conference, edited by Pisano, A., McCarthy, M. and Derby, S., Sep. 16-19, 1990, Chicago, Illinois, USA, pp. 115-125.

Webster's New Collegiate Dictionary (1981). G. & C. Merriam Company, Springfield, Massachusetts, USA.

Westbury, P.S. (1996). "The Development of the RSSB Tent", Proceedings of the 2nd International Conference MARAS 96 (Mobile and Rapidly Assembled Structures), edited by Escrig, F. and Brebbia, C.A., June 17-19, Seville, Spain, pp. 185-188.

Wichman, W.J. (1992). "Display Frame with Folding Display Attachment Devices", US Patent No. 5,125,205 (filed July 5, 1991).

Wittrick, W.H. and Williams, F.W. (1971). "A General Algorithm for Computing Natural Frequencies of Elastic Structures", Quarterly Journal of Mechanics and Applied Mathematics, Vol. 24, Pt. 3, pp. 263-284.

Yang, D.C.H. and Lin, Y.Y. (1985). "Pantograph Mechanism as a Non-Traditional Manipulator Structure", Mechanism and Machine Theory, Vol. 20, No. 2, pp. 115-122.

You, Z. (1996). "A Pantographic Deployable Conic Structure", International Journal of Space Structures, Vol. 11, no. 4, pp. 363-370.

You, Z. and Pellegrino, S. (1996a). "New Solutions for Foldable Roof Structures", Proceedings of the 2nd International Conference MARAS 96 (Mobile and Rapidly Assembled Structures), edited by Escrig, F. and Brebbia, C.A., June 17-19, Seville, Spain, pp. 35-44.

You, Z. and Pellegrino, S. (1996b). "Cable-Stiffened Pantographic Deployable Structures Part 1: Triangular Mast", AIAA Journal, Vol. 34, no. 4, pp. 813-820.

You, Z. and Pellegrino, S. (1997a). "Cable-Stiffened Pantographic Deployable Structures Part 2: Mesh Reflector", AIAA Journal, Vol. 35, no. 8, pp. 1348-1355.

You, Z. and Pellegrino, S. (1997b). "Foldable Bar Structures", International Journal of Solids and Structures, Vol. 34, no. 15, pp. 1825-1847.

Zanardo, A. (1985). "Extensible Arm, Particularly for Space Modules or Vehicles", US Patent No. 4,557,083 (filed Sep. 26, 1984).

Zanardo, A. (1986). "Two-Dimensional Articulated Systems Developable on a Single or Double Curvature Surface", Meccanica, Vol. 21, no. 2, pp. 106-111.

Zeigler, T.R. (1976). "Collapsible Self-Supporting Structure", US Patent No. 3,968,808 (filed Nov. 6, 1974).

Zeigler, T.R. (1977). "Collapsible Self-Supporting Structures", US Patent No. 4,026,313 (filed July 13, 1976).

Zeigler, T.R. (1984). "Collapsible Self-Supporting Structures", US Patent No. 4,437,275 (filed Aug. 7, 1981).

Zuk, W. and Clark, R.H. (1970). *Kinetic Architecture*, Van Nostrand Reinhold Company, New York.

IMAGE EVALUATION
TEST TARGET (QA-3)

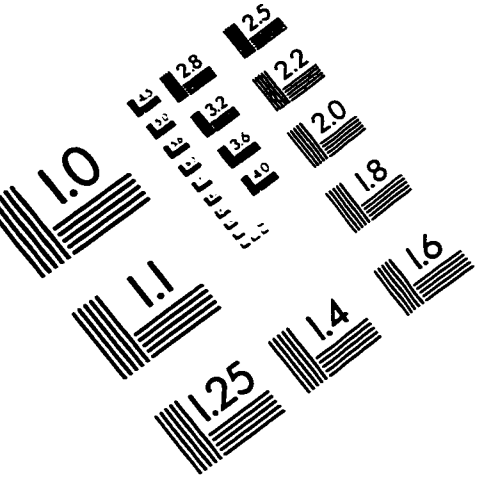

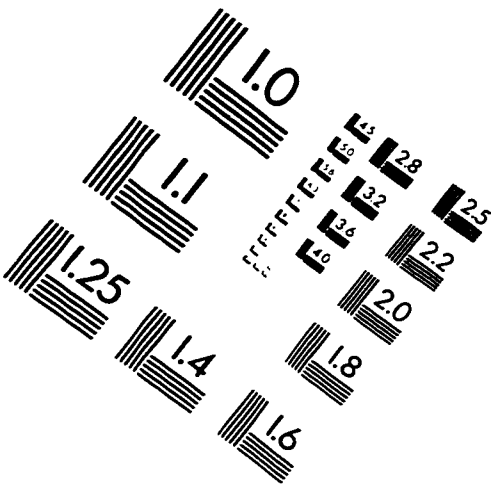

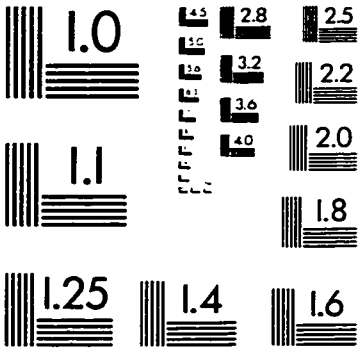

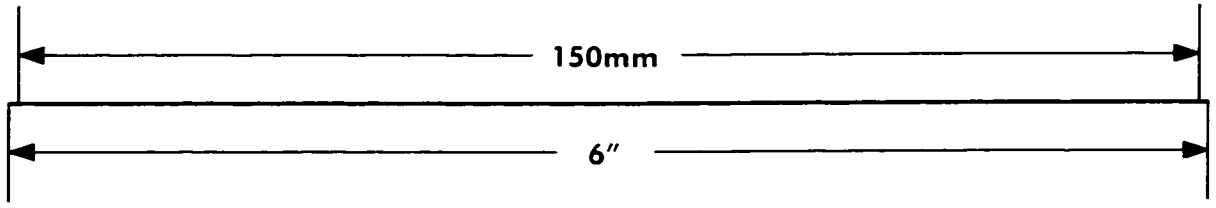

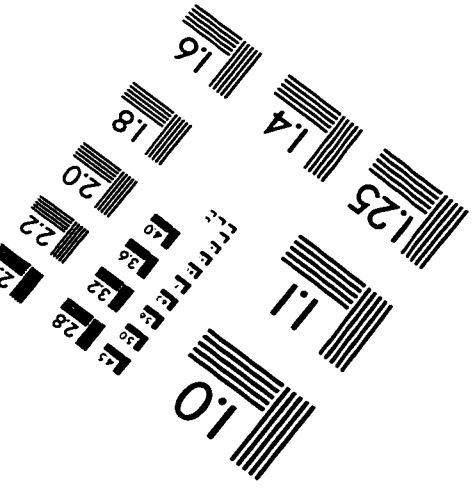

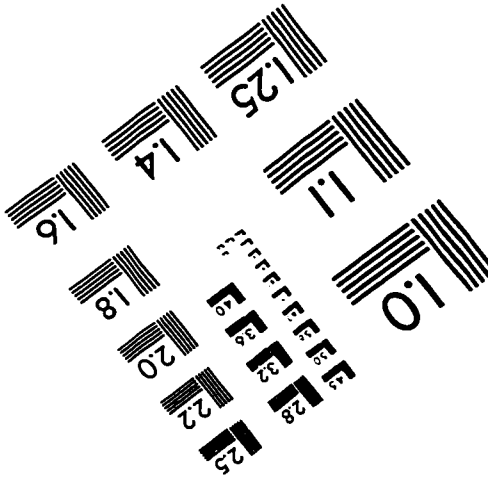

APPLIED IMAGE, Inc
1653 East Main Street
Rochester, NY 14609 USA
Phone: 716/482-0300
Fax: 716/288-5989

© 1993, Applied Image, Inc., All Rights Reserved